HYDROGENATION OF CARBON MONOXIDE OVER MODIFIED COBALT-BASED CATALYSTS

Saul Eric Colley

A Thesis submitted to the Faculty of Science, University of the Witwatersrand, Johannesburg, in fulfilment of the requirements for the degree of Doctor of Philosophy.

nary, 1991.

ABSTRACT

A disadvantage of the Fischer–Tropsch synthesis is that a broad product spectrum is obtained. Economic considerations however require an improvement in the optimization of the reaction to maximize the production of high value commercial products, in particular, short chain olefins and high molecular weight hydrocarbons. There is thus a potential for the development of improved catalysts that will show enhanced selectivities to a single product or narrow distribution of products. The majority of the investigations reported in this thesis have thus dealt with the study of, and modifications to, a previously developed co–precipitated Co/MnO matrix catalyst, to achieve these aims.
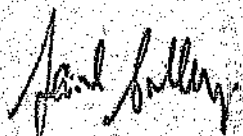
Co–precipitated Co/MnO oxide catalysts with improved product selectivities for the CO hydrogenation reaction, have been developed. This has been achieved by use of potassium– and chromium–promoters, respectively. These promoters were observed to influence catalytic performance differently, as was evidenced from the results obtained. The addition of small amounts of potassium promoter to Co/MnO resulted in an increase in the short chain (C_2 and C_3) olefin selectivity, coupled with a favourable decrease in methane formation. The presence of a chromium promoter on the other hand, substantially increased selectivity toward the longer chain hydrocarbons (i.e. C_{18}^+ fraction), without affecting catalyst activity. These desired product yields, from the respective promoted systems, were further increased by optimization of reactor operating conditions, viz. P(at constant conversion), T, and GHSV (and conversion).

Bulk changes in the Co/MnO catalyst (and related systems, viz. Co_3O_4, Co_3O_4/Al_2O_3, and $CoCr_2O_4$ oxide spinels) occurred during catalyst pretreatment, i.e. calcination and reduction, and under F–T synthesis conditions. The changes were followed *in situ* by a high temperature XRD/DSC investigation. Results of this study enabled the rationalization of the choice of the optimizaion conditions for catalyst pretreatment and activation. Furthermore, in all cases a novel Co(bcc) metastable phase was identified, after prolonged interaction with synthesis gas. The influence of the support did not play a significant role in the formation of this novel phase. Co(bcc) was proposed to form through a rearrangement of a cobalt–carbonyl intermediate. A correlation between the formation of Co(bcc) and the high selectivities toward the light alkenes for the Co/MnO catalyst, was made. This correlation was not obvious for the other Co systems investigated.

Tailoring of broad F–T product distributions has also been achieved by the consideration of alternative catalyst preparation techniques. Recently Shell Internationale Research has reported on the novel preparation of inhomogeneously supported cobalt–based catalysts. In these reports it was observed that 90% of the Co was situated in the outer volumes of the catalyst support. This effect was correlated with significant improved C_5^+ selectivity. We have reproduced an analogue of this Shell–type catalyst using a novel method of electroless cobalt deposition, onto Si/Al substrates. Support penetration by Co was found to vary with time of immersion in Pd activator solutions, whereas cobalt loading was observed to be a function of both cobalt bath concentration and plating bath temperature. Preliminary reactor studies were initiated.

DECLARATION

I declare that the work presented in this thesis was carried out exclusively by myself under the supervision of Prof. N.J. Coville. It is being submitted for the degree of Doctor of Philosophy at the University of the Witwatersrand, Johannesburg. It has not been submitted before for any degree or examination at any other University.

Saul Eric Colley

10th day of January, 1991.

To my mother

ACKNOWLEDGEMENTS

I would like to express my sincere gratitude to the following people who in some way or another became associated with this thesis:

My mother, for her endless support, understanding and motivation.

TABLE OF CONTENTS

CHAPTER 6: A NOVEL ELECTROLESS DEPOSITION METHOD OF CATALYST PREPARATION FOR IMPROVED C_5^+ SELECTIVITY

LIST OF TABLES

LIST OF FIGURES

CHAPTER ONE

INTRODUCTION

W..'e the credibility — or incredibility — of a reliable source of energy and chemical feedstocks will be argued to the end, the impact on over-extended global utilization is becoming unavoidable. This topic has become subjected to a flood of information and misinformation, conflicting viewpoints and varying interpretations — and for good and sufficient reason. For this subject is of daily relevancy and is entwined with the entire political, economic and social spectrum (1).

1.1 "Coal — a bridge to the future"

The gradual depletion of finite and limited world oil reserves, coupled with the uncertainty and expense of crude imports, has necessitated a search for alternative routes to liquid transportation fuels and chemical feedstocks. The total proven world resources of fossil energy carriers is approximately 5000 billion barrels oil — equivalent, made up of 75% coal, 13% crude oil and 12% natural gas (2). Forecasts predict a maximum in oil production shortly before the year 2000, with a steady state decline thereafter. At predicted consumption rates, natural gas reserves would seem to be sufficient for a further 30 — 35 years. Coal reserves which far exceed both oil and gas reserves will have a maximum production close to the year 2100. These statistics predict a world-wide return to coal as a fossil fuel source (2,3) — in fact coal has been described as a "bridge to the future" (4). At the present time coal is mainly used as a source of energy, especially for combustion to generate

electrical power. However, when coal is used as a chemical feedstock, the hydrogen to carbon ratio in the coal has to be increased to produce hydrocarbon derived compounds — a process known as coal liquefaction.

1.2   Coal as a chemical feedstock — coal liquefaction

Coal liquefaction is a general term used to describe a process in which a portion of the organic coal substance is converted to liquid products. In the widest sense this includes liquids extracted by solvents. More specifically, coal liquefaction involves producing liquids by chemically altering the coal structure and increasing the content of hydrogen relative to carbon. At the same time, nitrogen, sulfur, oxygen, and mineral matter are removed (5). Coal liquefaction can be classified as pyrolysis, direct liquefaction, and indirect liquefaction. In *pyrolysis*, coal is converted at temperatures above 400°C in a non-oxidizing atmosphere to gases, liquids, and char (the solid char usually being the main product). *Direct liquefaction* involves hydrogen addition to the coal by means of high pressure hydrogenation (Bergius Process) or coal extraction methods applying reactive hydrogen donor solvents (Exxon process). Conversion to liquids can be realised with or without added catalysts. According to the conditions chosen, the principal products can be high molecular mass fuels, distillate fuel oils, gasoline, or chemical feedstocks. In *indirect liquefaction*, coal is brought into contact with oxygen and steam at high temperature (coal-gasification) to produce a mixture of carbon monoxide and hydrogen (synthesis gas), which can be catalytically converted to liquid products. The best-known process, the Fischer-Tropsch (F-T) synthesis (6) [which will be discussed in greater detail in Sections to follow], produces a mixture of gaseous, liquid, and solid (waxy) hydrocarbons. A variant of the F-T synthesis gives methanol in yields that, unlike the hydrocarbon synthesis, approach 100%. Methanol can be used

as turbine and transportation fuel, although its energy content on a volume basis is only half of that of gasoline (5). It can also be converted almost quantitatively to high-octane gasoline by the Mobil methanol-to-gasoline (MTG) process. This process requires the use of the highly selective zeolite catalyst, ZSM-5 (7,8).

Both direct and indirect liquefaction have been used commercially to produce liquids from coal, with initial developments taking place in Germany during the 1920's and 1930's. However, commitments for large-scale liquefaction facilities have usually been based more on strategic considerations (because of inadequate or uncertain petroleum supplies), rather than on economics. Many industrialized nations have at some time made some investment in coal liquefaction research and development.

At the present time, coal is rarely used as a source of fuels and chemical feedstocks because of economic factors that dictate that the cheapest available resources i.e. oil, should be used first. An exception to this statement is the current commercial Sasol synthetic fuel processes in South Africa i.e. Sasol 1,2, and 3. South Africa has large deposits of coal (which are easy to exploit), 75% of which is low grade, high-ash coal (9). High-ash, unreactive coal is not suitable for direct coal liquefation, and therefore the indirect liquefation of this low coal via the Fischer-Tropsch synthesis is currently employed (10). Initial motivation for the construction of these plants was for political reasons, with the South African government wishing to become, and maintain, a certain degree of independence on the international energy markets.

This thesis is concerned with the abovementioned Fischer–Tropsch (carbon monoxide hydrogenation) process, as used in the commercially operating Sasol plants. For this reason, these topics (and some associated ideas) will be dealt with in more detail in the remainder of this Chapter.

1.3 The Fischer–Tropsch process

The Fischer–Tropsch synthesis can be defined as the catalytically induced hydrogenation of carbon monoxide, which produces higher hydrocarbons and/or oxygenates, the carbon chains of the molecules being predominantly straight in the range C_4 to C_{10} (6). This process is essentially a polymerization reaction, with carbon bonds being formed between carbon atoms derived from carbon monoxide, under the influence of hydrogen and a metal catalyst and with concurrent elimination of H_2O (11). The main reaction of the Fischer–Tropsch synthesis may be formulated as:

$$n(CO + 2H_2) \longrightarrow (CH_2)_n + nH_2O$$
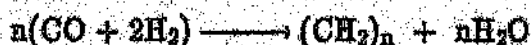
Depending on the catalyst and reaction conditions, the products are linear hydrocarbons, oxygenated derivatives thereof, or mixtures of both. Usually a wide range of molecules with different chain lengths and with a molecular weight distribution characteristic of polymerization reactions is formed.

The literature on the Fischer–Tropsch synthesis is remarkably varied and often confusing, such that any attempt to quantitatively correlate results from different publications on a given catalyst is difficult. The reasons for this situation are two fold: (i), the various authors are frequently vague about the precise nature and pretreatment of their catalysts; and (ii) there are no kinetic constants or selectivity parameters which universally and

uniquely described the results obtained (12). In this Chapter no attempt will be made to review the extensive F–T literature, and consequently only basic concepts will be presented here. However, the reader is referred to some well written books (13,14,6), and a number of review papers (15–18), for further information.

1.3.1 A brief histroy

The history of this process starts in 1902 with the observation by Sabatier and Senderson that methane was for.aed from mixtures of H_2 and CO over nickel and cobalt catalysts (19). Badische Anilin un Soda Fabrik (BASF) took out patents in 1913 on the preparation of hydrocarbons and oxygenates (synthol) at high pressure, typically over oxide catalysts (20). This work was not pursued further until the early 1920's when Franz Fischer and Hans Tropsch of the Kaizer Wilhelm Institute at Mülheim/Ruhr (later renamed the Max Planck Institute for coal research) reported their work on CO/H_2 reactions, using alkalized iron catalysts at high pressures (10 to 15 MPa). The liquid product was observed to be rich in oxygenated compounds (21). At lower pressures, hydrocarbons were produced over the iron catalysts; these catalysts were found to deactivate rapidly (22,23). This initiated further work on the metal catalysts (e.g. cobalt and nickel) operating at low pressures. After experimentation nickel was found to be unsuitable because of its high methane selectivity and rapid deactivtion. From 1933 to 1939, further development of cobalt catalysts including pilot plant tests, were made by Ruhrchemie AG. During this period Ruhrchemie AG were awarded the first Fischer–Tropsch plant patent licence using a cobalt thorium oxide catalyst. In 19?? Pichler demonstrated that with a ruthenium catalyst synthesis gas could be converted into a waxy material, "polymethylene" at low temperatures and very high pressures (24).

Intensive efforts in Germany, before and during World War II, led to the construction of large scale plants to supplement limited indigenous petroleum resources. The catalyst used was mainly the "standard" cobalt catalyst, with a composition of $Co:ThO_2:MgO:kieselguhr$ 100:5:8:200 (10). After World War II, interest in synfuel programs (particularly in the United States, in programs funded by the U.S. Bureau of Mines) were sustained by the fear that petroleum production could not keep pace with demand. Two German firms Ruhrchemie and Lurgi formed an *Arbeitgemeinschaft* (ARGE) and developed the fixed bed reactor using a precipitated iron catalyst to produce high yields of wax. In the USA several companies (e.g. Standard Oil and Hydrocarbon Research Inc.) developed fluidized bed reactors with the Kellogg Co. researching a circulating entrained catalyst version [fluidized bed reactors produce high yields of gasoline] of the reactor (10). However, coal liquefaction was rendered uneconomical by the discovery of immense reserves of cheap petroleum in the Middle East in the later 1940's and mid 1950's. Consequently interest in these processes waned. Since this period the major event in the further development of coal liquefaction was the construction of Sasol 1 (South Africa), which came on line in 1955 and has been in commercial operation ever since. The plant incorporated both the fixed bed Arge reactors and the entrained bed, Kellogg (Synthol) reactors. Research and development continued at Sasol in the 1950's and 1960's, although it had been largely discontinued elsewhere in the world. There were a few notable exceptions e.g. Pichler, Köbel and their co-workers in Germany (6) who continued research studies during this period.

Renewed interest in synthetic fuels was again initiated after the 1973 OPEC oil embargo, which greatly increased oil prices and clearly demonstrated the risks of excessive dependence on imports. Large investments

in Fischer–Tropsch research and development were made by the industrialized nations, the United States exerting a leading role. In the early and mid 1980's a surplus of petroleum crude was seen on the world market, and coupled with increasingly efficient use of fuel, lowered the demand for OPEC oil and led to price reductions. The investment in Synfuel research in the United States began to suffer a series of sharp reductions in 1981, and had declined to a comparatively minimal level by the late 1980's. This influenced other nations to reduce their investments in alternative energy resources. The possibility of new plants producing synthesis fuels from coal before the year 2000, are unlikely (6). However, in the wake of the current Gulf crisis there has been a distinct renewal of interest into the F–T reaction. This is evidenced by numerous papers on F–T synthesis being presented at recent international conferences on catalysis. Many excellent reviews have been written describing and summarizing this past work in F–T synthesis (6,13,14,25,26).

1.3.2 Preparation of synthesis gas

Coal gasification to synthesis gas (the so–called mixture of carbon monoxide and hydrogen) involves a thermal balance between the endothermic reactions of carbon with steam and carbon dioxide, and the exothermic reaction of carbon with oxygen (27). Additional processes occurring in gasifiers include coal devolatilization (coal → char + volatiles), the water gas shift ($CO + H_2O \rightarrow CO_2 + H_2$), and methanation ($CO + 3H_2 \rightarrow CH_4 + H_2O$) reactions (10,27). Dry–ash Lurgi fixed–bed gasifiers are used in the commercial Sasol process to produce the raw synthesis gas. These reactors use low–grade or high ash coals, and operate at high pressure with low oxygen consumption and high carbon conversion. Disadvantages of this operation include high steam consumption, and the production of methane, tars, oils,

and phenols (5). However, the product gas stream from the gasifier undergoes a step-wise purification process (Lurgi Rectisol purification), to produce a purified gas with hydrogen to carbon monoxide ratios of between 1.7 and 2.5.

1.3.3   Catalysts

For the F-T conversion of the coal derived syngas to products, the presence of a metal catalyst is necessary. The first reaction step of this process is the simultaneous chemisorption of CO and H_2 on the metal atoms of the catalyst (28). The 3d and 4f transition metals (i.e. group VIII metals) of the Periodic Table, or their inclusion compounds (e.g., nitrides, carbides), are particularly suitable for this chemisorption process (13).

(a)   Basic Metals

Virtually only cobalt and iron have found successful application in the F-T synthesis (6,10). Nickel produces mainly methane, making it unattractive for this process (10). As far as the platinum group metals are concerned, iridium, palladium, and platinum exhibit only very slight activity, and produce mainly alcohols. Rhodium and osmium have been observed to produce both oxygen-containing products and larger quantities of hydrocarbons at higher temperatures (29-32). Paraffins of high molecular weight have been synthesized using ruthenium catalysts at high pressure (6). Molybdenium, as a F-T catalyst, has been investigated by the US Burea of Mines (10), with the objective of developing a catalyst resistant to sulphur poisoning. Although reasonable activities were achieved, these were much lower than that of iron catalysts. Studies with Mo were also carried out at Sasol (10) where it was reported that high temperatures(400°C and higher) were required

for reasonable conversions, with methane selectivity also being very high.

So far titanium, vanadium, chromium, and manganese have not found application as the basic metal in F-T catalysts, because thier oxides are difficult to reduce, or may be even resistant totally to reduction to the metal at the temperature involved in catalyst manufacture. These metal oxides, have however been found to be important components in F-T catalysts when used either as structural and/or chemical promoters (33-37). This phenomenon will be discussed further in sections to follows.

The performance of a specific catalyst depends initially on the metal it contains. This performance is however strongly influenced by its environment i.e. the presence of promoters (structural and chemical – see Chapters 3 and 4), catalyst preparation (see Chapter 6) and pretreatments (calcination, reduction and activation – see Chapter 5), and by reactor operating conditions (10). There have been many attempts to tailor the broad F-T product spectrum (within the constraints of the Schulz–Flory distribution law), to a particular product or narrow distribution of products, by varying some of the abovementioned parameters. Tailoring the product distribution (selectivity) remains a challenging goal – see Chapters 3, 4 and 6.

(b) Promoters

As mentioned above, one approach in obtaining a high selectivity to a single product or narrow distribution of products, involves the use of catalyst promoters. Since the early years of the Fischer–Tropsch

reaction, it has been recognized that promoters are of paramount importance for these reactions. These promoters can be divided into two groups accoring to their mode of action. Difficult–to–reduce metal oxides (e.g. Al_2O_3, ThO_2, MgO, CoO,) are employed as *structural promoters* (6,13,33,38–40). The support effects high metal dispersions by its large surface area and inhibits recrystallization of the catalytically active phase. It also provides the desired mechanical properties of the catalyst and may hinder metal sintering. In addition, the support may favourably modify the catalytic properties of the metal by chemical interaction. The nature of this metal–support interaction depends both on the type of the metal and the type of support. These interactions are often intriguing and unpredictable (9). Titania is an example of a metal oxide support which has been found to modify strongly the properties of all group VIII metals. Hydrogen and CO chemisorption on TiO_2 supported metals are strongly suppressed when the metals are reduced at a high temperature. This effect, which was first described by Tauster *et al.* (38), is not observed (or to a much lesser extent) with SiO_2 or Al_2O_3 supported catalysts. For the observed phenomenon of suppressed chemisorption the expression Strong Metal Support Interaction (SMSI) has been introduced (41). The net result of the SMSI is a decrease in H_2 chemisorption, which in turn results in a decreased hydrogenation activity of the catalyst. This results in lower methane and higher olefin yields in the F–T reaction, when compared to non–SMSI catalysts. This effect has been rationalized by Hutchings (42) and Kugler (43).

The metal particles on the catalyst support may vary in size from clusters of a few atoms to larger particles of many atoms. Apart from the metal–support interactions, particle size may have a strong effect on

the catalytic properties of the metal. Very small metal particles may have properties that strongly deviate from bulk metal surfaces, for two reasons: (i) very small particles can have unusually high surface reactivity and, (ii) small particles do not have large ensembles of specific coordination number required by some reactions [structure sensitive reactions] (44,45).

Promotion by *chemical modification* (also termed energetic promoters) has been shown to affect both catalyst activity and selectivity, via an electronic mechanism -- this has been discussed in greater detail in Chapter 3. Chemically reactive structural promoters can also function as energetic promoters. Na, K, Rb, Li, and Cs all give rise to a comparable promoter effect for an equimolar quantity (46). The main effect of these alkali metal promoters is to induce a decreased H_2 chemisorption, coupled with an increased CO chemisorption and consumption (39). This causes an acceleration in chain growth, shifting the product distribution in favour of compounds with a higher carbon number. The drop in hydrogen adsorption suppresses the hydrogenation reaction, resulting in lower methane selectivities and higher olefin to paraffin ratios. The formation of oxygen–containing products has also been observed to be favoured. Copper can also be incorporated into the chemical–electronic group of promoters. Copper induces a more facile reduction of Fe, which, depending on the quantity of the Cu additive, makes it possible to decrease the reduction temperature (10).

(c) <u>Methods of catalyst preparation</u>

Successful, more selective F–T catalysts have not generally been developed from a consideration of the bulk and physical properties of

the catalyst constituents, but rather on a trial and error basis. Further, both direct experimentation and reference to similar experiments recorded in the literature have facilitated this search for new catalysts. In general, the method of catalyst preparation should produce a catalyst that, after suitable pretreatment (i.e. calcination and reduction), has a highly active and accessible surface area. The requirements of activity and mechanical strength will also vary depending on the type of reactor in which the catalyst is being employed. (Reactors used in F-T synthesis will be discussed in sections to follow). Techniques of catalyst preparation include, co-precipitation (detailed in Chapter 2), impregnation (detailed in Chapter 6), decomposition of metallic cluster compounds onto a support (34,47-50), solvated metal atom dispersion [SMAD] (51-53) and catalyst fusion (10). The subject of catalyst preparation is discussed further in Chapter 6.

1.3.4   Nature of the selectivity problem – Product distribution models

A limitation of F-T technology is the low selectivity to the desired products. There is an interdependence of selectivities, and product distributions are generally very broad. This is illustrated in Figure 1.1, which shows data for numerous Sasol iron catalysts run under a broad range of conditions. [The curves in Figure 1.1 represent an average of these data (54).]

As previously mentioned, the product selectivity depends on such variables as the catalytic metal, presence of promoters and support, operating conditions i.e. P, T, GHSV, syngas composition (examples of which are presented in Chapter 3), and reactor design (see Section 1.4.1). However, only in the case of methanol and methane can a product be produced with 100% selectivity.
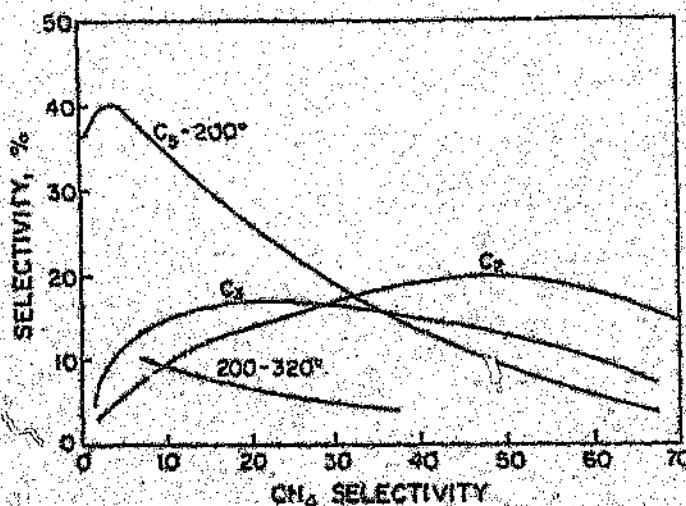
Figure 1.1: The interdependence of the product selectivities with F-T catalysts (54). Data are the average for a variety of Sasol Fe catalysts at 200 – 340°C, 5 – 40 atm.

On the basis of extensive experimental data, mathematical formulations have been derived which can adequately fit and rationalize the product distributions obtained using Fischer–Tropsch catalysts (11,55–59). These models are based on the assumptions that hydrocarbon chain growth proceeds via a polymerization mechanism, with growth occurring predominantly in single–carbon increments. The incremental increase in chain length, and the competing process for termination (by desorption into the gas or liquid phase as products), each have probabilities which are independent of the length of the oligomer chain attached to the surface. The nature of the monomer unit is the subject of current research and considerable controversy. However the exact nature of this C_1 monomer does not affect the fundamentals of the polymerization process.

The most probable distribution function, derived by Schulz and Flory, to describe the polymerization process i.e. the Schulz–Flory

distribution function (60), is identical to the analytical function derived by Storch .nderson, and co-workers (13) to describe their data for F–T synthesis, in the absence of chain branching. This equation which predicts the distribution of products as a function of carbon number n, is given by the expression.

$$\ln \frac{Wn}{n} = n \ln P + \ln \frac{(1 - P)^2}{P}$$ (1)

where Wn — weight fraction of product of carbon number n

P — chain growth probability factor — $r_p/(r_p + r_t)$

where r_p and r_t are the rates of propogation and termination respectively.

If this distribution function applies, then a plot of Wn/n should give a straight line, where both the slope and intercept give the same value of P. Figure 1.2 demonstrates how some commercial F–T data comply with the above relation (61).
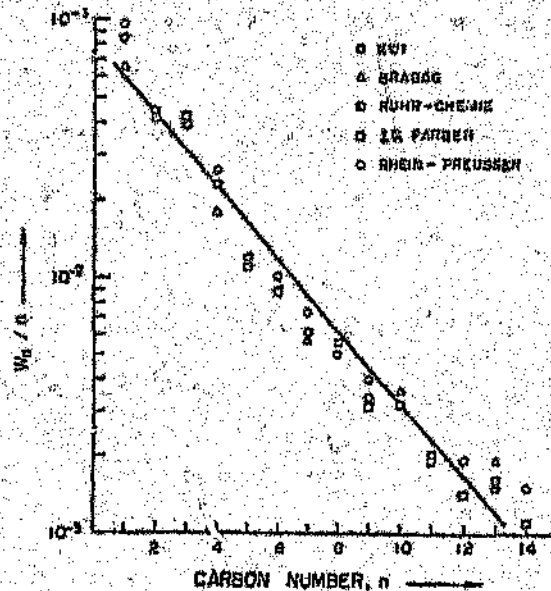
Figure 1.2: Hydrocarbon distributions for commercial iron catalysts plotted according to equation (1) [61].

Equation (1) suggests that once P is fixed, then the entire distribution is determined. This is supported by the commercial data for Sasol shown in Figure 1.1, where a strong interdependence on selectivity is observed. Figure 1.3 demonstrates more clearly the impact of the chain-growth mechanism on the selectivity of a number of groups of desired hydrocarbon products. [Here Wn is plotted as a function of the degree of polymerization, D, which is given by $(1-P)^{-1}$] (61).
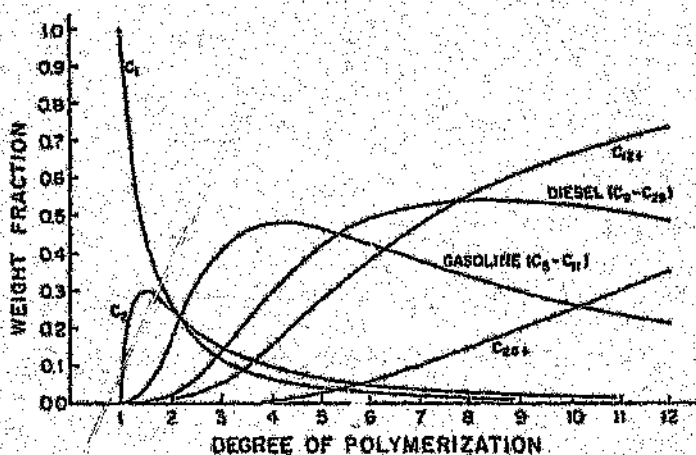
Figure 1.3: Selectivity limitations of F-T synthesis as determined by the Schulz-Flory distribution function (61).

Thus the Schulz-Flory equation predicts maximum yields for certain products, which are summarized in Table 1.1 (62).

It is obviously economically more logical to obtain a high selectivity to a single product or narrow distribution of products. Until recently, selectivity control for F-T reactions was limited to moderate shifts in the observed broad product distributions, within the selectivity constraints predicted by the Schulz-Flory distribution law. However, researches hav\ been quite successful (Sasol in particular) in learning to control and optimize

TABLE 1.1: Maximum yields of Cn products expected from a Schulz–Flory distribution

Product fraction	Maximum selectivity/% by mass
C_1	100
C_2	29
C_2–C_4	57
C_5–C_{11}	48
C_{12}–C_{25}	41

selectivities for the F–T process (10,63). Several approaches are currently being pursued in an effort to develop highly selective systems for the conversion of syngas to fuels and chemicals (61). These include (as previously mentioned), modification of F–T catalysts, optimization of reactor operating conditions and reactor design.

1.4   The Sasol Fischer–Tropsch process

The first commercial F–T plant in South Africa, Sasol 1 (Sasolburg), came on–stream in 1955 and has been in operation ever since. The plant produces waxes, liquid fuels, pipe line gas and chemicals. Following the Middle East oil crisis of 1973, two new and larger F–T plants, Sasol 2 and 3, w e built (at Secunda), which came on–stream in 1980 and 1982, respectively. These two new plants produce predominantly ethylene, gasoline and diesel. Based on over 34 years of commercial experience in F–T

operations, Sasol has identified factors for controlling the product slate with respect to fraction produced and yields. Experience with reactor types has demonstrated their advantages and limitations, while manipulation of the operating conditions has established control techniques for yields. The Sasol process has been reviewed by Dry (10,63-65).

As previously discussed, initial motivation for the construction of the Sasol plants was to enable South African to become less dependent on foreign oil suppliers. However, the very existence of these synthetic fuel plants has become very much more attractive from profits realized in the sale of the F-T by-products. Thus, from the original synfuels-from coal concept, petrochemical feedstocks from coal have become today's reality. Under normal world trading conditions with crude oil freely available, synthetic transport fuels were unable to compete with products derived from crude oil. However, for the half-year ended December 1988, Sasol achieved a 34.8 percent increase in earnings per share although there had been a 16 percent reduction in synfuels operating income (66). The key to the financial success of Sasol thus lies in the co-production of chemicals; the most important being: — ethylene

- ammonia and sulphur

- alcohols, aromatics and ketones

- phenols, and

- high molecular F-T waxes (Sasol waxes sell at approximately 4 times the price of liquid fuels — see Chapter 4).

Recently, a number of synfuels development and commercialization projects have been completed, improving in some cases on the 30-year-old technology — these will be discussed in sections to follow. Also, instead of oligomerising

programmed surface reaction (TPSR). Their results suggested two mechanisms for CO adsorption and hydrogenation operating on alumina–supported cobalt: (i) CO dissociation on the metal followed by hydrogenation of α–carbon (Reaction 1) and, (ii) spillover of CO and H_2 to the support where a CH_xO complex is formed, followed by diffusion of the complex to metal crystallites where it decomposes (Reaction 2). Reaction 1 was apparently favoured on large 3D crystallites, with Reaction 2 taking place on both large and inaccessible small crystallites. They suggested the distribution of these reactions to be a function of metal loading and reduction temperature; the fraction of methane formed by Reaction 1 increasing with increasing metal loading and extent of reduction.

The majority of the research performed for this thesis involved the use of a precipitated Co/MnO (1:1 % mole) matrix catalyst, developed by co–workers (84,85). Details of Co/MnO catalyst preparation and performance (including catalytic performance of similar systems) will be discussed in Chapter 2 and Chapter 3, respectively. Briefly, this catalyst was observed to show higher activities than those observed for Fe/MnO catalysts. Higher propene levels coupled with lower methane selectivities were also observed. A combination of Co and MnO has also been investigated by Varma *et al.* (86), however in this case, the active metal Co was *impregnated* onto the MnO support. While the catalyst was found to exhibit a high selectivity to olefins in the C_2–C_4 range, the total yield of hydrocarbons was low. Addition of Ni to the Co was observed to have improved the hydrocarbon yields, while still retaining good olefin selectivity.

Chemical modification of catalyst selectivity to produce a narrow range of molecular weights (i.e. by K promotion) has been widely studied and

all of the propene produced in the F–T process to low value liquid fuels, Sasol is constructing a polypropylene plant (63).

1.4.1   Sasol reactors

(i)   Commercial reactors

Until recently Sasol has only used two types of F–T reactors [extensively reviewed by Dry (10)], namely the fixed bed and circulating fluidised bed (CFB) reactors, as shown in Figure 1.4. CO hydrogenation over extruded precipitated iron based catalysts in the multi–tubular fixed bed Arge reactors – Figure 2A (operating temperature ~225°C), leads to the production of the high valued F–T waxes. Heat from the exothermic reaction is removed by converting water circulating on the outside of the tubes to steam (63). The circulating fluidised bed (CFB) Synthol reactors (Figure 2B), loaded with fused iron magnetite catalysts, produces low molecular mass olefins and oils. This reactor type operates at a higher temperature than the Arge reactor, namely 340°C, shifting the product spectrum toward the lower hydrocarbons. The production of heavier products are depressed as excessive wetting of the catalyst would result in particle agglomeration and hence defluidisation of the bed (63). The reaction heat is removed by heat exchangers and is absorbed by the gas (10). Both the gas throughput and the percentage conversion, on a cross–sectional area basis, is much higher for the CFB than for the fixed bed reactors (63).
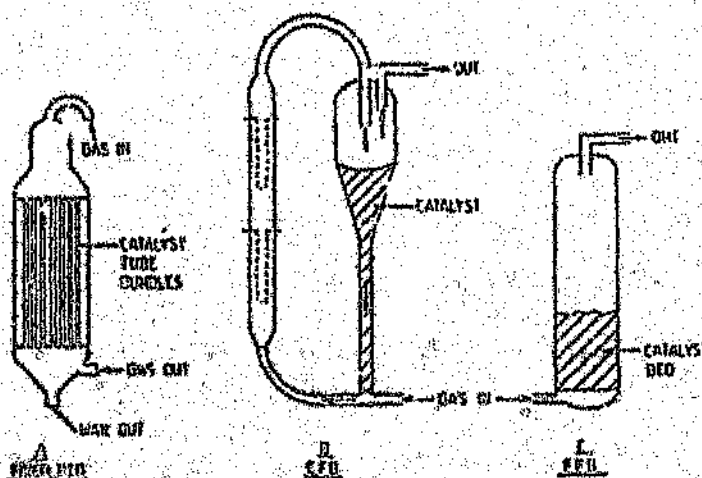
Figure 1.4: Sasol F–T reactors (63).

(ii) Recent reactor developments

(a) Higher pressure operation

By increasing the pressure (keeping gas residence time and percentage conversion constant, by increasing feed gas flow by the same proportion), the production per volume of reactor space can be increased in direct proportion to the pressure. This finding has been commercially utilised on two occasions at Sasol. New CFB reactors are physically larger and operate at higher pressures, thus having production capacities of three times that of the older units. In addition, a new fixed bed reactor operating at 45 bar (a 50% increase on the older units), has as predicted, increased wax production by 50% (63).

(b) Alternative fluidised bed reactors – the fixed fluidised bed (FFB) synthol reactor

The FFB reactor is the proud end result of a decade's research and development, which places Sasol on the threshold of tomorrow's synthetic fuels technology. The synthol FFB will be a strong contender for any future synthetic-fuels-coal/gas process in South Africa or abroad. A prime benefit is the cost of the FFB – nearly half that of the older technology. The FFB is more efficient, offers greater flexibility and significant savings on operating and maintenance costs. In the FFB the gas enters the reactor via a specially designed distributor and "bubbles" through the catalyst bed. The bed, although fluidised, is not transported as in the CFB case and is thus referred to as "fixed". A full scale commercial unit was constructed and came on stream in June 1989 (63,67).

(c) Slurry phase reactors

A slurry phase reactor is similar to a FFB reactor except that the catalyst is suspended in a molten F-T wax. This reactor is not seen as a competitor for the FFB/CFB systems, since studies have shown the slurry bed to have a lower conversion at 320°C. In addition, at this temperature, the wax is hydrocracked resulting in a loss of the liquid phase medium. As an alternative to the fixed bed reactor for the production of waxes at lower temperatures, however, the slurry phase reactor does have a major cost advantage. Due to a much simpler construction, the slurry is expected to be approximately 45% cheaper than the same capacity multi-tubular unit. Also, it has been

demonstrated that by regular fresh catalyst addition, a good conversion in the slurry bed can be maintained. This adds to the commercial advantage, since the slurry reactors can be kept on–line for long periods of time. The fixed bed reactors periodically have to be brought off–line for catalyst replacement. To fully evaluate the slurry process, Sasol has decided to operate a demonstration unit (63).

1.4.2   Product selectivity and final work–up

The Sasol F–T product spectra obtained under typical commercial conditions for the three reactor systems discussed are given in Table 1.2 (63).

TABLE 1.2:   Selectivity (carbon atom basis) for Sasol F–T processes[a]

	High Temp CFB/FFB	Low Temp Fixed Bed	Low Temp Slurry
CH_4	7.0	2.0	3.3
C_2H_4	4.0	0.2	1.0
C_2H_6	3.0	0.6	1.2
C_3H_6	10.7	0.9	3.2
C_3H_8	1.7	0.9	0.8
C_4H_8	9.3	1.0	3.1
C_4H_{10}	1.1	1.4	1.9
$C_5 + C_6$	16.5	4.8	6.1
$C_7 - 160°C$	20.0	6.2	7.6
$- 160° - 350°C$	15.5	18.3	17.0
$+ 350°C$	6.0	62.3	49.5
Oxygenates	5.1	1.4	4.4

[a] Data from Dry (63).

At low temperatures the main primary products are linear 1-alkenes, alkanes, alcohols and aldehydes. The C_9–C_{18} olefins are ideal for the manufacture of biodegradable detergents. The C_{10} to C_{18} cut is an excellent diesel fuel (the high cetane number of 75 and the presence of zero aromatics results in minimal exhaust pollution). The gasoline requires extensive isomerization and aromatisation, due to product linearity at these temperatures. At higher synthesis temperatures, secondary reactions occur which produce, for example branched hydrocarbons and aromatics. Hence the diesel cetane number decreases but the octane number of the gasoline increases. The olefinity of the hydrocarbons usually peaks at C_3 or C_4 (up to 90%) after which the olefinity decreases continuously; the waxes being essentially paraffinic (65).

Although the selectivity can be varied over wide ranges, the commercial constraints of feed gas composition, pressure, temperature and reactor type, determine to a large extent the straight run product distribution. The South African fuel market demands a gasoline to diesel ratio of about 1:1. However this ratio for the FFB/CFB system is 3:1. Thus to increase the final diesel fuel yield, Sasol employs two secondary processes, namely, olefin oligomerization (currently the dominant process) and wax cracking. Recently crystalline silica alumina catalysts (e.g. ZSM-5 types) have been shown to be particularly successful in converting C_3–C_5 olefins to liquid fuels. The wax produced in the fixed bed (low temperature) reactor can be cracked to extinction at relatively mild conditions to yield 80% diesel fuel and 15% gasoline (63).

1.5   Cobalt in F–T catalyst development

Since this thesis describes the research and development of *cobalt–based* catalysts, a review of the metal with respect to some of its properties, and in particular, previous and current research on cobalt F–T catalysts, would be appropriate.

1.5.1   Cobalt – some facts and uses

Cobalt is the 30th most abundant element on earth and comprises approximately 0.0025% of the earth's crust (68). It occurs in mineral form as arsinides, sulfides, and oxides; trace amounts are also found in other minerals containing nickel and iron, as substitute ions (69). The worlds largest cobalt reserves are in Zaire, Zambia, Morocco, Canada and Australia. Together the ores of these countries contain well over one–half of the world cobalt supply, the richest deposits being found in Zaire and Zambia. Smaller but commercially practical ore bodies also exist in the U.S.S.R., Finland, Uganda, South Africa, and the Philippines (70).

Chemically, cobalt resembles iron and nickel, which are its neighbours in the Periodic Table, and constitute the iron group. In nearly all of its compounds it exhibits a valence of +2 or +3. Cobalt has a formal valence of +1 only in a few complex nitrosyl and carbonyl complexes. Oxidation states of 0 and –1 are also found in certain Co complexes such as $Co_2(CO)_8$ and $Co(CO_4)^-$, respectively (71). Tetravalent cobalt exists solely in fluoride complexes and in one unusual series of binuclear peroxo compounds (70,71). The amines of cobalt were discovered by Werner (69) in 1890, and served as the basis for the formulation of the coordination theory in inorganic chemistry. The innumerable coordination compounds of cobalt(III) exhibit substantial   diversity   in   their   coordination   number,   geometric

structure, and stability, and in many aspects of their chemistry [the most common coordination number is 6] (71).

Cobalt and cobalt compounds have expanded from use as coloring agents in glasses and ground coat frits in pottery, to drying agents in paints and lacquers, and to their use in animal and human nutrients, electroplating materials, high–temperature alloys, high speed tools, magnetic alloys, alloys used in prosthetics, radiology, air–deodorizing filters, electric contacts, thermisters, and explosives (cobalt amine azides). It is also an effective catalyst or catalyst component in many homogeneous and heterogeneous processes (70). The catalytic reactions include hydrodesulfurization of petroleum, gasoline reforming, hydroformylation, F–T synthesis, hydrogenation and dehydrogenation, fluorination of hydrocarbons, polymerization (such as butadiene etc.), oxidation (xylenes to toluic acid, oxidation of hydrogen cyanide in gas masks or of CO in automobile exhausts), dehydration, CS_2 production, H_2S production, nitrile synthesis, amination of olefins, and reductions with borohydrides. Cobalt molybdates "CoMoX" which comprise of mixed oxides (Co–Mo, Ni–Co–Mo), are used in petroleum hydrogenation, desulfurization, denitrification, and hydrocracking (70).

1.5.2 Cobalt Fischer–Tropsch catalysts

From the time of the initial report by Sabatier and Senderens (1902) on the hydrogenation of carbon monoxide until the end of World War II, cobalt was the preferred metal for F–T catalysts. Cobalt catalysts gave the highest product yields and the longest lifetimes. Research at Ruhrchemie led to the development of the precipitated Co:ThO$_2$:MgO:kieselguhr (100:5:8:200) composition, which became the standard catalyst for commercial use in the German F–T reactors during the war. The high cost of

cobalt and the work on medium—pressure synthesis with iron catalysts however, led to the replacement of cobalt catalysts by the end of the war. Practically no further research was done on cobalt catalysts until the resurgence of interest in F—T synthesis during the 1970's. (This early work on cobalt catalysts has previously been discussed in Section 1.3.1.)

One of the main problems in F—T catalysis is a systematic description of catalytic systems that allows a splitting of global experimental results into a discrete set of catalytic effects (as previously mentioned — Section 1.3). Thus no attempt will be made to catagorise different research on cobalt catalysts here. Instead, this review will follow the progression, diversity and development of these catalysts from the late 1970's until the present time.

Significant variations in CO hydrogenation activities of supported cobalt catalysts with changes in pretreatment, dispersion, metal concentration, and promoter content have been observed by a number of laboratories. The origin of these variations is a matter of considerable interest and has stimulated a number of recent investigations. Dent and Lin (72) tested many different cobalt supported/promoted catalysts in a Berty reactor. They found the most active catalysts to be Co—Cr_2O_3—kieselguhr and Co—ZrO_2—kieselguhr. However, Co—MnO—alumina—K_2O catalysts seemed best for producing olefins. Borghard et al. (73) tested a Harshaw, cobalt on silica (100 Co:94 SiO_2) catalyst, which produced hydrocarbon products consisting of 90% gas and 10% liquid. For this catalyst a H_2/CO feed ratio of 2:1 gave better yields than 1:1 or 3:1 CO/H_2 feed ratios. Vanhove et al. (74) studied the relationship between pore size and metal crystallite dimensions and the length of the growing hydrocarbon chain. 2% Co on alumina catalysts

with different pore sizes were prepared by impregnation with solutions of $Co_2(CO)_8$. Products from the sample, with a mean pore radius of 300Å, had a maximum in the carbon-number-distribution at C_{18}, while a catalyst preparation with a mean pore radius of 65Å had a maximum at C_9. Catalysts with larger amounts of Co (5%) gave normal carbon number distributions. Further studies by Vanhove et al. (75), again showed catalysts prepared by the low temperature thermal treatment of dicobalt octocarbonyl impregnated supports (Al, Si-Al), to show high selectivities for restrained hydrocarbon cuts (low metal loadings). The chain length of the hydrocarbons was clearly related to the mean pore diameter and to the design of the supports.

Zowtiak et al. (76) used TPD to investigate H_2 adsorption/desorption on a series of cobalt catalysts. Experiments in which the adsorption temperature was varied revealed that H_2 adsorption on cobalt is an activated process, and is a function of catalyst support and metal loading. Desorption from unsupported, silica and alumina-supported catalysts involved one major peak in the TPD spectra, suggesting the presence of only one type of site. The titania- and carbon-supported catalysts, on the other hand, displayed multiple desorption peaks in the TPD spectra, providing evidence of a more complex distribution of surface sites, possibly as a result of SMSI. Reuel and Bartholomew (77,78) measured the specific activities and selectivities (using a single-pass differential reactor at low conversion) on unsupported Co, and Co supported on alumina, silica, titania, C, and magnesia. Their results indicated that specific activity and selectivity of Co varied with support, dispersion, metal loading and preparation method. The order of decreasing CO hydrogenation activity (1 atm, 225°C, 3% Co) was observed to be: Co/TiO_2, Co/SiO_2, Co/Al_2O_3, Co/C and Co/MnO. Specific activity was found to decrease with increasing dispersion. For Co/Al_2O_3 the activity and selectivity

for higher molecular weight hydrocarbons increased significantly with increased Co loading. Gopalakrishnan and Viswanathan (79) investigated, by TPD and IR techniques, the individual CO adsorption and co-adsorption of CO and H_2 on Co with additions of kieselguhr and thoria, and compared these studies with those on polycrystalline cobalt. Their studies showed kieselguhr and thoria to act as surface sites for H_2 adsorption by a spillover mechanism, thereby affecting the net adsorption properties of CO on the Co surface. They also found a considerable interaction between CO and H_2 on the promoted Co, but not on the polycrystalline Co surface (80). Further XPS, TPR and H_2 and CO adsorption studies (81) showed the kieselguhr to decrease the extent of Co reduction due to the stabilization of CoO by the support. However the presence of ThO_2 was found to increase the extent of reduction (by probably restricting the migration of kieselguhr). The CO/Co and H/Co adsorption ratios were found to decrease with decreasing Co loadings, indicating the possible interaction between Co and kieselguhr.

The kinetic behaviour in CO hydrogenation of partially reduced Co/Al_2O_3 catalysts, was studied by Moon et al. (82). Typical changes in catalytic properties observed with decreased catalyst reduction were, (i) suppression of H_2, and (ii) increased product selectivity for olefinic hydrocarbons. There was also an indication that the specific activity of methanation was enhanced by poor catalyst reduction. Their results thus suggested that unreduced cobalt oxide on the catalyst surface is not simply inert, but interacts with the reduced cobalt metal to modify overall catalytic properties. They then concluded that the extent of catalyst reduction is an important variable in determining the kinetic behaviour of supported Co catalysts. Lee and Bartholomew (83) studied CO hydrogenation over four (1, 3, 10 and 15 wt %) Co/Al_2O_3 catalysts using the technique of temperature

is reviewed in Chapter ? However other approaches to produce modifications of the kinetic behaviour of the F-T reaction, for example by alternative methods of preparation, encapsulation of Co active metal in the frame of zeolites or in porous carriers have been reported. The use of bimetallic Co catalysts and different reactor types, have also been investigated. Blanchard (87) has described the simultaneous formation of the active phase and the support using a [Co(acac)$_2$] precursor. This is reduced with alkyl aluminium (AℓEt$_3$) under conditions such that after the preparation, the active metallic phase is totally (or partially) reduced and aluminium species are transformed into alumina (the support). This procedure allows for a high dispersion of the active phase and also allows control of the global oxidation state of the catalyst. Meier et al. (88) investigated the preparation of Co catalysts using the solvated metal atom deposition technique, preparing Co on ( )a with less than 5 wt % of the metal. This alternative method of catalyst preparation led to systems that were considerably more active than catalysts with the same metal loading prepared by incipient impregnation procedures. These catalysts showed activity without H$_2$ pretreatment and at metal loadings which are considered low for cobalt F-T catalysts.

Frankel and Gates (89) investigated zeolite-encapsulated cobalt-cluster type systems as shape selective F-T catalysts. These catalysts offer the advantage of high selectivity and stability under conditions o? commercial significance. The catalysts were prepared by the reduction of Co^{3+} ions exchanged into A-type zeolite, giving propylene as the only detectable hydrocarbon product; (151°C, 1% CO conversion) and Y-type zeolite, giving n-butane as the main product with almost no C$_2$ or C$_3$ hydrocarbons (182°C, ≥ 15% CO conversion). Ishihara et al. (90) studied SiO$_2$ supported bimetallic catalysts of Fe-Co, Co-Ni, Ni-Fe for CO hydrogenation. These catalysts

were shown to have activities greater than those for the monometal catalysts, and product distributions were shifted to higher hydrocarbons by alloying of the metals. The Ni–Co alloys were the most selective for the formation of higher hydrocarbons, as well as the most active for CO conversion. Fornasari et al. (91) investigated the nature and catalytic activity, in the F–T synthesis, of Co, Cu, Zn, and Cr mixed oxides, for a wide range of compositions. A maximum in activity was obtained for catalysts containing comparable amounts of Co and Cu. This high activity was attributed to a synergic effect existing between Co and Cu. Barrault and Guilleminot (92) studied Co–lanthanum and Co–cerium carbon supported catalysts to identify the effects of rare earth elements on the F–T reaction. It was observed that these promoters gave rise t   crease in specific activity and turnover frequency, and the s....   ction increased from 4 to 40% (this fraction being essentially ....

Pannell et al. (93) presented carbon-n. .ber distributions for hydrocarbons from the use of Co catalysts in a Berty reactor (differential reactor with a large internal cycle) Maxima in carbon number distributions occurred at carbon numbers of 5 and 6. The ratio of olefins to paraffins and the average molecular weight decreased, with increasing H_2/CO feed (other conditions constant). Yokota and Fujimoto (94) carried out F–T synthesis over SiO_2 supported cobalt catalysts, conducted in a supercritical fluid medium using a fixed bed reactor. The rate of reaction was observed to be slightly lower than those in the gas phase reaction. However the removal of reaction heat and waxy product from the catalyst surface were found to be much more effective than those in the gas phase reaction. The supercritical phase reaction was also observed to produce a greater proportion of higher hydrocarbons (> C_{25}). than reactions in either the liquid or gas phase. Withers et al. (95) investigated the preparation, characterization and

involved in the catalytic action of our Co/MnO catalysts (and related systems viz. Co_3O_4, Co_3O_4/Al_2O_3, and $CoCr_2O_4$). This was attempted by following phase transformations *in situ* (using a DSC/XRD analytical combination), during the activation and use of such systems (Chapter 5).

Different methods of catalyst preparation have long been known to influence moderate shifts in the broad F–T product distributions. A novel F–T synthesis catalyst involving an inhomogeneously cobalt impregnated system, has been developed by Shell. The patent claims that if 90% of the Co is situated in the outer volumes of the support, then the selectivity toward C_5 can be enhanced. It was our aim to investigate the possibility of producing an active analogue of such a catalyst, using an electroless deposition technique. This technique is a totally novel method of catalyst preparation (Chapter 6).

outside of the particles, is introduced. This is determined with preliminary tests on aliquot samples of water. Our Co/MnO catalysts were promoted with different levels of K [K_2CO_3] and Cr [$Cr(NO_3)_3$] respectively, in the very same manner as detailed above. Promotion was with respect to the amount of active metal component present in the catalyst i.e. mass of Co, previously determined by AAS. Uniformity of promoters within the catalyst at this stage was not considered, since segregation from the bulk to the surface was observed to occur (from XPS studies, see Chapters 3 and 4) even during calcination for both promoters.

2.1.3 Catalyst pelleting and calcination

After promotion, the catalyst (in the form of a fine powder) was pressed into non uniform discs of ~2 mm thickness between two sheets of wax paper using a portable hydrolic press. The discs were then sieved and pelleted into 0.5 – 1.0 mm particles. The catalyst particles were then loaded into a muffle furnace and calcined in air at 500°C for 24 hours.

2.1.4 Analysis of metal content

The bulk metal composition of the Co/MnO catalysts used in this study was determined by atomic absorption spectroscopy. This was achieved by dissolving ~0.1 g of catalyst in aqua regia [3 HCl:1HNO$_3$], (~10 mℓ with boiling for 5 minutes) and diluting with distilled water by making all samples up to 1ℓ. The concentration of the metal components (on a molar basis) was then determined by AAS, using standard solutions as calibrants.

Construction of the respective reactor systems was from $1/4"$ stainless steel tubing and from stainless steel Swagelock connections (supplied by Johannesburg Valve and Fitting, South Africa). Premixed synthesis gas (typically CO 49.5%, H_2 49.5%, N_2 1% v/v — for Chapter 3 and CO 33.5%, H_2 66.5% v/v — for Chapter 4) and other reagent gases e.g. hydrogen (for reduction), were fed to the combined preheater/reactor at flow rates controlled using Whitey fine control needle valves, just upstream from the respective flow indicators (Aalburg Instruments and Control Inc., USA — maximum pressure 1350 kPa). The pressure was controlled using a back pressure regulator (GO BP3, with Cv flow coefficient modified to 0.003, pressure range 0 — 1725 kPa) located downstream of the reactor and condensors. The reactors were heated by means of electronic heating jackets (supplied by Heating Element Engineering, South Africa), and the temperature regulated by J-type thermocouples and thyristor controllers. Another thermocouple was inserted into the catalyst bed for accurate temperature measurements during the reaction. The locations of the respective thermocouples are shown in Figure 2.2 and 2.3. For all data quoted temperature control was better than $\pm$ 0.5°C, and for all conditions no exotherms were observed in the catalyst bed. All temperature control equipment was supplied by Temperature Controls (South Africa).

2.3   PRODUCT ANALYSIS

Gaseous products from the high pressure reactors were fed into an automated stream selection valve (SF8P, VICI AG, Valco), enabling the analysis of product gases from a *selected* reactor by an on-line dual detector (flame ionization detector — FID and thermal conductivity detector — TCD) Varian 3300 gas chromatograph. Gases from the selected reactor were injected (1 mℓ sample loop) into the respective separating columns

performance of cobalt carbonyl cluster type catalysts for use in slurry–phase F–T synthesis. A $Co_2(CO)_8/Zr(OPr)_4/SiO_2$ catalyst (3.5% Co, 6.6% Zr) was found not only to be the most active system in their F–T slurry system, but also gave the best liquid fuel selectivity (selectivities were found to correlate with S–F predictions).

The phase–out of lead containing anti–knock compounds from motor fuels is causing refiners to look for alternative metho   to enhance octane ratings. One approach being explored is the addition of oxygenates, such as alcohols or ethers as gasoline blending agents. The potential value of this market has led to renewed interest in the manufacture of methanol and higher alcohols via synthesis gas derived from coal or natural gas (96). Catalysts that have been studied for this reaction include a host of cobalt based systems. Pan *et al.* (97) produced methanol and higher alcohols during CO hydrogenation using $Cu/Co/ZnO/Al_2O_3/K$ catalysts. The overall yield of higher alcohols was observed to increase linearly with CO conversion, with the individual higher alcohols obeying a S–F distribution through $n-C_6H_{13}OH$. Takeuchi *et al.* (98) found C_2–O compounds to be effectivly produced by the hydrogenation of CO over cobalt catalysts doubly modified with Ru and alkali earths. Ru was observed to increase the catalytic activity by promoting the reduction of Co, with the alkali earths improving the selectivity of C_2–O, by controlling the oxidation states of the cobalt catalysts.

Recently there has been a considerable amount of commercial interest into the use of Co as the active component in F–T catalysts, despite the fact that Co is reported to be 230 times the cost of the current

commercial Fe catalyst [the price of Fe taken from the current price of millscale which is a reject byproduct in steel production] (63). In particular, recent claims have been made by Shell Internationale Research (36,37,99) on novel F–T catalysts showing better selectivities than conventional F–T catalysts. These claims deal with specific preparation techniques leading to catalysts that show a greater selectivity toward C_5^+ (a more detailed description of these catalysts is given in Chapter 6). These novel catalysts are to be used in the Shell Middle Distillate Synthesis Process (SMDS) at the new facilities to be constructed in Malaysia. Besides the Shell patents there have been further patent claims by the Exxon Research and Engineering Company, on different processes for F–T synthesis over cobalt based catalysts (100,101). In particular these latter patents describe the use of silicon oxide–promoted cobalt catalysts on titania supports for converting synthesis gas to heavy hydrocarbons (102).

1.6   Aims of this thesis

The *co–production* of high value commodity chemicals is the key to the financial success of today's synthetic fuel programmes. The most important of these high value products are short chain olefins (ethylene and propylene), and F–T waxes. The short chain olefins provide the basis for an important organic chemicals industry. Already Sasol is the only producer of ethylene in South Africa, and has recently announced a propylene recovery and polypropylene plant with a 120 000 ton capacity. This is expected to come on–stream in the very near future. Sasol F–T waxes, which have a wide variety of end uses, are marketed on a world–wide basis, and are currently sold at 4 times the price of liquid fuels. Waxes may also be hydrocracked to good quality diesel (80%) and gasoline (15%).

A limitation of Fischer–Tropsch technology is the limited selectivity to the above–mentioned high value desired products. There is an interdependence of selectivities and product distribution are generally very broad. Several approaches are currently being pursued in an effort to develop a highly selective synthesis within the constraints of the Schulz–Flory distribution law. One approach is the development of improved catalysts, or modification (by the incorporation of promoters) of existing catalysts, which are tailored to enhance the selectivity to a single product or narrow distribution of products. This type of endeavor is the basis of this thesis.

Initial studies involved the chemical modification of co–precipitated Co/MnO catalysts (originally developed by co–workers) for the hydrogenation of CO. The objective was to achieve high selectivity reactions on Co/MnO; (i) with the incorporation of potassium promoters, to produce short chain olefins, and (ii) with the incorporation of chromium promoters, to produce high molecular weight hydrocarbons. The addition of potassium promoters to supported group VIII metals in F–T synthesis has long been known to affect the performance of such catalysts in a variety of ways. However the use of chromium, specifically as a promoter in enhancing the selectivity toward heavy hydrocarbon formation, has not been previously reported. The effects of operating conditions i.e. T, P, and GHSV, on both the K and Cr promoted Co/MnO systems on catalytic performance, was also investigated. (Chapter 3 and Chapter 4).

It was considered important to investigate the structural changes occurring during calcination, reduction and under synthesis conditions of these unpromoted Co/MnO catalysts, since certain bulk changes could possibly be related to the final activity and selectivity of the working catalyst. An investigation was thus made to clarify some of the mechanisms

CHAPTER TWO

EXPERIMENTAL METHODS AND APPARATUS

2.1 CATALYST PREPARATION

2.1.1 Co-precipitation

The preparation of catalysts by co-precipitation of the salts of the constituent metals, usually produces an intimate mixing of the respective metal ions (103). The co-precipitation of cobalt and manganese nitrate salts from an ammoniacal solution was developed by co-workers (82,85), after consideration of several variations on the method outlined by Maiti et al. (104). This procedure facilitated the preparation of homogeneous reproducable catalysts on a small scale (~15 g per batch), under controlled conditions (temperature = 70°C, pH = 8.3). [Larger amounts (~100 g) of catalyst were prepared at the Chemical Engineering Department, University of Potchefstroom, Vaal Campus (South Africa) by a continuous co-precipitation method, based on the method by Deckwer et al. (105).] The small scale co-precipitation procedure is outlined in Appendix 1.

2.1.2 Promotion by the "incipient wetness" technique

"Incipient wetness" impregnation is the simplest and most direct method of deposition. The object is to fill the pores of the catalyst with an aqueous solution of promoter metal salt of calculated concentration to give the correct loading. The support is then heated in vacuo to remove pore moisture. This is not essential but speeds diffusion of the solute into the pores (106). Solution, in an amount just sufficient to fill the pores and wet the

2.2   CATALYST TESTING

2.1.1   Pretreatment and start-up procedures

Calcined catalysts (2 g) were loaded into fixed-bed laboratory microreactors (detailed in Section 2.2.2) and reduced *in situ* under H_2 (GHSV = 280 h^{-1}) at 400°C for 16 hours. The catalysts were subsequently cooled to 150°C (under H_2), afterwhich hydrogen was replaced by premixed CO/H_2 gas [1:1 by vol. (Chapter 3) and 1:2 vol. (Chapter 4)], obtained from Afrox, Special Gases Division (South Africa). Reactor operating conditions of pressure, temperature and gas hourly space velocity, were then brought up to the selected conditions within 30 minutes of start up. Steady state conditions were observed to have been achieved approximately 120 hours after start up, after which satisfactory mass balances (of ~150 hours) were obtained for all data presented.

2.2.2   High pressure microreactor system

CO hydrogenation activity and selectivity experiments were carried out using a bank of three fixed-bed laboratory microreactors, as illustrated in Figures 2.2 and 2.3 respectively. This enabled the testing of catalysts under approximately identical experimental conditions. The reactor system of Figure 2.2 was used in the investigation of the influence of K promoters on lower hydrocarbon olefin selectivity, as discussed in Chapter 3. This reactor system was later modified for heavy hydrocarbon (wax) handling capabilities, (Figure 2.3) in the investigation of Cr promoters for increased wax selectivities, as discussed in Chapter 4. The reactor housing, reactor insert and dual seal assembly, are detailed in Appendix 2. The room temperature condensor as in Figure 2.2, and the combination room temperature (~25°C) and hot condensor (~120°C), as in Figure 2.3, and are further discussed in Appendix 3.
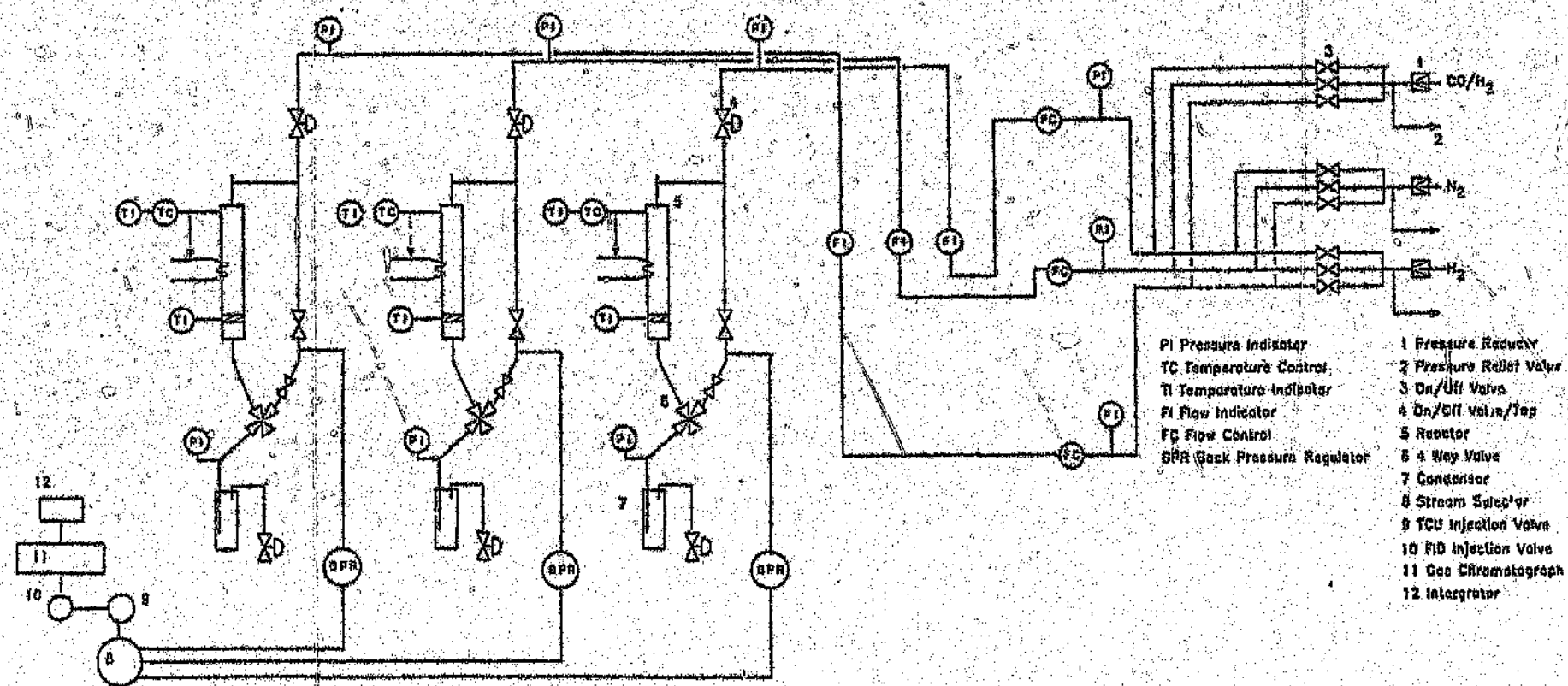
Figure 2.2: Schematic representation of the reactor system as used in the investigations of Chapter 3.

PI Pressure Indicator
TC Temperature Control
TI Temperature Indicator
FI Flow Indicator
FC Flow Control
BPR Back Pressure Regulator

1 Pressure Reducer
2 Pressure Relief Valve
3 On/Off Valve
4 On/Off Valve/Tap
5 Reactor
6 4 Way Valve
7 Condenser
8 Stream Selector
9 TCU Injection Valve
10 FID Injection Valve
11 Gas Chromatograph
12 Integrator
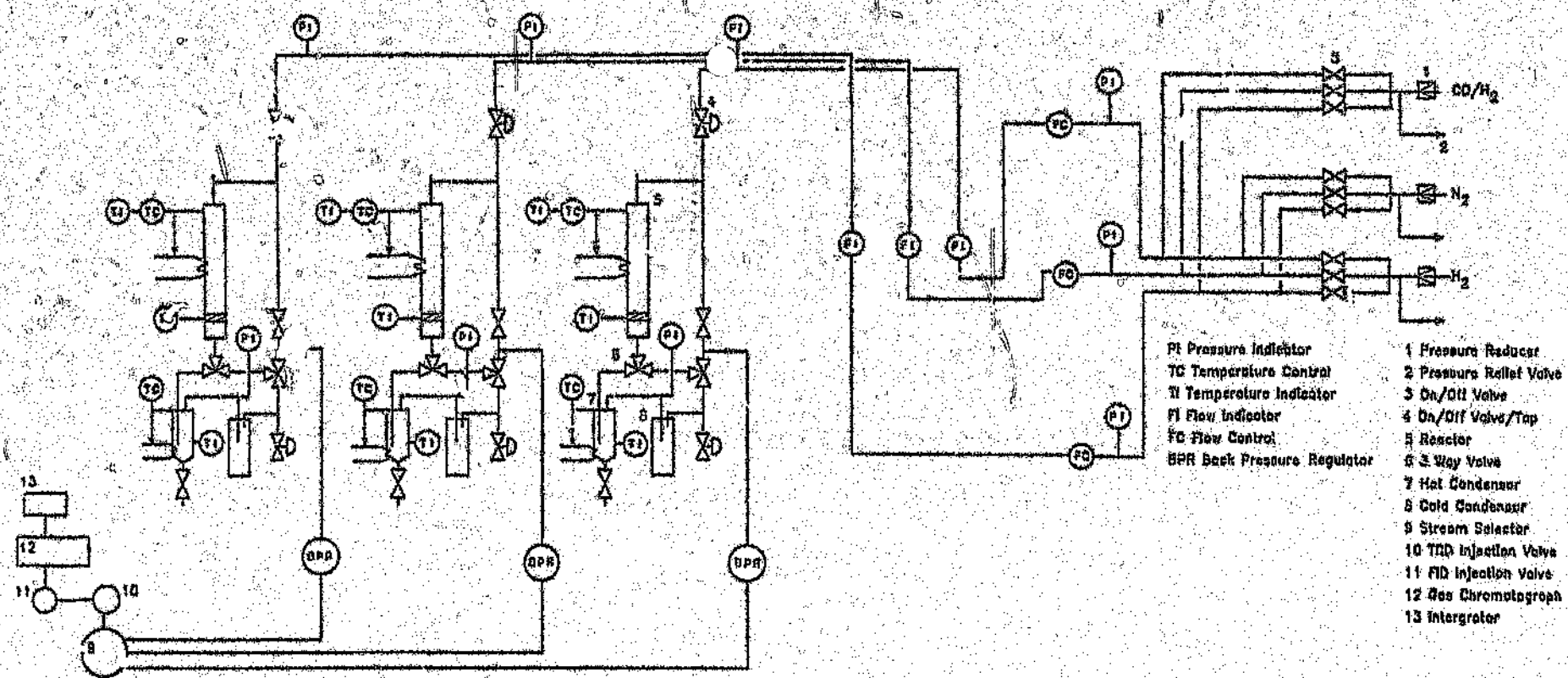
Figure 2.3: Schematic representation of the reactor system as used in the investigations of Chapter 4.

Porapak Q and Carbosphere columns) of the gas chromotograph by means of automated valves (Valco, 6 and 10 port valves). An on-line Varian 4270 integrater equipped with an external events module was used to fully automate this gas sampling procedure, and also allowed for the continuous sampling of each reactor in the multi-reactor system.

Gaseous hydrocarbons (C_1-C_{12}) were separated with a temperature programmed 2m x 1/8" stainless steel Poropak Q column and FID detector combination (using N_2 as a carrier gas). Separation was adequate for C_1, C_2 and C_3 olefins and paraffins, however hydrocarbons greater than C_4 could only be separated by carbon number only. The fixed gases i.e. CO, CO_2, N_2 and H_2 were separated with a temperature programmed 2m x 1/8" stainless steel Carbosphere column and TCD detector combination (using Ar as a carrier gas). The automatic on-column injection valve for this column also enabled a back-flushing facility, which was automatically triggered after the last fixed gas had been eluted. This procedure prevented the fouling of the column with the hydrocarbon products, and consequently lengthened the efficiency of the column considerably.

The condensed products trapped within the various knock-out systems, consisting of light to medium wax fractions and an oxygenated aqueous fraction, were analysed by an off-line Varian 3300 FID (and Varian 4290 integrator) equipped with a temperature programmed 30 meter capillary column (DB1 – 30N J+W Scientific Inc.) with a split flow facility. Separation of C_5^+ hydrocarbons and C_1^+ primary alcohols was adequate. The water content which was excluded from all final selectivity data, was quantified by comparison with alcohol standard mixtures. (The Varian gas chromatographs, integrators and Valco automatic valve were supplied by

SMM Instrumentation, South Africa.)

2.4 CALCULATION OF CONVERSION

The effect of conversion of carbon monoxide was used as an indication of catalyst activity. The equation used to calculate the percentage CO conversion is given below

$$\% \text{ CO conversion} = \frac{\text{moles CO}_{in} - \text{moles CO}_{out}}{\text{moles CO}_{in}} \times \frac{100}{1}$$

2.5 BULK AND SURFACE CHARACTERIZATION

2.5.1 Bulk characterization

(a) XRD analysis

X-ray diffraction measurements were carried out on a Rigaku Geigerflex D/max IIIA computer controlled wide angle diffractometer that was equipped with a high temperature X-ray attachment (HTA) for the in situ studies of Chapter 5. (These studies were performed at MATTEK, CJIR, Pretoria, South Africa). The HTA attachment is an airtight chamber (comprised of a removable top and stationary bottom dome) designed to maintain a specimen at high temperature and record its diffracted X-rays automatically under respective high temperature either in a vacuum, or in different atmospheres. The HTA furnace is made of an alumina framework, with Kanthell wire as a heating element, used in combination with a program temperature controller (Ero Electronic MPL programme and Athene 91Z zero voltage switching power controller) which allowed for the specimen temperature to be controlled precisely. A type R thermocouple placed less than 1 mm from

the sample surface was used for temperature measurement. Photos of the HTA showing the airtight chamber, and with the top dome removed showing the alumina furnace, are presented in Figures 2.7 and 2.8, respectively. The diffractometer operating conditions are given in Table 2.1

TABLE 2.1: X-ray diffractometer operating conditions

X-ray tube:

radiation	CuKα
voltage	45kV
current	30 mA
Divergence slit	1°
Receiving slit	0.3 mm
Scatter Slit	1°
Filter	Ni (part of heat shielding)

Step scan:

step size	0.02° 2Θ
time step	1 or 2 sec
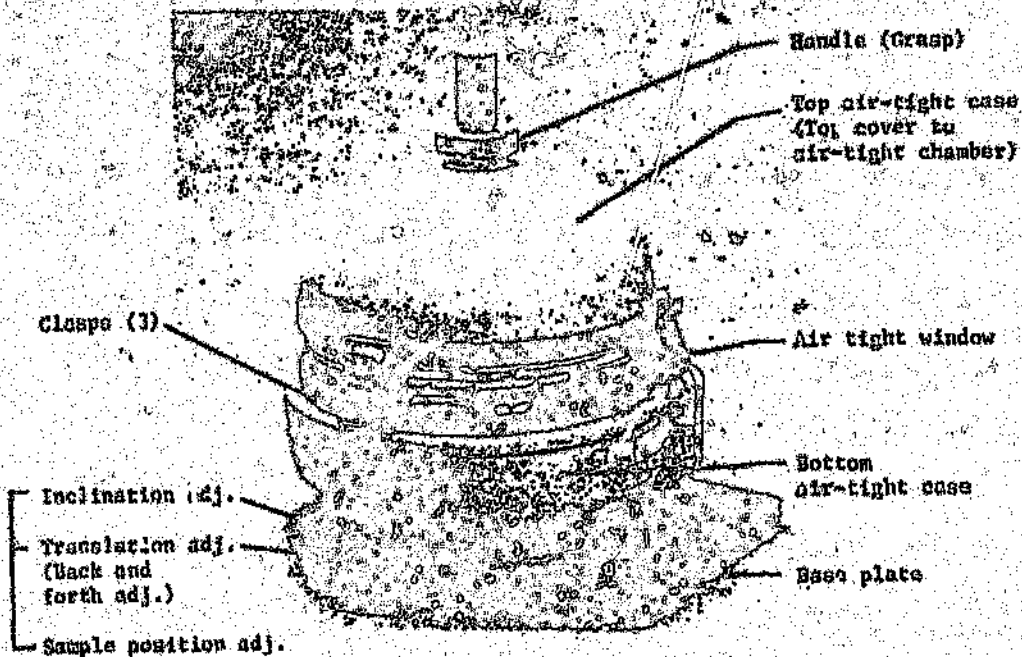
Figure 2.7: Photograph of the airtight HTA chamber with removable top and stationary bottom domes.
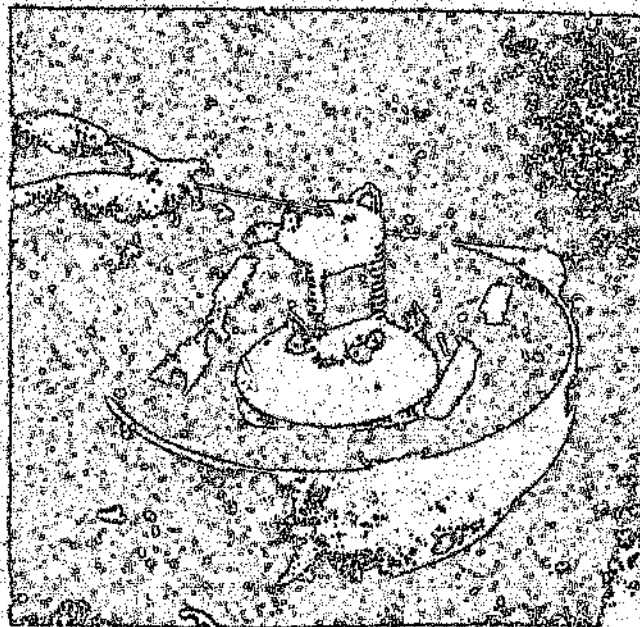
Figure 2.8: Photograph of the HTA chamber with the top dome removed, showing the wedge shaped heating furnace.

A ceramic heat shielding drum was used to stabilize furnace temperature fluctuations, and to shield the outer dome from excessive heat while allowing continuous flow of gas across the specimen. X-rays entered and exited the heat shielding drum via 0.006 mm Ni foil windows (which also filtered out K_β radiation), and through windows of the top dome of 0.03 mm $A\ell$ foil. The top dome of the HTA chamber was water cooled to protect the rubber sealing gaskets from overheating. A schematic illustration of the HTA chamber and goniometer arrangement are given in Figure 2.9.

The samples (approximately 0.7 g) were compacted onto a platinum mesh backing by means of a glass slide pressed by hand. This
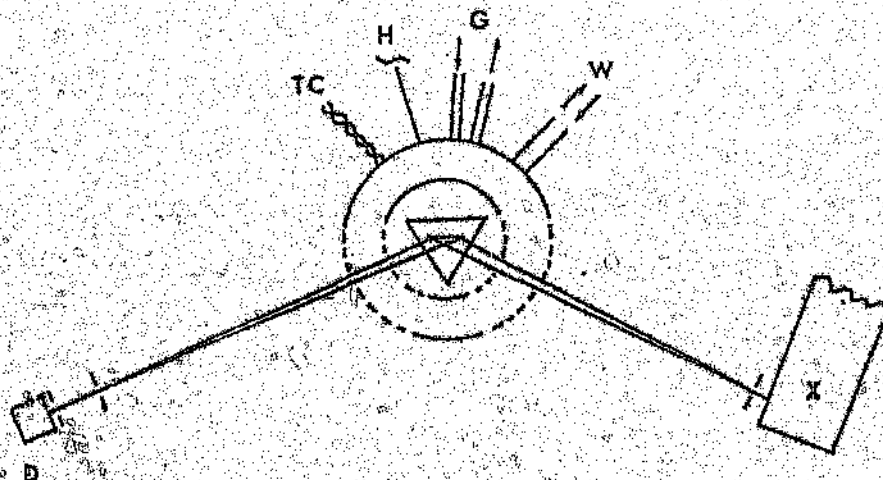
D=detector; TC=thermocouple; H=heater power;
G=gas; W=cooling water; X=x-ray tube.

Figure 2.9: Schematic illustration of goniometer with high temperature attachment.

part of the specimen loading procedure is critical, since the platinum mesh is mounted vertically inside the HTA furnace (horizontal goniometer), and the sample easily parts with the mesh during temperature cycling if not mounted properly. Alignment of the specimen was accomplished by removing the scintillator detector from the goniometer arm and shining a collimated beam of light via the scatter and receiving slits onto the specimen to check sample tilt with respect to the $\Theta/2\Theta$ axis.

For this investigation a gas flow ranging from 10 to 60 mℓ/min at just above atmospheric pressure was employed. The gas flow set up is depicted in Figure 2.10. The flow meters used were Aalborg FM 042–15

and FM 062-01 for H_2 and CO, respectively. Both flow meters were calibrated against a bubble flow meter at each change of flow rate. Gas flowed freely through the HTA chamber and then vented to the outside. A suction fan was installed in the radiation safety enclosure of the diffractometer, to prevent a possible build-up of dangerous gases in the laboratory due to leaks especially from the HTA chamber (not designed for over pressures).
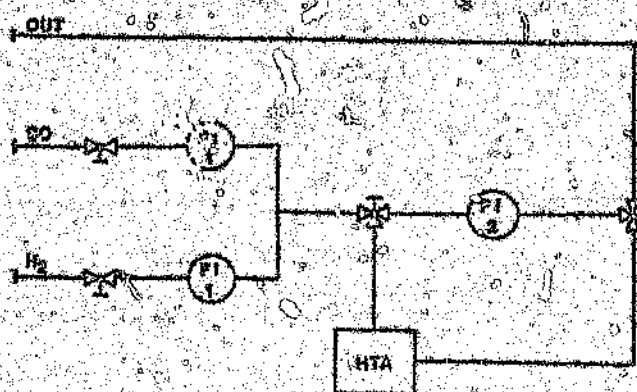
Figure 2.10: Schematic illustration of the gas manifold system (FI – flow control and indicator).

The goniometer was controlled and data captured by an Olivetti M24 through a RS232C serial port. The raw data needed quite extensive processing before the necessary information could be extracted from it. Cobalt fluoresces strongly in Cu radiation and in the absence of a monochromator a very high background was experienced. This problem was compounded by the effect of the irradiated area being wider than the specimen at low 2-thetas (as a result of the fairly wide

divergence slit employed in an effort to increase peak intensities). However a background correction routine managed to linearize and substract the baseline very well at all angles above 10° 2Θ. To avoid impractically long diffraction runs, the counting time per step was limited to a maximum of 2 seconds. The signal to noise ratio obtained with a 2 sec/step proved to be adequate after heavy smoothing of the spectrum. The identification of XRD patterns was aided by computer controlled peak search routines.

(b) Thermal analysis

Differential Scanning Calorimetry (DSC) was performed on a Dupont 910 DSC linked to a 9900 Computer/Thermal analyser used to control and track the progress of the experiments, collect data, and print results. The basic system consisted of a computer, a GPIB interface, a module interface (MI), at least one analysis module, and a plotter. The four basic functional components of the apparatus are illustrated in Figure 2.11.
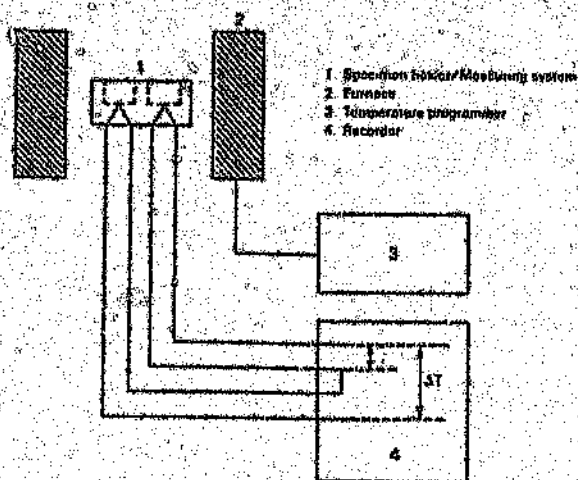
Figure 2.11:   Basic components of the Thermal Analyser.

The 910 DSC module was used to measure the differential power (heat input) necessary to keep the sample and reference isothermal as the temperature was changed. This DSC cell also allowed for the thermal analyses to be performed under different atmospheres with the use of a gas manifold system. Gas flow rates were typically of 50 mℓ min^{-1}, which was adequate in continually flushing the DSC cell, and then vented to the outside.

2.5.2   Surface characterisation

(a)   XPS analysis

X-ray Photoelectron Spectroscopic (XPS) measurements were performed at MICONTEK, CSIR (Pretoria, South Africa), with the use of a Vacuum Generators ESCALAB mk-II, equipped with a VG SIMS Lab (base pressure 1 x 10^{-11} mbar) incorporating a 45° hemispherical sector electron analyser.

(b)   Surface area measurements

Surface area measurements of the catalysts were performed using the N$_2$ adsorption method (and in some ca.. Krypton was also used) with a Micromeretics High Speed Surface Area Analyser, Model ASAP 2000. These analyses were performed by operators at Sastech, Sasol 1 (Sasolburg, South Africa). Certain analyses were also performed at MATTEK, CSIR (Pretoria, South Africa) using a Micromeretics High Speed Surface Area Analyser, Model 2200.

(c)   Scanning Electron Microscopy (SEM)

SEM measurements were performed at MATTEK, CSIR (Pretoria, South Africa) using a HISI SX-3/E equipped with a LINK analytical energy dispersive analyser.

CHAPTER THREE

THE INFLUENCE OF POTASSIUM PROMOTERS IN THE HYDROGENATION OF CARBON MONOXIDE USING COBALT MANGANESE OXIDE CATALYSTS

3.1   INTRODUCTION

It is generally believed that the hydrocarbon chain growth of classical F-T synthesis is a polymerization process giving a broad product distribution from methane to waxes, (107). Unsaturated hydrocarbons, especially those with two to four carbon atoms, constitute a large proportion of the feed stocks for the petrochemical industry; and thus direct synthesis of these lower olefins from synthesis gas using modified F-T catalyst is of great economic interest.

Moderate shifts in the broad product distributions may be obtained within the constraints of the Schulz-Flory distribution law by varying reaction conditions (6,10). However, to obtain high selectivity to a single product or narrow distribution of products requires the development of improved catalysts. One approach is the chemical modification of conventional F-T catalysts by the incorporation of promoters and other additives. The term *promoter* is difficult to define since there are many types of promoters and it is often difficult to make a distinction between the promoter, the active catalytic component and the carrier. An appropriate

definition seems to be: "A promoter is a substance added to a catalyst in a small amount, which by itself has little or no activity, but which imparts either better activity, stability or selectivity for the desired reaction than is realized without it" (108). It is likely to be difficult to achieve a high selectivity to a single product in this way; however, recent investigations using manganese oxide, in particular Fe/MnO (104,109–113), led to the formation of low olefins (C_2–C_4) in high yields. In general, for these Fe/MnO catalysts, high olefin selectivities are only achieved under mild reaction conditions and are not stable at realistic CO conversions or reaction conditions (114). Also the propensity of the Fe to form carbides (Fe_5C_2) in the presence of CO (115,116), causes a deterioration in catalyst selectivity. It would thus seem that Fe would be an unsuitable candidate on which to base an improved catalyst design.

Studies involving the promotion of cobalt by manganese oxide has been investigated at low metal loadings (<10%). For example, Barrault et al. (117) has studied these catalysts on various supports, such as keiselguhr and alumina. Varma et al. (86) have studied the performances of MnO supported Co and Ni catalysts, and with varying compositions. Although these catalysts resulted in improved selectivity, particularly to propene, these systems were demonstrated not to be stable for any appreciable time scale. The modification of cobalt with MnO has also been investigated by co–workers (84,85,118) in our research group, who have shown that a Co/MnO catalyst with Co:Mn mole ratio of unity, can give decreased methane yields together with enhanced propene formation, and showed stable catalytic performance of up to 1000 hours time–on line.

The addition of small amounts of potassium to supported group VIII metals for F–T synthesis has long been known to affect the performance of such catalysts in a variety of ways; detailed examples of which have been described in relevant sections of this chapter. In general, the potassium promoter has been shown to increase the olefin to paraffin ratio, the average molecular weight of the products, the content of oxygenates and to decrease the methanation activity of the catalyst (10,13,14,46,72,119,120). This is believed to arise from the alkali–induced chemisorption changes, with the relative surface concentration and dissociation probability of CO and H_2, significantly altered, affecting both reaction mechanism and product distribution (121–123). As a result we have investigated the effect of potassium on our Co/MnO catalysts in an attempt to:

— firstly; further enhance the selectivity toward the commercially viable C_2 and C_3 olefins, and

— secondly; to further suppress methane formation, and thus prevent the loss of an expensive carbon source to a commercially less–viable product.

3.2   EXPERIMENTAL

The apparatus and techniques for this study have been discussed in detail in Chapter 2. Briefly, cobalt manganese oxide catalysts (Co/Co+Mn = 0.5) were prepared by co–precipitation from a solution of mixed nitrates with aqueous ammonia under controlled conditions (pH = 8.3, T = 70°C), by

using the method of Maiti *et al.* (104). The Co/Mn ratio in the prepared catalysts was controlled by selection of the appropriate initial mixed nitrate solution. Promotion of the catalysts with various percentages of potassium (as K_2CO_3), was achieved by incipient wetness, the method of which has previously been reviewed by Acres *et al.* (103), (the promotion with potassium was with respect to the mass of the active component, i.e. mass of Co, present in the catalyst sample). Catalyst precursors were pelletted and sieved (0.5 – 1.0 mm particles) and then calcined in air (500°C, 24 hours). Catalysts were subsequently reduced *in situ* at 400°C for 16 hours, in a hydrogen atmosphere (GHSV = 280 h⁻¹). Catalyst (2 g) were loaded into three multi-fixed-bed laboratory reactors (Figure 2.2, Chapter 2), which enabled CO hydrogenation of different catalysts under almost identical experimental conditions (CO/H_2 ~ 1:1, T = 220°C, P = 500 kPa and GHSV = 250 h⁻¹). A stabilization period of ~ 120 hours after initiation of F–T synthesis was allowed before mass-balance data collection was commenced. Analysis of product gases were determined by on-line gas chromatography capable of analysis for hydrocarbons (FID detector, poropak Q column) and CO, CO_2, H_2 and N_2 (TCD detector, carbosphere column). Condensed liquid products were analysed by using off-line gas chromatography (FID detector, 30 m J+W BD1 capillary column).

3.3   RESULTS

The effects of potassium loading on the performance of Co/MnO catalysts during the hydrogenation of carbon monoxide are presented in Table 3.1. The addition of only small amounts of potassium was shown to effect the performance of such catalysts in a variety of ways. Particular attention was

given to the effects of potassium on catalyst activity, methane and heavy hydrocarbon selectivity, olefin to paraffin selectivity and primary alcohol selectivities. Each of these effects as a function of K loading are graphically illustrated, and will be discussed in-turn, in sections to follow.

3.2.1 Catalyst activity and selectivity

The selectivity data of Table 3.1 was derived from processed data of ~ 170 hour mass balance runs ("total mass of input, feed = total mass of output, products), under steady state conditions. Prior to these stable steady state conditions being realized, there was a required stabilization or "bedding-in" period, during which time the catalysts presumably reached a stable surface and bulk configuration, yielding constant activity and product distributions.

(a) Stabilization/activation "bedding-in" period

The activity of freshly reduced Fe catalysts in the F-T synthesis starts initially from zero and increases slowly to a maximum with time on stream. In this respect Fe differs from other F-T active metals such as Co, Ni and Ru where the activity reached equilibrium more rapidly. On introducing synthesis gas to partly reduced $Fe-Cu-SiO_2-K_2O$ catalysts at normal synthesis temperatures, the metallic iron is very rapidly converted to the Hägg carbide (Fe_5C_2) (10). Further reduction/carbiding continues slowly for several days and the activity increases somewhat during this period due no doubt to the continued creation of more active sites. Although our Co/MnO catalysts showed

TABLE 3.1: Selectivities of CO hydrogenation using K promoted Co/MnO catalysts.

% K promotion	0.0	0.01	0.05	0.1	0.25	0.5
pressure/kPa	540	500	550	500	580	500
reaction time/h	170	103	170	144	170	144
temperature/°C	220	220	220	220	220	220
GHSV/h^{-1}	268	236	253	254	267	251
CO conversion (%)	44.1	43.0	38.8	39.0	37.5	28.7
Hydrocarbon Selectivity (% m/m)						
CH_4	8.3	6.9	5.8	4.2	4.7	6.0
C_2H_4	2.3	2.3	1.7	1.9	2.7	3.1
C_3H_6	3.5	3.0	1.4	1.4	0.8	0.8
C_2H_6	13.6	13.6	12.2	10.1	9.9	8.6
C_3H_8	3.7	3.4	2.7	2.2	1.8	1.8
C_4	9.3	9.3	9.5	7.4	7.9	7.7
C_5^+	38.2	39.3	40.1	47.2	47.8	48.5
total C_6 hydrocarbon	17.3	17.2	14.9	12.3	11.7	10.4
Alcohol Selectivity (% m/m)						
CH_3OH	0.6	0.5	0.6	0.6	0.3	0.2
C_2H_5OH	2.0	1.8	1.3	1.4	0.8	0.4
$1-C_3H_7OH$	3.9	3.7	3.6	3.5	3.8	2.0
$1-C_4H_9OH$	1.0	1.4	1.7	1.6	1.3	0.9
C_5OH	8.3	9.1	11.9	11.5	14.1	16.6

an almost immediate acti ·· , ~25% CO conversion after only 1 hour time on stream, the catalyst still required a stabilization or "bedding-in" period of ~120 hours (T = 220^{0}C, P = 500 kPa and GHSV ~250 h^{-1}), for a maximum stable activity and selectivity to be attained. During this period the activity increased to ~43% CO conversion, which was also accompanied by a decrease in methane selectivity and a corresponding increase in both the C_2, and C_3 selectivity; as shown in Figure 3.1 (a) and (b) (which by this time had also shown an increased olefinity of these products). It may also ! · observed (Figure 3.1 (b)) that the duration of this stabilization period, was not altered by the incorporation of the potassium promoters into the catalyst system (this was found to be consistent for potassium loadings as high as 1.0%).

From *in situ* XRD studies performed on a working Co/MnO catalyst (Chapter 5, Section 5.3.4), a correlation could be made between the growth of the metallic Co partic a (identified as the body centered cubic, bcc, phase of Co) and an increase in propene selectivity, with time on stream. A maximum in the intensity of the Co(bcc) lines was observed after ~120 hours of CO/H_2 synthesis, which coincided with the generation of a maximum in the propene selectivity. A similar correlation could also be made with the decrease in methane selectivity and a corresponding increased growth of the Co(bcc) phase. This somewhat controversial statement is discussed further in Section 5.3.4. The activation/stabilization period of the Co/MnO catalysts, could thus be associated with the generation of a less hydrogenating system, which in turn may be associated with the formation of the "true" active form of the metallic cobalt i.e. Co(bcc) during this period.
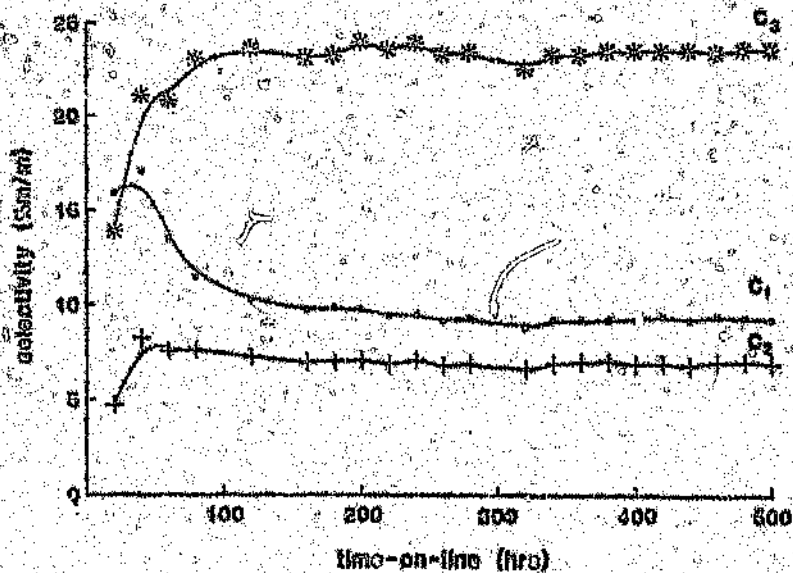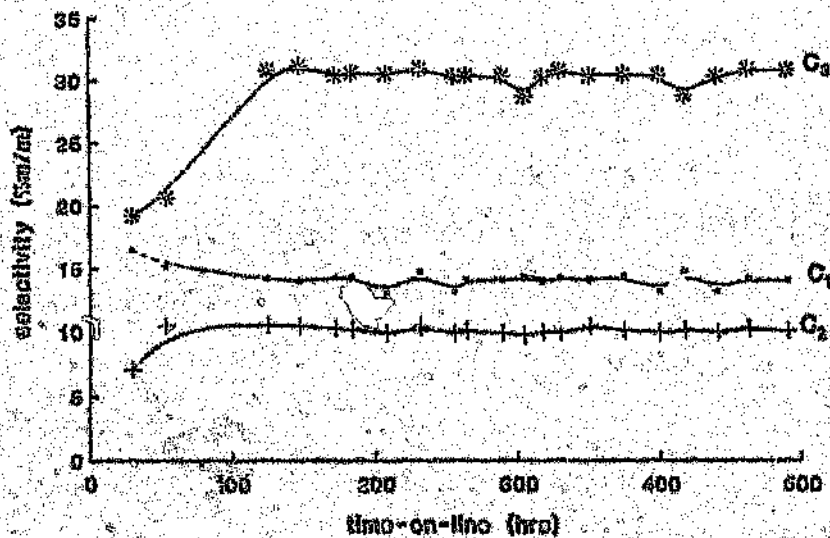
C_1, C_2, and C_3 selectivities versus time on stream, showing the stabilization period for the Co/MnO catalyst with a, 0.0% K and b, 0.25% K.

[*] The data used in these plots do not reflect selectivities from complete mass balance calculations, but rather % m/m selectivities from the gaseous fraction alone.

All catalyst activity and selectivity data was thus obtained from mass balance runs (of ~170 hours), performed only after ~120 hours of initial CO/H_2 synthesis, i.e. only after steady state conditions had been attained. No changes in the maintained activity and selectivity (of both the non-promoted and promoted catalysts) were observed for the duration of the different catalysts that were tested (in some cases for as long as 500 hours); see Figure 3.1(a) and (b).

(b) Catalyst activity

The effects of potassium loading on catalyst activity (in terms of % CO conversion) is presented in Table 3.1 and Figure 3.2. The data indicated that only low levels (between 0.01 and 0.25%) of potassium were required to produce the desired effects of decreased methane and increased olefin selectivities, which was accompanied by only a small decrease in catalytic activity. At the observed lower K loading i.e. between 0.1 and 0.2% K, CO conversion decreased by only ~6.0%, when compared to its unpromoted analogue. A significant decline in activity resulted from the addition of higher levels K with the 1.0% K promoter catalyst exhibiting a reduced CO conversion to levels of half that of the unpromoted system. (Catalyst deactivation as a result of high K loadings was found to be consistent with noticeable increases in the methane selectivity — this will be discussed further in the following section.)

The amount of potassium required for optimum catalytic activity depends on the nature of the metal and the catalyst support. Apparently, there must be sufficient alkali metal to enhance dissociative chemisorption of CO, but there must not be a level such that the

hydrogen adsorption is totally suppressed (124). The low levels of alkali content used for optimum catalytic performance of our Co/MnO catalysts, seem to be consistent with the alkali loadings used for the promotion of similar catalysts. For example, Yang *et al.* (125) have found the alkali effect to approach near saturation at 0.2 g/100 g Fe. On conventional fused iron and precipitated iron catalysts, the K/Fe levels
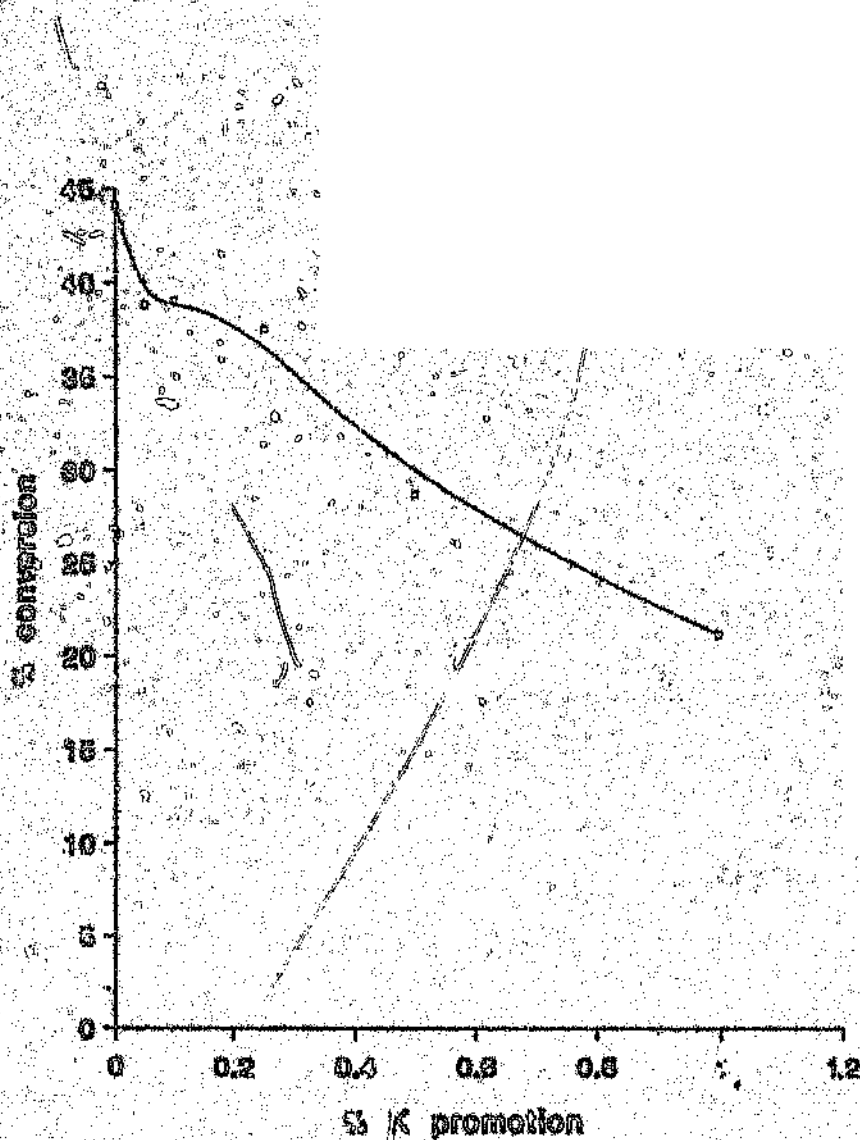
Figure 3.2: Influence of % K content on CO conversion.

of 0.005 – 0.01 by weight were required for maximum activity (6) [when acidic oxides are present as structural promoters or supports, e.g. Al_2O_3, larger amounts of alkali metal are generally required (6)].

Although it is well known that alkali promoters significantly modify the catalytic activity of metals for CO hydrogenation, there is disagreement in the literature on what effect they have. Yeh *et al.* (126) found that for silica supported iron systems, the K promoted catalysts were less active than those catalysts without K. Similarly, Chen *et al.* (127) studied CO hydrogenation over carbon-supported iron-cobalt and carbonyl cluster-derived catalysts, and found that in general, the family of unpromoted catalysts (as well as the Co only sample) were much more active than the K-promoted clusters. Chuang *et al.* (128) showed the rate of CO conversion for Ru/TiO_2 catalysts to decrease in the order unpromoted >Li>K>Cs. However, work by Arakawa *et al.* (129) on alumina-supported iron catalysts, showed the turn-over frequency for CO consumption, N_{co}, to have increased initially, and then passed through a maximum as the K/Fe ratio was increased. According to Dry (10), the activity of fused catalysts operating at high temperatures in a fluidized bed, increased sharply with K_2O content and then levelled out, while at low temperatures in a fixed bed, the activity decreased as the K_2O content was increased, possibly owing to the accumulation of heavy hydrocarbons which deactivated the catalyst.

The observed decline in CO conversion upon alkali-metal addition could possibly be explained in terms of: (i) the extent of CO and H_2

chemisorption as a function of K and, (ii) the effect of K on the reducibility of Co^{2+}, ie. :—

(i) The potassium promoter increases the electron donation to the active metal and thus generates a surface with greater electron density (122,130). The metal–carbon interaction is strengthened, the extent of dissociative CO adsorption increases, and the formation of carbon monomers that participates in hydrocarbon formation is enhanced. The increased electron density on the metal, and subsequent rise in surface carbon coverage, suppresses hydrogen chemisorption (110,123,131). In addition, K has also been observed to increase the binding and activation energies for H_2 over Group VIII metals. This results in a decreased H_2 adsorption and consequently a decreased hydrogen atom erage (119a, 119b). A decrease in the hydrocarbon formation rate can thus occur as a consequence of a hydrogen–deficient surface.

(ii) XPS studies by co–workers (132) on K promoted and unpromoted Co/MnO catalysts, showed that the K inhibited the Co reduction at the catalyst surface. The authors also made the assumption that the metallic cobalt was mobile, and that the reduction may have started in the bulk. The presence of K_2CO_3 would lower the number of cation vacancies in the MnO lattice, resulting in the metallic cobalt having a lower diffusion capability. This would result in a lower number of active sites (i.e. Co metal sites) at the surface, with increasing K promoter, which could thus result in a decreasing activity. This finding is in agreement with the studies performed on K promoted Fe/Mn catalysts by Lindner et al. (133), who observed that samples with 1 and 2% of K in the bulk, showed smaller amounts of metallic Fe on the surface, and should therefore have shown a clearly lower activity for F–T synthesis.

(c) <u>Methane and heavy hydrocarbon selectivity</u>

The K promoter has proven to be a good candidate for meeting the desired objective of lower methane selectivities in Co/MnO catalysts. The proportion of methane in the product spectrum was shown to decrease on addition of small amounts of K, with an optimum decrease in C_1 yields occurring between 0.1 and 0.2% K — see Table 3.1 and Figure 3.3. Further increases of promoter resulted in a slight increase in methane yields, until 0.5% K, after which the methane yields increased further, which was also accompanied by an overall deactivation of the catalyst (conversion dropped to ~21% for a 1.0% K loading). As mentioned previously, increasing the potassium promoter beyond its optimum loading had resulted in a decreased activity, which has been shown (6) to be associated with increased methane yields.

The effect of K promotion on the methane selectivity of F-T catalysts has been the subject of numerous reports in the literature. Dry and Oosthuizen (46) have studied the effect of surface basicity on hydrocarbon selectivity on a number of magnetite catalysts. Data have been presented that showed a good correlation between higher surface basicity with a lower methane selectivity. Yang and Oblad (125) reported that the methane had decreased correspondingly as the potassium content increased from zero to 0.2 g K/100 g Fe. The incorporation of K into carbon-supported iron-cobalt corbonyl cluster derived catalysts, examined by Chen et al. (127), was shown to result in reduced methane formation. Work undertaken by Gonzalez and Muira (134) on a series of silica-supported Ru catalysts, showed the turnover number for methane formation to decrease. The effects of K_2CO_3

coverage of an Fe foil on F–T synthesis has been studied by Bonzel and Krebs (136), whose results had revealed that K had once again resulted in a decrease in the rate of methane formation.
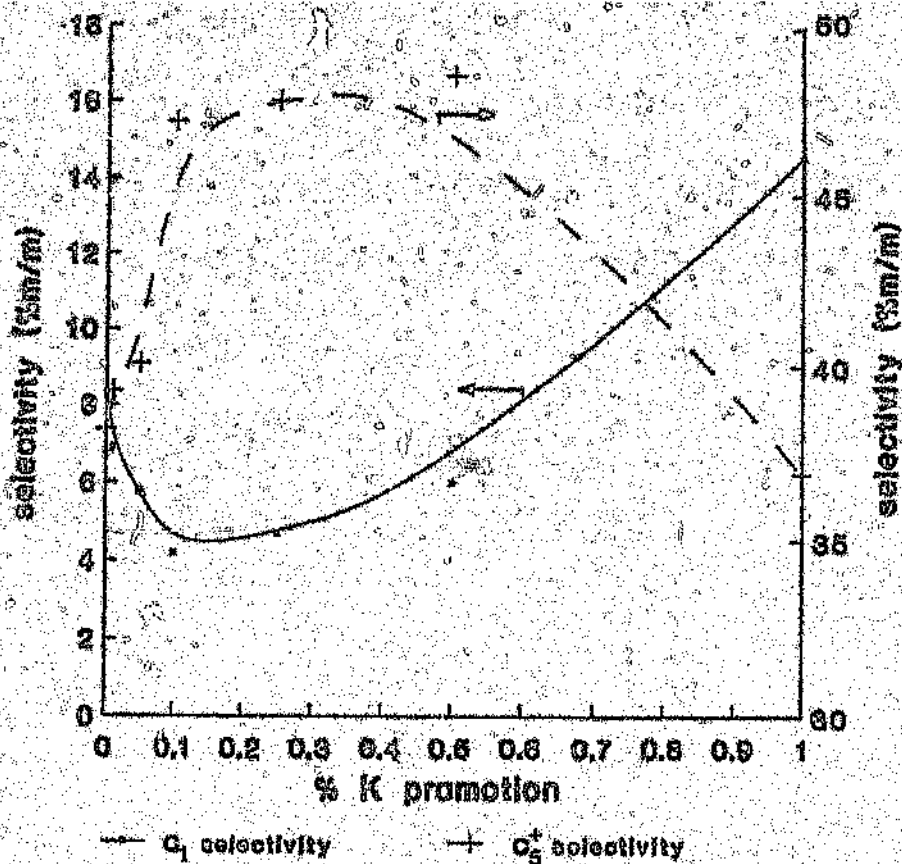
Figure 3.3: Effect of K promoter on methane and heavy hydrocarbon selectivity.

Consideration of the weight fractions for the carbon number ranges C_1, C_2–C_4 and C_5^*, shows that the decrease in methane selectivity coupled with a corresponding decrease in the C_2–C_4 fraction, see Table 3.2, was accompanied by an increase of the high molecular weight C_5^* formation, on addition of K promoter (Figure 3.2).

The observed shift to higher molecular weight hydrocarbons with K promotion was substantiated from increased chain growth probability factors α, calculated from Schulz–Flory plots for the set of K–metal addition catalysts. The α values presented in Table 3.3, indicated that the probability of C_1 monomer propogation increased with increasing

TABLE 3.2 Selectivities for the C_2–C_4 light hydrocarbon formation as a function of K loading.

% K loading	C_2–C_4 fraction (% m/m)
0	32.4
0.1	31.8
0.05	28.5
0.1	23.0
0.25	21.9
0.5	21.8
1.0	41.8[a]

[a] non–comparable due to the decreased activity from high K loadings.

alkali metal content. Higher α values imply a shift to higher molecular weight products, at the expense of the lighter molecular weight hydrocarbons.

Although only one value for α was calculated for our promoted and non-promoted Co catalysts (i.e. no break in the Schulz–Flory distribution was observed for our carbon range chosen), considerable uncertainties remain as to whether or under what circumstances the F–T products from a promoted catalyst may be characterized by a

TABLE 3.3: Chain growth probability factors, α, as a function of K content.

K (%)	α^a
0	0.79
0.01	0.84
0.05	0.84
0.1	0.86
0.25	0.86
0.5	0.85

a α values were found from the slope when the $\log \frac{Wn}{n}$ was plotted against n, from the Schulz–Flory distribution equation $\log \frac{Wn}{n} = n \log \alpha + \log \frac{(1-\alpha)^2}{\alpha}$; where n is the carbon number (in our case n = 1–15) and Wn is the weight fraction hydrocarbon product with carbon number n.

65

single value of α, rather than by two or more values. Huff and Satterfield (136) have presented selectivity data for the F–T reaction, supporting the theory that two distinct sites existed on potassium promoted iron catalysts, characterized by different chain growth probabilities. Studies by Konig and Gaube (120) and Shliebs and Gaube (137), have also reported data supporting the two site theory for iron catalysts promoted with potassium. Ertl et al. (123), have shown, from spectroscopic surface analysis of reduced–potassium–promoted iron catalysts, the potassium to be non–homogeneously distributed over the catalyst surface. From these observations it was difficult to argue that only two types of sites existed. Rather it was more reasonable that a distribution of sites existed, each with a unique probability of chain growth, and a corresponding value of the local K concentration. However, both the two–site model and the distributed site model have been shown to be equivalent in their ability to fit the molecular weight product distribution from an iron catalyst that has been promoted with potassium (138).

The observed shift to longer chain hydrocarbons with alkali–metal addition has long been known to be a phenomenon of supported group VIII metals (14). Dry and Oosthuizen (46), showed that the addition of K to reduced magnetite catalysts produced more useful larger chain hydrocarbons. Also, several researchers have observed these product shifts using different K–promoted iron based catalysts, for example, iron supported alumina catalysts (129), silica supported Fe–nitride catalysts (126) and precipitated iron catalysts (137).

(3) **C₂ and C₃ olefin selectivities**

> One of the principle objectives for the incorporation of the K promoter into the Co/Mn catalysts, besides its proven candidacy for suppressed C_1 fractions, was to achieve a greater selectivity potential to produce C_2 and C_3 olefins. The selectivity data from Table 3.1 showed that this objective had indeed been achieved, with those entries containing K promoter showing enhanced olefin selectivities for the C_2 and C_3 fractions, with the optimum K loading again being between 0.1 and 0.2% K. Although an overall decrease in the selectivities for the total C_2 and C_3 hydrocarbons, as shown in Table 3.4, was observed, the addition of promoter however, generated an increasing percentage of olefins in these C_2 and C_3 light gas fractions. This result is better demonstrated from calculated olefin to paraffin ratios given in Table 3.4 and Figure 3.4, showing dramatic increases in these ratios with addition of K promoter.

TABLE 3.4: Total C_2 and C_3 hydrocarbon selectivities with percent olefin content as a function of K promoter.

% K promotion	0.0	0.01	0.05	0.1	0.75	0.5	1.0[a]
Total C_2 ($C_2^- + C_2^=$)	5.6	5.3	4.1	3.3	3.3	3.2	9.6
Total C_3 ($C_3^- + C_3^=$)	17.3	17.2	14.9	12.3	11.7	10.4	18.7
$C_2^=/C_2^-$	0.66	0.77	1.33	1.35	4.50	5.17	5.53
$C_3^=/C_3^-$	3.66	4.05	4.52	4.59	5.50	4.76	4.50

[a] non comparable result due to decreased CO conversion from high K loading.

The variations in the alkene/alkane ratios observed with the above catalysts, could be due to variations in the primary alkene selectivity or to variations in the secondary hydrogenation of the primary alkene products. Schulz (139) has shown that for certain matrix catalysts, the primary alkene selectivity could be quantified in terms of the average mole % alkene in the C_3/C_4 fraction. Similarly, secondary alkene hydrogenation could be characterized as the mole % alkene in the C_2
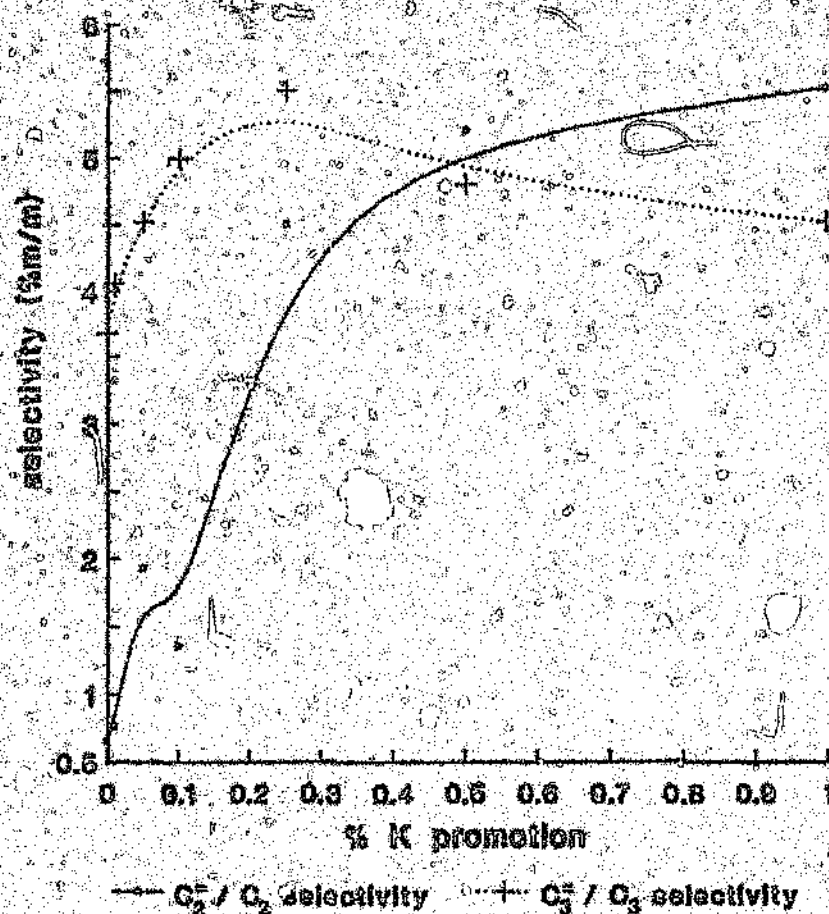
Figure 3.4: C_2 and C_3 olefin/paraffin ratios as a function of K promoter.

fraction compared to the mole % alkene in the C_2 fraction, which when close to 1.0, indicated a system of primarily alkene selectivity. If this ratio were to be significantly less than 1.0, then this could describe a system in which a high proportion of secondary hydrogenation was occurring. This analysis was based on the observation that since ethene is the most reactive alkene with respect to secondary hydrogenation, when compared to propene and the higher alkenes, its selectivity would thus be highly dependent on secondary hydrogenation.

The ratios for describing primary alkene selec[.]vity and secondary hydrogenation for the K promoted and non–promoted Co series are given in Table 3.5.

TABLE 3.5:   Primary alkene selectivity and secondary hydrogenation ratios for the Co series.

% K promotion	0.0	0.01	0.05	0.1	0.25	0.5[a]	1.0[a]
primary alkene[b] selectivity	0.09	0.09	0.100	0.10	0.11	0.17	0.26
secondary hydrogenation	0.18	0.19	0.43	0.40	0.81	1.08	1.25

[a] the data for the higher % K loading system may exaggerate these observed trends, due to non–comparable lower CO conversions, which has been shown to effect the values of primary alkene selectivities (85).

[b] in our case the primary alkene selectivity has been defined as the % C_2H_4 in the C_2 fraction (85).

The primary alkene selectivity ratios remained approximately constant whereas the approach to the value of 1.0, for the secondary

hydrogenation ratio increases dramatically with increasing K promoter (~4.5 fold increase between 0 and 0.25% K loading). From this data it becomes apparent that although the K promoter may have a minor influence in increasing the selectivity toward the primary alkenes, its major role would seem to be in its ability to suppress secondary hydrogenation of the primary alkene products. Similar results for Fe/Mn catalysts have been observed by Schulz and Gokcebay (140) who claimed that the addition of K to their catalysts had also reduced secondary olefin hydrogenation. This reasoning was further substantiated from CO/H_2 chemisorption studies on K promoted catalyst surfaces, which were shown to display decreased hydrogenating properties, due to increased CO and reduced H_2 chemisorption in the presence of the K promoter (122,123,141).

Numerous studies on a host of catalysts have shown the addition of K promoter to invariably increase the percentage of olefins in the light gas fraction. Anderson et al. (13) have reported an increase in the olefin to paraffin ratios up to about 0.5 parts of K_2O per 100 parts by weight of Fe. Arakawa et al. (129) also using Fe based catalysts, had shown the C_2^+ product to be almost exclusively olefinic, at high K/Fe ratios. Research performed on cobalt based catalysts with different combinations of Mn, kieselguhr, Al_2O_3 and ZnO, showed that for those entries which contained alkali (K_2O), the selectivities for C_3-C_4 olefins were high (72). Unconventional K promoted Fe–Co carbonyl cluster–derived catalysts has also been shown to greatly enhance the selectivity to olefins (127). Co which is known to produce a high degree of paraffins (6,13), was modified by the K so that it produced a marked enhancement of olefin selectivity (at low conversions). Similarly, the

addition of a K atom to the Fe–Mn bimetallic carbonyl cluster derived catalysts, supported on high surface area amorphous carbon black, was shown to further enhance the selectivities toward the light olefins (34).

(a) Primary alcohol selectivities

Primary alcohol selectivies are given in Table 3.1, with $C_1OH \rightarrow C_4OH$ and C_5OH^+ fractions being plotted as a function of K, and presented in Figure 3.5. These results showed that the presence of K favoured the formation of longer chain alcohols accompanied by decreases in selectivity toward the $C_1OH \rightarrow C_4OH$ fraction. These trends held true for K loadings of up to ~0.4% K, whereafter dramatic decreases in the C_5OH^+ fraction also occurred. This sudden decrease in the selectivity toward the C_5OH^+ fraction occurring together with an ever decreasing selectivity of the C_1OH-C_4OH fraction, is due to the decreased CO conversions occurring as a result of high K loadings (at low conversions, decreased organic and aqueous condensates are formed, with zero yields being observed for high K loadings). The formation of these longer chain alcohols was consistent with the observed selectivity shift toward longer chain hydrocarbons, coupled with the presence of increased concentrations of CO (available for possible CO insertion in the formation of alcohols) observed with K promoted surfaces (122,123,132).

It is known that the addition of alkali salts to methanol synthesis catalysts often resulted in increased yields of higher alcohols (128). It has been suggested that the selectivity to alcohols during CO hydrogenation on Rh catalysts varies with the basicity or acidity of the support (142). Also, Anderson et al. (13) using Fe/Al₂O₃ catalysts,

found that the content of oxygenated products increased with K promoter up to 0.5 g K/100 g Fe.
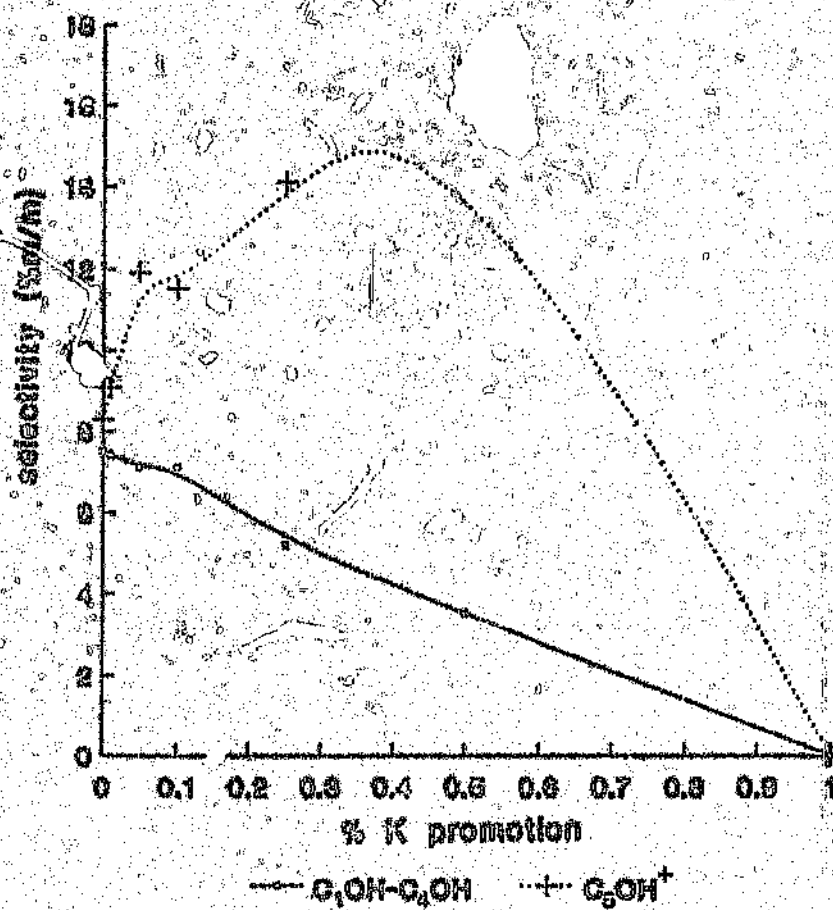
Figure 3.5: C_1OH-C_4OH and C_5OH^+ alcohol fractions as a function of K promoter.

(f) Mechanism of promoter action

The influence of K on the distribution of products is consistent with the effects of this promoter on the electronic properties of the catalyst surface. Essentially, K influences the competition between dissociative CO chemisorption and H_2 adsorption on the active catalyst sites.

The mechanism of CO adsorption during the F-T reaction occurs via metal σ bonding and the simultaneous back donation of transition-metal valence electrons into the antibonding 2π orbitals of the carbon in CO (130). During this back donation process there is a strengthening of the metal-carbon bond, and a simultaneous weakening of the carbon-oxygen bond. If the C-O bond is sufficiently weakened in the adsorption process, then dissociative CO adsorption will occur, generating the building blocks for carbon chain formation.

Surface spectroscopy studies of CO adsorbed on alkali metal-doped transition-metal surfaces, indicated a significant weakening of the CO bond, and an increase in the extent of CO adsorption (121,135). A charge transfer has been shown to take place from the alkali metal to the vacant d orbitals of the active metal, as evidenced by the lowering of the metal work function (143). The additional electron density imparted to the metal serves to increase the extent of back-donation into the 2π antibonding orbitals of CO, causing a weakening of the CO bond. This was indicated by a noticeable decrease in the CO stretching frequency upon addition of alkali promoter (144,1`5). UPS work showed that the saturation coverage of the adsorbate, the rate of dissociative adsorption, and the adsorption energy had increased on the

alkali–promoted metal (146). Measurements of the heat of adsorption of CO on Fe + K surfaces had also indicated the ΔH_{ads} increased, with increasing alkali metal content (119).

On the other hand, the presence of an electron–donating species on the catalyst surface suppresses the adsorption of hydrogen, as hydrogen itself donates an electron to the metal upon adsorption (10). It has also been shown that the presence of CO and surface carbide, decreases the hydrogen adsorption on metals (119,131). Furthermore, the heat of adsorption of H_2 decreases with increasing alkali metal (119, 119a, 119b), confirming the notion that alkali–metal addition suppresses H_2 adsorption. If it is assumed that K has a similar effect on the chemisorptive properties of the working catalyst, then the observed reduction in CH_4 formation and, the increase in olefin/paraffin ratios, with addition of K, can be attributed to the suppression in the relative concentration of H_2 with respect to CO, which decreases the hydrogenating properties of the catalyst surface. Also, the reactivity of the carbidic species of K promoted Co foils (122) has been shown to be reduced by K, helping to explain the lower observed methanation rates. The observed increase in α values is also associated with a decreased hydrogenating capability of the K promoted surface, which is reasonable since methanation is a competing reaction to chain growth on the surface. It has been shown (31,147) that there is an inverse relationship between higher hydrocarbon selectivity and the H_2 reactant partial pressure during CO hydrogenation. Apparently the effect of K on the reaction is similar to that of a lower H_2 partial pressure. It has been

suggested (148,149) that this could arise from the competition between adsorbed C and H atoms (as discussed), resulting in the decreased hydrogenation capability of the promoted surface.

3.3.2 Effect of operating conditions on the alkene/alkane ratios

The C_2 and C_3 olefin to paraffin ratios has been studied as a function of reactor operating conditions. CO hydrogenation was carried out with various promoted and non-promoted Co/MnO catalysts varying the reaction temperature, pressure, H_2/CO ratio and gaseous hourly space velocity. Similar optimization studies have been performed by van der Riet et al. (85) in establishing the effect of operating conditions on the alkene/alkane ratios of non-promoted Fe/MnO and Co/MnO catalysts.

(a) Effect of reaction temperature

Typical hydrocarbon product distributions for 0.0 and 0.25% K promoted Co/MnO catalysts at three different temperatures of 190, 220 and 250°C are shown in Table 3.6 (at fixed pressure and space velocity of 500 kPa and 280h^{-1}, respectively). On increasing the temperature, the methane increased significantly and became a major hydrocarbon product at the expense of the higher hydrocarbons. As the temperatures decreased, the olefin to paraffin ratios for the C_2 and C_3 fractions increased dramatically for both the promoted and non-promoted catalysts (Table 3.6). Thus, at high temperatures secondary hydrogenation of the primary alkenes is favoured.

TABLE 3.6: Hydrocarbon distribution at different temperatures for promoted and non-promoted Co/MnO catalysts[a]

	0.0% K			0.25% K		
T/°C	190	220	250	190	220	250
% CO conversion	17.3	44.1	56.4	13.8	37.5	45.9
Product Selectivities/% m/m						
C_1	6.9	8.3	16.7	4.3	4.7	12.9
C_2	4.9	5.8	6.8	2.9	3.3	5.1
C_3	11.8	17.3	18.3	9.3	11.7	14.9
C_4	11.1	9.3	9.7	9.4	7.9	6.3
C_5^+	43.5	38.2	29.4	41.5	47.8	36.9
Total oxygenates	tr	15.8	11.5	tr	20.3	15.9
Olefin to Paraffin ratios						
$C_2^=/C_2^-$	1.0	0.7	0.3	7.8	4.5	2.7
$C_3^=/C_3^-$	4.9	3.7	2.0	8.0	5.5	3.2

[a] P = 500 kPa, GHSV = 280 h^{-1}

The influence of temperature on product selectivity has been found to be consistant for most F-T catalysts, in so far as the observed product selectivity shifts to lighter molecular mass products, with increasing operating temperature (10). Research on cobalt catalysts has shown the percentage of olefins in the various carbon-number cuts to remain constant or to decrease as the temperature was increased (14). Arakawa et al. (129) using K promoted and non-promoted alumina supported Fe catalysts., showed the average molecular weight, the olefin to paraffin ratios, and the proportion of alcohols formed to increase as the temperature decreased. As can be seen from Table 3.7, Sasol

fluidized iron catalysts also showed all trends mentioned above, namely, as the temperature increased the CH_4 selectivity increased, the olefinity of the products and the alcohols and acids decreased (10).

TABLE 3.7 The influence of temperature on the selectivity of fluidized iron catalysts (Sasol)[a]

Temperature/°C	Selectivity/% C atom			
	CH_4	$C_2^=/C_2$ ratio	Alcohols	Acids
310	10	6	2.3	0.3
330	14	10	2.3	0.4
350	17	9	1.6	0.2
360	20	8	1.3	0.2
370	23	6	0.8	0.1
380	78	4	0.5	0.1

[a] Table by courtesy of M.E. Dry (10) Sastech (R and D), Sasolburg, South Africa.

In the choice of an optimum operating temperature for the production of lower hydrocarbon alkenes, factors such as acceptable levels of methane formation and CO conversion should also be considered, in conjunction with high alkene/alkane ratios. For example, low temperatures result in low CO conversions (i.e. T of 190°C = 17.4% CO conversion) which are synonymous with high alkene/alkane ratios (85), however the low CO turnover numbers may be economically unacceptable for industrial plant operations.

(b) <u>Effect of gas hourly space velocity</u>

The space velocity was varied by changing the gas flow rate for a given mass of catalyst at a fixed pressure (500 kPa) and temperature (220°C). Figure 3.6 shows a plot of C_2 and C_3 olefin to paraffin ratios as a function of space time (reciprocal of space velocity), for a series of 0.0, 0.1 and 0.25% K promoted Co/MnO catalysts. Slight decreases in the alkene/alkane ratios were observed in changing the space time from 1.7 x 10^{-3} h to 6.7 x 10^{-3} h (i.e. gas hourly space velocity from 600 h^{-1} to 150 h^{-1}). The C_2 fractions seemed to be more sensitive to change than their C_3 counterparts, with a greater decrease in the C_2 olefinity being observed with increasing space time (i.e. slopes for the C_2 alkene/alkane ratios were more inclined than for the C_3 alkene/alkane ratios). This is consistent with earlier observations that the ethene was the more reactive of the olefins (139), and would consequently be more susceptible to any change that increased the hydrogenating properties of the system.

These decreases in olefinity are a result of increased contact times (from increasing space time), which would consequently increase the probability of secondary hydrogenation of the primary alkenes. Similar trends of decreasing olefin to paraffin ratios with increasing space time, was also found to be consistent with conclusions of Bussemeier et al. (111), that the primary products of reaction are the α-olefins which are hydrogenated to corresponding paraffins (occurring to greater extents with increased contact times). Arakawa et al. (129) have shown the olefin to paraffin ratio to increase with increasing flow rate, again indicating that olefins are a primary synthesis product, and that a substantial portion of the C_2^+ paraffins are formed by hydrogenation of the olefins.
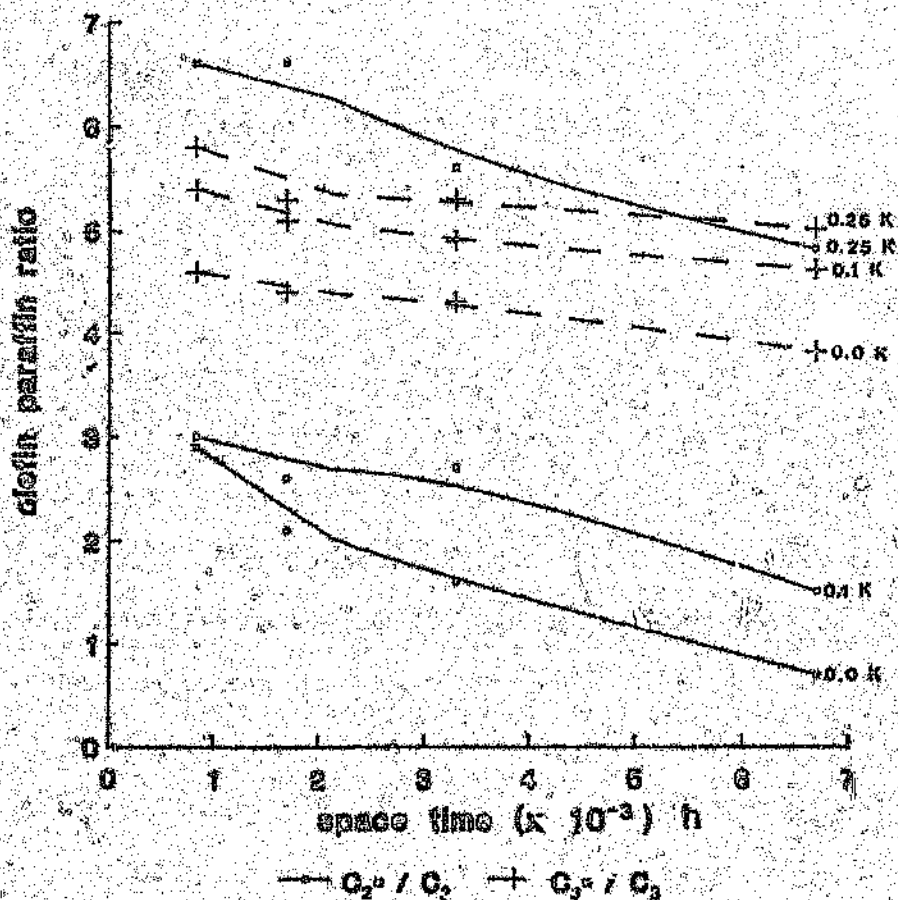
Figure 3.6: Effect of space time on the C_2 and C_3 alkene/alkane ratios ($P \approx 500$ kPa, T)

It is difficult to isolate the effect of space time, since inevitably conversion increases with increasing space time. Thus a plot of C_2 and C_3 olefin to paraffin ratios as a function of varying conversions, for the same series of catalysts is given in Figure 3.7. Similar trends, as for effect of space time, i.e. slight deceases in the olefin to paraffin ratios for

the C_2 and C_3 hydrocarbons were observed with increased CO conversions; with the C_2 fraction again being more sensitive to change than its C_3 counter part. (It should be noted that the C_2 alkene from the potassium free system, was more sensitive to change in the hydrogenation properties of the catalyst as a result of varying space time and conversion, when compared to its K promoted analogues – see Figures 3.6 and 3.7. This further substantiates the suppressed secondary hydrogenation properties of the K promoted catalyst – as discussed earlier.)

The above results are consistent with work done by co-workers (85) on non-promoted Fe/MnO and Co/MnO catalysts, who have shown the alkene/alkane ratios to decrease steadily with increasing space times and conversions. Studies by Varma et al. (86) on MnO supported Co and Ni catalysts, also observed decreased olefin to paraffin ratios with increasing space times and conversions. Chen et al. (127) using K promoted Co and Fe carbonyl cluster-derived catalysts, showed that at low conversions (below 7%), C_2 and C_3 paraffins were almost never observed.

Although optimum alkene/alkane ratios were observed to occur at lower space times i.e. low conversions, this may again be e..nomically non-feasible (in the case of industrial plant operation), as a result of low CO turnover frequencies.
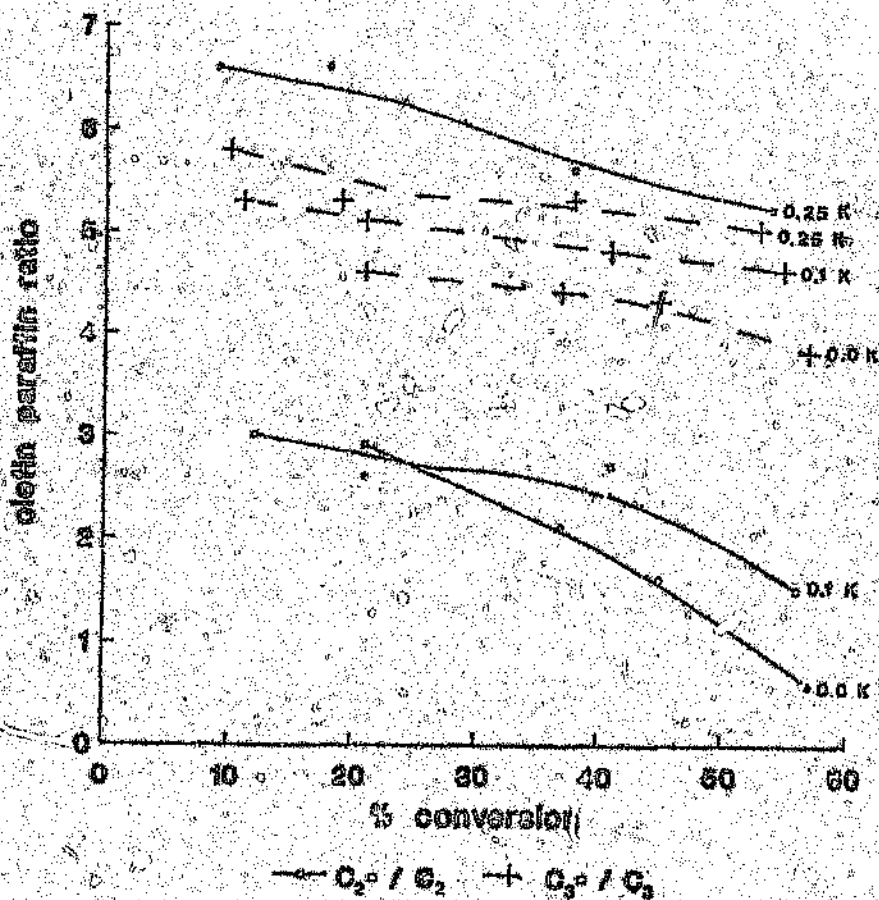
Figure 3.7: Effect of conversion on C_2 and C_3 alkene/alkane ratios ($P \approx 500$ pKa; $T \approx 220°C$).

(c) Effect of pressure

CO hydrogenation was performed on the same series of Co catalysts as in the previous section i.e. 0.0, 0.1 and 0.25% K, each at three different pressures of 300, 500 and 1000 kPa respectively ($T \approx 220°C$). For comparative purposes the pressures were varied maintaining

a *constant contact time*, i.e. since contact time is proportional to pressure but inversely proportional to GHSV, a constant contact time was maintained by compensating increasing pressure with increasing gas hourly space velocity.

The effect of pressure on the alkene/alkane ratios is shown in Figure 3.8, which demonstrated that on increasing pressure, slight decreases in alkene selectivity for both the C_2 and C_3 hydrocarbons had occurred. These results are consistent with work performed by co-workers (85), who showed that, in general, increasing the reaction pressure decreased the alkene selectivity for both Fe and Co manganese oxide supported catalysts. The C_2 and C_3 alkene/alkane ratios from the 0.25% K promoted catalyst showed a greater sensitivity to change in pressure than their comparative counterparts (Figure 3.8). Similar results were observed by Chen *et al.* (127) on K promoted Co and Fe carbonyl cluster–derived catalysts, who showed that the addition of K to a given cluster usually made the partial pressure dependence of CO more negative, whereas the H_2 partial pressure dependence became more positive.

Further investigations of the influence of pressure on alkene selectivity was performed by changing pressure, at a *constant GHSV* i.e. *variable contact time*, rather than a constant contact time, as previously. Since contact time is related to pressure, increasing the pressure from 300 to 1000 kPa, would have the effect of increasing the contact time by almost three fold. The results of increasing pressure (at GHSV $\approx$ 250 h^{-1}) on C_2 and C_3 alkene/alkane ratios are given in Figure 3.9.
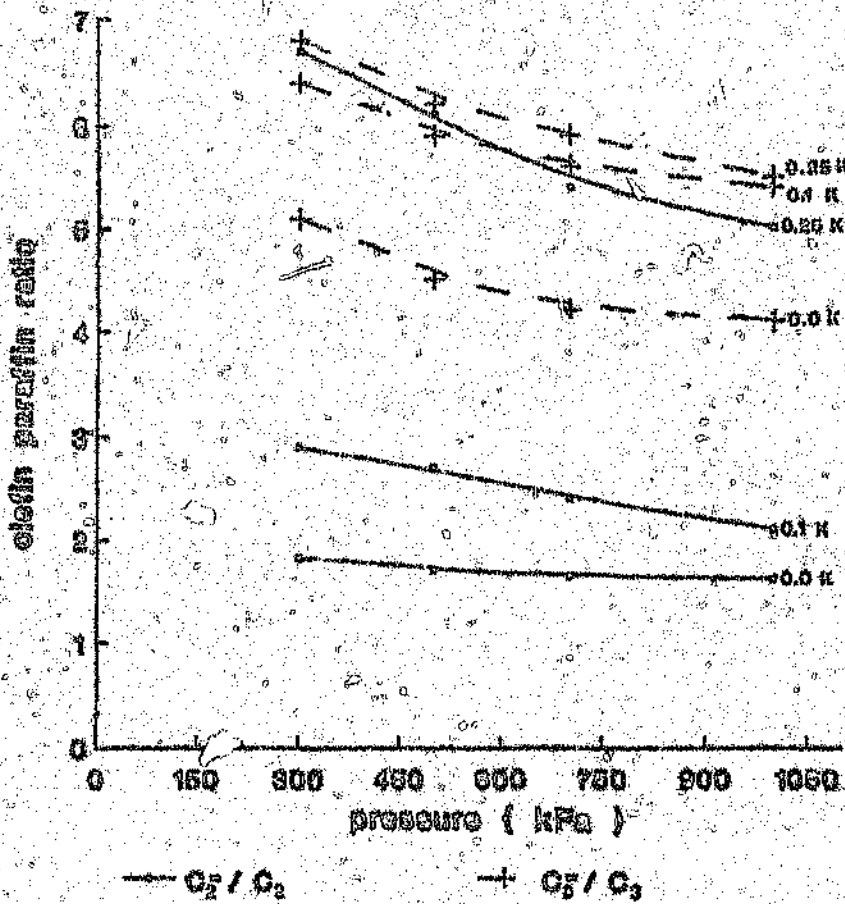
Figure 3.8: Effect of pressure (*constant contact time*) on alkene/alkane ratios for the C_2 amd C_3 hydrocarbon fractions (T ≈ 220°C).
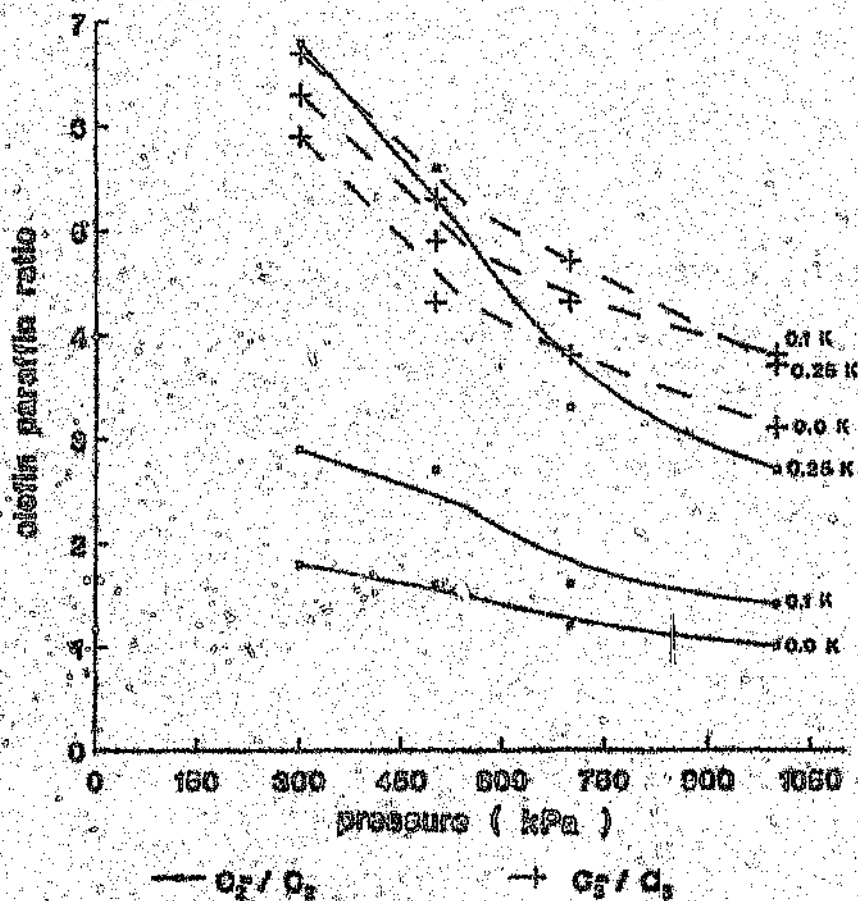
Figure 3.5: The effects of pressure (*variable contact time*) on C_2 and C_3 alkene/alkane ratios.

These results showed that on increasing pressure (with increasing contact time) a marked decrease in olefinity of the products had occurred, when compared to only slight decreases in olefinity observed for increasing pressure at a constant contact time – cf. Figure 3.8. This result is reasonable since by increasing contact time, the probability of

secondary hydrogenation of the primary alkenes increases, decreasing the alkene/alkane ratio, as observed. Thus, in order to operate the F–T synthesis reaction to lower hydrocarbon olefins at *high* pressures, the effect of increasing contact time with increasing pressure, could be compensated, by increasing GHSV.

(d) Effect of H_2/CO ratios

To observe the effect of the H_2/CO ratio on catalyst performance, the proportion of H_2 in the feed gas was increased from H_2/CO = 1 to H_2/CO = 2. Results of CO hydrogenation on *non-promoted* Co/MnO catalysts using the two different feed gas ratios are presented in Table 3.8.

TABLE 3.8: Effect of H_2/CO ratios on catalyst performance[a].

H_2/CO ratio	1	2
pressure/kPa	495	500
T/°C	220	220
GHSV/h^{-1}	263	255
% CO conversion	44.3	55.2
Product Selectivity (% m/m)		
C_1	8.3	12.4
C_2	5.8	10.5
C_3	17.3	21.1
C_4	9.3	11.0
C_5^+	43.5	33.4
Total oxygenates	15.8	11.2
Olefin to Paraffin ratios		
$C_2^=/C_2^-$	0.7	0.2
$C_3^=/C_3^-$	3.7	2.1

[a] CO hydrogenation was performed on two non-promoted Co/MnO catalysts.

These results indicated that increasing the H_2/CO ratio of the feed gas from 1 to 2, resulted in a decrease of the percentage olefins in the lower hydrocarbon products, with the alkene/alkane ratios decreasing by factors of almost 4 and 2, for the C_2 and C_3 fractions respectively. In addition, an increase in methane selectivity coupled with decreases in both the higher molecular weight hydrocarbons and total oxygenates were observed. An increase in the CO conversion on increasing the H_2/CO ratios was also observed. Decreased alkene selectivities could be explained in terms of an increased partial pressure of H_2 with respect to CO (since the proportion of H_2 in feed was increased), thus increasing the chance of secondary hydrogenation of the primary alkenes.

Although the catalytic performance of K promoted catalysts with increased H_2/CO ratios was not tested, we may predict that similar trends i.e. decreased olefinity, would occur with the Co/MnO catalysts of varying K loadings. (These predictions may be made due to similar trends that have already been observed between promoted and non-promoted Co catalysts during T, P and GHSV optimization studies).

Our results are consistent with studies performed by other workers, for example, Arakawa *et al.* (129) using Fe catalysts, showed that as the proportion of H_2 in the feed gas was increased, the rate of reaction increased, and concurrently, the average product molecular weight, the olefin to paraffin ratio, and the formation of alcohols all decreased. Using a cobalt catalyst at 180 °C and atmospheric pressure Kölbel (10) found that changing the H_2/CO ratio of the feed gas from

0.56 to 2 resulted in no change in the CH_4 selectivity. However, other studies on cobalt catalysts (14) showed that on lowering the H_2/CO ratio, the molecular mass of the product increased as did the olefin and alcohol content. Ruhrchemie tests (14) using Co:Ni:ThO$_2$:Mn:kieselguhr catalysts showed that a H_2/CO ratio of 1 had resulted in a lower CH_4 selectivity and a higher olefin content in the liquid hydrocarbon products, than a H_2/CO ratio of 2 feed gas. Studies at the US Bureau of Mines (10) using iron lathe turnings as catalyst, showed that although the $C_1 + C_2$ selectivity had increased on increasing the H_2/CO ratio of the feed gas from 1.36 to 2.91, the olefinity of the product had decreased. Thus, the overall effect of increasing the H_2/CO ratio of the feed gas was to yield products of lower olefinity.

3.3.3 Bulk and surface characterization

An investigation into the structural changes of co-precipitated Co/MnO catalysts during calcination, reduction and F–T synthesis has been detailed in Chapter 5. In summary, the calcined catalyst precursors were found to consist of mixed Co–Mn oxide spinels identified as $(Co,Mn)(Co,Mn)_2O_4$ and $CoMnO_3$, which were subsequently reduced to a solid solution of Co(fcc) + MnO. After an extended period of synthesis (~120 hrs), the Co(fcc) had transformed into a body centered cubic form [Co(bcc)], which has been proposed to be its "true" active phase for CO hydrogenation.

Although an *in situ* investigation of the K promoted Co catalysts was not performed, *ex situ* XRD studies performed on a series of K promoted (0.0 – 1.0% K) calcined (500°C, in air) Co/MnO catalysts, suggested that the incorporation of the alkali did not in any way effect

the bulk structure of the catalysts. This was confirmed by a DSC characterization, performed on the same series of catalysts, during their calcination (temp. ramp 25 → 550°C at 5°C min⁻¹). These results are consistent with observations by Dry *et al.* (150), that potassium and iron do not form solid solutions. Futhermore, spectroscopic surface analysis of reduced-potassium-promoted iron catalysts (123), showed the surface to be significantly enriched in K, with large clusters of K several micrometers across. In addition, the use of low K loadings (< 1.0%) for the promotion of our catalysts, coupled with the fact that K has been found to segregate to the surface, even at the calcination stage (132), further substantiated the accuracy of the above observations.

If absent in the bulk, the K promoter would then essentially occupy the catalyst surface, and would consequently influence the surface composition and topology of the catalyst; which would not be detected from bulk XRD and DSC characterization. These changes were thus monitored by certain surface sensitive techniques, e.g. from BET surface analysis, and *especially* from X-ray photoelectron spectroscopy (XPS), performed by co-workers (132) on a 0.25% K promoted Co/MnO catalyst. The BET surface areas of a series of calcined (500°C, 24 hrs) alkali-impregnated catalysts are given in Table 3.9.

TABLE 3.9:   Influence of the K promoter on the BET surface areas[a]

% K promoter	BET surface area ($m^2 g^{-1}$)[b]
0.0	15.7
0.0 (treated with H_2)	13.2
0.01	10.1
0.05	11.1
0.1	11.9
0.25	14.2
0.5	16.6
1.0	17.0

[a] outgassing temp. 150°C – 170°C, outgassing time 16 – 18 hrs, outgassing pressure 5×10^{-6} mbar, adsorption temp. 76° K (liquid nitrogen), adsorption gas = N_2.

[b] the surface areas were corrected for the physical influence of H_2O (as used in the promotion procedure), reflecting the change in surface areas due to the influence of K promoter alone.

The BET data from the above table shows clearly that K influences the surface areas. The area decreased initially with increasing alkali content, and then increased and eventually exceeded that of the non–promoted entry. These results are consistent with those of Dry. et al. (46), who showed that the alkali promoter decreased the surface areas of reduced iron catalysts, and that a greater loss in areas was recorded the more basic the alkali added (alkali promotions were in the order of between 0 and 2.0g/100g Fe).

The surface areas with corresponding specific activities for the K promoted series, is illustrated in Figure 3.10.
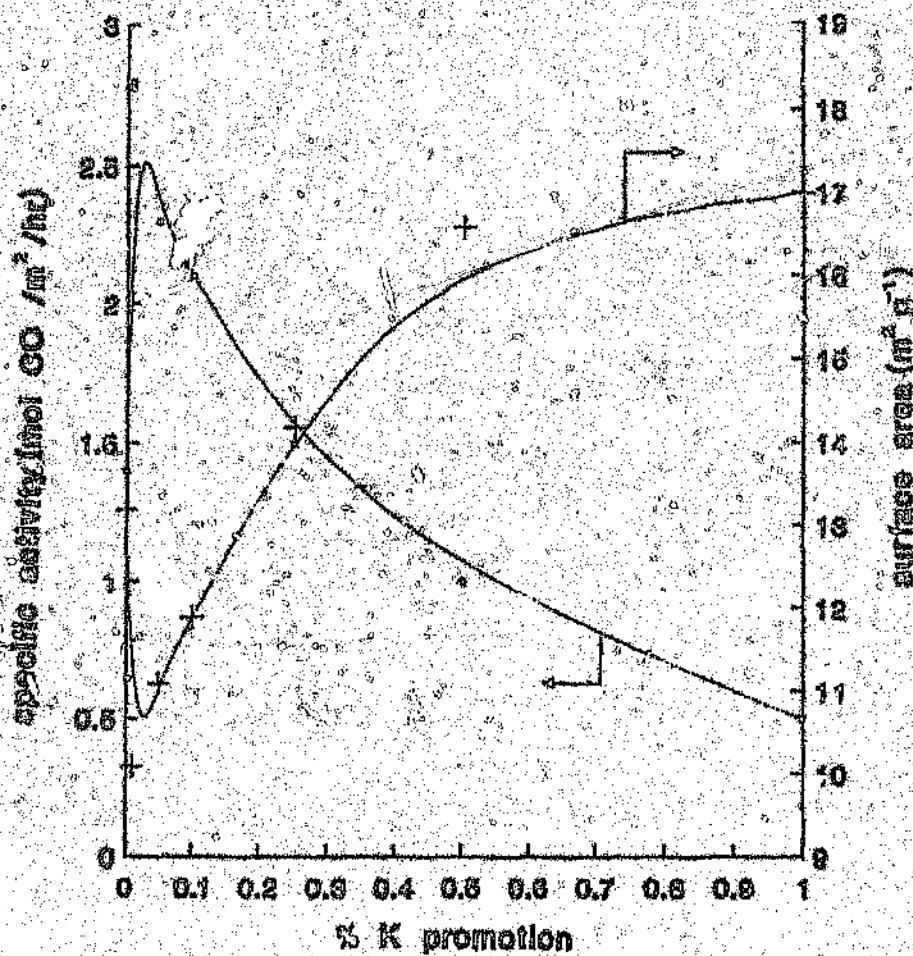
Figure 3.10: Surface areas and corresponding specific activity versus K promotion.

Figure 3.10 shows the specific activity to initially increase with increasing K content (with corresponding decreases in surface area),

and then to decrease (accompanied by corresponding increases in the surface area). Although the overall CO conversion has been shown to decrease with increasing K content (Section 3.3.1(b)), the *specific activity* increases initially and then starts to rapidly decline with increasing promoter content.

XPS has been shown to be a powerful tool for the identification and behaviour (physical and chemical) of adsorbed intermediates on the catalyst surface (Section 3.3.1(f)), and it has been used by co-workers (132) in an attempt at identifying the influences of the K promoter on the *physical* nature of the catalyst surface during pretreatment and synthesis. The catalyst surface compositions often vary considerably with respect to bulk compositions under the influence of temperatures and pressures, under which surface segregation of the different elements or molecules from the bulk can occur. Our promoted catalyst was thus analysed by XPS in the following sequence of calcination, reduction, F-T synthesis, re-reduction and finally Ar⁺ bombardment (132). A summary of the results from this surface analysis is listed below:

(i)   As already mentioned, segregation of the potassium from the bulk was shown to occur during calcination, reduction and synthesis.

(ii)   Before reduction the manganese at the surface was found to be less oxidised compared with the non-promoted Co/MnO. This indicated that CO_3^{2-} (from K_2CO_3) may be present in the

lattice sites previously occupied by excess O^{2-} ions, along with K^+ in the cation vacancies. This would limit the diffusion of metallic Co (previously claimed to have become reduced in the bulk, from Ar^+ bombardment) through the MnO lattice. Consequently this would explain why Co in the catalyst bulk is more reduced than at the surface, when compared to its non-promoted analogue. (This was mentioned in Section 3.3.1(b), in an attempt at explaining the observed decrease in activity to the decrease in the number of surface Co metal sites.)

(iii)   Evidence for small amounts of adsorbed CO can be used to explain the increased tendency for alcohol production over the K promoted catalysts (Section 3.3.1(e)), which probably occurs via CO insertion into the growing hydrocarbon chains.

3.4   CONCLUSIONS

CO hydrogenation performed on the Co/MnO catalysts prepared by co-precipitation techniques, showed that the response of these catalysts to potassium addition was atypical.

As was noted in many studies, a maximum in activity was obtained at a particular level of K; however for our systems, a small decrease in CO conversion was observed at the optimum K loadings of between 0.1 and 0.2% K (promotion beyond this optimum level had resulted in a more dramatic decrease in activity).

The alkali metal was observed to decrease the hydrogenation

ability of the cat.   st, as indicated by a decrease in methane selectivity and
an increase in product (C_2 and C_3) olefinity; thus demonstrating the principle
objective for which the catalyst was promoted. There was also an observed
shift to higher molecular weight hydrocarbons with K promotion, which was
substantiated by increased chain growth probability factors α, calculated
from Schulz-Flory plots for the set of K-metal addition catalysts. Our results
showed that the presence of K had also favoured the formation of longer chain
alcohols, accompanied by decreases in selectivity toward the C_1OH-C_4OH
fractions.

From a literature survey, the mechanism of promoter action was
thought to be through the influence of potassium on the electronic properties
of the catalyst surface, creating a competition between dissociative CO
chemisorption and H_2 adsorption on the active catalyst sites. An observed
increase in the CO dissociative adsorption, accompanied by a suppression of
H_2 adsorption, was simply due to the enhancement of the electron-donating
character of the active metal with alkali promotion.

Selectivity of the C_2 and C_3 alkenes was studied as a function of
reactor operating conditions. Increasing reaction temperature resulted in the
catalyst becoming increasingly hydrogenating, as was observed by dramatic
increases in methane yield, (at the expense of higher hydrocarbons), and
decreases in the olefinity of the C_2 and C_3 products. Alkene selectivity was
found to decrease with increasing space time and conversion and, at constant
conversion, increasing pressure. These effects se as a result of increasing
contact times, which would in turn increase the chance of secondary
hydrogenation of the primary alkenes. Similar observations were found to be
true on increasing the H_2/CO ratio from 1 to 2, thus increasing the partial

pressure and thus the hydrogenating capabilities of the system.

XRD and DSC characterization performed on the series of K promoted catalysts, suggested that the incorporation of the alkali did not in any way affect the bulk structure of the catalysts. The K promoter should then essentially concentrate on the catalyst surface, and changes in surface composition were demonstrated from BET surface area measurements and XPS studies. BET measurements showed the surface area to initially decrease at low alkali levels, and then to increase to levels consistent with the non-promoted entry. XPS studies showed surface segregation of the potassium from the bulk oxide during calcination, reduction and synthesis. It also showed a de_____ ____ of surface Co sites as a result of diffusion limits set-up in

4.3   RESULTS

The catalytic synthesis of hydrocarbons from mixtures of CO and H_2 was measured for a series of chromium promoted Co/MnO catalysts. Synthesis was performed under reaction conditions of $T = 220°C$, $P = 500$ kPa and GHSV = 250 h^{-1}, i.e. at those conditions that were found to yield optimum catalytic performance by the pioneering work performed by co-workers on non-promoted Co/MnO systems (84,85) [conditions of catalyst calcination and reduction pretreatment was also in accordance with previous studies performed by co-workers on the non-promoted Co systems].

Prior to mass-balance data collection, the catalysts were stabilized in H_2/CO for ~140 hours, which has previously been described [cf. Section 3.3.1(a)] as a "bedding-in" or stabilization period. During this time the conversion and product selectivity attained values which indicated that a steady state, non-transient behaviour of the catalysts had been achieved. A plot of methane selectivity as a function of time-on-line is shown in Figure 4.1, illustrating the stabilization period (decreasing methanation activity), and the subsequent steady state region. In addition, no significant change composition of the effluent gas was observed over the time period of the mass balance runs (~170 hours).

Our choice of Cr promoter levels (with respect to the trial Co content), was based initially upon optimum Cr loadings in the promotion of similar catalysts (claimed to be in the region of ~4.0% w.r.t. the active metal component), as determined by researchers at Sastech, Sasol R & D (156) [higher levels of Cr promotion, i.e. greater than 4.0%, were investigated

vacuo (110°C, 16 hrs), and then pelleted and sieved (0.5 – 1.0 mm particles), followed by a calcination in air at 500°C for 24 hours. The catalyst precursors were then loaded (2g) into multi–fixed–bed laboratory reactors (as previously, c.f. Section 3.2) and reduced *in situ* at 400°C, under H_2 for 16 hours (GHSV = 280h^{-1}). Premixed synthesis gas (CO/H_2 ~1:2, T = 220°C, P = 500 kPa and GHSV = 250h^{-1}) was subsequently fed over the catalysts and the system was allowed to reach steady state (~140 hrs) before mass balance data were collected. Certain modifications (for improved wax handling capabilities) were carried out on the reactor testing apparatus used for the K–promotion studies of Chapter 3. Here liquid and solid condensates were collected in two separate condensors; one heated (~130°C) containing the heavier hydrocarbons (~C_{16} – C_{40}), and the other at room temperature, containing mostly aqueous and oxygenated products, in addition to lighter hydrocarbons (~C_4 – C_{12}). A detailed description of the modified testing apparatus is given in Section 2.2. Analysis of product gases and condensed liquid and solid products were determined by on– and off–line gas chromatography respectively (cf. Section 2.3). CO hydrogenation experiments were typically of 170 hours duration and conversions were determined at regular intervals (every 24 hours).
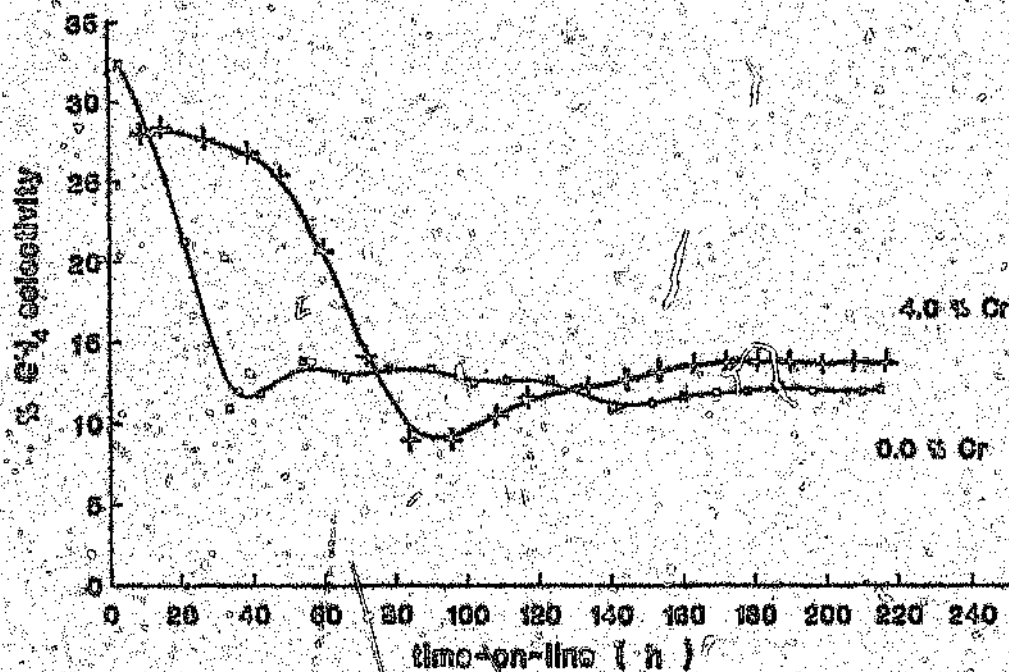
Figure 4.1: CH₄ selectivity as a function of time-on-line, showing the stabilisation priod and subseq ent steady state region.

at an attempt at determining the levels at which the catalyst would deactivate — results of which are discussed in sections to follow]. Product distributions of the total hydrocarbons (consisting of gaseous hydrocarbons and fractions of condensed hydrocarbons including oxygenated products), from the CO hydrogenation of a series of Cr promoted Co/MnO catalysts, are given in Table 4.1. The selectivity data are represented as the number of

4.3.1 Light and medium wax selectivity

Particular attention is given to the hydrocarbon fraction [referred to as the light (C_{16}–C_{25}) and medium (C_{26}–C_{35}) wax fraction], which consists of linear hydrocarbons having at least 16 and at most 40 carbon atoms per molecule. Examination of the selectivity data of Table 4.1, shows that the addition of Cr promoter substantially increases the selectivity toward these longer chain hydrocarbons; thus exhibiting the principle objective for which the catalyst was promoted. In order to better demonstrate the influence of the Cr promoter on this selectivity shift, the total fraction >C_5 has been fractionated into C_5–C_{10}, C_{11}–C_{15}, C_{16}–C_{20}, C_{21}–C_{25}, C_{26}–C_{30} and >C_{31}+ fractions, and the data presented in the form of a bar chart, are illustrated in Figure 4.2. It is evident that as the carbon number increases from C_5 to C_{31}+, so the selectivity toward the longer chain hydrocarbons of the promoted system increased markedly. For example, there is only a moderate two fold increase in the selectivity toward the C_{16}–C_{20} fraction, compared to a substantial 8 fold increase in the selectivity of the C_{26}–C_{30} fraction, on addition of promoter. Furthermore, the non-promoted Co catalysts were found not to produce hydrocarbon products of chain lengths longer than C_{30}, whereas the addition of Cr promoter generated longer carbon chain lengths; even C_{38} has been detected in this work.

The levels of chromium promotion that were required to bring about the abovementioned selectivity shifts, are consistent with the optimum levels (as previously discussed) found by other researchers, based on similar catalysts (156). It is also evident that Cr loadings as low as 2%, are sufficient to bring about the observed selectivity shifts. Increasing C loadings
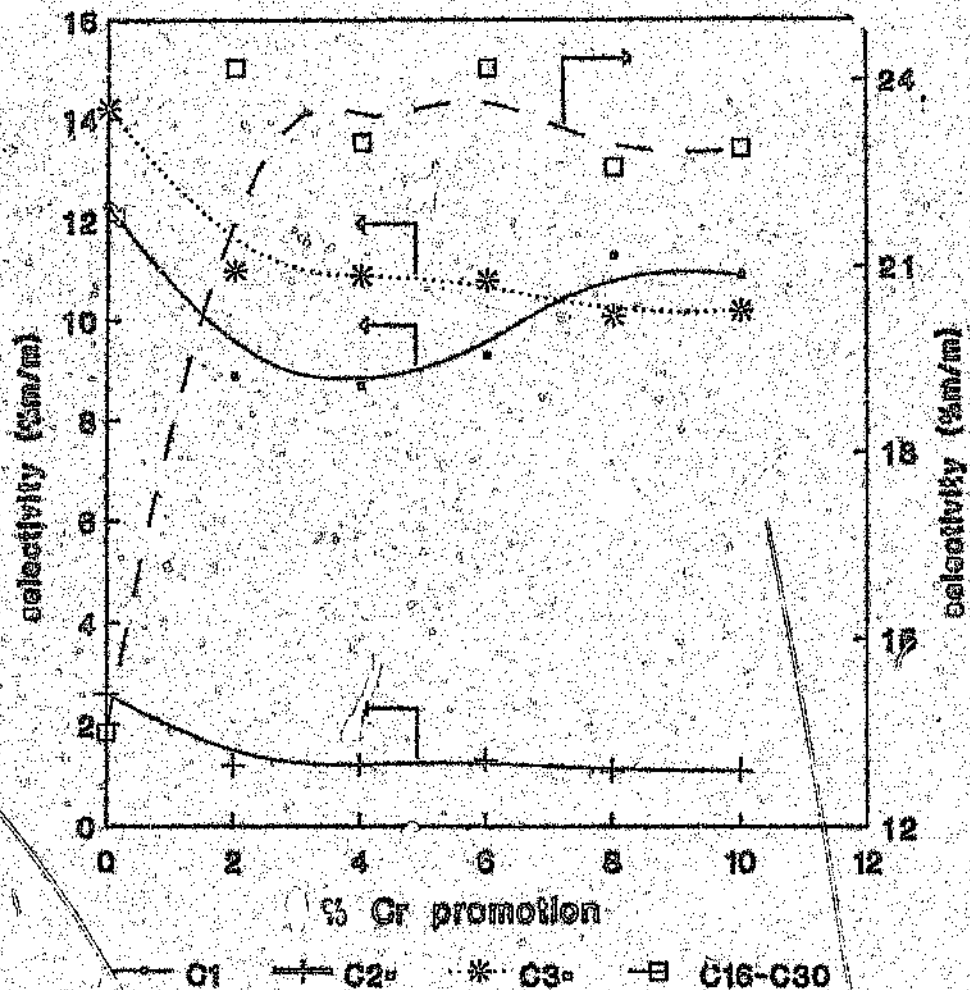
Figure 4.3 Plots of C_1, C_2, C_3, and C_{10}–C_{30} fractions as a function of Cr promotion.

It is apparent from from Figure 4.3 that after 2% Cr promotion, a plateau region is found and that no further changes in catalytic selectivity occurred on increasing the Cr loading beyond this level. These observations will be discussed in greater detail in sections to follow.

CHAPTER FOUR

AN INVESTIGATION INTO THE USE OF CHROMIUM PROMOTED Co/MnO CATALYSTS FOR CO HYDROGENATION TO LONGER CHAIN HYDROCARBONS

4.1 INTRODUCTION

Although petroleum fractions produced from coal-based processes may be of strategic importance, these synthetic fuels have a limited market value since they cannot compete with current world oil prices. However, the existence of synthetic fuel plants have been made very much more attractive from profits realized in the sales of certain by-products of F-T processes (151). One of the more intractable by-products of the F-T process (Sasol process) is the loosely-defined entity "wax". Waxes are mixtures of aliphatic organic compounds which are large, chainlike molecules. Crystallization is promoted by cohesion but waxes also contain some amorphous material (152). It is not generally realized that the commercial-scale version of the F-T processes produces considerable quantities of different types of waxes. Since these waxes are being marketed on a worldwide basis, it is important to maintain a programme of research which could further improve the selectivities towards, and quality of, these high value products.

Sasol plants (South Africa) employ multi-fixed bed reactors (low temperature, high pressure) using an extruded precipitated iron based catalyst, for the production of high value linear F-T waxes, which are free of aromatics (10,151) [this latter feature is of great importance when considering

the health regulations associated with many of the end-products]. Typically the wax product can be cut into 'gatch' (320° – 370°C) 'medium wax' (370° – 500°C) and 'hard wax' ($>500^\circ$C), [all boiling points are at 101 kPa]. Depending on the requirements, some of the cuts are further refined e.g. 'medium' and 'hard' waxes are hydrogenated over Ni-based catalysts to remove all traces of oxygenated hydrocarbons and olefins. Some hard wax may be subjected to a controlled oxidation process to produce several types of oxidised waxes (151). Waxes have a wide variety of end uses, and depending on their chain length, they are used for instance in the manufacture of industrial petroleum jellies, polishes, lubricants, crayons, candles, water proofings, paints, plastics and anti-corrosion coatings for metals. (151). Also, waxes can be cracked to extinction at relatively mild conditions to yield 80% (high quality) diesel fuel and 15% gasoline (153).

Apart from the wax selective precipitated iron catalyst, considerable interest has been shown in Co-based catalysts, in particular by Shell Internationale for the synthesis of longer chain hydrocarbons [for use in their MDS process] (63). Co on different catalyst supports e.g. SiO_2, Al_2O_3, TiO_2 and ThO_2, and modified by the incorporation of different promoters e.g. Zn, Ti, Cr and Ru, have been reported (36,110,154). Ru is another metal renowned for its selectivity toward heavy hydrocarbons (6,151,155). However the very high cost of this metal probably eliminates it from commercial application. Furthermore, due to the limited world stock of Ru metal, it's use in large commercial F-T plants is not possible unless the Ru content is limited to ~0.1% (63).

In an attempt at increasing the selectivity toward the light and medium wax fractions of our Co/MnO formulations, it had been suggested

that the use of a chromium promoter (156), might prove to be a good candidate. Chromium salts on silica supports (Phillips Catalysts) are used as industrial catalysts in the polymerization of ethene (157–160). Thus initially it was thought that the Cr promoters in our Co catalysts could have become active polymerization centers, polymerizing $C_2^=$ and $C_3^=$ products obtained from F–T synthesis, to longer chain products (see later). Apart from small amounts of Cr being added to the Shell Co–based catalysts (99,154), no further investigations into the use of Cr promoters in F–T synthesis to promote selectivity of heavy hydrocarbons has been reported in the literature. However the use of Cr as a component in catalysts for the synthesis of methanol and higher alcohols, has been well studied (35,161–163).

Performance of cobalt manganese oxide catalysts with varying percentages of added Cr, in the CO hydrogenation reaction in order to produce increased selectivity toward light and medium wax fractions, has been investigated. An optimization study of the system with respect to reduction temperature and reactor operating conditions of temperature, pressure and gas hourly space velocity, has also been performed.

4.2   EXPERIMENTAL

Preparation of the Co/MnO catalysts was again by co–precipitation of corresponding metal nitrate solutions with aqueous ammonia solution. The detailed method and apparatus used in this catalyst preparation is as described in Chapter 2. The resulting precipitate was dried in vacuo (110°C, 16 hrs) and then impregnated with different levels of $Cr(NO_3)_3$ promoter (w.r.t. to the active Co metal component), by the incipient wetness technique (103), as described in Section 2.1.2. The catalyst was again dried in

carbon atoms per molecule, and concentrations are given as mass percents of total products.

TABLE 4.1: The catalytic performance for a series of Cr promoted Co/MnO catalysts for the hydrogenation of CO[a].

% Cr promotion	0	2	4	6	8	10	15	20	25
% CO conversion	55.2	56.5	53.1	52.5	56.6	54.8	53.2	51.3	53.0

Hydrocarbon Selectivities (% m/m)

	0	2	4	6	8	10	15	20	25
C_1	12.3	8.9	8.7	9.7	9.3	11.3	10.9	11.5	14.1
$C_2^=$	2.6	1.2	1.1	1.3	1.1	1.1	1.0	1.0	0.8
C_2	7.0	6.7	6.5	7.0	8.0	8.1	7.1	8.1	9.6
$C_3^=$	14.2	11.0	10.9	10.8	10.1	10.2	9.1	9.8	10.0
C_3	6.9	5.5	5.	.4	6.2	6.5	6.2	6.6	8.6
C_4	12.3	11.0	10.x	..0	11.2	10.9	10.7	10.5	11
C_5-C_{10}	21.2	18.6	18.4	17.1	16.8	16.5	16.6	16.9	15.9
C_{11}-C_{15}	6.6	6.1	6.6	6.2	5.9	5.5	5.7	5.0	3.7
C_{16}-C_{20}	4.3	8.2	8.4	7.7	7.3	7.5	7.7	7.9	7.3
C_{21}-C_{25}	2.1	7.9	6.8	7.9	7.8	8.1	8.1	7.1	6.4
C_{26}-C_{30}	0.5	4.2	3.7	4.3	4.0	3.9	3.8	3.6	2.1
$C_{31}^=$	—	3.9	4.1	4.3	3.5	3.4	3.9	3.3	2.3

Oxygenate Selectivity (% m/m)

	0	2	4	6	8	10	15	20	25
C_1OH	0.9	0.7	1.0	1.1	0.9	0.8	1.6	1.7	1.1
C_2OH	2.3	2.1	2.4	2.8	2.7	2.7	2.7	2.6	2.3
C_3OH	1.0	0.9	1.2	1.2	0.9	0.9	2.0	2.0	1.2
C_4OH	0.8	0.5	0.7	0.6	0.4	0.4	0.9	0.9	0.8
C_5OH^+	1.1	0.9	1.1	0.8	0.9	0.9	1.0	1.0	0.9

a (i) typical reaction conditions: T = 220°C, P = 500 kPa and GHSV = 250 h^{-1}

(ii) product selectivities are from processed data of ~170 hour mass balance runs.
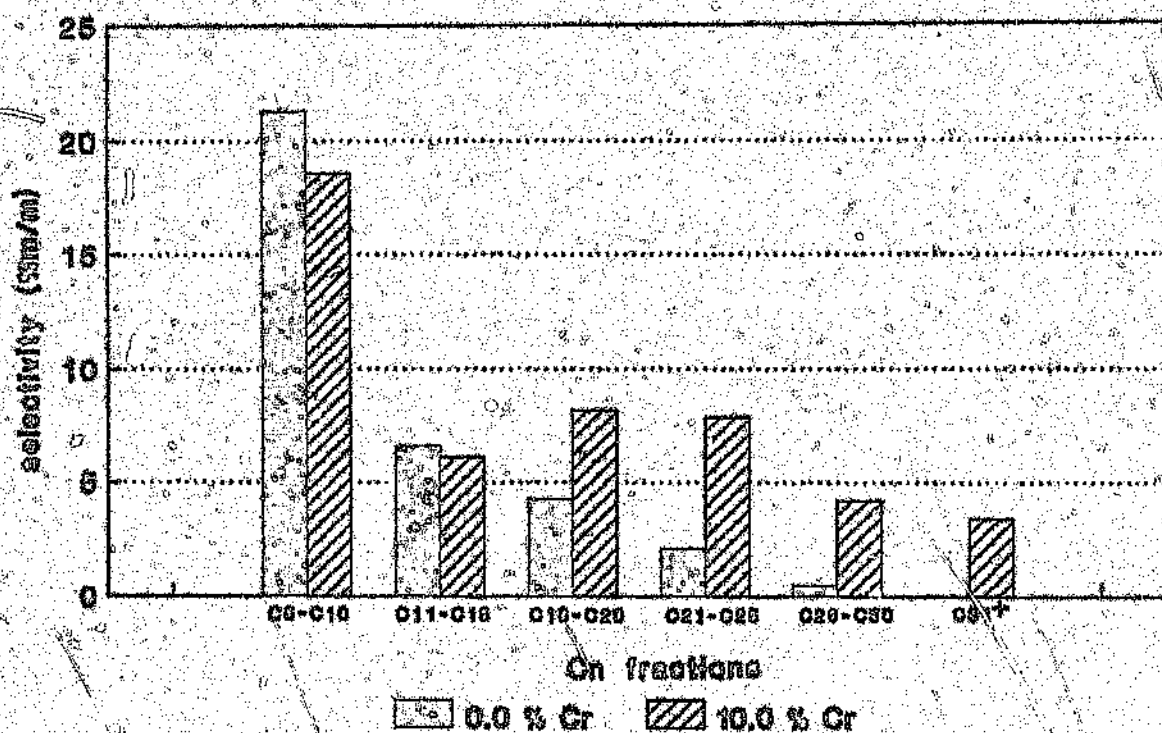
Figure 4.2: A bar chart showing the influence of the Cr promoter on the hydrocarbon distribution.

above this level did not result in further increases in the formation of heavy hydrocarbons, with the catalyst selectivity and activity in general, remaining almost constant with increased Cr content. This is further illustrated in plots of C_1, C_2, $C_3^=$ and $C_{16}-C_{50}$ fractions as a function of Cr content, presented in Figure 4.3.

Shifts in selectivity toward the long chain hydrocarbons on addition of Cr promoter, were further recognised from increased chain growth probability factors α_1 and α_2, (Table 4.2). The chain growth probability factor, α, is the ratio of the rate of chain propogation to the rate of propogation plus termination, and is a known method for describing the product distribution of the F-T reaction (164,105). The α value is indicative of the selectivity of the catalyst for producing heavy hydrocarbons from synthesis gas. The α values were calculated from the so-called Schulz-Flory distribution law (55), described by the equation (also described in Section 1.3.4).

$$\ln Mn = n \ln\alpha + \ln [(1-\alpha)^2/\alpha]$$

where, on plotting $\ln Mn$ against n (where n is the carbon number and Mn is the mole fraction hydrocarbon product with carbon number n), the values of α can be found from the slope or from the intercept at $n = 1$.

In early studies on F-T synthesis catalysts it was proposed that only one chain growth probability factor, α, existed for the Fischer-Tropsch reaction (56,57,164). In certain cases however, researchers have discovered a break to occur in the Schulz-Flory plot at approximately carbon number 9, producing a second, larger chain growth probability factor, α_2 (58,137,165,166). In a recent publication the Schulz-Flory distribution law was extended to include this second growth probability factor (58), given as

$$Mn = A\alpha_1^{(n-1)} + B\alpha_2^{(n-1)}$$

where α_1, α_2 = chain growth probability factors 1 and 2

A and B = constants related to the process parameters

TABLE 4.2: Chain growth probability factors α_1 and α_2 for the series of Cr promoted and non-promoted Co/MnO catalysts[a]

% Cr promotion	α_1	α_2	C_{18}^{+}
0	0.82	0.90	6.9
2	0.81	0.94	24.2
4	0.81	0.94	23.0
6	0.80	0.95	24.2
8	0.79	0.96	22.6
10	0.80	0.95	22.9
15	0.80	0.93	23.3
20	0.79	0.94	21.9
25	0.79	0.94	18.1

[a] again no significant changes in the α values beyond the 2% Cr level were observed.

The shift to longer chain products with addition of Cr promoter is clearly manifested by an increase in α_2 (0.90 to 0.94), accompanied by an increase in the C_{18}^{+} selectivity from 6.9 to 24.2% m/m, between the non-promoted and 2% Cr promoted systems – see Table 4.2. Plots of product distribution from which the α values were calculated, for the two catalysts, as described by the Schulz-Flory distribution law, are illustrated in Figure 4.4(a) and (b), respectively. A significant difference in the slopes of the lines that refer to the product distrubution greater than C_{18} (from which the α_2 values were calculated) is observed, graphically illustrating the shift in product distribution on addition of promoter.
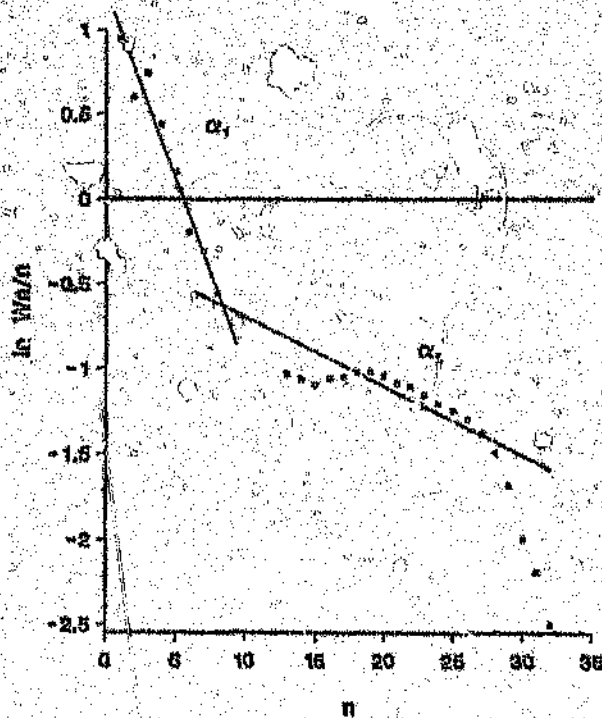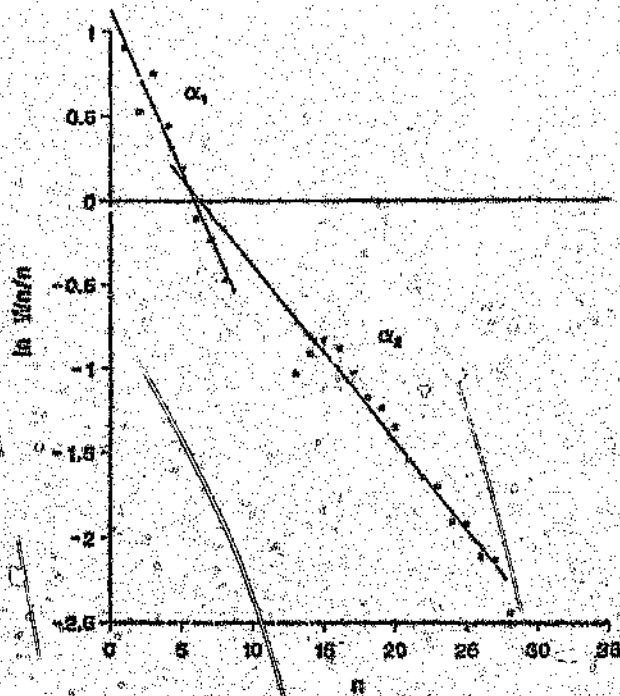
Figure 4.4(a) and (b): Schulz–Flory distribution plots of, a, non–promoted and b, 2% Cr promoted Co systems, showing the slopes from which the respective α_1 and α_2 values were calculated.

Thermogravimetric analysis was performed on the condensed hydrocarbon fractions collected from the non-promoted and promoted (2% Cr) catalyst systems, [thermogravimetry involves measuring the mass of a sample as its temperature is increased, and a plot of mass versus temperature permits an evaluation of the sample composition (167)]. The respective thermograms for the two samples are shown in Figure 4.5(a) and (b) respectively. Attention was given to the percent mass loss of sample over the same temperature range (ramping from 20°C → 160°C at 5°C min⁻¹) for both samples as demonstrated by the respective thermograms. A moderate 9.33% mass loss was observed for the condensate of the promoted entry, whereas a substantial 46.92% mass loss was observed for the condensate of the non-promoted entry (over the same temperature range). This further substantiates the shift in selectivity toward the higher melting/boiling point hydrocarbons with addition of Cr promoter.

4.3.2 Lower hydrocarbon selectivity

As expected, the observed shift in selectivity toward higher molecular weight hydrocarbons was accompanied by a small overall shift in selectivity away from the lower hydrocarbon gas fractions, with addition of Cr promoter – see Table 4.1 and Figure 4.3. Since the selectivities of the lower gas fractions, in particular ethene and propene did not change markedly on catalyst promotion, chain growth via olefin polymerization of alkene monomers does not appear to have taken place. (The proposed mechanisms for increased chain growth as influenced by the addition of Cr promoter, will be discussed in greater detail in Section 4.3.7.).
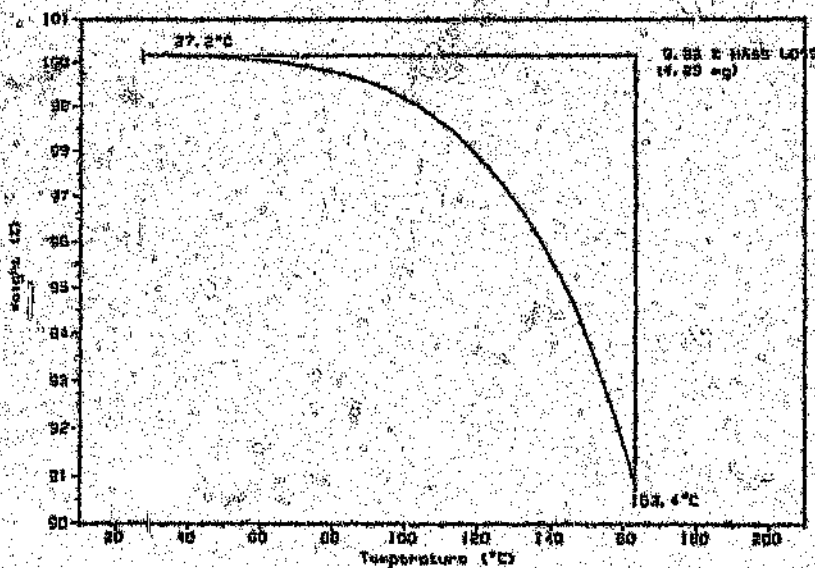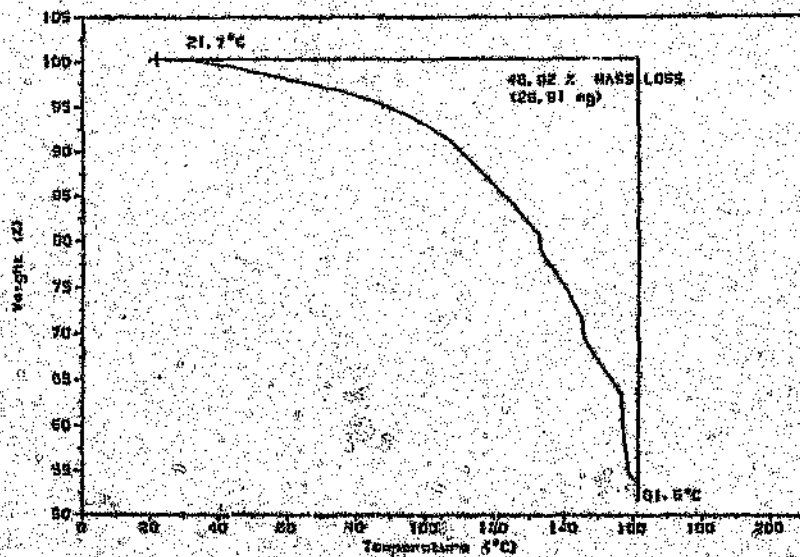
Figure 4.5(a) and (b):   Thermograms from the thermogravi-
metric analysis of the condensates from
a, non-promoted and b, 2% Cr
promoted systems.

The hydrogenation activity of the catalyst system was found in general, to increase with increasing Cr metal loading — see Figure 4.6.
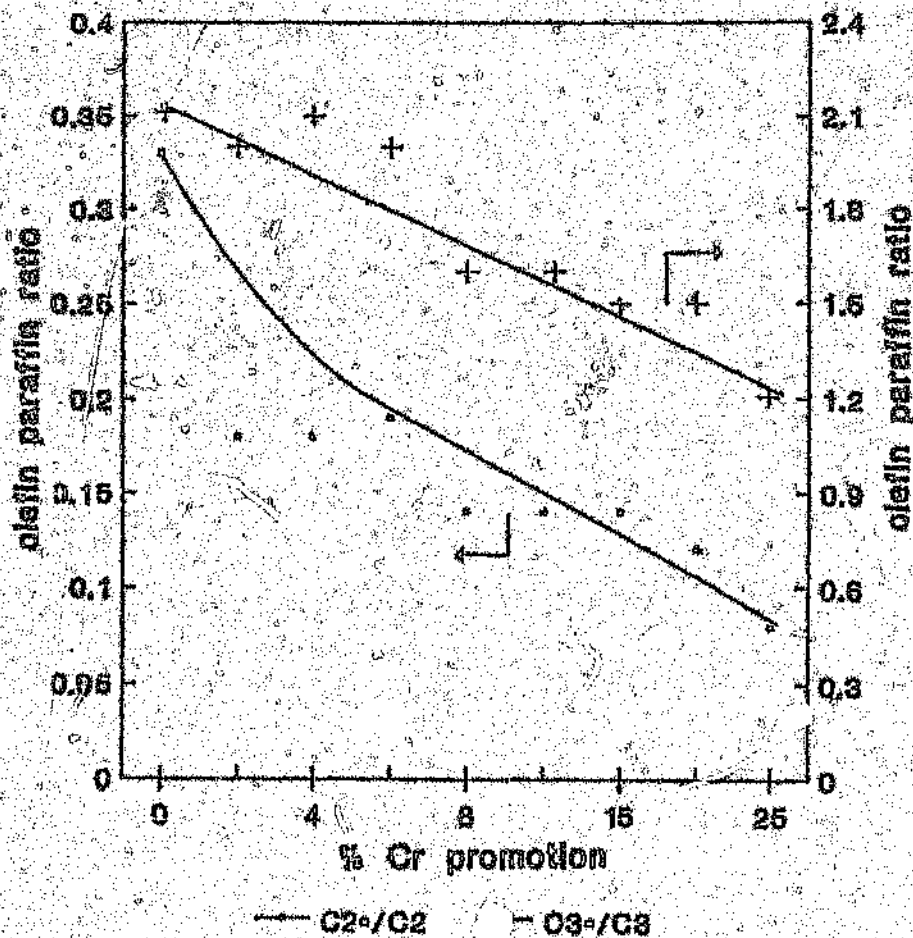
Figure 4.6: Plots of C_2 and C_3 olefin to paraffin ratios as a function of Cr promotion.

The ethene olefin paraffin ratios showed an initial marked decrease on addition of only small amounts of Cr (i.e.2%), beyond which the ratios decreased steadily at approximately the same rate as for the C_3 fraction. This decrease in C_2 olefinity with initial 2% loading, initially suggested the

possibility that some of the ethene may have become included in the polymerization to the longer chain hydrocarbons.

4.3.3   Catalytic activity

A surprising observation in this study was that *no* significant deactivation was apparent with increasing Cr promotion (even as high as 25% loading), during synthesis studies – see Table 4.1 and Figure 4.7.
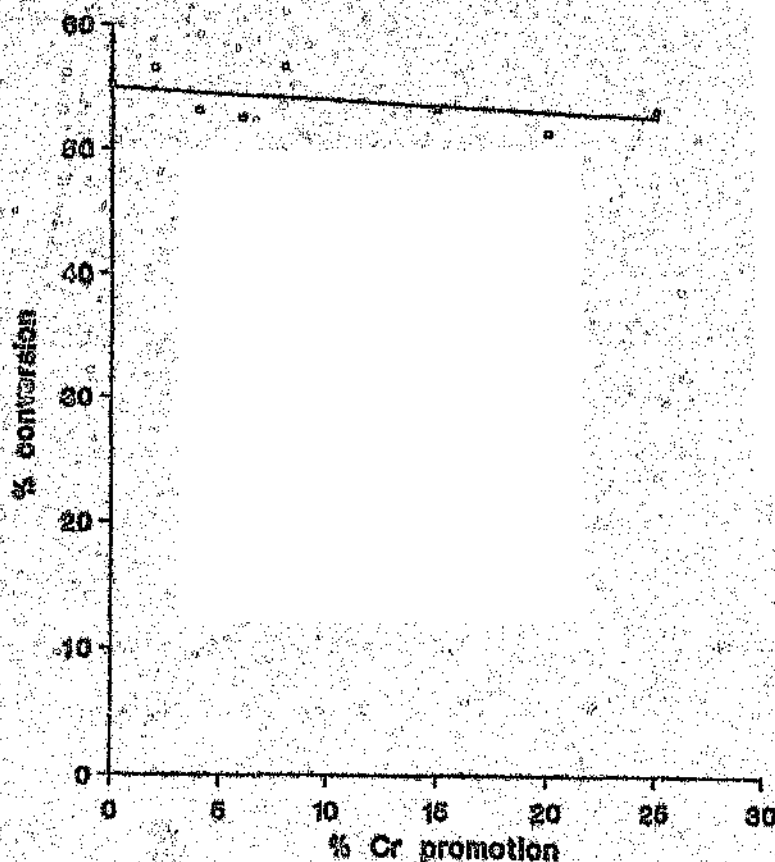
Figure 4.7:   A plot of catalyst activity (% CO conversion) as a function of Cr promotion.

This would lead one to believe that the Cr promoter was not participating in, or exerting an influence on a chemical step (i.e. electronic interaction) in the

F—T synthesis. It is to be remembered that only small amounts of the electronic promoter K (e.g. ~0.2% K promotion — Chapter 3) was found to be optimum for increased olefin selectivities of the same Co catalysts. The Cr promoter could thus probably be exerting a minor structural influence, modifying for example, the texture and porosity of the catalyst surface, that would consequently influence the small change in catalyst selectivity. Surface and bulk characterization measurements (i.e. XPS, surface area and XRD analysis) performed on the catalyst systems, were consistent with the fact that certain surface changes had occurred on Cr promotion. This will be discussed in further detail in Section 4.3.6.

4.3.4   Optimization studies

The influence of reactor pressure, space time and temperature on selectivity toward the light to medium wax fraction was investigated in an attempt at maximizing these selectivities with reactor operating conditions. The optimization studies were performed on 10% Cr promoted Co/MnO catalysts.

(a)   Effect of pressure

Increasing the pressure had a marked effect on increasing the selectivity toward the longer chain hydrocarbons, and also increased both the extent of conversion and oxygenate content. This is illustrated by the data of Table 4.3 and Figure 4.8, and the trends are to be expected on thermodynamic grounds because of the contraction in volume which takes place upon reaction (6).

TABLE 4.3: Effect of pressure on activity and selectivity[a]

Pressure	CO conversion (%)	wax	% converted CO to oxygenates[b]	gaseous hydrocarbons
220	39.3	7.2	1.3	87.5
500	54.8	22.0	5.7	69.7
1000	55.6	37.2	8.1	52.3

[a] constant operating conditions: $T = 220°C$ and GHSV ≈ 250 h^{-1}
[b] oxygenates = primary alcohols
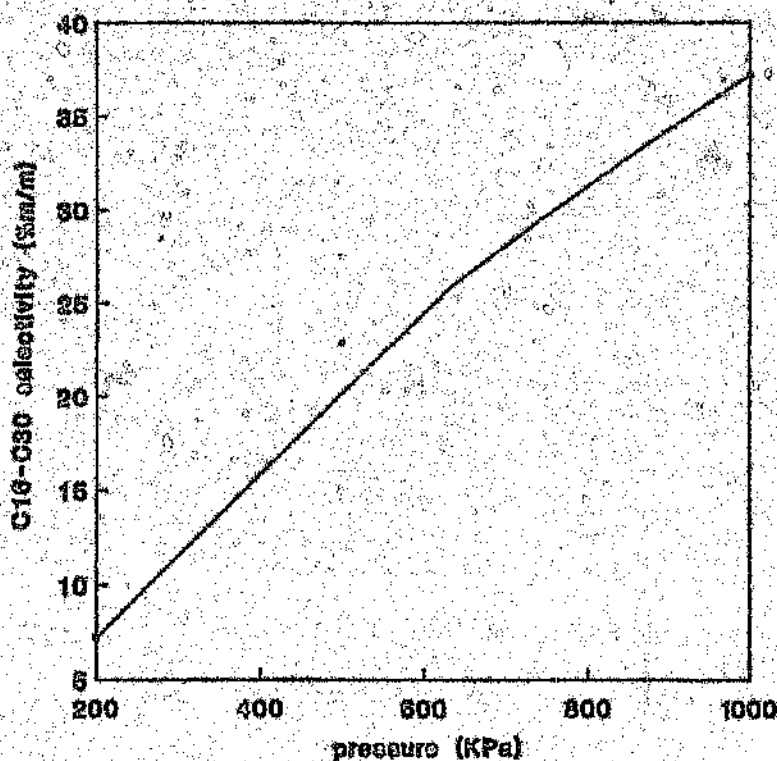
Figure 4.8: Plot of $C_{16}-C_{30}$ selectivity as a function of reactor pressure.

Our results are consistent with work performed by other authors who indicated that in general, on increasing pressure the hydrocarbon

selectivity shifted toward the heavier products. For example, the effect of pressure on product chain length over a ruthenium catalyst at 453 K is given in Figure 4.9 (26). Figure 4.9 also shows that beyond a certain point the yield of heavy products begin to fall off with further increase of pressure. This has been attributed to carbonyl formation, but may also be due to the blocking of the catalyst surface by high molecular weight products (26).
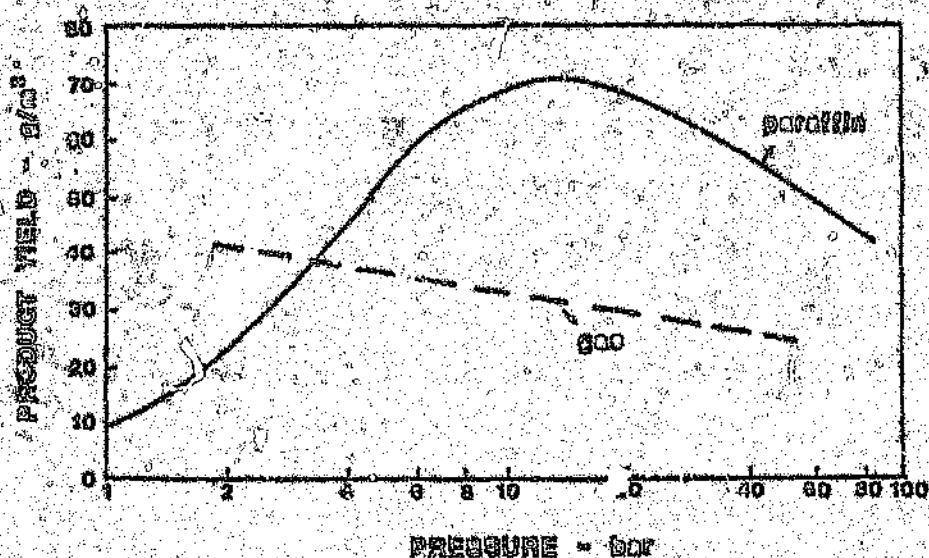
Figure 4.9:   Effect of pressure on chain length (26) [From Pichler. H., "Gasoline synthesis from carbon monoxide and hydrogen" *Advances in Catalysis*, Vol. IV, (1952)].

Similar results were observed by Fischer and Pichler (10), who found that on increasing the pressure from 0 to 15 MPa, the wax selectivity of their cobalt catalysts increased up to 1.5 MPa and then decreased, corroborating the trends shown in Figure 4.9. Furthermore, new high pressure fixed–bed reactors which operate at 45 bar (a 50% increase),

which were successfully commissioned at Sasol 1 (South Africa) in 1987, and increased the Sasol F-T wax production by 50% (63).

The observed influence of pressure is not likely to be due to the total pressure per se, but to the partial pressures of CO, H_2, CO_2 and H_2O (10). Studies performed with an alumina supported ruthenium catalyst in the temperature range 170° to 300°C showed that the partial pressure of CO was the dominant parameter which controlled the selectivity spectrum (155). Thus, on lowering the H_2/CO ratio of the feed gas for such a system, the average molecular mass of the product is expected to increase, and this was found to be the case for studies performed on certain Co catalysts (14). Although the mechanism of the F-T synthesis is not completely understood, it would seem likely that the greater the surface hydrogen concentration the greater the likelihood of chain termination. Conversely, the greater the surface carbon concentration, the greater will be the probability of chain growth (10). Thus the ratio of the chemisorbed hydrogen and carbon entities should play a role in determining the product selectivity. If it is assumed that the relative amounts of surface hydrogen and carbon is proportional to the partial pressures of H_2 and $CO + CO_2$ respectively, then the factor which controls selectivity could have the general form $ap_{H_2}^x/(ap_{CO}^y + cp_{CO_2}^z)$ (it). Factors which may influence the relative values of the constants a, b, c, x, y, z are for example the presence of promoters, temperature and the use of various catalyst supports.

(b) Effect of temperature

The influence of temperature on the product selectivity is presented in Table 4.4.

TABLE 4.4: Effect of temperature on activity and selectivity[a]

Temperature/°C	160	190	220	250
conversion/%	7	18	54	78
Product Selectivity (% m/m)				
C_1	3.2	12.0	10.9	27.5
C_2	1.7	11.2	9.2	9.3
C_3	3.6	22.1	16.7	21.5
C_{16}–C_{30} fraction	tr	tr	22.9	5.6
% of genates[b]	tr	tr	5.7	10.3

[a] constant operating conditions: p = 500 kPa and GHSV ≈ 250 h⁻¹
[b] oxygenates = primary alcohols

The data of Table 4.4 shows that as the operating temperature is increased the rate of reaction increases and the product selectivity shifts to lighter molecular mass compounds. [At low temperatures and consequently low conversion no condensate material was collected and thus it can be assumed that the formation of these products was negligible (cf. Chapter 3).] The oxygenate content was also observed to increase with increasing temperature. Other workers reported similar findings; operating nickel and ruthenium catalysts at low temperatures (< 200°C) produces a high proportion of wax, but at higher temperatures (> 300°C) methane is the principle product formed (10). King (168), using Ru/Aℓ₂O₃ catalysts, also showed a shift to methane formation from heavier products on increasing the reaction temperature from 175° to 250 °C. The influence of temperature on the selectivities of a Sasol precipitated iron catalyst operating in a fixed bed

is demonstrated in Table 4.5 (10). The selectivity is shown to shift away from the heavier products.

TABLE 4.5: The influence of temperature on the selectivity of a fixed bed Sasol iron catalyst

Temperature/°C	Hard wax[a] selectivity/% C atoms
213	47
227	34
237	24
247	17

Table by courtesy of M.E. Dry (10), Sastech (R and D), Sasolburg, South Africa.

[a] Hard wax is that fraction boiling above 500°C.

(c) Space time

The influence of space time on the light to medium wax function selectivity was investigated by increasing the feed-gas flow rate at fixed pressure (500 kPa) and temperature (220°C). The average molecular weight of the products was found to be sensitive to changes in space time, increasing as the space time increased – see Table 4.6 and Figure 4.10. For space times greater than ~4 x 10^{-3} h^{-1} (i.e. GHSV ~250 h^{-1}), the wax selectivity (C$_{16}$$^+$) remained relatively constant, which suggested that at increased conversions and contact times, the selectivity toward the heavier hydrocarbons was high.

TABLE 4.6: The effect of space time on activity and selectivity[a]

space time/h	0.8×10^{-3}	3.8×10^{-3}	7.7×10^{-3}
conversion/% CO	11.4	54.8	64
Hydrocarbon selectivity/(%m/m)			
C_1	14.1	10.9	9.8
$C_2^=$	0.6	1.1	1.8
C_2^-	9.3	8.1	6.4
$C_3^=$	8.2	10.2	14.1
C_3^-	11.6	6.5	7.0
C_4–C_{15}	48.8	28.5	29.4
$C_{16}^=$	3.3	26.6	22.8
oxygenates	0.9	5.7	6.1

[a] Constant temperature (220°C) and pressure (500 kPa)
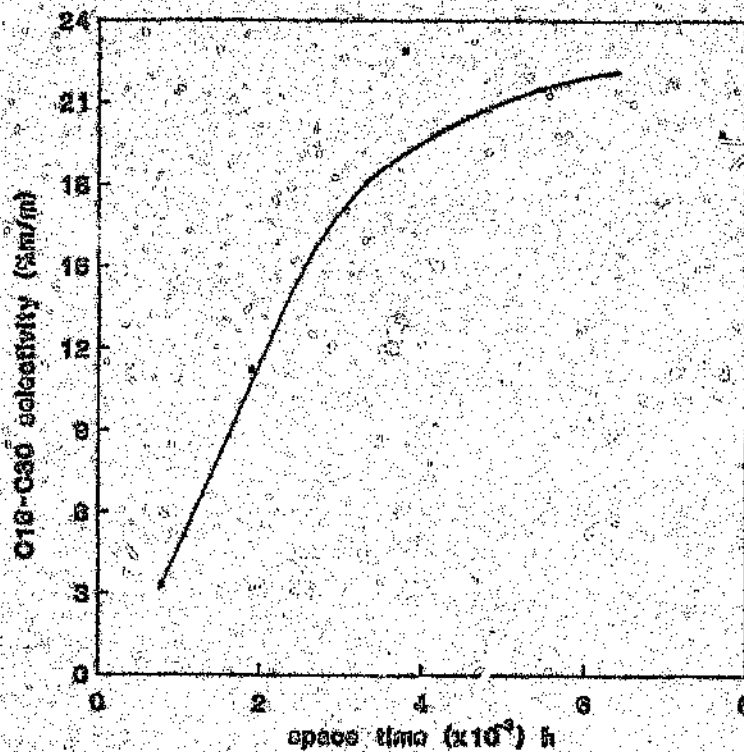
Figure 4.10: Effect of space time on the selectivity toward the C_{16}–C_{30} fraction.

As previously mentioned [cf. Section 3.3.2(d)] it is difficult to isolate the effect of this variable, since conversion decreases with decreasing space time [low conversions have been found to be synonymous with low C_{10}^+ fractions (cf. Chapter 3)]. However, the observed decrease in selectivity toward the heavier hydrocarbons may be attributed to decreased contact times as a result of decreased space times, which would consequently decrease the probability of chain growth. Also, on increasing space time, the catalyst appeared to become less hydrogenating, as was evidenced by decreased methane yields and an increase in olefinity of the C_2 and C_3 fractions (Table 4.6). Decreased hydrogenation activity with increased space times, could influence the termination step during chain growth, thus promoting longer chain products. These results are consistent with studies performed by Arakawa and Bell (129), who also observed increases in the average molecular weight of the products and increased olefin to paraffin ratios with increasing space times – see Table 4.7.

TABLE 4.7: Effects of space velocity on product distribution[a]

(Catalyst: 20% Fe/Al_2O$_3$)

GHSV (at STP)	CO conv./%	C_1	$C_2^=$	C_2^-	$C_3^=$	C_3^-	C_4	C_5	C_6^+
3000	11.7	27.3	6.4	2.4	17.2	0.5	10.8	8.2	14.9
6000	7.1	32.5	20.3	0.8	20	0.3	11.2	5.4	7.1

[a] From Arakawa and Bell (129)

4.3.5 Reduction procedure

As previously mentioned, it was initially assumed that the Cr promoter could adopt the function as a polymerization agent, as in the

Phillips Catalysts (158,160,162). If this were to be the case, then essentially a bifunctional catalyst would exist, one active for CO hydrogenation (Co/MnO), and the other involved in the polymerization of F–T products, i.e. C_2^* and C_3^* (Cr(II) active sites). Thus an optimum reduction procedure favouring both catalytic systems would have to be determined.

The oxidation state of the active Cr sites for the Phillips catalyst has been proposed as Cr(II) obtained from the reduction of Cr(VI) [158–160,169,170]. The removal of water during the reduction is crucial, since at high temperatures ($> 300°C$), H_2O becomes mobile and chemically more active, oxidising Cr(II) to Cr(III). It also has the tendency of existing in the form of Cr^{3+} clusters, which apparently are stabilized by a strong crystal field, which is characteristic of α-Cr_2O_3 (157), as shown in equation 1. Even at a low relative water vapour pressure ($P_{H_2O}/P_{H_2} > 8 \times 10^{-9}$) chromium(II) oxide is not thermodynamically stable. This effect of water influences the degree of reduction directly [157]. It has also been shown that reduction

reduction   Hydrolysis   cluster formation   (1)
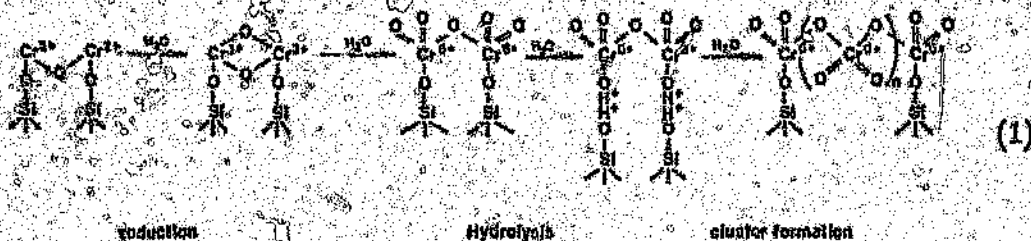
at 350°C improves activity, whereas higher temperatures destroy the activity (169). It has been thought that this may indicate the rearrangement of the Cr(II) into a less coordinatively unsaturated form — possibly aggregates (169) — see equation I.

During the reduction of our Co/MnO catalyst (for which the optimum reduction temperature of the non–promoted catalyst has previously

been shown to be at 400°C — cf. Chapter 5), the Cr would be subject to exposure to H_2O formed during the reduction process. Under these circumstances the presence of the active Cr polymerization valency of (II) i.e. Cr^{2+}, would be highly improbable since in the presence of H_2O the oxidation of Cr^{2+} to Cr^{3+} has been shown to take place. Rather a clustering of Cr^{3+} ions, similar to that illustrated in equation 1, probably associated with MnO, would occur.

From the above discussion, coupled with the selectivity data for ethene and propene formation of Table 4.1, it may be concluded that Cr did not act as a polymerization centre, but possibly acted as a structural promoter in our reactions. The reduction procedure could thus be important in influencing certain structural properties such as pore volumes and surface areas, as a result of possible Cr clustering occurring during the reduction. The variation of reduction temperatures of a 10% Cr promoted Co/MnO catalyst was thus investigated, with reduction being carried out at temperatures of 200°, 300°, 400° and 500°C. Subsequent catalytic performance for CO hydrogenation is given in Table 4.8 The reduction temperature for the Co/MnO catalyst promoted with 10% Cr, was also found to be optimum at 400°C. High methane and low wax selectivities, are as a result of incomplete reduction of the Co metal, for reductions carried out at 200° and 300°C. Reduction at 500°C also resulted in a drop in activity and low wax selectivity, possibly as a result of Co sintering at these high reduction temperatures. Furthermore, the behaviour of the Cr/silica catalysts has been shown to be dependent on the activation temperature, with activity dramatically increasing on increasing temperature from about 400° to 600°C (157,158,169). There has also been shown to be an inverse correlation between the activity of the catalyst and the hydroxyl population on the silica, with

the catalyst becoming more dehydroxylated with increasing temperature, and consequently becomes more active for the polymerization of ethylene. The operating temperatures of our Cr promoted Co/MnO catalysts were well below the optimal temperature range quoted for the Cr/silica activation (i.e. dehydroxilation). Also the presence of free water in the reactor would poison the active Cr sites by possible hydroxylation. These factors further corroborate the unlikelihood of our Cr–Co/MnO system assuming the Phillips–catalyst type polymerization behaviour.

A Cr additive has been shown to increase the activity and selectivity of a silica–supported Ni–Cr solid (tested for ethane

TABLE 4.9: **Effects of different reduction temperatures on catalyst activity and selectivity[a]**

reduction temperature/°C[b]	200	300	400	500
conversion/% CO	4.3	17.2	54.8	22.0
Product Selectivity/% m/m				
C_1	29.3	29.7	10.9	8.4
C_2	16.2	11.9	9.2	10.2
C_3	14.9	13.7	16.7	27.0
C_4–C_{15}	38.4	41.7	32.9	49.3
C_{16}–C_{50}	tr	tr	22.9	2.1
% oxygenates[c]	tr	tr	5.7	0.4

[a] reactor operating conditions, T = 220°C, P = 500 kPa and GHSV = 250h⁻¹
[b] catalysts were reduced at each of the above temperatures for 16 hrs under H_2.
[c] oxygenates = primary alcohols

hydrogenolysis, and benzene and CO hydrogenation). It was proposed that the presence of Cr considerably promoted the reduction process (162). An incomplete reduction of these Ni–Cr catalysts was reported to be due to the existence of an irreducible compound such as $NiO–Cr_2O_3$. This was not found to be the case for our Co/MnO catalysts, as was manifest by the activity and selectivity remaining approximately constant with addition of Cr promoter. Similar compounds such as $MnO–Cr_2O_3$ could be present in our Co/Mn system and associated with the formation of Cr aggregates (as previously mentioned).

4.3.6 Bulk and surface characterization

The surface and bulk compositions of Cr promoted (and non-promoted) Co/MnO catalysts were investigated by several techniques; namely XRD and XPS analysis and surface area measurements. This study was carried out in an attempt at formulating a better understanding of the mode of operation of the Cr promoter.

(a) XRD analysis

X-ray diffraction was performed on a series of calcined Co/MnO catalysts promoted with increasing levels of chromium (i.e. from 0 to 30%). From the resulting diffraction spectra [examples of which are given in Figure 4.11(a) and (b)], the calcined catalyst precursors were identified as the mixed Co/Mn oxide spinel, $(Co,Mn)(Co,Mn)_2O_4$ – (cf. Chapter 5). The series of diffractograms for the various Cr promoted catalysts suggested that no change in the bulk structure had occurred as a result of Cr addition, even for catalyst containing 30% Cr – see Figures 4.11(a) and (b).

Thus if absent in the bulk, the promoter should be concentrated on the catalyst surface; — this was verified by an XPS analysis performed on the catalyst surface.

(b) XPS analysis

XPS analysis was performed on a 10% Cr-promoted catalyst before and after calcination (500°C, 24 hrs in air); results of which are given in Table 4.9.
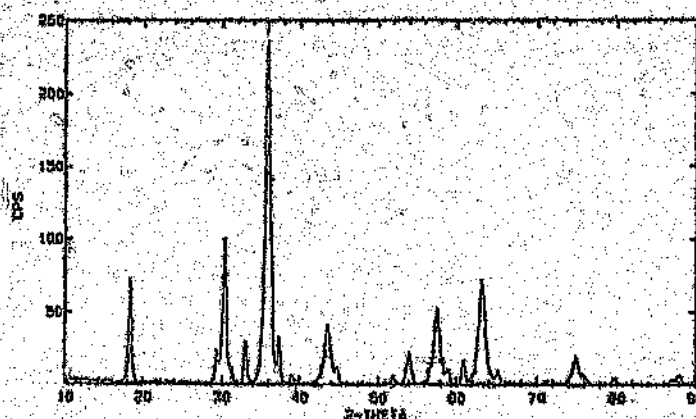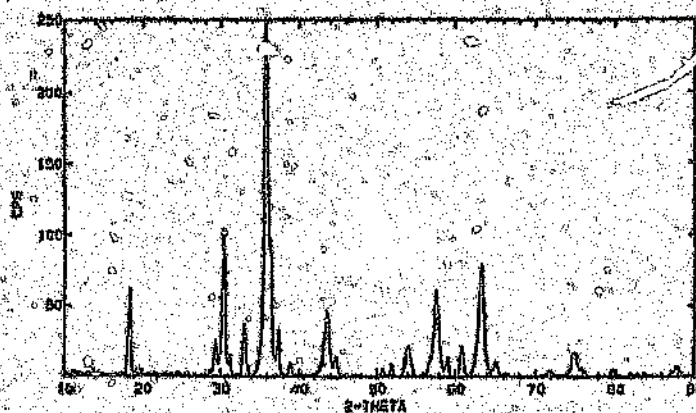
Figure 4.11(a) and (b): X-ray diffraction spectra of a calcined Co/MnO catalyst with a, 0% and b, 30% Cr promotion.

TABLE 4.9: XPS analysis of a 10% Cr-promoted Co/MnO catalyst before and after calcination

	C	O	Mn	Cr	Co	
before calcination	19.3	25.7	22.9	3.4	28.8	Relative mass %
	29.7	42.7	11.1	1.7	14.8	Relative atomic %
after calcination	4.5	31.4	34.0	7.6	22.3	Relative mass %
	10.6	55.6	17.5	4.2	12.2	Relative atomic %

From the XPS data of Table 4.9 it is evident that the Cr promoter is observed on the catalyst surface. After catalyst calcination there is an observed increase in the surface % Cr concentration, (see Table 4.9). Thus after calcination, the majority of the Cr promoter is concentrated on the catalyst surface, corroborating the observation from the XRD analysis. Also, after calcination the Co surface concentration was shown to become slightly depleted, whereas the Mn surface concentration was observed to increase. This suggested a possible Cr–Mn support interaction (171), possibly in the form of $MnO–Cr_2O_3$ or $MnO + Cr^{3+}$ aggregates as previously mentioned (cf. Section 4.3.4). Decreased C and increased O surface concentration are as a consequence of the calcination procedure.

The presence of Cr on the catalyst surface, as well as the changes in peak intensity of the relative components of the catalyst system before and after calcination, are demonstrated in Figure 4.12(a) and (b) respectively (the respective peaks are marked).
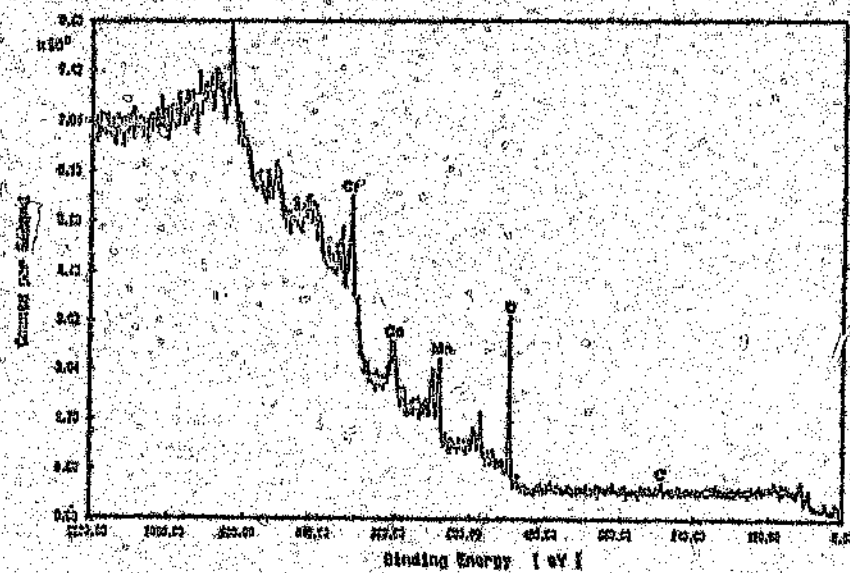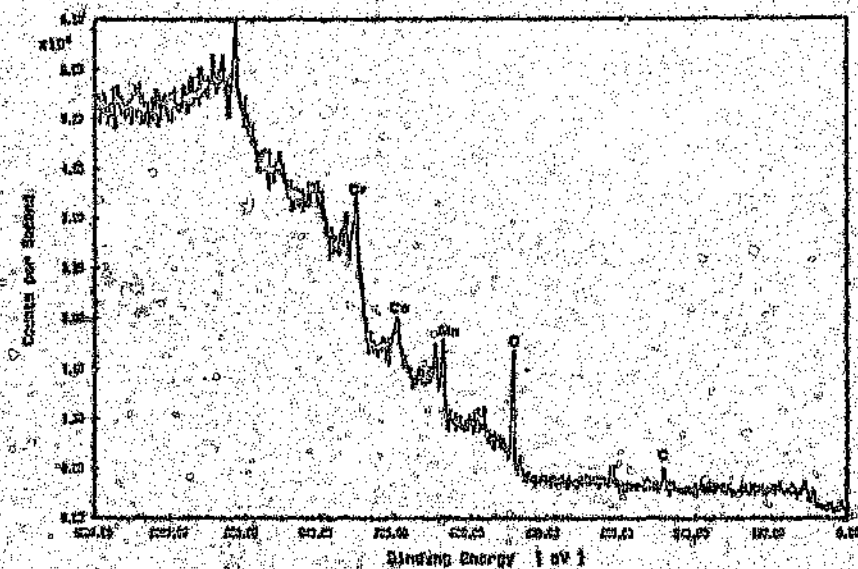
Figure 4.12(a) and (b):   X-ray photoelectron spectra of a 10% Cr-promoted Co/MnO catalyst a, before and b, after calcination (note the change in intensity of the relative peaks before and after calcination

(c) <u>Surface area measurements</u>

BET surface area measurements were performed on a series of calcined Cr–promoted Co catalysts; results of which are given in Table 4.10.

<u>TABLE 4.10:</u>   <u>BET surface areas of a series of Cr promoted Co/MnO</u>
<u>catalysts</u>

Cr promotion/%	BET surface area/m^2 g^{-1}
0	11.6
2	11.6
4	11.7
8	12.9
15	16.0
25	16.7

The surface area measurements of Table 4.10 showed that no significant change in the surface area had occurred, with addition of Cr promoter. As previously determined (XPS analysis), the Cr promoter is concentrated on the catalyst surface, thus at 25% Cr promotion, one would expect there to be more significant change in surface area than is actually observed. The absence of an increased surface area with higher Cr loadings could be due to the formation of possible surface Cr conglomerates (discussed earlier), which would minimize their influence on surface area.

4.3.7   <u>Possible mechanism of promoter action</u>

Although our understanding of the mechanism of Cr promotion in the formation of longer chain hydrocarbons remains incomplete, certain

proposals can be made from catalyst characterization studies (surface and bulk), coupled with inferences made from the literature on the behaviour of Cr–based catalyst in similar enviroments.

Initially it was thought that the Cr promoter could have become an active site for polymerization (polymerizing $C_2^=$ and $C_3^=$ products from F–T synthesis), based on Cr/silica industrial catalysts (Phillips Catalysts) for the polymerization of ethene (169). Owing to the sensitive parameters required in thermal activation of such catalysts (15, 59,169), which are dissimilar to thermal treatments performed in the pretreatment of our Co/MnO catalysts (85), the likelihood of forming an active Cr site with the correct valency (Cr^{2+}) and coordination, is minimal. Also, Cr^{2+} has been reported to be thermally unstable (157) and easily oxides to Cr^{3+} in the presence of H_2O, which also has the tendency to form clusters (α–Cr_2O_3) on the catalyst surface (as previously discussed). Since H_2O is a primary product of CO hydrogenation, the survival of the active Cr^{2+} site (if at all present from initial catalyst pretreatments) would be highly unlikely. In addition, no significant decrease in selectivity toward propene or ethene fractions, with addition of Cr (i.e. with increased wax yields) were observed, thus corroborating the above argument.

The relatively constant catalytic activity observed with increasing Cr promoter, minimized any influence of Cr as an electronic (chemical) promoter. In contrast, the addition of only small amounts ($< 0.5\%$) of potassium (electronic promoter, cf. Chapter 3) to the catalyst system was shown to decrease activity; increased loadings ($> 0.5\%$) result in catalyst deactivation. [In general, the influence of chemical promoters originate from electronic interactions with the catalytically active metal which modifies

catalytic activity (172)]. In silica–supported nickel–chromium solids, the presence of Cr has been shown to affect neither the electronic properties of nickel nor its activity in ethene hydrogenolysis and benzene hydrogenation, at low temperatures. However in CO hydrogenation, Cr addition was observed to indirectly increase activity, resulting from the increased reducibility of nickel in the presence of chromium (162). Although the *individual* oxides, ZnO, MnO and Cr_2O_3 have been shown to be efficient catalysts for methanol synthesis, it has been proposed that in the mixed oxide $ZnO–MnO–Cr_2O_3$, Zn and Mn may be the active elements, with Cr_2O_3 activity as a structural promoter (35).

From the foregoing discussion, the function of Cr (in our Co/MnO catalysts) as a polymerization agent or an electronic promoter appear to be discounted. The role of Cr as a structural promoter, physically influencing chain growth in some way, was thus considered. Structural promoters are in general, difficult to reduce high melting oxides such as Al_2O_3, ThO_2, MgO and CoO. Their principal function is to modify the physical attributes of the catalytically active phase, such as increasing the surface area of the reduced catalysts and improving temperature stability by inhibition of crystal growth (10,172). The chromium promoter could be in the form of Cr_2O_3 (as previously described) conforming in part to the above description of a structural promoter. Although Cr was observed not to significantly increase surface areas (Table 4.10), thermal stabilization of the surface active Co metal sites from a physical Co–Cr interaction could be possible. Cr has been thought to act as a physical promoter in Zn–based catalysts for alcohol synthesis (161), by stabilizing the active ZnO species through formation of a Zn–Cr spinel, which acts as a support and increases the surface area. In this study Cr was suggested to act as a chemical promoter by decreasing the

activation energy in the decomposition of methanol. Furthermore, the physical effects of mean pore diameter have been shown to be related to the chain length of the hydrocarbon products (75). Adsorption–desorption kinetics have shown pore condensation and filling can occur with products which have a chain length related to the pore size. Increased residence times as a result of smaller pores, increase the chance of product re–adsorption, and thus increase the probability of chain growth, resulting in longer chains. Cr/silica catalysts have been shown to exhibit a strong correlation between their porosity and the molecular weights of the polymer produced; the larger the average pore diameter of the silica, the lower the molecular weight of the product (169). Modification of pore diameters due to Cr clustering on the Co/MnO catalyst surface (*after the reduction and subsequent CO/H₂ reaction*) could play a role in increasing the molecular weight of the hydrocarbon products.

4.4   CONCLUSION

The incorporation (by incipient wetness) of the Cr promoter into the co–precipitated catalyst system substantially increased the selectivity toward the longer chain hydrocarbons i.e. C_{10}^+ fraction. This effect was observed with the lowest Cr level studied i.e. 2% Cr, with activities and selectivities remaining approximately constant on further addition of promoter (to levels as high as 25% Cr). Shifts in selectivity toward the heavy hydrocarbons on addition of Cr promoter was substantiated from the increased chain growth probability factor. In addition, thermogravimetric analysis performed on wax samples from promoted and non–promoted catalysts, demonstrated a greater sample mass loss, over the same temperature range, for the non–promoted sample.

The observed shift in selectivity toward the higher hydrocarbon fractions was accompanied by a general shift in selectivity away from the lower hydrocarbon fraction (with no light carbon fraction in particular, being observed to significantly decrease). The hydrogenation activity of the catalyst was found to generally increase with increased Cr promotion, as evidenced from increasing CH_4 yields, and decreasing C_2 and C_3 olefin to paraffin ratios. An unusual observation was that no significant activity loss was apparent with increasing Cr promotion (even with a 25% loading), suggesting an unlikely electronic influence of the promoter.

The investigation of reactor operating conditions showed high pressures and lower temperatures with moderate space time, to be optimal for increased light to medium wax selectivities. The optimum reduction temperature ($400^\circ C$) was observed not to be influenced by the presence of Cr promoter, with incomplete reduction and possible Co sintering occurring below and above the optimum reduction temperature respectively.

The location of the Cr promoter in the catalyst system was determined by XRD and XPS analysis. XRD analysis suggested that since no change in the bulk structure of a series of calcined Cr promoted catalysts, had occurred, the Cr promoter was probably concentrated on the catalyst surface. This was verified from XPS analysis performed on a calcined and uncalcined 10% Cr–promoted catalyst, which showed high concentrations of Cr on the catalyst surface. After calcination, a further increase in surface Cr concentration was observed, Cr segregation occurring from the bulk to the surface, during this process. An observed increase in Mn surface concentration after calcination, suggested a possible Mn–Cr interaction. No significant change in surface area with increased Cr levels was observed. This suggested

that the Cr could be located on the surface in aggregates due to Cr^{3+} clustering in the presence of H_2O, an effect which did not contribute significantly to the surface area.

The role of the Cr promoter in the selectivity of high molecular weight hydrocarbons has not been completely clarified. The possibility of the Cr promoter becoming an active site for polymerization (polymerization of $C_2^=$ and $C_3^=$ F–T products), was discounted on the basis that the formation of the correct 2+ oxidation state would seem improbable in an oxidizing (F–T active) environment. The active Cr^{2+} would oxidise to Cr^{3+}, which has also been reported to cluster in the presence of H_2O and form stable α–Cr_2O_3 on the catalyst surface. In addition, no significant decreases in ethene or propene selectivities (from F–T synthesis) were observed, corroborating the above suggestion. Since no change in catalytic activity was observed with increasing Cr levels, the influence of Cr as an electronic (chemical) promoter, was assumed to be minimal. The role of Cr as a structural promoter, physically influencing chain growth in some way has to be considered.

CHAPTER FIVE

AN *IN SITU* HIGH TEMPERATURE X-RAY DIFFRACTION
INVESTIGATION OF COBALT/MANGANESE
OXIDE CATALYSTS AND RELATED SYSTEMS

5.1 INTRODUCTION

A large number of inorganic compounds and crystalline phases are known to
be involved in the formation, activation, and deactivation of Fischer–Tropsch
(F–T) catalysts (10,14,104,109). Due to the difficulties of investigating these
materials under typical F–T conditions of high temperatures and reactive
atmospheres, F–T catalysts have often been developed with little knowledge
of the true chemical and physical behavior of the working catalyst. A great
deal of time and effort is presently being spent to identify the chemical and
physical properties which influence a particular catalyst's activity, selectivity
and lifetime.

There are a number of techniques, as summarized in Table 5.1,
that may be applied to the detection and identification of:—

— absorbed species and microscopic action at catalytic surfaces
(surface characterization); and

— various crystalline phases of the catalyst, (bulk characterization).

TABLE 5.1: Characterization techniques used in heterogeneous catalysis

Property sought	Technique used	Reference
location of active material potential poisons	EPMA (electron probe microanalysis)	(10)
characterization of supported catalytic species	TPR, TPO (temperature programmed reduction and oxidation)	(173)
to obtain a detailed picture of atomic environment and coordination, e.g. bond distances and coordination numbers	EXAFS (X-ray absorption edge fine structure)	(174)
direct observation of metal dispersion	SEM,TEM(scanning and transmission electron microscopy)	(10)
to estimate the mean size of supported metal crystallite/dispersion of metal on support	X-ray line broadening, EM	(150)
surface areas	BET and Langmuir chemisorption isotherms	(46)
surface composition	IRAS (infrared reflectance-adsorption spectroscopy)	(175)
	AES(Auger electron spectroscopy) XPS (X-ray photoelectron spectroscopy)	(176)
	SIMS (secondary ion mass spectroscopy)	(177)
extent of reduction/ support interaction	TPR/Mössbauer spectroscopy (Fe)	(10)
crystalline (bulk) homogeneity/phases present	XRD (X-ray diffraction analysis)	(178)
evidence for clusters/ free metals	Mössbauer (Fe) Magnetic susceptibility	(179)
cluster shape	high resolution EM	(180)

The instrumental techniques outlined in Table 5.1, used singularly (or in various combinations) have the potent'l to increase our understanding of heterogeneous catalysts. Although *ex situ* or "post mortem" studies of practical catalysts are capable of yielding useful information about the relationship between structure and reactivity (91,115,133 181,182), such measurements are of limited value for air–sensitive materials. The application of *in situ* physical methods offers the possibility of major progress in this field (181,183,184,186,188). *In situ* methods of catalyst characterization allow for the continuous analysis of catalysts to be performed under realistic reaction conditions, that is, under controlled atmospheres and elevated temperatures. These allow the continuous monitoring of catalyst transformations that occur during catalyst pretreatment and subsequent synthesis.

The identification of more selective CO hydrogenation catalysts has been the subject of considerable recent research in a number of centres (42,187,188). There has been a particular interest in the study of catalysts that demonstrate high selectivities for the production of C_2–C_4 alkenes (as described in Chapter 1 and Chapter 3).

Research has centred on catalysts exhibiting strong metal support interactions for metals supported on, or in solid solution with, a particuly reducible oxide, e.g. $XMnO_x$ (where X is normally a transition metal ion) (43,104,109,110,189). The promotion of cobalt by manganese oxide at low metal loadings, has been found to demonstrate high yields of light alkenes (72,117,190). Recent commercial interest in Co (99,154), coupled with several fundamental studies of cobalt–containing F–T catalysts (42,86,117,190–192), has led to further investigations of our cobalt manganese oxide formulation, which has previously been shown (33,84) to give decreased

methane yields together with enhanced propene formation.

An investigation was made into some of the mechanisms involved in the catalytic action of these cobalt/manganese oxide catalysts (and related systems), by following phase transformations *in situ*, during the activation and operation of such a catalyst. It was considered important to define the nature of the structural changes during calcination and reduction processes as well as under synthesis conditions, since these changes are probably related to the final activity and selectivity of the catalyst system.

Thermal analysis, i.e. Differential Scanning Calorimetry (DSC) was used to study the phase transformations that Co/Mn oxide precursors undergo during pre-synthesis calcination and reduction procedures. Although DSC studies are excellent for pinpointing temperatures at which phase changes take place, this technique is not very specific as to the nature of the various phases involved. On the other hand, powder X-ray diffraction (XRD), has been used routinely for the unambiguous identification of crystalline phases under normal atmospheric conditions and ambient temperatures.

X-ray diffraction of samples under special atmospheric conditions (e.g. vacuum, inert, reducing, etc.) and elevated temperatures, are capable of producing a reliable qualitative phase analysis in most cases. It was thus considered the ideal technique to investigate apparent transformations at temperatures established by DSC, and under the appropriate atmospheric conditions. An *in situ* high temperature X-ray diffraction study was also performed on the Co/MnO catalyst to follow phase transformations, after prolonged periods of F-T synthesis.

5.2   EXPERIMENTAL

The cobalt manganese oxide catalysts (Co/(Co + Mn) ≈ 0.50) used in this investigation were prepared by the co-precipitation procedure as outlined in Section 2.1.1. DSC studies, under the appropriate atmospheric conditions, were performed on a Dupont (9900) Thermal Analyser, as detailed in Section 2.5.1(b). The *in situ* XRD measurements were carried out on a Rigaku Geigerflex D/max IIIA computer-controlled wide angle diffractometer equipped with a high temperature X-ray diffractometer attachment (HTA). A detailed description of the layout and operating conditions of the HTA and diffractometer are   in Section 2.5.1(a). Since X-ray diffraction is a bulk technique and analyse the entire solid matrix of the sample, it was therefore less sensitive than DSC which measures the heat flow to and from the sample with a much greater sensitivity (178). Based on this knowledge the XRD results may not have correlated directly with the DSC, and thus higher temperatures for the XRD analysis were selected to correlate with those temperatures as pinpointed by the DSC thermogram.

5.3   RESULTS

5.3.1   An *in situ* DSC/XRD characterization of structural changes occuring during calcination and reduction of catalyst precursors

Most CO hydrogenation catalysts require a calcination and reduction stage to render the metal species on the catalyst active and in the correct dispersion. Extensive research has been performed by numerous authors (31,32,72,76,189,193,194) on the effects of different pretreatment conditions on catalytic properties. Previous studies with Co/MnO catalysts have shown that the conditions of calcination and reduction of catalyst precursors, can have significant effects on the selectivity and activity of the

final catalyst (85). DSC/XRD experiments were carried out over a range of conditions to characterize the structural and chemical behaviour of the catalyst precursors, and the catalysts derived from them.

5.3.1(a) *In situ characterisation during calcination of catalyst precursors*

The route for producing an intimate mixture of cobalt and manganese oxides at the molecular level is based upon the co-precipitation of the nitrate salts of the respective elements, from an ammoniacal solution. The initially precipitating solid is often found to be a complex mixture of hydroxylic compounds, which are subsequently decomposed to the oxides by heating in air; a process referred to as calcination. Trends have been observed by researchers who have shown that the calcination step can have important effects on the surface and bulk compositions of the catalyst, surface area and pore volumes, the amount of metal support interaction and the degree of metal dispersion on the catalyst support (104,109,117,185,196).

Calcination at a temperature of 500°C for a period of 24 hours, has been shown to be optimal for the Co/MnO system (85). Comparisons of uncalcined and calcined catalysts have indicated the former to show a comparable selectivity but at a depressed activity (62); see Table 5.2. Other comparisons have shown the uncalcined catalysts to produce very high alkene yields with low methane, during the early stages of the CO/H$_2$ reaction. Similar results have been reported by Barrault *et al.* (195), where catalysts calcined at low temperatures were observed to be more active and selective, with the high hydrocarbon fraction containing olefins as major components. On increasing the calcination temperature, a decrease in both the activity and in light olefin selectivity, especially of propene was observed. It has also been observed (62), that the performances of uncalcined and calcined Co/MnO

catalysts (tested under identical experimental conditions), converge with reaction time due to a changing of their surface composition to a common configuration.

The calcination of a fresh, Co/MnO catalyst precursor was monitored in a DSC/XRD experiment, in an attempt to correlate phase composition with the catalytic activity data from Table 5.2. The DSC experiment was performed in the temperature range $25^{\circ}C \rightarrow 500^{\circ}C$, ramping at $5^{\circ}C$ min^{-1}, in air; the thermogram of which is shown in Figure 5.1. The instrument allowed for continuous real–time monitoring and data collection during the calcination procedure. X–ray diffraction patterns were then collected, ex situ, at the temperatures pinpointed by the DSC thermogram, where probable phase changes had taken place (the catalyst samples were held at each of those temperatures for at least 8 hours before an XRD was carried out).

TABLE 5.2: CO hydrogenation of uncalcined and calcined Co/MnO catalysts[a]

	uncalcined	calcined[b]
CO conversion/%	25	43
Hydrocarbon selectivity/% m/m		
CH_4	10.0	8.5
C_2H_4	3.4	3.3
C_2H_6	4.1	3.6
C_3H_6	17.1	16.1
C_3H_8	4.3	3.7
C_4	11.5	10.0
C_5^+	49.6	46.7
total oxygenates	0	8.1

(a) GHSV = 263 h^{-1}, P = 585 kPa, T = $220^{\circ}C$, time–on–line = 275 hours, 2 g catalyst.

(b) calcined in air T = $500^{\circ}C$ for 24 hours.
[Results provided by M. van der Riet] (62).
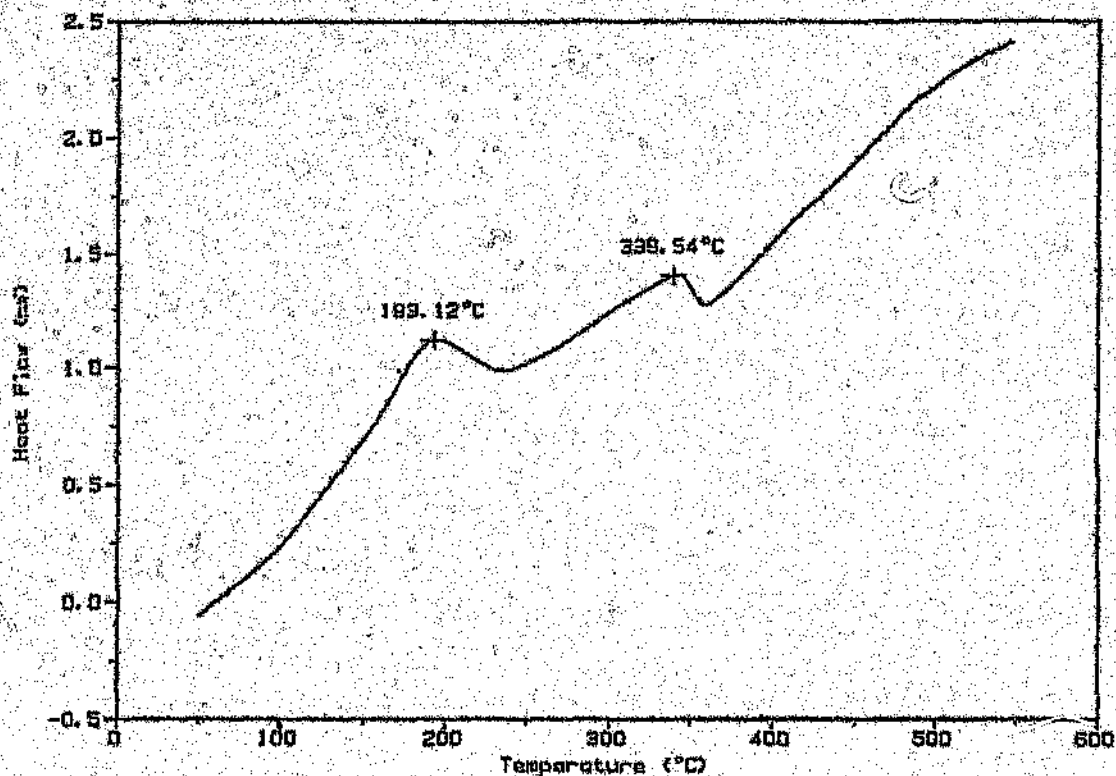
Figure 5.1: DSC thermogram from the calcination pretreatment of a Co/Mn mixed oxide catalyst precursor.[a]

a, DSC thermogram was performed in the temperature range $25^oC \rightarrow 500^oC$, ramping at 5^oC min^{-1}, and then kept isothermal at 500^oC for 1 hour, in air.

An XRD measurement was performed on the uncalcined oxide precursor to determine the initial phases present, as shown in Figure 5.3(a). The diffraction profile was indexed to the "Co/Mn oxide mixed spinel", $(Co,Mn)(Co,Mn)_2O_4$, in which the cobalt and manganese cations occupy each site non-exclusively. The term "mixed-oxide spinel" may be referred to as a structurally active solid-solution of varying composition with a lattice of considerable complexity (62,197). Similar spinel phases of Co/Mn oxide systems, have also been observed by Kuznetsova et al. (197), who reported the presence of a $Co_xM_{3-x}O_4$ mixed oxide after calcining in air at 400°C. A diagram of a simple spinel structure is presented in Figure 5.2.
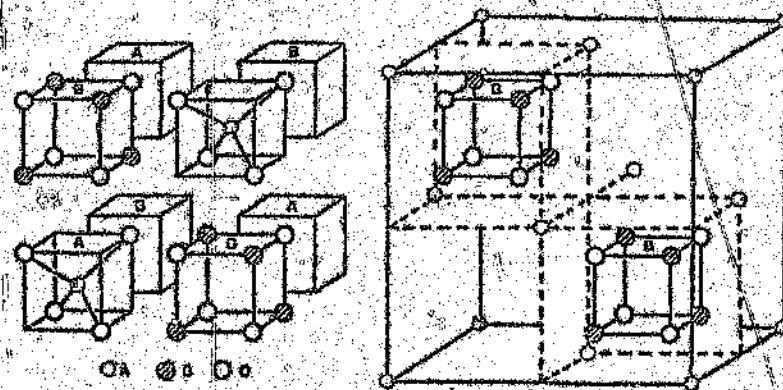
Figure 5.2:   The spinel structure AB_2O_4. The structure can be thought of as eight octants of alternating AO_4 tetrahedra and B_4O_4 cubes as shown in the left-hand diagram.
[From D.M. Adams, Inorganic Solids – John Wiley and Sons, 1974] (198).

The two exotherms of Figure 5.1, at ~195°C and ~340°C, suggested that the calcination of the catalyst involved a two-stage process to its final calcined state. Corresponding diffraction patterns that were collected after calcination at 210°, 360° and 500°C, are shown in Figure 5.3(b), (c), (d) respectively.

These diffractograms showed an increase in peak intensity, indicating a higher degree of crystallinity resulting after each increased calcination temperature. This heightened crystallinity could have been due to an increased degree of substitution of the Co and Mn cations in the octahedral and tetrahedral sites of the spinel structure. The calcination pretreatment thus resulted in the enhanced crystallinity of the Co/Mn oxide precursor (from XRD data), with major crystal growth and structured reordering possibly occurring at ~195°C and ~340°C respectively (from the DSC thermogram).

In order to explain the activity data of Table 5.2, an attempt was made to correlate the effect of calcination on subsequent reduction. Differential scanning calorimetry (ramping from 20°C – 600°C, at 5°C min^{-1}), was thus performed under a flowing hydrogen atmosphere to monitor the differences in the reduction behaviour of an uncalcined and calcined catalyst precursors. The resulting thermograms are presented in Figure 5.4 and Figure 5.5 respectively. The effect of calcination on the subsequent reduction process can be derived from differences in the shapes of the exothermic peaks of the respective thermograms. The exothermic peaks of Figure 5.4 (especially at ~200°C) are broader and less Gaussian than the exothermic peaks of Figure 5.5. This indicated the possibility of a slower reduction process as a result of interference from crystal growth and structural reordering of the oxide spinel,
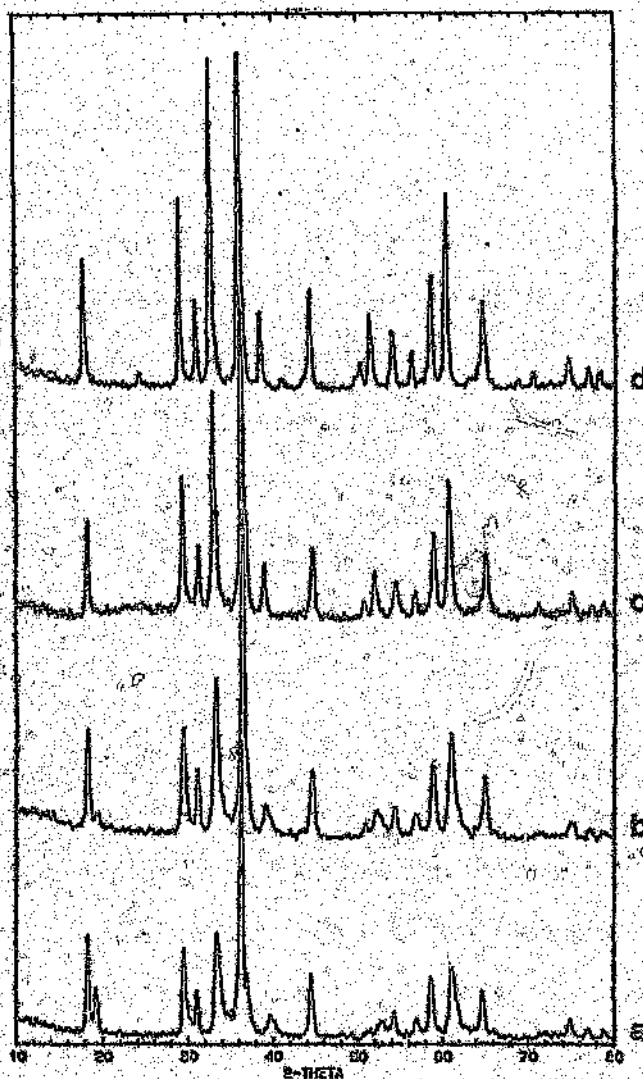
Figure 5.3(a)–(d):   Corresponding diffraction patterns obtained from the calcination procedure of a Co/Mn oxide catalyst precursor.

(a)–(d)   XRD diffraction patterns were collected from an *ex situ* study with diffraction patterns being collected at calcination temperatures of 20°, 210°, 320° and 500°C (in air).

which should have otherwise occurred during the calcination step. This is reflected by the initial lower syngas conversion of the uncalcined catalyst — see Table 5.2. In support of this statement, the exothermic peaks associated

with the thermogram during calcination (Figure 5.1) that also coincide with the exothermic peak positions during reduction, were found to be broad, suggesting some influence of the changes associated with calcination occurring during reduction of the uncalcined sample. Also, the slow reduction of the uncalcined catalyst is corroborated with the earlier observation, that the uncalcined and calcined precursors reach some common configuration only after long periods of reaction with CO/H_2. This would lead one to believe that structural ordering and further reduction of the uncalcined sample occurs, under the influence of CO/H_2, during this period.

5.3.1(b) An in situ characterisation during reduction of the calcined catalyst precursor

The high temperature H_2 reduction of mixed transition metal oxide catalysts generally reduces them down to a low oxidation state, and this in turn affects the activation of such catalysts. Several researchers have established that the reduction temperature of such catalysts e.g. Fe/MnO (199,200) and Co/Al_2O_3 (82), can have decisive effects on their structure and properties, with respect to phase composition, crystallite size, degree of reduced metal dispersion on support, strong metal support interaction and surface areas.

CO/H_2 reactions over a Co/MnO ca   after reduction have shown (62) that the reduction has to be effected at a temperature of 400°C for at least 16 hours if optimal catalytic properties are to be attained – see Table 5.3. From these results it is obvious that for the catalyst treated at 200°C, the reduction is far from complete and thus resulted in an inactive catalyst when compared to the catalyst whose reduction was carried out at a temperature of 400°C.
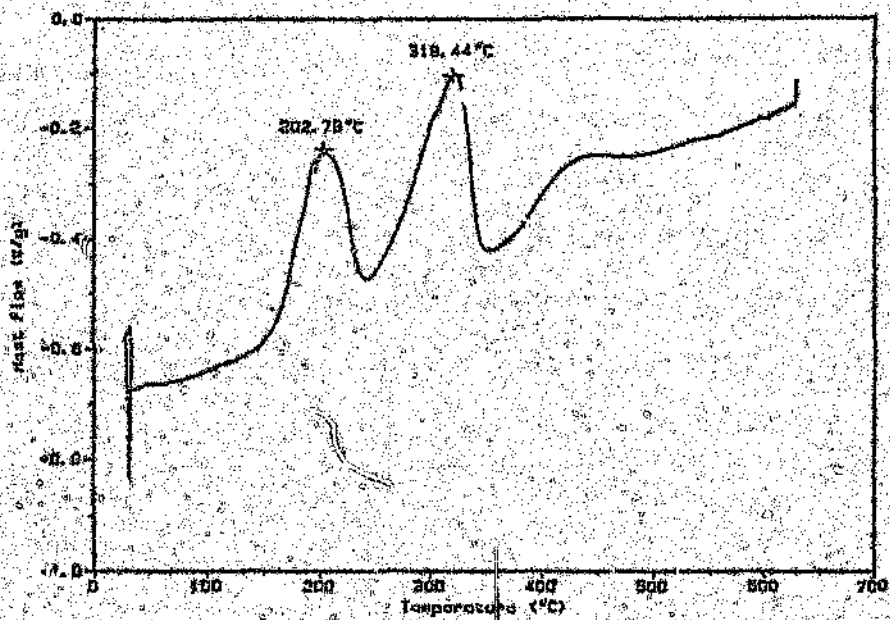
Figure 5.4: DSC thermogram of the *in situ* reduction of an uncalcined Co/Mn oxide precursor.
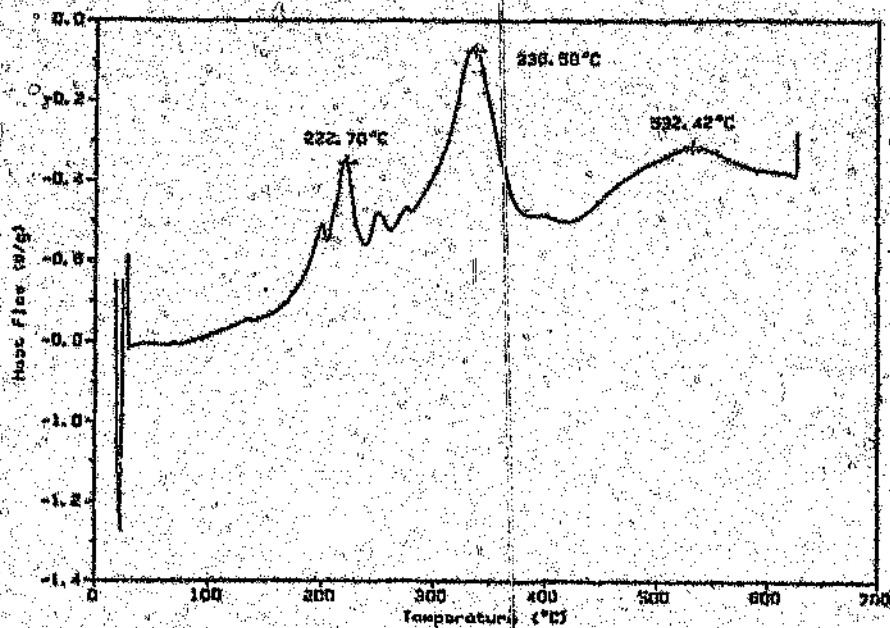
Figure 5.5: DSC thermogram of the *in situ* reduction of a calcined Co/Mn oxide precursor.

The reduction, after calcination of a Co/MnO catalyst was also followed by *in situ* DSC/XRD analyses in an attempt to correlate changes in catalyst composition and structure, during this reduction, to subsequent activity data (e.g. Table 5.3). Particular attention was given to following the evolution of the various solid phases with increase of temperature under a hydrogen environment. DSC measurements of the reduction were performed under a controlled hydrogen atmosphere, with the temperature being increased from 20 to 500°C, at a rate of 5°C min⁻¹. A resulting thermogram is shown in Figure 5.6.

TABLE 5.3:   Effect of reduction temperature on the performance of a Co/MnO catalyst [a]

Reduction T/°C	200	400	430
Time-on-line/h	79	47	88
GHSV/h⁻¹ [b]	290	310	269
CO Conversion/%	1	31	14
Hydrogen Selectivity/% by mass			
CH_4	100	6.1	6.6
C_2H_4	Tr	1.7	1.0
C_2H_6	0	1.0	0.5
C_3H_6	Tr	6.7	2.7
C_3H_8	0	1.1	0.6
C_4	0	8.8	2.7
C_5^+	0	74.6	62.1
oxygenates	0	0	24.0

[a] $CO/H_2 = 1:1$ v/v, T = 190°C, P = 585 kPa, 2.0 grams of catalyst;
[b] measured at STP.

[Results provided by M. van der Riet] (82).

After a further 12 hours under H_2 at 400°C, an additonal diffractogram was obtained. At this stage it was found that the metallic Co peak (as in Figure 5.7) had appeared to have grown in size, and it was therefore decided that a series of diffractograms would be taken after 31, 36 and 44 hours, under H_2 at 400°C. There was no indication of further growth of the Co peak as demonstrated by the series of diffre..ograms shown in Figure 5.9. The temperature of the HTA was then lowered to 220°C, in preparation for the syngas experiments, and after 6 hours at this temperature under H_2, an XRD was run. The diffraction profile showed the catalyst to have remained in its reduced state, at that temperature.
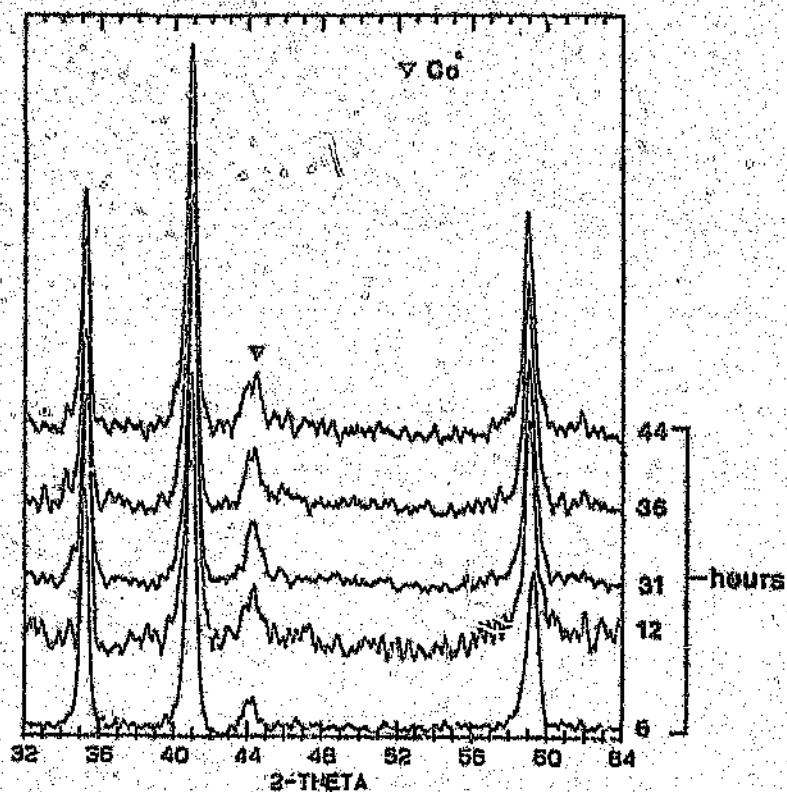
Figure 5.9: A series of diffractograms performed over a period of 48 hours, under H_2 at 400°C.
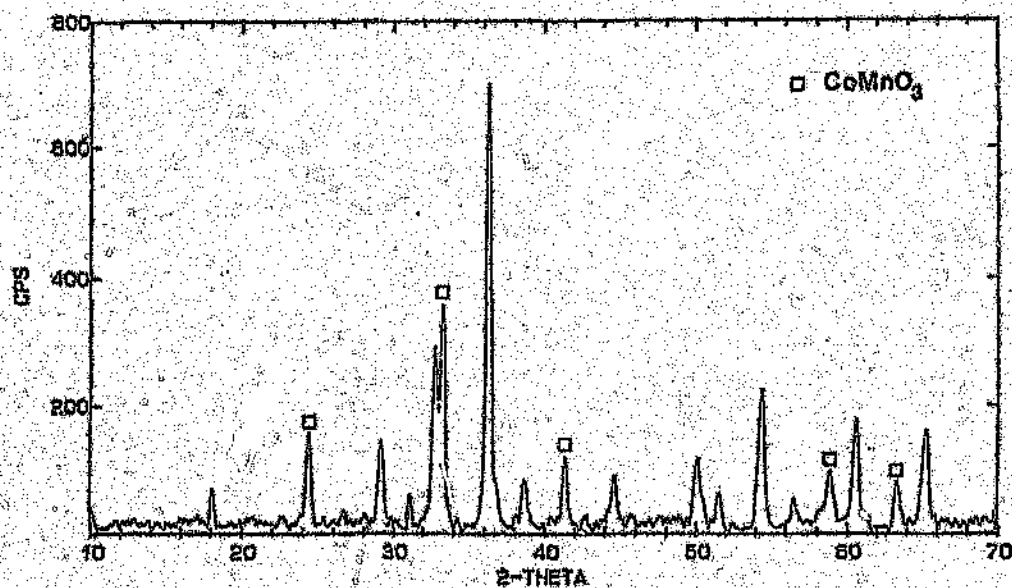
Figure 5.11: Diffractogram of the calcined C-2 precursor. The $CoMnO_3$ peaks are marked.

The structural changes of C-2 that occurred during reduction at the various temperature stages, as shown in Figure 5.12(a) – (e), proceeded via a similar route to that followed during the reduction of C-1. After reduction of the initial spinel phases, at 270°C, under H_2, the main phase was again indexed as MnO, with a poorly crystalline metallic cobalt phase appearing after reduction at 400°C. Although the two catalyst samples, C-1 and C-2, were of different precursor origin i.e. (Co,Mn) $(Co,Mn)_2O_4$ versus $CoMnO_3$ + $(Co,Mn)(Co,Mn)_2O_4$ respectively, they appear to follow the same phase transformation route to a common reduced state. This suggests that the exact form of the precursor Co/Mn oxide phases might not be a good criterion by which to forecast the performance of such a catalyst.

A synopsis of the identifiable phases of the two catalyst precursors, C–1 and C–2, present during the calcination and reduction pretreatments, is presented in Table 5.4.

Table 5.4: Identifiable phases present at different temperatures and atmospheres of initial catalyst pretreatment

temp (°C)	atmosphere	treatment time (hours)	identifiable phases present	
			C1	C2
20	air	0	(Co,Mn)(Co,Mn)$_2$O$_4$	(Co,Mn)(Co,Mn)$_2$O$_4$ + CoMnO$_2$
20	H$_2$	0		no change
150	H$_2$	8		no change
270	H$_2$	8		MnO
320	H$_2$	8		no change
400	H$_2$	6		MnO + traces of metallic Co
400	H$_2$	12		slight growth in Co peak
400	H$_2$	44		no change
220	H$_2$	8		no change

From these studies it may be concluded that the Co/Mn oxide spinel was reduced by H$_2$ at 400°C to MnO and elemental Co, through the formation of MnO + "CoO" as possible intermediate phases.

The course of the reduction can thus be represented by the following

These results indicated the existence of a sharp exothermic peak at ~230°C, followed by a fairly broad exothermic region, possibly consisting of two overlapping peaks, the first a shoulder at ~300°C, and the other a more defined transition at ~380°C. This suggested that the reduction of the catalyst proceeded via a possible three stage phase change to its final state. As previously mentioned, DSC thermograms do not always reveal the details of complex thermo—structural behaviour, thus; an X-ray diffraction study was undertaken in order to determine the structural changes taking place during the reduction.
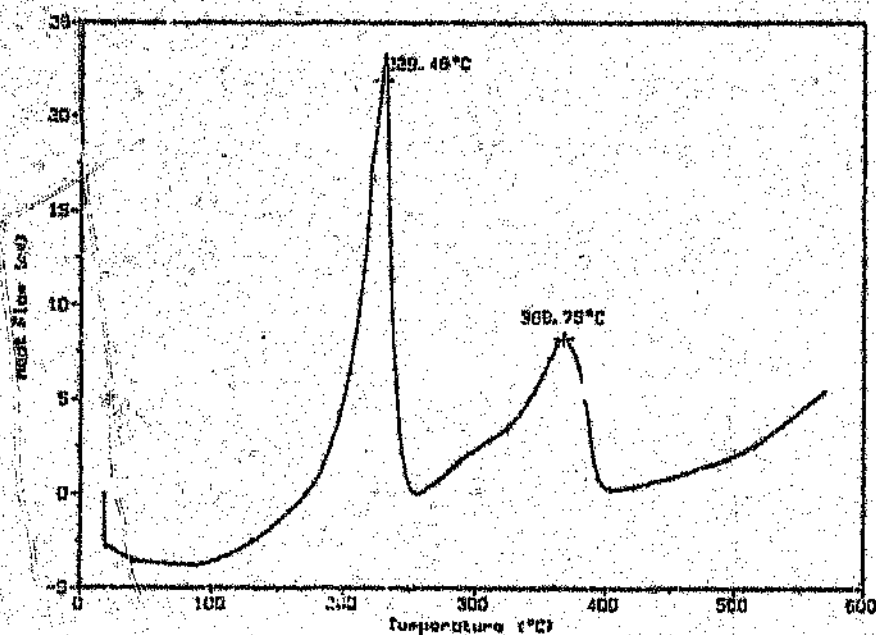
Figure 5.6: DSC thermogram of the *in situ* reduction of the calcined Co/MnO catalyst.

XRD patterns were collected *in situ* under a hydrogen atmosphere in the region of those temperatures, i.e. 270°, 320°and 400°C, indicated by the DSC exotherms, where probable phase transformations had taken place. A diffractogram was performed to establish the initial phases present in the

sample at room temperature, under H₂. The diffraction profiles of the spinel phase present, viz. (Co,Mn)(Co,Mn)₂O₄ was indistinguishable from that of the calcined sample discussed in Section 5.3.1(a). The sample was then heated to 150°C and an XRD taken after 4 hours under H₂ at that temperature. No phase changes were expected, and none was observed.

The temperature was then increased to 270°C, and after further treatment with H₂ for 8 hours, the diffractogram shown in Figure 5.7, was obtained. The X-ray diffraction pattern was indexed as only a single phase, namely cubic MnO. MnO has also been shown to be one of the predominating phases of similar catalysts (104), at the early stages of reduction, i.e. at temperatures below 300°C. X-ray diffraction studies by Barrault (117) on silica supported Co-Mn catalysts (where the total metal content was ~10%) further showed that due to the much greater resistance to reduction to metal, manganese was found to be in the oxide form MnO, rather than the metal Mn⁰, in the catalyst.
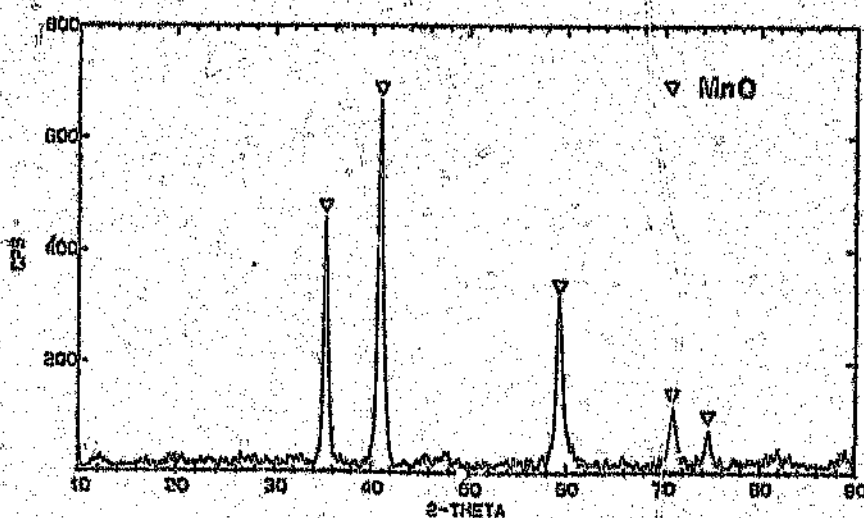
Figure 5.7: Diffractogram of catalyst at 270°C after 8 hour treatment under H₂ showing MnO phase.

Although MnO was the only crystalline phase detected after this initial reduction at 270°C, the cobalt that must have been present at this stage, possibly in the form of CoO, was undetected. It was believed that this could have been due to the CoO being present in a finely divided form as an amorphous product, and was consequently not observed by XRD analysis. XPS studies performed by co-workers on the surface of a Co/MnO (1:1) catalyst (132), have shown that the cobalt, prior to the reduction temperature being increased to 360°C, exists in the form of CoO. This is supported by reduction studies of Co–ThO₂–MgO–kieselguhr by Sexton *et al.* (173), who have shown that the cobalt oxide (Co_3O_4) present in all the air–calcined catalysts, reduced rapidly to CoO at temperatures below 300°C. CoO was then found to reduce more slowly to Co metal, at temperatures of 400°C.

Thus, these initial results established that the early stages of reduction of the Co/Mn oxide spinel, was found to occur at ~ 230°C (corresponding to the first exotherm of the DSC thermogram), and which may be attributed to the transformation to MnO and amorphous CoO (from X-ray diffraction data).

In order to identify the exothermic shoulder of the thermogram at ~ 310°C, an X–ray diffraction was performed after the temperature of the catalyst had been increased to 320°C in H_2 for 8 hours. The subsequent X–ray diffraction pattern indicated that no further change had transpired. Consequently, the phase change as indicated by the thermogram, could possibly be due to an increased crystalline growth of CoO, which was still too finely divided or amorphous in structure to be detected by XRD analysis.

Finally, to characterize the last stage of the reduction of the catalyst sample, the temperature was further increased to 400°C, and after 6 hours at this temperature, the diffractogram shown in Figure 5.8, was obtained.
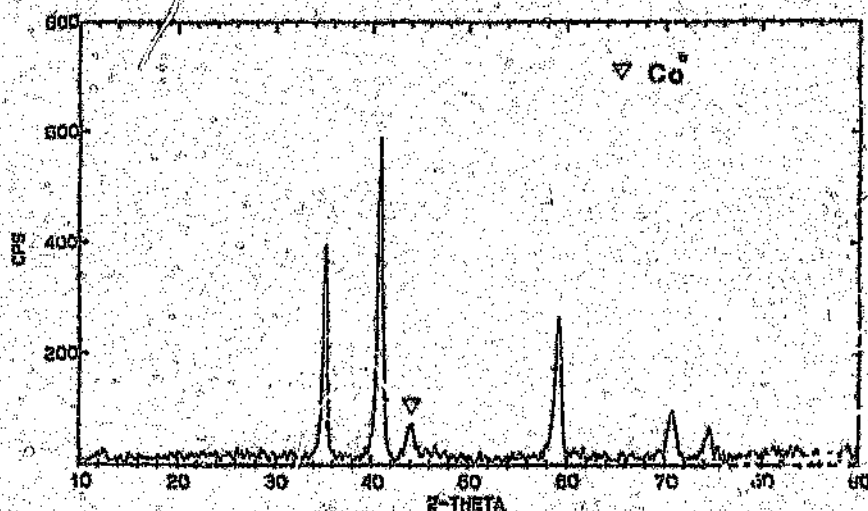
Figure 5.8: Diffraction pattern collected after reduction at 400°C, showing the emergence of the metallic Co phase.

The predominant phase remained MnO, but a small peak at $2\Theta = 44.20°$ suggested the possibility of metallic cobalt emerging as a second phase. An *in situ* XPS study of the reduction of the Co/MnO catalyst, which had previously been investigated by co-workers (132), showed that the surface cobalt was seemingly unaffected by H_2 at a temperature of 260°C, but was reduced to metallic Co at 360°C and remained so at 400°C. This was illustrated by both the chemical shift of the $Co(2p_{3/2})$ peak from a binding energy of 780.3 to 778.1 eV, and the disappearance of the shake-up satellite

associated with the high-spin (d^7) Co^{2+} ion. It was also observed that on reduction at these temperatures, a significant decrease in the Co/Mn surface ratio from 0.44 to 0.12 had occured, indicating high enrichment of Mn with respect to cobalt at the surface. Similar effects of surface enrichment of Mn with respect to the active metal after reduction has been observed with Fe/MnO catalysts (104,110,196). Research by other groups has shown that the reduction of cobalt oxide to metallic cobalt under H_2 occurs between 200° and 700°C, depending on the catalyst support and the method of preparation (14,82,132,173,185,201).

Due to limited crystal growth occurring, only the main peak of metallic Co could be detected; thus uncertainty existed as to the exact crystal structure of the metallic cobalt phase at this stage. However, the Co peak was close to that of face-centered cubic structure [Co(fcc)], and thus one would have to accept this as the most probable cobalt phase. Face-centered cubic cobalt has been shown to be stable at temperatures above 400°C, and the hexagonal close-packed structure [Co(hcp)] to be stable at temperatures below 400°C (14). In addition, certain researchers have considered some of their cobalt phases to be essentially a mixture of face-centered cubic and disordered close-packed structures (14). Srinivasen *et al.* (201), studied several cobalt catalysts on a silica support, and showed that after reduction, metallic cobalt was found to be present in the hcp and fcc forms in the ratio of 7:3. We have performed similar *in situ* reduction studies on Co_3O_4, Co/Al_2O_3 and $CoCr_2O_4$ samples respectively, where the metallic Co could unambiguously be indexed to that of face-centered cubic cobalt at the final stage of reduction. These results are discussed in following Sections 5.3.4.

From the aforementioned results it can be concluded that the final stage of the reduction, corresponding to the exotherm of the thermogram at ~ 380°C, may be characterized as the reduction of cobalt oxide (CoO) to metallic cobalt. The extent of the reduction to metallic cobalt was difficult to calculate, since both the CoO and the Co metal were too amorphous or finely dispersed to be completely detected by XRD analysis. Although precipitated Co_3O_4 has been shown to be reduced quantitatively to Co metal at temperatures as low as 200°C (14), under these conditions supported cobalt catalysts have been shown to be difficult to reduce due to the dispersed cobalt particles being stabalized by the interaction with the support material (14,202–205). Co/Al_2O_3 catalysts studied by Reuel and Bartholomew (77,78) were reduced by only 11 to 44% after reduction at 375°C for 20 hours.

In summary, a series of diffractograms showing the various phase transformations of the Co/Mn oxide spinel precursor, during its reduction at the different temperature stages, to its final reduced configuration, is shown in Figure 5.10.

The pretreatment conditions of calcination and reduction were again performed on a Co/MnO catalyst that had been selected from a different batch sample. The conditions of co–precipation for this catalyst remained essentially the same as for the aforementioned Co/MnO catalyst (the former and latter Co/MnO catalysts are from hereon referred to as C–1 and C–2 respectively). The diffraction profile of C–2 after calcination in air (500°C for 24 hours), showed the presence of an additional spinel phase (viz. $CoMnO_3$) over and above the $(Co,Mn)(Co,Mn)_2O_4$ mixed spinel that had earlier being indexed as the initial phase present in C–1. The presence of this

additional phase, could be a result of synthesis conditions during catalyst preparation e.g. temperature and pH, not being kept exactly the same for different catalyst batches. It could also be a result of further oxidation of the $(Co,Mn)(Co,Mn)_2O_4$ spinel in air, i.e. the oxidation of $CoMn_2O_4$ to $CoMnO_3$. The diffraction pattern of the calcined C-2 precursor showing the $CoMnO_3$ phase is shown in Figure 5.11.
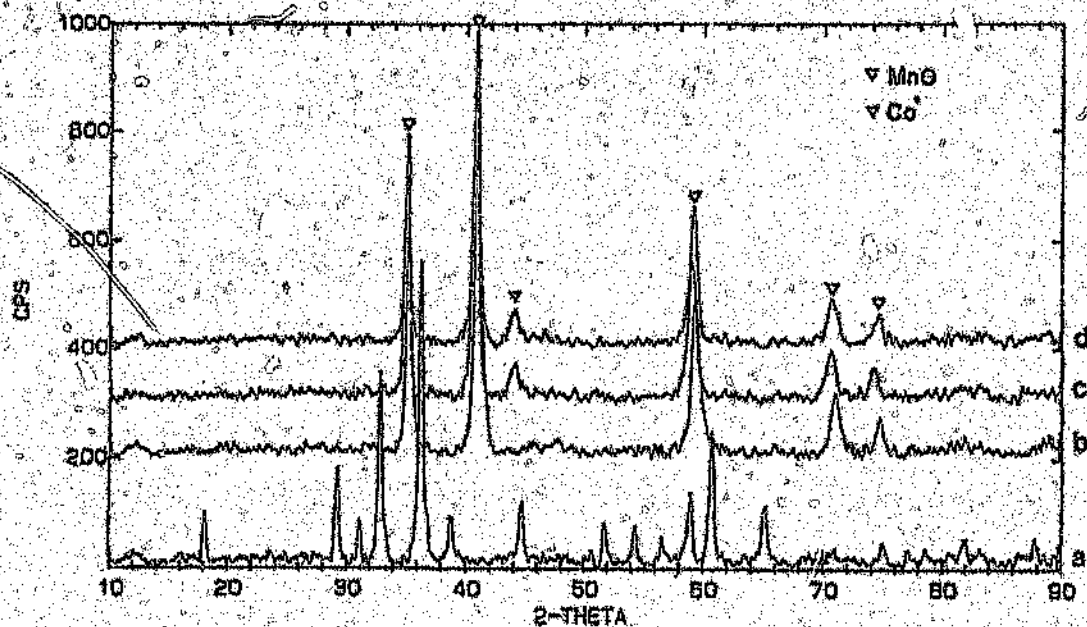
Figure 5.10: Series of diffractograms of the Co/Mn oxide spinel during its reduction. XRD's were collected after:

a, calcination showing $(Co,Mn)(Co,Mn)_2O_4$ spinel,

b, after reduction at 270°C showing MnO phase,

c, after reduction at 400°C showing appearance of the Co metal,

d, no change occurred on cooling the catalyst to 220°C under H_2.
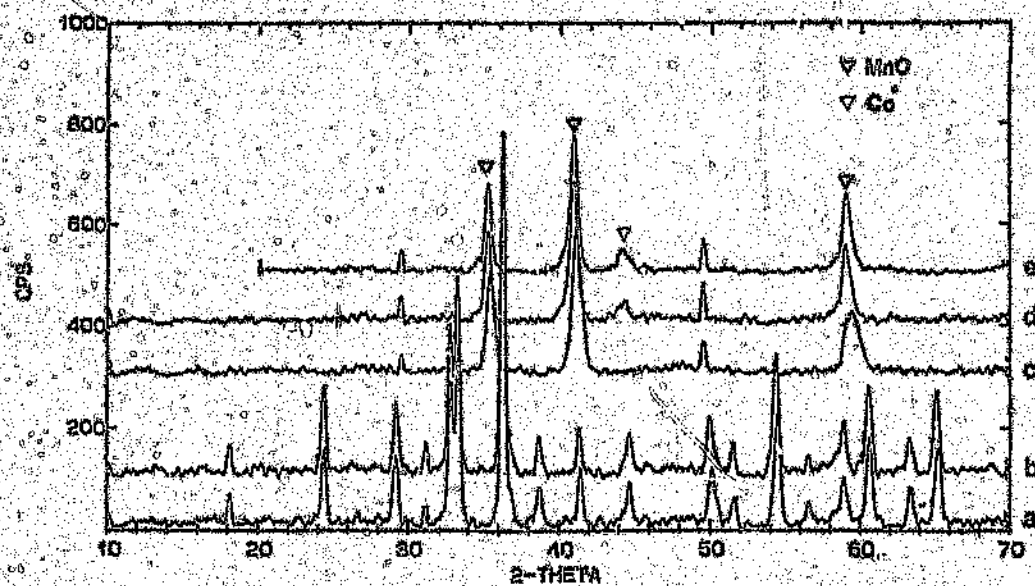
Figure 5.12(a)-(e): Full series of the diffractograms collected during the reduction procedure of C-2, after:

a, calcination, showing $(Co,Mn)(Co,Mn)_2O_4$ + $CoMnO_3$ spinel phases,

b, reduction at 150°C, no change,

c, reduction at 270°C, showing MnO phase,

d, reduction at 400°C, showing MnO + metallic Co,

e, at 220° under H_2, no change.

scheme:--

$(Co,Mn)(Co,Mn)_2O_4$

$(Co,Mn)(Co,Mn)_2O_4+CoMnO_3$ $\quad\xrightarrow[H_2]{270°C}MnO+"CoO"$

$\qquad\qquad\qquad\qquad\qquad\xrightarrow[H_2]{400°C}MnO+Co(fcc)+"CoO"$
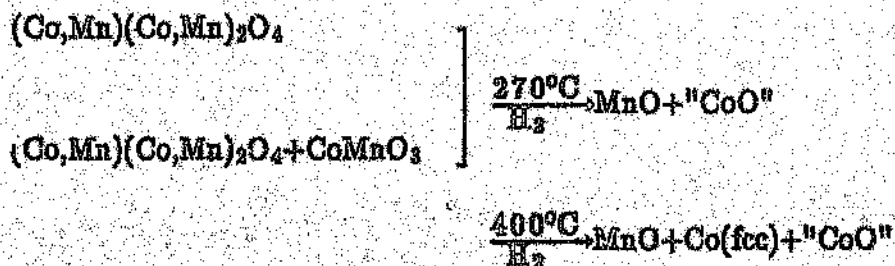
The specific reduction temperature for the Co/MnO catalysts of 400°C, which had previously been determined (62), to yield optimal subsequent catalytic performance, (Table 5.3), cor'' l be rationalized from the *in situ* XRD reduction studies as having been the temperature at which the reduction of CoO to metallic Co had occurred. For reductions carried out at temperatures *below* this required minimum, incomplete reduction and activation of such catalysts is found. For reduction at a temperature *above* this optimum, loss of catalytic activity, (possibly from sintering) is also observed. As an example, (from Table 5.3), H_2 reductions of the catalyst precursor at 200° and 430°C, resulted in CO conversions of only 11 and 14% respectively.

5.3.2 An *in situ* X-ray diffraction characterization of the Co/MnO catalyst during reaction with CO/H₂

As was previously discussed, the use of *in situ* X-ray diffraction methods has the potential to increase our understanding of catalyst performance by investigation of the structural behaviour of these materials under realistic process conditions. The power of this method in the characterization of working catalysts, has recently been demonstrated by several research groups, who utilized this method to explore several diverse catalysts, treated under various reaction conditions, e.g. Fe and cerium intermetallic alloy catalysts (181,184) for ammonia synthesis reactions, cobalt

CO–hydrogenation catalysts supported on silica (201) and ZSM–5 (185), palladium hydroxide hydrogenolysis catalysts (206), and methanol synthesis with rare earth copper alloys (183).

One of the main objectives of this study was to provide a complete structural and morphological description of the phases present in the catalyst during reaction with CO/H_2, under "realistic" reaction conditions. An *in situ* X–ray diffraction study under F–T synthesis conditions was performed on a Co/MnO catalyst from the batch sample previously identified as C–1. X–ray diffraction patterns collected after pretreatment calcination (500°C, 24 hrs., air) and subsequent reduction (400°C, 16 hrs, H_2), again indicated the initial presence of a (Co,Mn)(C   )ide spinel, being reduced to MnO and a metallic cobalt phase   (b)). The optimum operating temperature for CO hydrogenation ...   O) been found to be ca. 220°C (62), at which the catalyst sn.   methane selectivities, with corresponding increased propene selectivity (higher temperatures resulted in the catalyst becoming more hydrogenating, whilst lower temperatures generated low catalytic activity). Thus, after reduction at 400°C under H_2, the sample temperature was then allowed to stabilize at 220°C and, after 2 hours under flowing H_2 at this temperature (during which no further phase changes were detected), the gas was substituted for a 1:1 (by volume ratio) mixture of CO/H_2 at a flow rate of 40 ml min^{-1}. Previous studies (118) have indicated that under such conditions (T = 220°C, P ∼ 1 atm, GHSV ∼ 280 h^{-1}), hydrocarbon production from synthesis gas had begun almost immediately and that a stable performance was achieved after ∼ 100 hrs on–line. Although MnO has been shown to have a short–lived hydrogenation capability (85), (which may be related to the presence of excess O^{2-} ions and associated cation vacancies in the structure), the metallic

5.15(e) and (f). This indicates that Co(bcc) is metastable as was witnessed from this rapid transformation to Co(fcc). Also present, was some residual Co(bcc), appearing as a small shoulder at $2\Theta = 44.73^\circ$, – see Figure 5.15. This pattern showed, in addition, two weak peaks at 2Θ values of ∼ 34° and 49°, resulting from an unidentified phase. This may possibly represent a product generated during the transformation of an impure Co(bcc) phase to a pure Co(fcc) phase, which would indicate the presence of interstitial atoms, such as carbon, in the Co(bcc) structure; they did not correspond to known Co carbide phases, however.
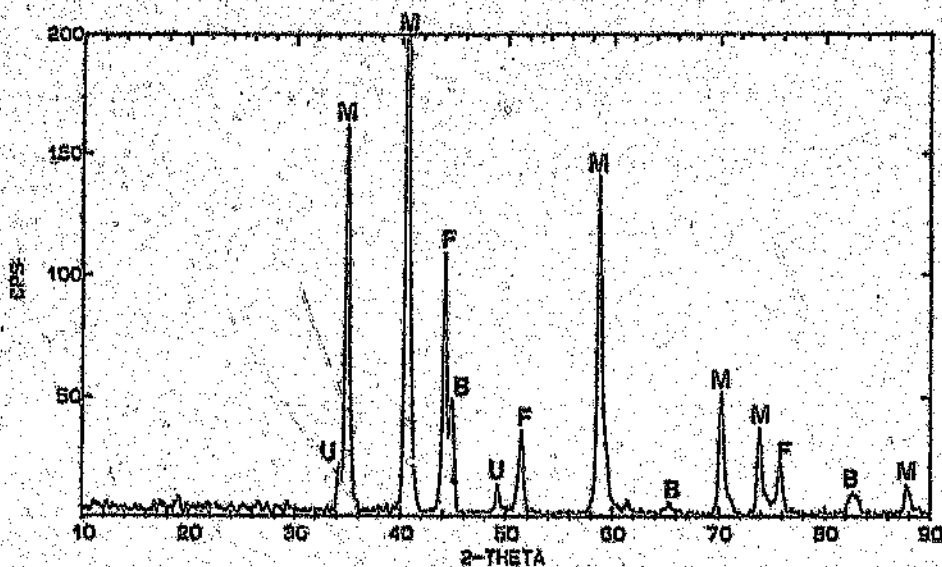
Figure 5.15: Diffractogram of the specimen crushed in air showing the transformation of Co(bcc) to Co(fcc). M = MnO; F = fcc; B = bcc; U = unknown.

The fact that crystal growth of the Co(fcc) to Co(bcc) takes place at lower temperatures (i.e. no increase in crystallinity was observed with prolonged reaction of Co(fcc) in H_2 at 400°C), suggests that the action of CO coupled with *lower* temperatures, may play some role in the formation of the
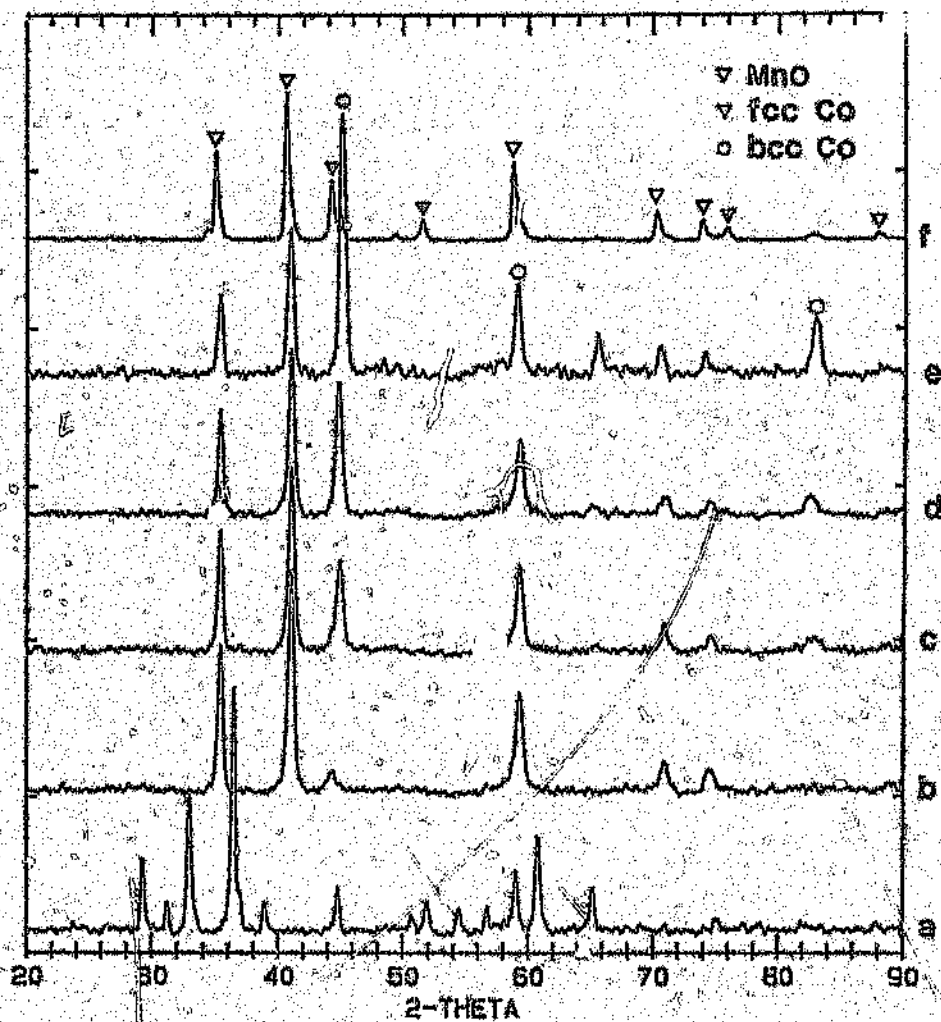
Figure 5.18(a)-(f): XRD patterns for the Co/MnO system at various stages of chemical treatment.
a, $(Co,Mn)(Co,Mn)_2O_4$ mixed oxide spinel after calcination at 500°C for 24 hours, in air.
b, MnO + Co(fcc) after final reduction at 400°C for 16 hours, under H_2.
c-e, after 24, 72 and 112 hours reaction with CO/H_2 at 220°C, showing the evolution of the Co(bcc) peaks.
f, resulting sample crushed in air, showing the transformation of Co(bcc) back to Co(fcc).

(i.e. forming a possible forced body centered cubic structure). This investigation was extended by attempting to form the Co(bcc) phase on additional catalyst supports, namely Al_2O_3 and Cr_2O_3, under similar experimental conditions.

The Co_3O_4 oxide spinel system

The XRD patterns resulting from the various stages of chemical treatment performed on the Co_3O_4 oxide spinel are collectively illustrated in Figure 5.17 (a) – (f).

Figure 5.17   (a)   The XRD data collected at room temperature after calcination of the sample (500°C, 24 hrs. in air), was indexed as a Co_3O_4 oxide spinel.

(b)   after reduction at 400°C for 18 hours, under H_2, the complete transformation of Co_3O_4 to metallic Co was observed. Unlike the case of Co/MnO (Section 5.3.1(b)) the reduced Co could unambiguously be identified as the fcc phase [the Co(fcc) lines are marked in Figure 5.17(a)]. As previously found, the absence of the strong Co(fcc) peaks of Co/MnO could have been a result of high metal dispersion on the support with a low degree of crystallinity. In contrast, the Co_3O_4 system showed a good degree of crystallinity with strong Co(fcc) lines from the X-ray diffraction of larger metallic particles.

(d)–(f) the diffraction patterns collected after 84(d), 151(e) and 175(f) hours after continuous CO/H$_2$ exposure, showed the strongest peak at ~44° to grow to about 3 times its initial height. With the appearance of the other diagnostic lower intensity peaks at approximately 2Θ = 65°, 82° and 102°, by 175 hours, a positive identification of the bcc phase of Co could then be made. (The respective fcc and bcc phases are marked on the figure.)

Figure 5.17(f) is shown in an expanded version of the diffraction pattern, in Figure 5.18. A mixture of the fcc and bcc phases of Co, after 175 hours of F–T synthesis is clearly evident.
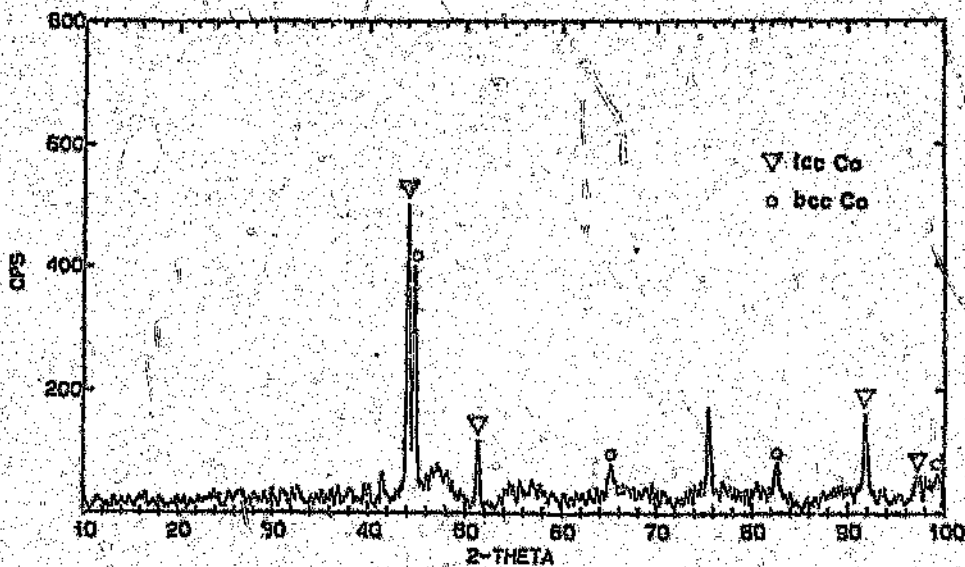
Figure 5.18: XRD pattern showing the mixed fcc and bcc phases of Co, resulting after CO/H$_2$ reactions, from the Co$_3$O$_4$ precursor.

cobalt observed, was considered to be the catalytically active and stable phase.

After 6 hours of CO/H_2 reaction in situ, no further phase change was observed, but after 24 hours, some new peaks of low intensity appeared in the diffractogram which grew in intensity; after 112 hours these peaks were stronger than those characteristic of the MnO phase – see Figure 5.13(a) – (f). The new diffraction peaks at 2Θ values of 44.73°, 65.13° and 82.54°, corresponding to (hkl) reflections of (110), (200) and (211) respectively, could only be indexed to a bcc cobalt phase, with relative intensities similar to those of iso-structural α-Fe. (A more detailed description of Co(bcc) identification is given in Appendix 5.) Further evidence for the transformation to this novel phase was observed from the gradual shift, with time-on-line, of the metallic Co (fcc) peak position at $2\Theta = 44.20°$ to the Co(bcc) peak position at $2\Theta = 44.73°$, as is demonstrated in Figure 5.13 (a) – (f). The lattice parameter a, for Co(bcc) was calculated to be 0.286 nm in contrast to that of 0.354 nm for Co(fcc) (the calculations were performed using MnO as an internal standard after back calibration with silicon using equation 1.2 of Appendix 5). This compares favourably with the lattice constants of Co(bcc) as determined by EXAFS of 0.282 nm (174) and X-ray diffraction of 0.283 nm (207) on thin films. The smaller lattice parameter for Co(bcc) can be explained from an inspection of the different atomic packing arrangements, as shown in Figure 5.14 (a) and (b), with the lattice parameters given by $\dfrac{4r}{\sqrt{2}}$ and $\dfrac{4r}{\sqrt{3}}$ for the fcc and bcc crystal structures respectively (r = atomic radius of Co).
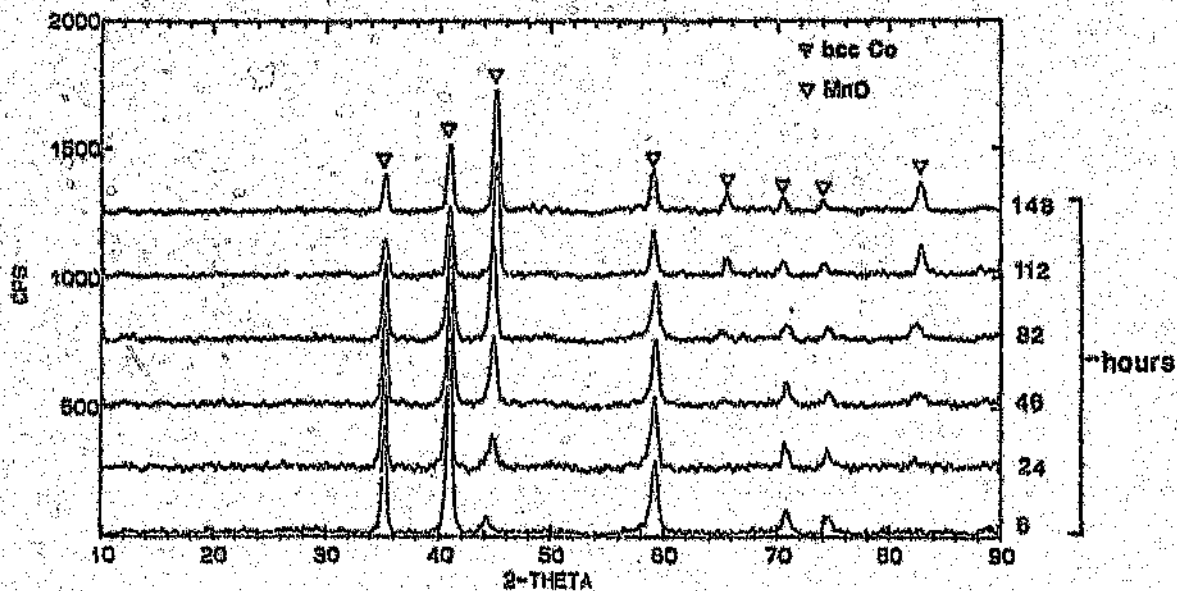
Figure 5.13(a)-(f):   A series of diffractograms showing the growth in the Co(bcc) peaks under CO/H_2 after 6, 24, 46, 82, 112 and 148 hrs on-line. (The Co peaks are marked.)

Views of the two cubic structures (a) fcc and (b) bcc with
the formulae of the respective lattice parameters.

$$a = \frac{4r}{\sqrt{2}}$$

$$a = \frac{4r}{\sqrt{3}}$$
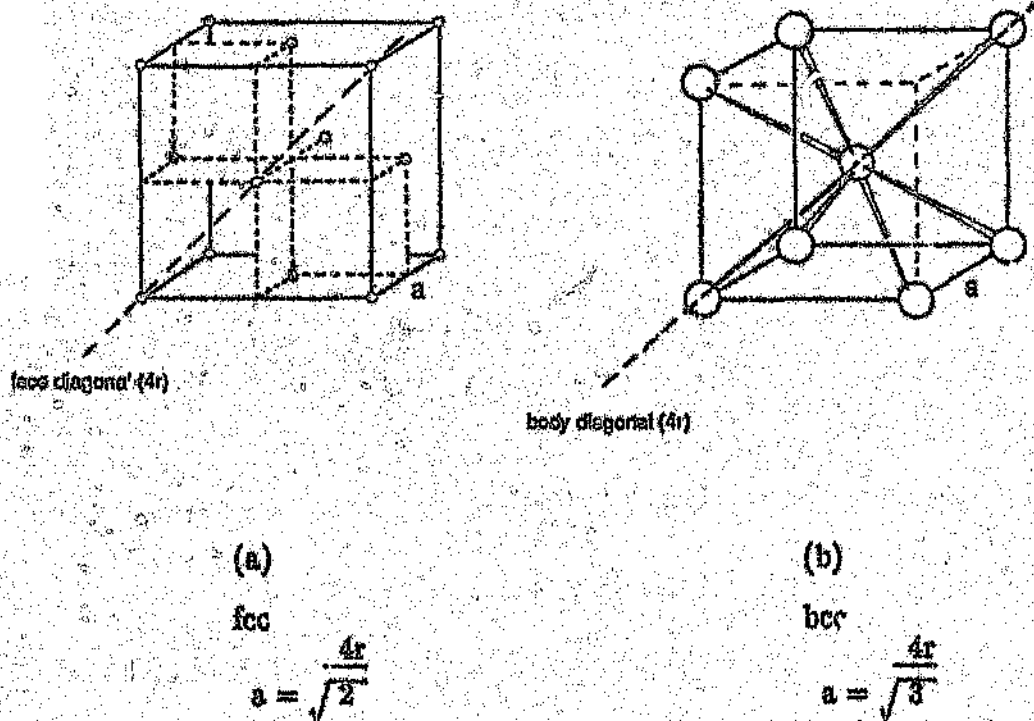
Figure 5.14: Views of the two cubic structures (a) fcc and (b) bcc with
the formulae of the respective lattice parameters.

After reaction for 148 hours with syngas at 220^0C, the catalyst
sample containing the Co(bcc) was cooled to 20^0C still under CO/H_2. The
XRD measurement indicated that no structural change had occurred as a
result of cooling. Even after exposure of this sample to air for 3 hours, only
cubic MnO and Co(bcc) were present, indicating a certain stability of Co(bcc)
in air. However, by lightly crushing a portion of this specimen and leaving it
for a further 3 hours in air, XRD revealed that a phase transformation back
to Co(fcc), the more stable form of metallic Co, had occurred – see Figure

Co(bcc) structure. Furthermore the possibility of a small amount of *disordered interstitial* carbon in the metallic structure cannot be discounted. Also, an equal shift of the (110), (200) and (211) lines of Co(bcc) was observed, suggesting an overall shrinkage of the unit cell. These peak shifts are not from specimen movement, as the MnO peaks did not shift, nor from thermal expansion, since all XRD's were performed at 220°C; but could however, be due to the formation of some intermediate structure, which transforms into a smaller, more stable, final bcc arrangement.

A correlation between catalytic performance and the generation of this Co(bcc) phase will be discussed in Sections to follow.

Figure 5.16 (a) — (f) and the corresponding Table 5.6, provide a summary of the phases that were present in the Co/MnO system at various stages of chemical treatment under calcination, reduction and hydrocarbon synthesis conditions.

5.3.3   Implications of the Co(bcc) structure

Until now (186), no direct confirmation of the bcc structure of the bulk phase of cobalt had yet been published. However, surface XRD investigations (179) of sputtered polycrystalline Co–Cr films prepared by compositional moldulation (vacuum deposition techniques), have provided evidence for the epitaxial–growth of a Co(bcc) phase on a Cr substrate, under special conditions of film thickness. It was thought that the formation of this new phase may be due to the heats of solution of Co in Cr o. Cr i Co compared with the difference of their surface enthalpies. More recent molecular–beam– epitaxy (MBE) experiments (208) under ultrahigh–vacuum conditions, coupled with high–energy electron diffraction, have identified

TABLE 5.6: Summary of the Co phases that evolved after various chemical treatments and conditions

temperature/°C	atmosphere	time—on—line	identifiable phases
20	air	0	$(Co,Mn)(Co,Mn)_2)O_4^o$
200	H_2	2	no change
220	H_2/CO	6	no change
220	H_2/CO	24	Co(bcc) growing
220	H_2/CO	46	Co(bcc) growing
220	H_2/CO	82	Co(bcc) growing
220	H_2/CO	112	Co(bcc) peaks stronger than MnO
220	H_2/CO	148	Co( ) peak growth rate decreased
20	H_2/CO	14	no change
20	air	3	no change
20	air/(crushed)	3	MnO + Co(fcc) + traces of Co(bcc)

Co(bcc) formed epitaxially on GaAs (110) surfaces, having a lattice parameter of 0.2827 nm. Also, electronic band theory calculations (209,210) used to study the different structural and magnetic phases of cobalt, have shown Co(bcc) to exist only as a ferromagnet (with the moment close to its hcp value), while Co(fcc) shows the co–existence of a ferromagnetic and nonmagnetic phase. Total–energy calculations (209) showed the bcc phase to be metastable and to occur at an equilibrium energy slightly higher (0.06 eV/atom) than the calculated minimum for the fcc phase. Other total–energy calculations (211) showed that the minimum of the fcc phase was only 0.03 eV/atom higher in energy than the minimum for the hcp phase, which is the lowest–energy phase.

True metastable phases (a local minimum of the total energy under conditions of zero pressure or applied field), of which the thin film epitaxy specimens are an example, should be differentiated from forced structures which are externally maintained (nonequilibrium morphology by imbedding in a foreign matrix), of which the polycrystalline Co–Cr films might be an example (208). The excess energy of the metastable phase above the thermodynamically stable structure should be manifest by interesting magnetic and electronic behaviour, making these phases possibly more technologically interesting and scientifically valuable than their more stable counterparts.

5.3.4 Further investigations into the generation and stabilization of the thermodynamically metastable Co(bcc)

Similar *in situ* experiments to those completed on Co/MnO were performed on Co_3O_4, i.e. in the absence of the MnO matrix, in order to establish the function, if any, of the host matrix in the formation of Co(bcc)

(c) the temperature of the catalyst was reduced to 220°C in
H₂, and CO introduced into the HTA chamber to form
a 1:1 (by volume) mixture of CO/H₂. A diffraction
pattern collected after 16 hours showed that no further
change had occurred, until after 58 hours of exposure to
syngas, the emergence of a small peak at 2Θ ~ 44° was
observed. This indicated the possible initiation of the
conversion of the fcc form of Co to its bcc phase.
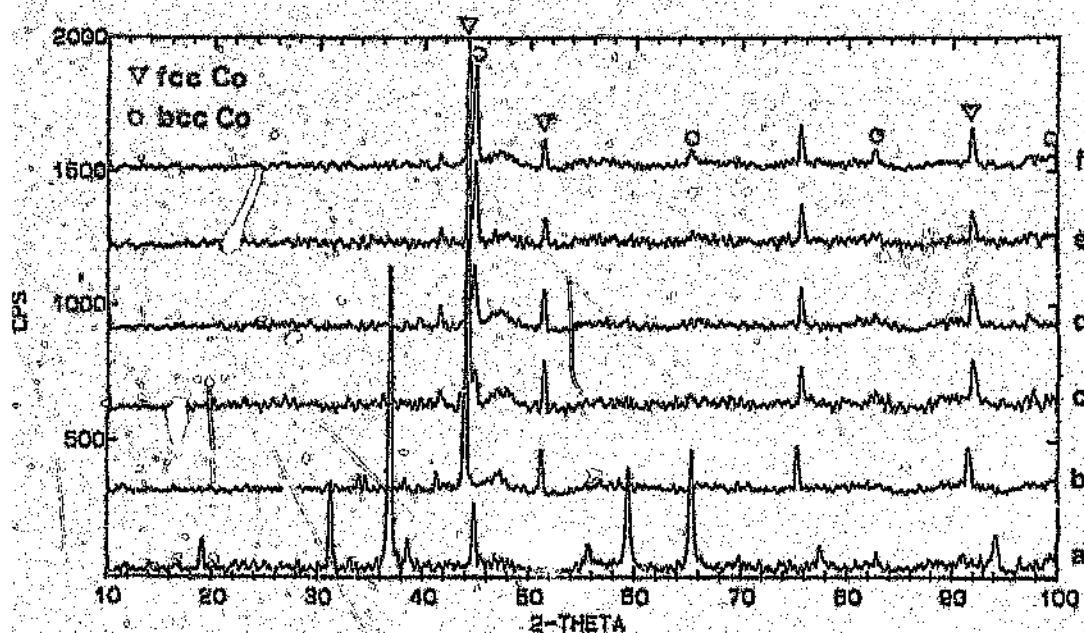
Figure 5.17(a)-(f): XRD patterns for the Co₃O₄ system at
various stages of chemical treatment.

a, Co₃O₄ oxide spinel after calcination.

b, after reduction at 400°C with H₂, showing
the resulting Co(fcc) phase.

c-f, after 58, 84, 151 and 175 hours reaction
with synthesis gas at 220°C, demonstrating
the growth of the Co(bcc) phase (the
different phases are marked).

The growth of the metastable Co(bcc) phase from the Co_3O_4 precursor, in the absence of the host matrix MnO, minimised any influence that the matrix may have played in forcing or generating this unusual cobalt structure.

The Co_3O_4/Al_2O_3 system

This catalyst was obtained from R & D Dept. Sastech (Sasolburg, South Africa), and had been prepared by impregnating 5% by mass Co_3O_4 onto a γ-Al_2O_3 support, from an aqueous solution of cobalt nitrate, dried at 120°C, and calcined at 500°C in air.

The resulting XRD patterns collected after calcination, reduction and continued F–T synthesis, are given in Figure 5.19(a) – (f).

Figure 5.19(a)   The room temperature diffraction pattern collected under H_2 (after calcination) established that the sample was a mixture of the Co_3O_4 and Al_2O_3 spinel phases; of which both phases, but more so the alumina were poorly crystalline. This made it difficult to identify the specific alumina present. (The Co_3O_4 and Al_2O_3 peaks are marked.) The $CoAl_2O_4$ spinel phase was not observed.

(b)   after reduction at 400°C in 1 bar H_2 for 13 hours, the Co_3O_4 appeared to have been fully reduced to Co metal in the fcc form, with the alumina remaining unchanged (again, unlike in the case of Co/MnO, the metallic Co could unambiguously be identified as the fcc phase. The fcc peaks are marked.)
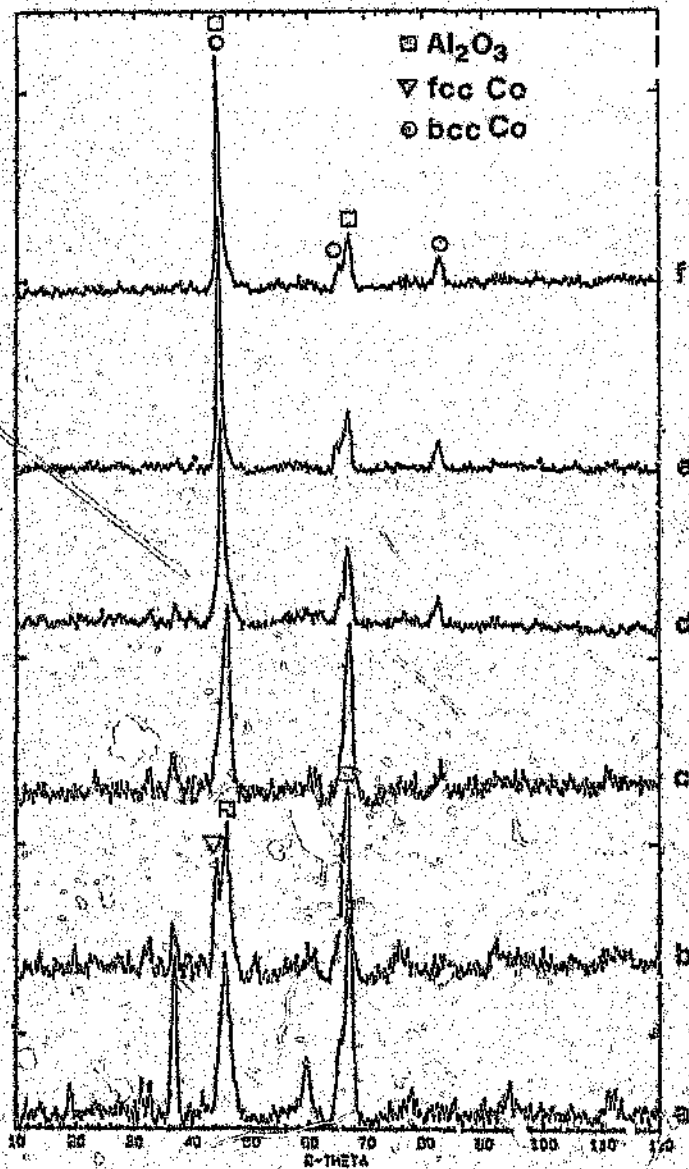
Figure 5.19(a)–(f): XRD patterns for the Co_3O_4/Al_2O_3 system collected after various stages of chemical treatment.

a, Co_3O_4 and Al_2O_3 spinel phases after calcination.

b, after reduction, showing the resulting Co(fcc) and Al_2O_3 phases.

c–f, after 9, 24, 48 and 72 hours reaction with CO/H_2, showing the growth of the Co(b) phase with time. (The various phases are marked.)

(c) after 18 hours at 400°C, the sample was cooled down to 200°C, and CO was introduced into the sample chamber, producing the final CO/H_2 (1:1 by volume) mixture. After only 9 hours of synthesis, the indications were that Co(fcc) had already largely transformed to Co(bcc). It should be noted, however, that the generally poor quality diffraction patterns obtained with this catalyst made the interpretation of subtle changes difficult.

(d) after 24 hours under synthesis conditions, the resulting XRD showed a more positive identification of Co(bcc). However, interference from the alumina peaks (which unfortunately persisted throughout this study), prevented a definite identification. The intensity ratio of the peaks at approximately $2\Theta = 45°$ and $67°$, showed the expected values for Al_2O_3 after calcination and subsequent reduction. This was not however, the case under synthesis conditions, where the peak at 45° grew to more than *four times the expected height*, introducing the presence of a second overlapping peak, possibly Co(bcc). Thus, the diffraction peak at ~ 45° appeared at this stage to be composed of a small crystalline component (believed to be alumina) and a more crystalline component [believed to be Co(bcc)]. The resolved double peak observed at ~ $2\Theta = 45°$ and 67°, again corresponded to Co(bcc) and alumina, with the bcc peak probably being stronger if it were not for the overlap. The second

strongest peak of Co(bcc), which was completely free from any interference from alumina, was observed at $2\Theta \sim 82^\circ$. Although the strong fcc and bcc Co peaks at $\sim 45^\circ$ are close to one another and are therefore difficult to resolve under these circumstances, no signs of the secondary peaks of Co(fcc) were detected, whilst definite secondary peaks at positions corresponding to Co(bcc) were observed. We conclude that there was no Co(fcc) present after 24 hours CO/H_2 reaction, and that the second phase present was almost certainly Co(bcc).

(e)–(f)   diffraction patterns collected after 48 and 72 hours under synthesis conditions showed very strong evidence for Co(bcc).

The formation of Co(bcc) on the Al_2O_3 support, corroborated the conclusions of the previous experiments with Co_3O_4, i.e. in eliminating any influence of the MnO matrix in the formation of Co(bcc).

The CoCr₂O₄ – mixed oxide spinel system

This spinel ($\sim 26\%$ Co by mass) was obtained from Merck Chemicals. Summarized in Figure 5.20(a) – (c) are the XRD patterns collected after the various chemical treatments.

Figure 5.20(a) the room temperature XRD collected after calcination was indexed as a $CoCr_2O_4$ mixed oxide spinel.

(b) the XRD pattern from the H_2 reduction of the oxide spinel at 400°C (~ 20 hours) showed that no structural change had occurred at this temperature. The reduction temperature was thus increased by multiples of 100°C, at which temperatures further reductions were performed (for ~ 12 hours at each of these temperatures). *Only after a temperature of 800°C was reached under H_2, was the reduction of $CoCr_2O_4$ to Co(fcc) + Cr_2O_3, observed.* (The various peaks are marked.) Clearly, in this instance, the matrix (Cr_2O_3) *does* have a strong influence on the reduction behaviour of the Co^{2+} ions.

(c) after the temperature had been reduced to 220°C, synthesis gas mixture was introduced into the HTA chamber. *Only after 7 days of continued CO/H_2 exposure, was the formation of a small peak at 2Θ ~ 44° observed,* indicating the presence of a possible Co(bcc) phase (the other Co(bcc) peaks were not observed). The relevant XRD Co(bcc) line is marked on Fig. 5.20.

From the above study, it would seem that under the present conditions of reduction and synthesis, the $CoCr_2O_4$ system was more reluctant in the generation of a Co(bcc) phase, than the previous Co systems considered. This could possibly be a result of the formation of a very stable Co(fcc) phase, that was formed at a high reduction temperature of 800°C.
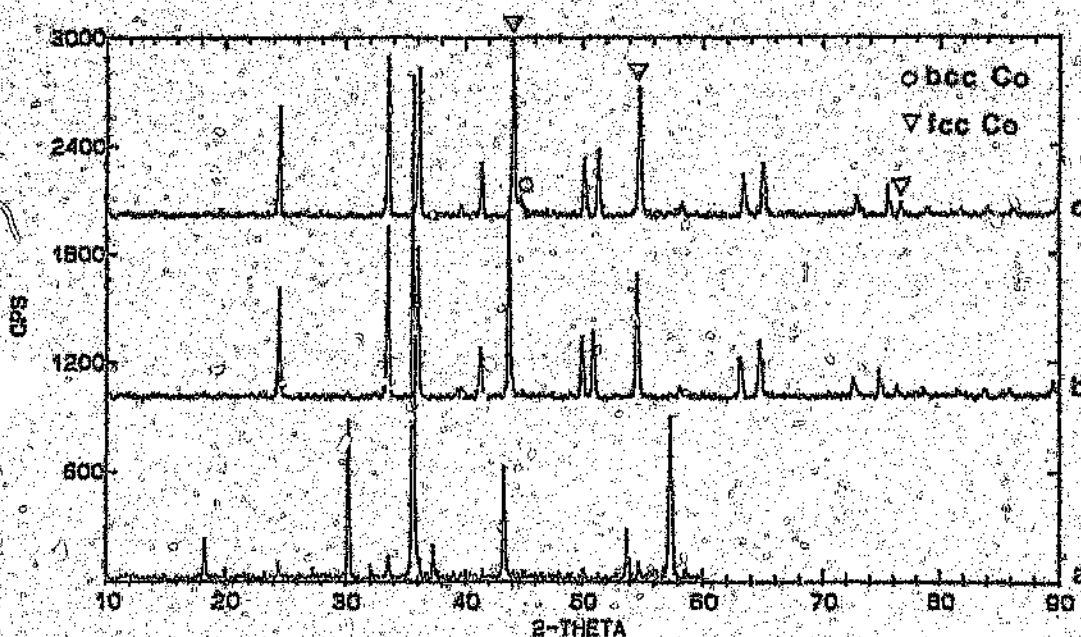
Figure 5.20(a)–(c): Summary of the XRD patterns resulting from the different chemical treatments.

a, CoCr$_2$O$_4$ mixed oxide spinel (after calcination).

b, Co(fcc) + Cr$_2$O$_3$ after reaction at 800°C for 16 hrs (under H$_2$).

c, after 7 days CO/H$_2$ reaction, showing the emergence of the possible Co(bcc) phase. (The various phases are marked.)

High selectivities toward propene (coupled with low methane selectivity) has already been established for the Co/MnO system (see Chapter 3), which may be correlated to the formation of Co(bcc), as shown in Figure 5.21. These selectivities however, were not observed with Co/Cr₂O₃ [high alcohol production (163)] or Co₃O₄ [high methane and low propene selectivity (118)]. In the case of Co/Al₂O₃, the reported catalytic data claim high selectivity to light olefins but at very low CO conversions (40). This correlation is purely speculative and is based on limited data. Johnson et al. (211a) have proposed the CO hydrogenation reaction to probably be structure-insensitive. Further surface characterization studies (eg. specific activity, active site density measurements and XPS studies) with time-on-line from start-up, would help put these controversial statements into a better perspective.
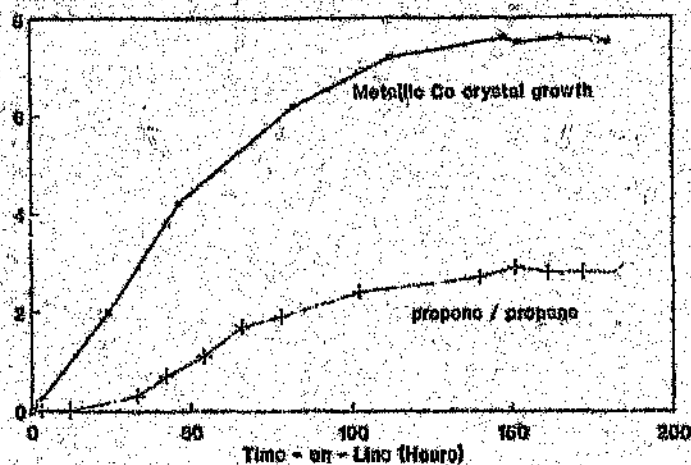
Figure 5.21: The correlation between increased propene selectivity and increased metallic crystal growth of Co(bcc).

In all the above systems investigated (under typical F-T conditions), the novel Co(bcc) metallic phase was identified after prolonged interaction with synthesis gas. The influence of the support was found not to play any significant role in forcing or generating the Co(bcc) phase. The role

of the reactant gases i.e. CO and H_2, and the possible influence of temperature, thus needed to be considered.

5.3.5 The possible role of CO, H_2, and temperature, in the formation of Co(bcc)

Whilst more work remains to be done to elucidate the precise effects of the parameters associated with this process in the formation of Co(bcc), we have proposed the following to occur. The interaction of CO with the catalyst material is thought to "open-up" the solid systems forming *cobalt-carbonyl* type intermediates. These cobalt-carbonyl intermediates are then thought to be further acted upon by H_2 and/or by temperature (thermal effects at 220^oC), causing a rearrangement of the intermediates to the metastable Co(bcc) phase. Strong evidence for the above mechanism is from the reluctancy of the $CoCr_2O_4$ spinel to form Co(bcc) — as previously discussed. After reduction of this spinel at 800^oC, an extremely stable $Co(fcc)/Cr_2O_3$ matrix system had resulted which was resistant to attack by CO. Consequently, few or no cobalt-carbonyl intermediates (for further rearrangement to Co(bcc)) could be formed. This was further substantiated from bulk sulphiding studies on Co/MnO and $CoCr_2O_4$ oxide spinel systems, performed by co-workers (212). They observed the Co/MnO catalyst to form a predominant Co_9S_8 phase after sulphiding at 400^oC. However, at similar temperature ranges, the Co/Cr system was reluctant to form any bulk sulphide, and only at temperatures greater than 550^oC, was sulphiding of this system observed. This showed the Co/Cr system to be resistant to attack by sulphur, much as in the same way as it was resistant to attack (in our case) by CO; thus the reluctance of this system to form possible cobalt-carbonyl intermediates for rearrangement to Co(bcc), under the influence of H_2 and/or temperature.

5.4   CONCLUSION

An investigation was made into some of the mechanisms involved in the catalytic action of cobalt/manganese oxide catalysts (and related systems), by following phase transformations *in situ*, during the activation (calcination and reduction) and operation of such systems. *In situ* DSC and XRD analytical methods were utilized in the study of these materials, which allowed us to probe the thermostructural behaviour of the systems under typical process conditions.

Initial studies followed phase transformations during calcination and subsequent reduction of the Co/MnO systems. The initial phase of the uncalcined oxide was indexed to the mixed oxide spinel $(Co,Mn)(Co,Mn)_2O_4$, in which the Co and Mn cations occupy each site non-exclusively. The calcination pretreatment was shown to result in the enhanced crystallinity of the Co/MnO oxide spinel (from XRD data collated after calcination at 210°, 360° and 500°C), with major crystal growth and structural re-ordering, possibly occurring at ~195°C and ~340°C respectively (from exotherms of the DSC thermogram). The catalytic performance of an uncalcined and calcined catalyst, showed the former to exhibit similar selectivities but at a depressed CO conversion, when compared to the latter. (DSC studies performed during the reduction of uncalcined and calcined samples, suggested that this depressed activity could have been due to a slower reduction rate of the less crystalline uncalcined sample.) Subsequent reduction of the calcined catalyst precursor was observed to occur via a two stage process (from exotherms of the DSC thermogram at 230° and 380°C) to its final reduced state. XRD patterns collected *in situ* identified these two changes as an initial reduction at 230°C to MnO, plus possibly CoO (which, if present, was too amorphous and too finely dispersed to be detected by XRD); followed by the final

5.4 CONCLUSION

An investigation was made into some of the mechanisms involved in the catalytic action of cobalt/manganese oxide catalysts (and related systems), by following phase transformations *in situ*, during the activation (calcination and reduction) and operation of such systems. *In situ* DSC and XRD analytical methods were utilized in the study of these materials, which allowed us to probe the thermostructural behaviour of the systems under typical process conditions.

Initial studies followed phase transformations during calcination and subsequent reduction of the Co/MnO systems. The initial phase of the uncalcined oxide was indexed to the mixed oxide spinel $(Co,Mn)(Co,Mn)_2O_4$, in which the Co and Mn cations occupy each site non–exclusively. The calcination pretreatment was shown to result in the enhanced crystallinity of the Co/MnO oxide spinel (from XRD data collated after calcination at 210^0, 360^0 and 500^0C), with major crystal growth and structural re–ordering, possibly occurring at $\sim195^0$C and $\sim340^0$C respectively (from exotherms of the DSC thermogram). The catalytic performance of an uncalcined and calcined catalyst, showed the former to exhibit similar selectivities but at a depressed CO conversion, when compared to the latter. (DSC studies performed during the reduction of uncalcined and calcined samples, suggested that this depressed activity could have been due to a slower reduction rate of the less crystalline uncalcined sample.) Subsequent reduction of the calcined catalyst precursor was observed to occur via a two stage process (from exotherms of the DSC thermogram at 230^0 and 380^0C) to its final reduced state. XRD patterns collected *in situ* identified these two changes as an initial reduction at 230^0C to MnO, plus possibly CoO (which, if present, was too amorphous and too finely dispersed to be detected by XRD); followed by the final

reduction at 380°C of th CoO to Co metal (the extent of the reduction to Co metal was not measured). The reduction temperature of 400°C for the Co/MnO precursor (which had previously been determined to yield optimal subsequent catalytic performance) could thus be rationalized from this reduction study.

An *in situ* X-ray diffraction study was then performed on the preconditioned catalyst to follow phase transformations under typical F-T conditions. After prolonged exposure (112 hours) of the reduced catalyst to CO/H_2, new peaks at 2θ values of 44.73°, 65.13° and 82.54°, corresponding to (hkl) reflections of (110), (200), and (211) respectively, had appeared. These new peaks could only be indexed to a bcc cobalt phase, with relative intensities similar to those of iso-structural α-Fe. Further evidence for the transformation to this novel phase was observed from the gradual shift, with time-on-line, of the metallic Co(fcc) peak position at 2θ = 44.20° to the Co(bcc) peak position at 2θ = 44.73°. Even after exposure of this sample to air, only cubic MnO and Co(bcc) were present, indicating a certain stability of Co(bcc) in air. However, after lightly crushing a portion of this sample (and leaving in air for a period of time), XRD had revealed that a phase transformation back to Co(fcc) had occurred. This rapid transformation back to Co(fcc) suggested that Co(bcc) is a metastable phase. The lattice parameter a, for Co(bcc) was calculated to be 0.286 nm, in contrast to that of 0.354 nm for Co(fcc). Until now, no direct confirmation of the bcc structure of the bulk phase of cobalt had yet been published. However, surface XRD investigations (under special conditions) have provided evidence for the epitaxial-growth of Co(bcc) on certain substrates.

To determine the influence of the host matrix, MnO, on forcing or

generating the Co(bcc) phase, similar experiments were performed on Co_3O_4 (i.e. in the absence of the MnO matrix). After calcination, the Co_3O_4 oxide spinel was reduced to metallic Co(fcc) under hydrogen at 400°C. After exposure of the reduced sample to CO/H_2 at 220°C for 175 hours, the observed peak at $2\Theta \simeq 44°$ had increased to about 3 times its initial height, and with other diagnostic lower intensity peaks appearing at approximately $2\Theta = 65°$, 82° and 102°, a positive identification to the bcc phase of Co could be made. Thus the formation of the metastable Co(bcc) phase from the Co_3O_4 precursor, in the absence of a host matrix, minimised any influence of the support in forming this novel phase.

This investigation was extended by again performing *in situ* XRD investigations under similar experimental conditions, on additional catalyst supports namely Al_2O_3 and Cr_2O_3. The room temperature XRD temperature collected after calcination of the 5% Co_3O_4 on Al_2O_3 system, established that the sample was a mixture of Co_3O_4 and Al_2O_3 spinel phases. After reduction, (under H_2 at 400°C) the Co_3O_4 appeared to have fully reduced to Co(fcc) metal. After continued exposure (48 hours) of this sample to synthesis gas, the observed peak at $2\Theta = 45°$ had increased to more than four times its original height, with secondary peaks at the positions corresponding to Co(bcc), again appearing. The formation of Co(bcc) on the Al_2O_3 support, corroborated the conclusions of previous experiments with Co_3O_4, i.e. in eliminating any influence of the MnO matrix in the formation of Co(bcc). Reduction of the calcined $CoCr_2O_4$ system to Co(fcc) + Cr_2O_3, was only achieved at a temperature of 800°C. Clearly, in this instance, the matrix (Cr_2O_3) does have a strong influence on the reduction behaviour of the Co^{2+} ions. Also, only after 7 days of continued CO/H_2 exposure, was the formation of a small peak at $2\Theta \sim 44°$ observed, indicating the presence of a possible

Co(bcc) phase (the secondary Co(bcc) peaks were not observed). The CoCr$_2$O$_4$ system was thus more reluctant to form Co(bcc). This could have been due to the possibility of a very stable Co(fcc) formed at the high reduction temperature of 800°C.

High selectivities toward propene (coupled with low methane production) that had previously been established for the Co/MnO catalysts, could be correlated to the formation of Co(bcc). These selectivities, however, were not observed with Co/Cr$_2$O$_3$ (high alcohol production) or Co$_3$O$_4$ (high methane and low propene selectivities). In the case of Co/Al$_2$O$_3$, catalytic data report high selectivities to light alkenes, but at low CO conversion.

Since the role of any support in the formation of Co(bcc) could be discounted on the basis of this phase being formed with Co$_3$O$_4$; the role of CO, H$_2$ and temperature needed to be considered. It was proposed that Co(bcc) was formed through the formation of a *cobalt–carbonyl intermediate*, which then by further action upon by H$_2$ and/or temperature, would generate the Co metastable phase.

CHAPTER SIX

A NOVEL ELECTROLESS DEPOSITION METHOD OF
CATALYST PREPARATION FOR IMPROVED C_3^+ SELECTIVITY

6.1 INTRODUCTION

Supported catalysts are one of the most common forms of heterogeneous catalysts in practical use (9,213,214), and consist of a catalytically active metal component dispersed in a porous support of high surface area. Advantages of these supported–metal catalysts lie in their high surface–to–volume ratio and the high thermal stability endowed by the dispersion (215). Such catalysts are commonly produced by liquid–phase impregnation (being the simplest and most direct method of deposition) in which dry or wet pellets of the porous support are impregnated with a solution of a compound of the desired catalytic constituent (215,215a). During impregnation and subsequent drying, small crystallites of the catalyst precursors are deposited on the internal surface of the support material.

6.1.1 Metal support impregnation

The impregnation and drying steps involve mass and/or heat transfer processes which often do not reach equilibrium, resulting in non–uniform concentration profiles of impregnant, "impregnation profiles" along the radius of the support pellet (215). The metal loading profile of the supported catalyst is an important factor in determining the performance of the catalyst (213,215,215b). Examples of these impregnation profiles (along with activity profiles) are shown in Figure 6.1.
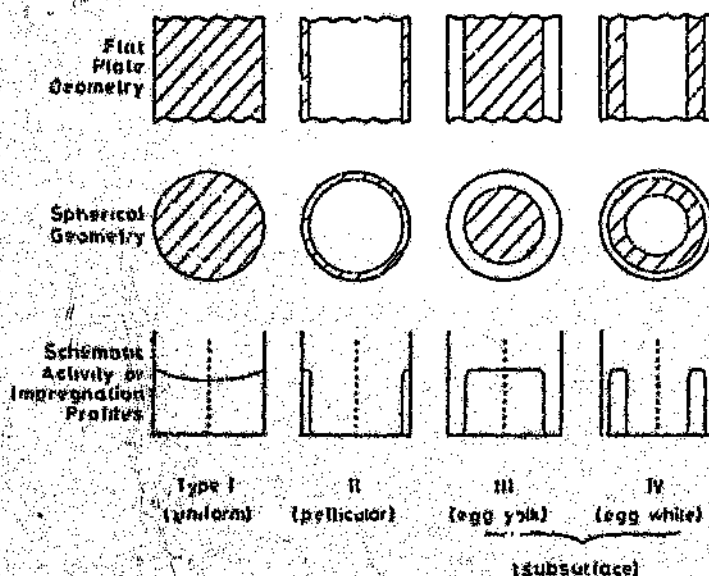
Figure 6.1: Four limiting types of impregnation or activity profiles. Hatched areas in the cross sections of slabs and pellets (top and middle rows) indicate the regions where active components are deposited. The bottom row shows schematic examples of impregnation or activity profiles (215).

The Type I profile is sometimes referred to as "uniform", although the local activity or local metal concentration may not be constant with respect to pellet radius, as shown by the schematic profile. Type II is often referred to as "pellicular" or "egg-shell", Type III as "egg-yolk", and type IV as "egg-white". Types III and IV, in which bands devoid of active material are established on the exterior of the support pellet, are also termed "subsurface impregnation" types (213,216). The effect of nonuniform activity profiles on the performance of catalyst pellets was first discussed by Shadman–Yazdi and Petersen in 1972 (215c). It is of considerable industrial as well as academic interest to predict and control these impregnation profiles. For example, in automotive emission control used in a real outer exhaust gas converter, the

egg–white distribution w ꞏ found to be best for Pt/Al$_2$O$_3$ catalysts, judged by both activity and stability (215). Also, the egg–white and egg–yolk catalysts have been shown to be beneficial in applications where severe attrition occurs, since only he inert and inexpensive support is worn off and the precursor active metals are saved (213).

Several studies on the effect of nonuniform activity distribution on parallel and consecutive reaction selectivity, have been conducted by exploring various monoparametric activity distribution profiles (215d–215h). For the use of parallel reactions in pellets used for C$_2$H$_4$ epoxidation, selectivity to ethylene oxide was found to increase as the catalyst concentration increased toward the external pellet surface (215f). The problem of determining the optimal catalyst profile for selectivity maximization in parallel and consecutive reactions, was recently solved analytically for arbitrary catalytic reaction kinetics in both isothermal and nonisothermal pellets (215j–215k).

6.1.2   F–T catalyst preparation

The preparation of supported F–T catalysts of prescribed activity and selectivity has long remained a somewhat artistic and proprietary matter, because of the large number of physicochemical factors involved that are not well understood and difficult to control (38,77,217). The need for new catalysts able to lead to a selective production of chemical feedstocks, such as olefins or alcohols from syngas, promoted a new apporach for their preparation as soon as it became clear that the structure of the catalysts was a key factor for their properties (87). In search for an ideal catalyst, it is perhaps instructive to establish a relationship (probably empirical), between

the kinetic parameters and such innate catalyst properties as, dispersion, percent loading, composition, and metal particle size (218). Studies by Reuel and Bartholomew (77,78) suggested that α (Schulz–Flory chain growth probability factor) is strongly sensitive to these catalytic properties. Also for catalysts prepared by the decomposition of zerovalent metallic complexes on a support, the chain length of the products for this type of catalyst has been shown to be governed by the pore size distribution of the support (75). Research on the scientific basis of catalyst preparation has grown rapidly with improved impregnation and preparation techniques (95,99,154,214,219–221). Methods of catalyst preparation has also been discussed in Section 1.3.3(a).

6.1.3   The Shell cobalt impregnated catalyst

Of particular interest is the novel synthesis catalyst developed by Shell Internationale Research [for their Middle Distillate Synthesis (MDS)], in which the active Co metal was impregnated on the support in such a manner as to adopt the Type II or "eggshell" profile – the process for the preparation of such catalysts have been patented by Shell (36,37). The patents relate to a process for the preparation of such catalysts by immersing a porous carrier (either alumina, silica or an alumina/silica combination), once or several times in a solution of cobalt in hydroxyethylcellulose, or in organic solvents, such as ethanol or glycol. The liquid is then removed from the composition after each immersion by drying or calcining. It was found that the catalysts having an inhomogenous cobalt distribution showed significantly improved C_5^+ selectivity as related to catalysts with a homogenous cobalt distribution, only when the inhomogenous cobalt distribution is such as to meet the

requirement

$$\frac{\Sigma V_p}{\Sigma V_c} < 0.85 \quad ,$$

where ΣV_p —   total peel volume containing 90% of the quantity of Co present in the total volume.

and ΣV_c —   total volume of the catalyst pellets under consideration.

The claimed enhanced C_5^+ selectivity (of which the commercial importance has been detailed in Chapter 4) obtained with these catalysts has been thought to be associated with temperature gradients across the catalyst pellets (222). For uniform or homogenous type distribution, temperature is thought to increase along the radius of the pellet maximizing in the pellet centre. The collective effect in this case would be to produce a greater proportion of shorter chain hydrocarbons, especially methane. For "egg–white" or inhomogenous Shell–type distributions (where 90% of the cobalt is situated in the previously described peel volume) the catalysts would be less subjected to temperature gradients, and would thus consequently produce the proposed longer chain hydrocarbons i.e. increased C_5^+ selectivity.

It was our aim to investigate the possibility of producing quantities of active silica/alumina – supported cobalt catalysts; the metal being deposited only on the outer zone of the support pellets, so as to comply with the previously discussed Shell patent formulation.

6.1.4 Initial considerations of a novel electroless deposition technique for supported metal catalyst preparation

An alternative method for making supported catalysts by the electrochemical techniques of anodization and electrodeposition has been studied by Miller et al. (124). Anodization of aluminum foil in an inorganic acid creates a highly porous aluminum oxide substrate into which the transition metal is electrochemically deposited. This method allows for the facile control of the catalyst structure, as the pore size and the density are determined by the electrochemical parameters and the strength of the acid employed in the anodization process. The metal particle size distribution and the metal content are controlled by deposition voltage, time, and frequency.

The suggested ease over the control of catalyst structure and metal deposition of the above study, makes these electrochemical methods of catalyst preparation an attractive alternative. After careful consideration it was decided that electrochemical methods could in fact be investigated in the preparation of our Shell type analogues. However, since our support (silica-alumina) is a non-conducting material (unlike the aluminum foil of the above study), electrochemical methods would have to be discounted and replaced in our case by *electroless deposition methods* (i.e. in the absence of an externally applied potential). [A brief introduction into the theory of electroless deposition is given in the section to follow.] Our investigation followed an electroless plating technique, whereby the outer layers of the support (peel volume) would be electrolessly plated with Co metal, such that at least 90% of the metal would be deposited in this peel volume and satisfy the quotient $\Sigma V_p / \Sigma V_c < 0.85$.

6.1.5   Theory of electroless plating

Electroless plating is the autocatalytic reduction of dissolved metal ions from solution to produce a coherent film of metal, without the use of an externally applied potential (223,224). This reduction of metal ions occurs only on a surface of a suitable catalytic substrate in contact with the plating solution. A chemical reducing agent in the solution supplies the electrons for the reduction of the metal salts to their elemental form, i.e.

$$M^{2+} + 2e^- \text{ (supplied by the reducing agent)} \xrightarrow{\text{catalytic surface}} M^0$$
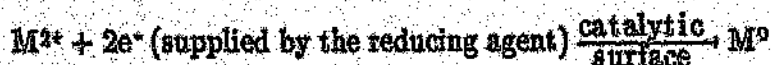
Electroless plating can occur on non-conductors, for example on our silica/alumina support (where direct electroplating is of course not possible), once the surface has been made catalytic by a suitable activation treatment [as described in Section 6.2.2] (223). The metal being deposited must itself be catalytic in order that the deposition be maintained (224).

Electroless plating baths are invariably aqueous solutions which include some or all of the following components: a metal salt (source of M^{n+}), reducing agent (source of e^-), buffering reagents (plating rate and bath stability may be sensitive to pH), complexing agent for the metal ion (especially important for baths operating under alkaline conditions), stabilizers (to prevent spontaneous decomposition of the plating bath which are inherently thermodynamically unstable), and substances which accelerate the deposition rate. Generally plating baths may operate from room temperature up to the boiling point of water (223–225). Since impurities of 1 ppm or less can profoundly affect the plating process, it is not surprising to find that the behaviour of these plating baths can be quite unpredictable. Hence, published bath formulations may not work in everybody's hands, and baths which work well on one substrate may fail totally on another (223).

The electroless plating of cobalt (and other group VIII metals) is a novel technique in catalyst preparation. The electroless plating of certain of these metals are used extensively in a variety of industrial applications. Electroless plating of Ni produces a layer of excellent properties (when incorporated with phosphorous and boron), and boasts a $100 million industry (226). Electroless copper plating with formaldehyde as the reducing agent, always gives crystalline metal layers, and has a wide application in the manufacture of printed circuit boards (227,228). Deposition of gold, palladium and gold: palladium alloys (from acidic baths of low metal content), allows for the fabrication of multilayered heterostructures which could come to good use for ohmic contact preparation onto n–GaAs (229). The electroless plating of Co–P films has been recognized to be a useful and

le procedure in high–density magnetic recording technology, and has generated an enormous amount of research (230–232). A variety of metals such as Ni, Co, Pd, and Cu are used for contact filling, via hole filling, and for conductor patterns in integrated circuit fabrication (233). These materials are selectively deposited onto a variety of surfaces such as silicon, silicide, Al–Si, and photoresist. Although this process is still in its early stages of development, very promising results have already reported to have been achieved.

In this Chapter we discuss the initial stages and modifications in the development of an electroless plating procedure for the production of silica/alumina – cobalt supported catalysts. This objective was to produce catalysts which would comply with the Shell type specifications for enhanced C_5^+ selectivity in F–T synthesis.

6.2 EXPERIMENTAL

6.2.1 Catalyst support

The cobalt electroless plating experiments were performed on proprietary extruded silica–alumina pellets obtained from Sastech (Sasol 1, Sasolburg, South Africa).

6.2.2 Support preparation

For the electroless plating of non–conducting materials, an activation step is required to render the surface catalytic to plating. This is achieved using stannous chloride and palladium chloride (or nitrate) solutions (223–225). To produce a catalytic film, the support was treated first with acidified $SnCl_2$ (solution of 0.053M $SnCl_2$ + 0.040 M HCL) which adsorbed onto the surface. After thorough rinsing in water, the support was then immersed in acidified $PdCl_2$, and in later experiments $Pd(NO_3)_2$ (solutions of 1.41 x 10^{-3} $PdCl_2$ + 2.50 x 10^{-3} M HCl; 2.17 x 10^{-3} M $Pd(NO_3)_2$ and 2.50 x 10^{-3} M HNO_3), which produced a surface on which electroless plating could be initiated. Simplistically, the process might be represented by equation (1).

$$Sn^{2+} + Pd^{2+} \rightarrow Sn^{4+} + Pd \tag{1}$$
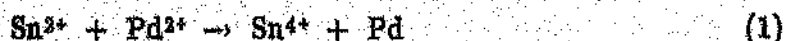
Detailed surface investigations have indicated that a more complex situation takes place (223). The degree of penetration of Co plating, and thus the V_p/V_c ratio was found to depend largely on the Sn and Pd pretreatment procedure. Variables such as soaking times and washing procedures related to Co penetration are discussed in detail, in sections to follow.

It was later found that since the support was porous in nature, the $SnCl_2$ treatment to initiate anchorage of Pd onto the surface, was unnecessary. Later experiments thus involved support pretreatment with

$PdCl_2$ or $Pd(NO_3)_2$, only.

6.2.3 Cobalt bath components

Cobalt was electrolessly deposited from an alkaline hypophosphite–based aqueous solution. Essentially, cobalt ions are catalytically reduced to the metal in alkaline solution by hypophosphite ions, which are thereby oxidized to orthophosphite ions, as shown in equation (2).

$$Co^{2+} + (H_2PO_2)^- + OH^- \xrightarrow[\text{surface}]{\text{catalytic}} Co^0 + 2H^+ + (PO_3)^{2-} \tag{2}$$
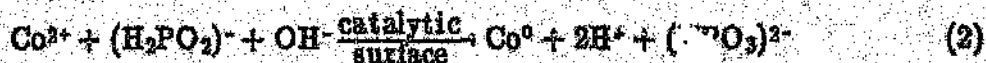
At the same time, elemental phosphorous, which immediately alloys with the cobalt, is produced through reduction–hydrolysis of a fraction of the hypophosphite ions. Simultaneously, more hypophosphite anions are oxidised to phosphite with evolution of H_2, as shown in equation (3).

$$(H_2PO_2)^- + OH^- \rightarrow (HPO_3)^{2-} + H_2 \tag{3}$$
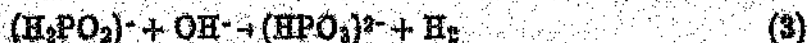
The plating baths contain a cobalt salt and a reducing agent. In addition, a complexing or chelating agent, generally a citrate salt (sodium citrate), is also needed. This stabilizers the solution and tends to inhibit the production of cobalt phosphite precipitates. The very nature of these side products will tend to slow down the plating rate of a bath (224). A buffering agent is also used in order for the bath pH to be maintained between 9 – 10. Even with the use of buffers, chemical plating baths require additions of an alkaline compound such as ammonium hydroxide to maintain the bath within the pH operational parameters. As the pH drops so does the plating rate until a point is reached where the solution will not initiate or sustain deposition (223).

The electroless cobalt bath components are shown in Table 6.1 (233).

TABLE 6.1: Bath composition for electroless cobalt deposition

cobalt chloride/nitrate[a] (deca hydrate), g/ℓ	30, 60
sodium hypophosphite, g/ℓ	20
sodium citrate, g/ℓ	30
ammonium chloride/ammonium nitrate[a], g/ℓ	50
pH (adjustment by addition of NH_4OH)	9 – 10
temperature, °C	30 – 90

[a] In later experiments, the bath composition was modified in order to eliminate the presence of chlorides, which are known to poison F–T catalysts (10).

6.2   Catalyst characterization

(a) Optical microscopy

Optical microscopy was used to determine the degree of penetration of Co into the support, and thus the Vp/Vc ratios. At a microscopic magnification of 50 times, 50 lines in the microscopic field represent a real distance of 1 mm. The respective dimensions of the catalyst i.e. diameters of plated and non–plated regions and pellet length, could be determined. The respective volumes for the Vc/Vp ratios could thus be estimated from equations (4), (5) and (6) as demonstrated in Figure 6.2.
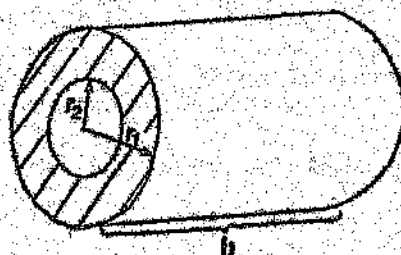
Figure 6.2:   Determination of Vc and Vp by optical microscopy.

$$V_c = \text{total volume of the catalyst pellet} = \pi r_1^2 h \qquad (4)$$

$$\text{where} \quad r_1 = \text{radius of pellet}$$

$$h = \text{length of pellet}$$

$$V_s = \text{volume of support not plated} = \pi r_2^2 h \qquad (5)$$

$$\text{where} \quad r_2 = \text{radius of area not plated (i.e. inner core)}$$

$$V_p = \text{volume of peel containing plated Co} = V_c - V_s \qquad (6)$$

$$= \pi h (r_1^2 - r_2^2)$$

(b) **Determination of percentage mass of Co in peel volume by AAS**

The percentage mass of Co in the peel volume was determined by AAS. The samples were prepared for analysis by crushing and soaking 0.2 g of catalyst in 10 mℓ of aqua regia (HCℓ:HNO$_3$ = 3:1) for a period of ~20 minutes. These solutions were subsequently heated at boiling point for 1 minute, then made up to 1ℓ volumes in distilled water, and absorbances measured.

(c) **Reactor studies**

CO hydrogenation was performed over the electrolessly Co plated catalysts in laboratory microreacters, as previously described in Chapters 2, 3 and 4.

6.3 RESULTS

The plating techniques and optimization studies of penetration are now discussed. The outer layers of the silica–alumina supports were electrolessly plated with Co, to achieve a ratio requirement of $V_c/V_p < 0.85$ (as previously described from Shell patent claims). Furthermore, for

acceptable F–T activity levels, the concentration of the active Co metal within the so–called "peel volume" should be greater than 10% (78,88), and thus attempts to maximize this concentration was also investigated.

6.3.1   Initial plating studies

Due to the novelty of this procedure in F–T catalyst preparation, it was decided that initial plating and optimization studies would involve the use of a recommended Co plating bath only (224). Once certain plating and depth controlling variables could be defined, necessary modifications to the bath components could be made. For example, variations in activation pretreatments i.e. controlling Co depth profiles within the support, and elimination of chloride reagents (which are known to poison F–T catlysts) on the catalyst synthesis were eventually attempted.

Pellets were activated by successive treatments in $SnCl_2$ for 2 – 5 minutes each. After each respective treatment the pellets were thoroughly rinsed with H_2O. The plating bath (using the bath as described in Section 6.2.3 with $CoCl_2$ as a cobalt source) was heated to 85°C, with the pH maintained between 9 and 10 by the addition (dropwise) of a concentrated ammonium hydroxide solution. The activated pellets were then placed into the plating bath. Plating occurred almost immediately as manifested by a black layer of Co metal that was deposited onto the surface of the white support, coupled with vigorous evolution of gas. Plating was allowed to continue for 30 seconds after which the pellets were removed, rinsed with H_2O, and allowed to dry (in air). The plated pellets were broken in half and the plated layer and profile measured. In all of the plated pellets, the deposited Co layer appeared to be continuous and not to have penetrated into the support. Rather the Co had formed a plated layer on the support surface

only. Since *penetration* of the Co layer *into* the support was necessary, certain modifications to substrate activation were needed, and are discussed in the following section.

6.3.2   Removal of surface support plating initiators to effect Co penetration

In order to effect Co penetration within the support, the surface plated layer had to be prevented, which was obviously inhibiting further plating of Co within the pores of the substrate. This was achieved by the selection of suitable solvents in order to remove the surface Sn and Pd sensitisers, and in effect remove the surface plating initiators. Thus, the activation pretreatment was modified such that after the stannous treatment, the pellets were thoroughly washed in alcohol; and after the palladium treatment, the pellets were thoroughly washed in aceton_____. pellets were then plated as previously. The plated pellets now revealed plated Co penetration within the support, rather than the formation of an outer surface layer only. Enhanced plated Co penetration was further achieved by optimizing immersion time in the activation pretreatments – this is discussed in the sections to follow. The two Co plating profiles as obtained from plating the support before and after the solvent washing modification, are well illustrated by the optical and electron micrographs as shown in Figure 6.3(a) and (b), respectively. The data suggest that it should be possible to control deposition of the active component within the support, to form the different intra– concentration profiles of the catalytically active metal and activity profiles as shown in Figur 6.1 (215).

6.3.3 Support activation and subsequent Co plating in the absence of SnCl₂

As previously discussed, activation of non-conducting materials involved sensitization with both stannous chloride and palladium chloride solutions. The primary function of SnCl₂ is to adsorb onto a smooth surface onto which subsequently Pd may anchor. This process is known as cementation and can be described by the following equation:

$$Sn^{2+} + Pd^{2+} \rightarrow Sn^{4+} + Pd^{0}(surface)$$

An attempt was made to see if the SnCl₂ step could be removed from the process since silica-alumina is known to have a rough texture. A plating bath was thus prepared, as previously, into which pellets activated by PdCl₂ treatment only (5 min. soak in PdCl₂, followed by an acetone rinse) were placed. Vigorous plating of these pellets occurred forming a continuous Co plated layer within the support. From this study it was concluded that treatment with SnCl₂ for the purposes of anchoring the Pd catalyst onto the support, could be avoided in future work. This result was particularly important in later bath-modification studies, in the elimination of chloride ion reagents.

6.3.4 Effect of activation and bath plating variables on plated Co penetration and percent mass loading

These experiments were undertaken in an attempt at establishing a control over Co plated penetration and percent mass loading on the support, by investigating such variables as, time of immersion of support in PdCl₂, Co salt bath concentration, effect of plating times at different
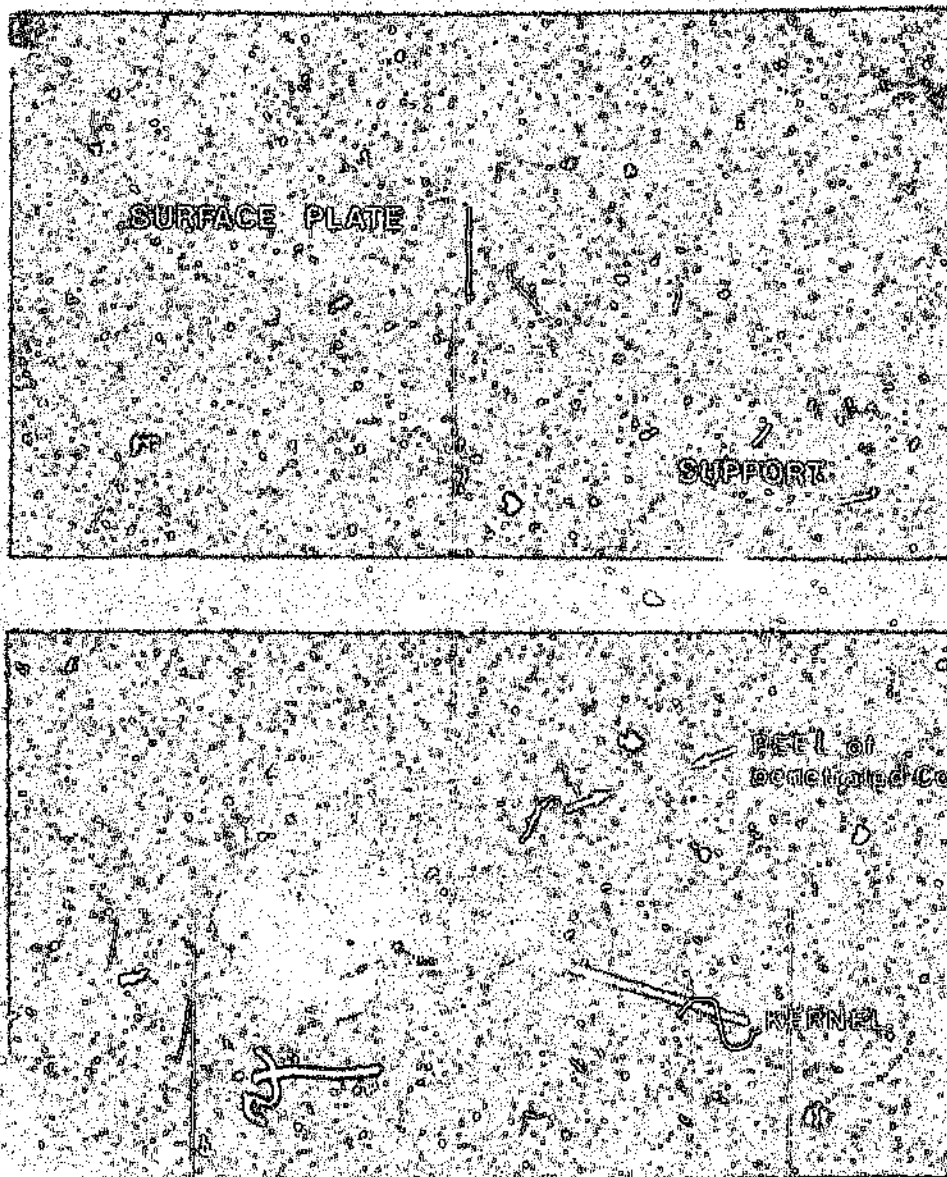
Figure 6.3(a) and (b):

a, electron micrograph (1400x) of the plated support *before* the solvent washing modification, showing plating on the *pellet surface only* (no Co penetration).

b, optical micrograph (20x) of the plated support *after* the solvent washing modification, showing the penetration of plated Co into the support, with minimal Co plating observed on the substrate surface.

temperatures, and the effect of PdCl₂ activation treatment at different temperatures. These effects will now be discussed in turn.

(a) Effect of immersion time of support in PdCl₂ during activation

Catalyst support was soaked in PdCl₂ solution for times of between 5 and 180 minutes. After each respective PdCl₂ soak, the support was washed in acetone, and then plated in an alkaline CoCl₂ bath at 65°C for one minute. The experiment was then repeated, but using Co(NO₃)₂ as a cobalt source (80°C, one minute). Plated catalysts were broken in half and penetration depths for the two experiments then determined [by optical microscopy as previously described in Section 6.2.4(a) and (b)]. The results are shown in Table 6.2, and Figures 6.4(a) and (b) respectively.

TABLE 6.2: Effect of PdCl₂ soaking time on plated Co depth penetration

PdCl₂ soak time/min	plated Co penetration/mm[a]	
	CoCl₂ bath	Co(NO₃)₂ bath
5	0.20	0.18
10	0.24	0.22
20	0.33	0.36
30	0.51	0.52
60	0.87	0.92
120	1.11	1.10
180	1.25	1.28

[a] A comparison between the two Co sources (plated at different bath temperatures) w.r.t. Co penetration can be made, since it has been shown (in later studies) that bath temperature does not significantly affect Co support penetration, only % Co loading – see Table 6.4.

From the results of Table 6.2, it is evident that depth penetration of plated Co into the support can be controlled by the time of immersion in the $PdCl_2$ activator solution, which migrates into the pores of the support, and thus locally activates subsequent plating. In addition, successful plating was also achieved by substituting the cobalt chloride salt with that of a nitrate salt, furthering our objective of eventually avoiding the use of chloride containing reagents. It may also be concluded that the source of cobalt ions did not affect the degree of plated Co penetration into the substrate. An immersion time of 60 minutes corresponded to a V_p/V_c ratio of approximately 0.69 (for both cobalt sources), which met the V_p/V_c Shell claim requirements of being less than 0.85. However, determination of total metal content for this ratio, showed the cobalt loading to be less than 2% by mass. This is an insufficient concentration for acceptable F–T activity. Additional experiments were performed to determine the Co loading as a function of the time of immersion in $PdCl_2$ (i.e. Co plated penetration). Support was soaked in $PdCl_2$ for various time periods and was then plated in a $Co(NO_3)_2$ bath for 2 minutes at a temperature of 70°C. Results of plated Co penetration and loading are given in Table 6.3.

From Table 6.3, it is evident that although plated Co penetration increased with increased $PdCl_2$ immersion time (as previously shown), the percent Co loading did not increase, but remained approximately constant.

The poor F–T catalyst activity at low metal loadings appears to be related to the interaction of metal oxides with the support and the influence of this interaction on the reducibility of the oxide (88). Metal
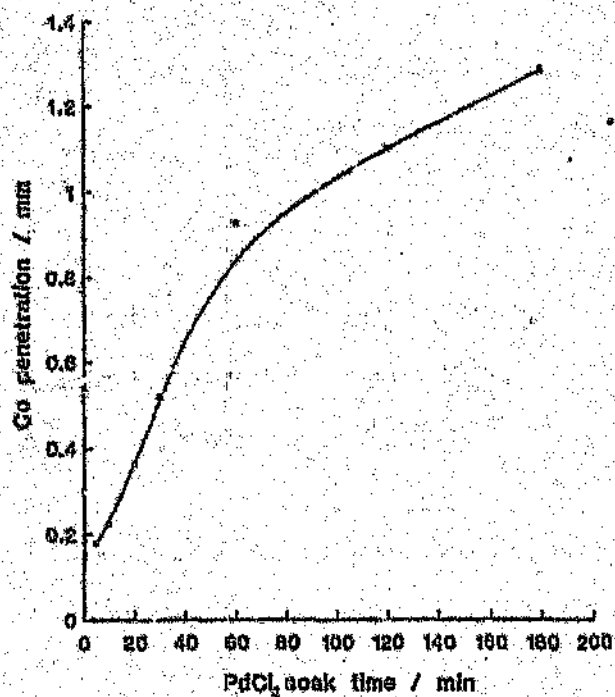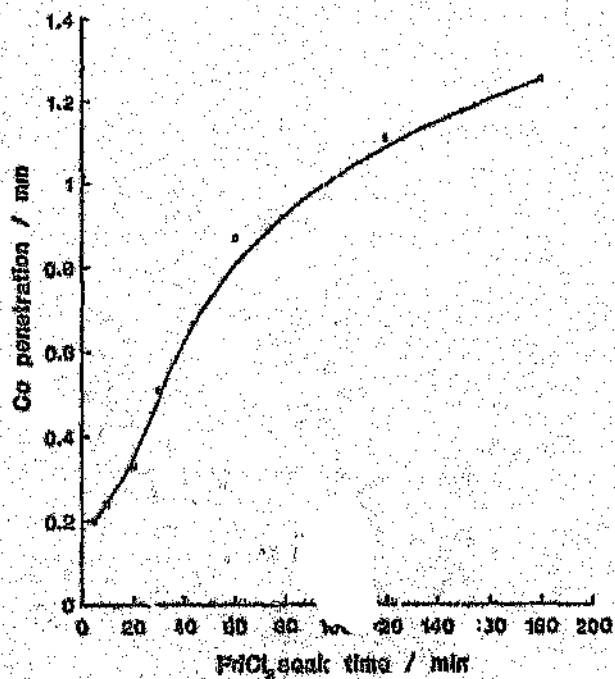
Figure 6.4(a) and (b):   Penetration of plated Co into support as a function of $PdCl_2$ soaking time, for catalysts plated in, a $CoCl_2$ and, b $Co(NO_3)_2$

TABLE 6.3: Effect of immersion time in PdCl₂ on plated Co p~ _tration and % mass loading

PdCl₂ immersion time/min	Plated Co penetration /mm	Vp/Vc	Co loading /% by mass
10	0.64	0.72	7.0
30	0.54	0.64	6.5
60	0.76	0.81	7.0
120	0.86	0.87	5.7
180	0.92	0.90	6.7

cations may interact strongly with supports such as silica and alumina (216), forming silicates and aluminates (234), which are not as easily reducible as the bulk oxides. As the metal loading is increased a more easily reducible "bulk-like" phase forms on the surface of the catalyst, and the catalyst becomes increasingly active.

Experiments were thus performed in an attempt at increasing the cobalt concentration to acceptable levels (> 10% by mass), but keeping within the desired Vp/Vc ratios of less than 0.85.

(b) The effect of Co(NO₃)₂ bath concentration on plated Co loading

Support was immersed in PdCl₂ for various time periods and subsequently plated in Co(NO₃)₂ baths of 30 and 60 g dm⁻³ respectively. Vp/Vc ratios corresponding to plated Co concentrations were determined, the results of which are given in Table 6.4.

From the results of Table 6.4, it is evident that increased plated cobalt loadings may be realized by increasing the Co bath concentration. However, increased V_p/V_c ratios were also observed to have occurred with increased Co bath concentration which exceeded the limit of 0.85, as illustrated in Table 6.4 and Figure 6.5 (this being especially true for shorter soak times i.e. < 60 minutes). Further optimization studies were thus required involving different plating times and at different bath temperatures, in order to maximize plated Co loading within the limits of the V_p/V_c ratio, i.e not exceeding 0.85. [The control used in this study was support not activated with $PdCl_2$ (i.e. immersion time = 0)]. Here, Co loadings were also observed to have increased with increased Co bath concentration, but obviously no plating had occurred, and the Co was homogeneously distributed throughout the pellet with $V_p/V_c = 1$.

TABLE 6.4:   Effect of Co bath concentration on plated Co support penetration and loading

Co bath concentration/gdm⁻³	PdCl₂ immersion time/min	Vp/Vc		Co loading/% by mass	
		30	60	30	60
	0	1.00	1.00	6.5[a]	9.9[a]
	60	0.75	0.91	4.0	10.0
	120	0.88	0.96	4.8	10.3
	260	0.97	0.98	4.8	7.8

[a] *At this stage* optimum plated Co loadings (i.e. > 10% Co) had not yet been achieved, and higher levels of Co were obtained by simple impregnation with the control samples. The presence of the Pd activator for the plated samples has been shown to limit the diffusion of Co into the kernel of the support (see Section 6.3.2).
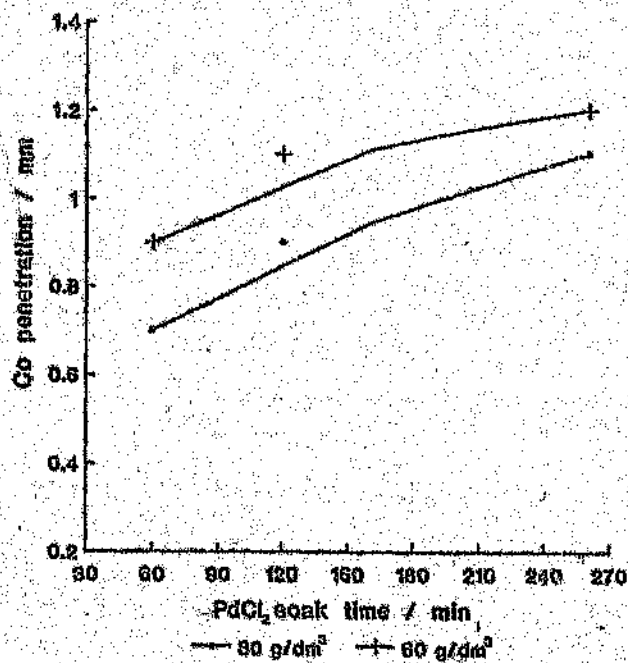
Figure 6.5:   Plated Co support penetration with Co(NO₃)₂ plating bath concentration of 30 and 60 g dm⁻³ respectively.

(c) Effect of plating time at different bath temperatures

Silica–alumina support was immersed in PdCl$_2$ for one hour, and subsequently plated in a Co(NO$_3$)$_2$ bath (60 g dm^{-3}) at 50° and 70°C respectively, for periods of between one to thirty minutes. Results of plated Co loading and Vp/Vc ratios as a function of plating time for the two bath temperatures are shown in Table 6.5.

TABLE 6.5: Results of plated Co loading and Vp/Vc ratios as a function of plating time at bath temperatures of 50° and 70°C, respectively.

bath temperature /°C	plating time/min	Vp/Vc		Co loading/% by mass	
		50	70	50	70
	1	0.78	0.62	6.9	10.5
	2	0.86	0.80	9.0	8.7
	5	0.90	0.86	8.8	13.4
	10	0.94	0.89	7.6	15.1
	15	0.97	0.92	11.8	12.4
	20	0.99	0.98	12.3	13.0
	30	1.0	0.99	17.7	24.0

From the data in Table 6.5 it is observed that increased bath temperatures (i.e. 70°C) had resulted in higher plated Co loadings, accompanied by lower Vp/Vc ratios (i.e. degree of Co penetration), for any given plating time. The degree of plated Co penetration was also observed to be dependent on the length of plating time, increasing with increasing plating time. Thus, certain plating bath variables may be manipulated in various combinations in order to maximize Co loadings

within the limits of Vp/Vc < 0.85. For example, plating at 50°C for 2 minutes resulted in a Co loading of 9% with a corresponding Vp/Vc ratio of 0.86. However, plating of 70°C for a period of 5 minutes resulted in a Co loading of 13.4% with a corresponding Vp/Vc ratio of 0.86.

6.3.5   Elimination of chloride reagents from the Co plating bath

The presence in the feed stream of small quantities of certain substances can cause the activity to fall markedly. This common cause of deactivation is called "poisoning", which is due to strong chemisorption of these substances on the active sites, thereby blocking them for reaction (10). Strong alkali metals of Group I promote the activity of metal catalysts, and thus it may be expected that highly electronegative elements, e.g. sulphur, will act as poisons. Chloride ions (in small quantities) have been known to be effective poisons in F–T synthesis over iron catalysts (10), and thus similar effects were thought to become relevant over cobalt based catalysts (222). The total removal of chloride containing reagents from our plating baths had thus become a priority if this was to become an alternative method of Co catalyst preparation. Initially the removal of chloride ions was attempted by long periods (24 hours) of soxhlet extraction, after plating in $CoCl_2$ (30 g dm^{-3}) for one minute at 65°C (using $PdCl_2$ as the sensitizer). XPS and EDAX analysis performed on these samples had shown there to be a considerable decrease in the chloride ion concentration (from observed decrease in the respective signals toward Cl ions) after soxhlet extraction. However chloride ions not removed by this process were present in sufficient quantities for there to be a potential poisoning concern. (XPS and EDAX analysis were preformed at the CSIR, Pretoria.)

One step in partially resolving this problem was from successful

plating observed using a $Co(NO_3)_2$ bath (as previously mentioned). The remaining chloride in the bath was derived from the $PdCl_2$ support sensitiser, thus an alternative Pd salt needed to be considered. Activation using a $Pd(NO_3)_2$ solution (0.25 g dm^{-3}, after dissolving $Pd(NO_3)_2$ in HNO_3) was attempted by soaking the support in this solution for 60 min, followed by subsequent $Co(NO_3)_2$ bath treatment at 70°C for 10 minutes. Under these conditions no plating was observed, but rather simple impregnation of the Co into the support had occurred. It was thought that this could have been due to an insufficient $Pd(NO_3)_2$ concentration, i.e. a concentration too low to initiate plating.

A study was thus conducted to determine the minimum possible concentration of $Pd(NO_3)_2$ required to activate Co plating onto the support. This was achieved by soaking pellets in various concentrations of $Pd(NO_3)_2$ solutions for 2 minutes, and subsequently placing the pellets into a $Co(NO_3)_2$ bath at 70°C for one minute. The quality and extent of Co plating was then observed.

This study showed that the lowest possible concentration of $Pd(NO_3)_2$ for which acceptable Co plating was initiated is 0.6 g dm^{-3}, corresponding to almost double the $PdCl_2$ concentration required to initiate the same standard of plating. (A possible reason for this could be due to the effect of the respective counterions on the adsorption of the Pd^{2+} ions onto the support). However, the plating of a cobalt layer onto a silica-alumina support had shown to be successful in the absence of any chloride reagents. Penetration of a cobalt layer with Vp/Vc < 0.85 and loading > 10% had been achieved by immersing the support in $Pd(NO_3)_2$ (0.6 g dm^{-3}) for 60 minutes and then plated in an alkaline $Co(NO_3)_2$ bath (60 g dm^{-3}) at 70°C for 10

minutes. The resulting sample had a Vp/Vc of 0.84 and a Co loading of 12.3% (m/m).

It had also been brought to our attention that phosphorous (from the reducing agent sodium hypophosphite, which alloys with the Co metal during plating) is also an effective F–T poison (222), and should thus also be taken into consideration for the modified bath formulation. It has been reported that phosphorous loadings of up to 8% (by mass) may alloy with cobalt during plating (224,225,235), and thus it is import:)t for an alternative reducing agent to be investigated. This study is currently been undertaken by colleagues at the Catalysis Research Programme (University of the Witwatersrand), with alternative reducing agents such as borohydrides. These reagents have been successfully used as the reducing agent for electroless plating of Ni (225).

6.3.6   Preliminary catalyst characterization

From the X–ray photoelectron spectroscopy performed on the sample of Section 6.3.5, cobalt was also observed to exist as CoO and not as metallic cobalt, as had been previously surmised. It was thought that the cobalt was initially plated as Co metal, which then subsequently oxidized to CoO in the presence of O_2 and H_2O; this process being promoted by redox contributions from acidic SiO_2/Al_2O_3 support. This war ˙ ˙uced from the transformation of the initially black Co peel (i.e. Co metal,   dark navy blue Co peel (i.e. CoO), with time after plating. This was no cause for concern since the plated cobalt on the support would be reduced to the metal by heating *in situ* to 400°C under a stream of H_2, prior to F–T synthesis.

An electron micrograph (1200 x) of the cobalt surface deposit, showed the microstructure which developed during plating to consist of relatively large crystallites separated by crevices, as shown in Figure 6.6 The development of this surface characteristic could be explained by assuming that phosphorous acts as a growth inhibitor (231,232). When the phosphorous concentration at the metal-solution interface is low, growth can continue predominantly laterally i.e. perpendicular to the surface. Such free growth would lend to the relatively large crystals that were observed. The crevices probably form because the phosphorous content at the metal-solution interface increases as the reduction reaction proceeds, as proposed by Frieze et al. (231).

6.3.7. Catalytic reactor study

An attempt was made to compare the catalytic performance of the plated catalyst with $Vp/Vc = 0.64$ (and Co loading of 12.3% m/m), to that of a catalyst prepared by impregnation i.e. by soaking support in a Co bath (60 g dm^{-3}), with $Vp/Vc = 1$ (and Co loading of 7.8% m/m). From the F-T selectivity data of the above catalysts, the Shell Patent claims as previously discussed, (i.e. of $Vp/Vc < 0.85$ then C_5^+ higher), could be tested.

The catalysts were loaded (2.5 g) into two fixed-bed microreactors (as described in Chapter 2) and calcined in situ at 500°C for 1. hours, in air. The catalysts were then reduced in situ under H_2 for 16 hours at 400°C. Subsequent F-T synthesis was carried out at 220°C and 500 kPa, using a 2:1 H_2/CO syngas mixture, GHSV = 280 h^{-1}.

Since the activity for both catalysts was very low, i.e. the CO conversion was less than 4%, no meaningful comparison of the selectivities
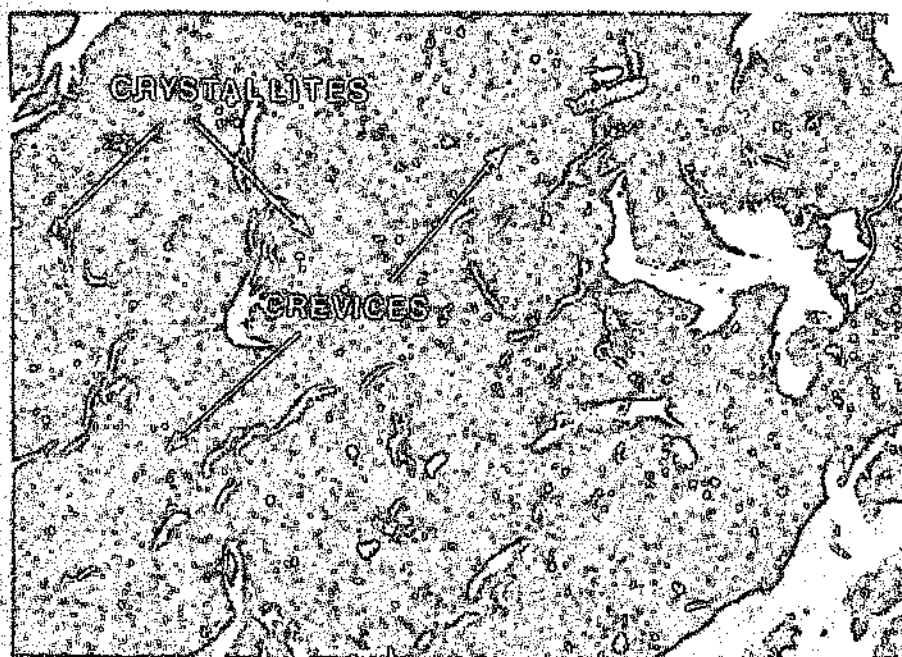
Figure 6.6: Electron micrograph (1200 x) of the Co plated peel, showing the large crystallites separated by crevices.

between the two catalysts could be made. Optimization of catalyst activation i.e. conditions of calcination, reduction and synthesis start–up, are currently being investigated. Deactivation due to phosphorous poisoning could also not be discounted.

6.4 CONCLUSION

The cobalt electroless plating of silica/alumina pellets with metal loadings of greater than 10%, and satisfying the Shell quotient of $V_p/V_c <$ 0.85, was achieved. Certain modifications to the initial plating procedure as given in the literature were made in a quest to optimize the process within our specifications. A Pd surface treatment (i.e. in the absence of the anchoring Sn treatment) was sufficient to produce the catalytic film required
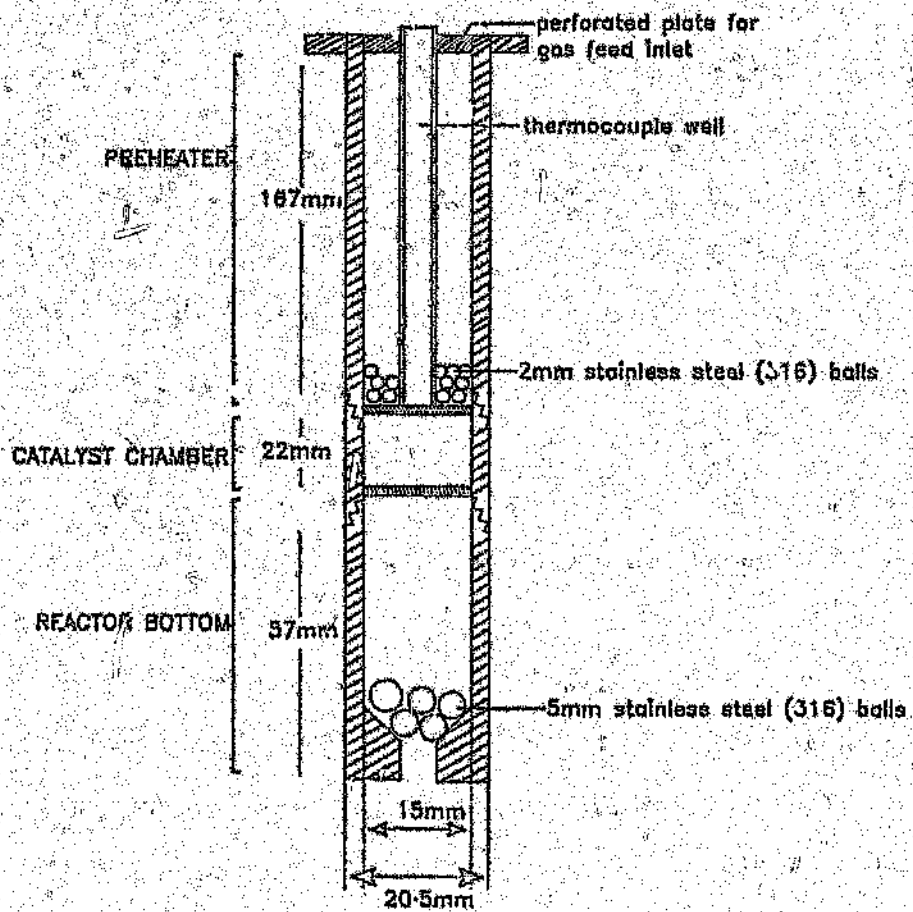
Figure 2.5: The reactor insert assembly.

for plating activation (with the Pd being able to anchor itself onto the porous support). Washing of the Pd activated pellets in acetone was necessary to achieve subsequent Co penetration. This important wash step prevented pellet surface plating by removing Pd activator, that would otherwise inhibit this required penetration. The depth of penetration i.e. V_p/V_c ratios, was controlled by the time of immersion in Pd activator solution, coupled with the subsequent acetone wash. These two parameters could be varied to produce the industrially important "impregnation-profiles" discussed in Section 6.1.

Cobalt metal loading was found to be dependent on both Co bath concentration and plating bath temperature, and was consequently maximised by optimising these variables. Co metal penetration and loading seems to be controlled by more than one variable, and the influence of one factor may depend on others. Comprehensive and systematic experiments to cover the number of variables would thus be necessary.

Since chlorides are known F-T poisons, they had to be removed from the plating bath formulation. The plating activation and bath formulation was thus modified by substituting Pd and Co chloride salts for Pd and Co nitrate salts i.e. $Pd(NO_3)_2$ and $Co(NO_3)_2$. Since phosphorous (from the reducing agent hypophosphite) is also a known F-T poison, work is currently been performed in the search for alternative reducing agents e.g. borohydrides.

XPS measurements showed the cobalt to exist as CoO, with the Co metal being oxidized in the presence of H_2O and O_2, promoted by the acidic medium of the support. Electron micrographs showed the plated

surface to exist of large crystallites separated by crevices produced by phosphorous, which has been thought to act as a plating inhibitor.

Initial reactor studies were unsuccessful due to inadequate activation of the plated catalysts – optimization of catalyst activation is currently being investigated. Deactivation due to phosphorous poisoning should also be considered (alternative reducing agents are also being investigated). Comparisons in catalytic performance (i.e. C_5^+ selectivity), between homogeneous and inhomogenous distributed Co catalysts could not be made at this stage.

Although this novel method of catalyst preparation is in the early stages of its development, it seems to show some promising attributes, especially in the relatively easy control of the active metal impregnation profiles. These profiles have been shown to be industrially important, with the different profiles showing optimal behaviour under varied industrial and commercial applications.

CHAPTER SEVEN

CONCLUSION

Most current interest in F-T technology derives from the need to develop non-petroleum based alternative methods of producing fuels and chemical feedstocks. Although fuels may dominate the picture as far as strategic matters are concerned, the production and sales of chemical feedstocks, regarded as by-products of the F-T synthesis, have significantly increased the economic viability of the F-T process. Economic considerations thus dictate the development of new and improved catalysts for enhanced selectivities toward these high value commercial F-T by-products.

The need for improved catalysts which produce more selective chemical feedstocks from syngas, such as olefins and higher molecular hydrocarbons, prompted a study of the effects of promoters, on an existing co-precipitated Co/MnO catalyst. We have shown that the addition of K and Cr promoters significantly modified the catalytic properties of the Co/MnO catalyst in syngas conversion. The influence of K-promoters on catalyst activity and selectivity has been known since the infancy of F-T catalysis. Potassium proved to be a good candidate for meeting our objective of effecting increased light olefin selectivity and decreased methane formation. In addition, the average molecular weight of the hydrocarbons, and the selectivity toward longer chain alcohols were both favoured by addition of K promoter. A small decrease in CO conversion was observed at optimum K loading, beyond which a more dramatic decrease in activity was observed.

Selectivity of the short chain olefins was observed to decrease with increasing temperature and space time (and conversion) and at constant conversion, increasing pressure. The K promoter was found not to influence the bulk structure of the catalyst, with promoter action being thought to be influencing the electronic properties of the catalyst surface.

No studies on the addition of Cr promoters to catalysts for increased wax selectivities have previously been reported (except where Cr is used as a constituent in Shell catalysts). The Cr-promoter used in our Co/MnO catalysts substantially increased the selectivity toward the longer chain hydrocarbons, and has now become an important constituent in the study of new catalysts for enhanced wax selectivity, in our research group. CO conversion was observed not to be affected by the addition of the Cr promoter, even at high loadings. High pressure and lower temperatures coupled with moderate space times, were shown to be optimal for higher hydrocarbon selectivity. Characterisation studies showed the Cr to have had no influence on the bulk structure of the catalyst. The exact method of promoter action is not completely understood.

A high temperature *in situ* XRD/DSC study of the Co/MnO catalyst (and related systems) was undertaken to characterise phase transformations taking place during catalyst pretreatment and under realistic F-T conditions. Results showed that an increase in the crystallinity occurred during calcination of the Co/MnO mixed spinel. This was later observed to be an important prerequisite to subsequent catalyst reduction. An optimal 400°C reduction temperature for this catalyst could be rationalised in terms of the presence of metallic Co phase (i.e. the active phase), being detected only at

these temperatures. After prolonged exposure of the reduced Co/MnO catalyst to syngas, new peaks had appeared in the XRD spectrum which could only be indexed to a novel bcc cobalt phase, with relative intensities similar to those of iso-structural α-Fe. The rapid transformation of this phase back to Co(fcc), after light crushing in air, suggested that Co(bcc) was metastable. The host matrix MnO, has little influence on the formation of this phase, since Co(bcc) was observed with other systems e.g. pure Co_3O_4, and Co_3O_4/Al_2O_3 (also under prolonged F-T conditions). For a $CoCr_2O_4$ mixed oxide spinel investigated, Co was only reduced at 800°C, which, after subsequent F-T synthesis was observed to form Co(bcc) with reluctance. This was thought to be due to the formation of very stable Co(fcc) formed at 800°C. Clearly in this case, the matrix Cr_2O_3, does have an influence on the behaviour of the Co^{2+} ions. The formation of Co(bcc) was proposed to have formed through the rearrangement (under the influence of H_2 and/or temperature) of a cobalt-carbonyl type intermediate. High selectivities toward propene could be correlated with the formation of Co(bcc) for the Co/MnO catalysts. These selectivities however were not observed with the other Co systems investigated.

Recently Shell has reported on the novel synthesis of F-T catalysts that show an enhanced C_5^+ selectivity. In their reports it is implied that 90% of the Co must occupy the outer volumes of the catalyst support, to have the required catalytic properties. We have reproduced an analogue of this catalyst using a novel electroless deposition method, plating Co metal onto a Si-Al substrate. Co metal loadings of greater than 10%, and satisfying Shell specifications, were achieved in this way. Co support depth penetration was found to be dependent on the time of immersion of the support in Pd activator solution. Co metal loading was found to be dependent on both Co

bath concentrations and plating bath temperature. Initial reactor studies were unsuccessful due to inadequate activation of the plated catalyst. Although this novel method of catalyst preparation is still in the early stages of development, it seems to show promising attributes, especially in the relatively easy control of the active metal impregnation profiles. These profiles have been shown t be of industrial and commercial importance, with different profiles having optimal behaviour for different applications.

After seventy–five years of research, development, and production, F–T technology is reported to be in a mature state of equilibrium (`36). F–T technology is not more widely used at present because of the economic domination of petroleum. Where it is used (i.e. Sasol), F–T synthesis is economically and effective because of special local economic considerations. At least three new synfuels plants are approaching commercialization i.e. Norway's Statoil GMD slurry process, Shell's SMD process and South Africa's Mossgas project. All will use natural gas as a source of synthesis gas. This commercial thrust is one aspect of the current state of F–T synthesis which has indicated the necessity of dedicating more time and effort into further research and development in this field. In the near term, improvements in existing or emerging technologies are indicated e.g. Sasol's high pressure fixed bed reactor modification. In the medium to long term, it is imperative that further studies be continued in synthesis–gas chemistry e.g. in the development of advanced gassification processes, and in the development of cheap selective catalysts. During this term, chemicals and fuels from coal–derived synthesis gas are likely to become competitive with petroleum–based processes.

APPENDIX 1

The co-precipitation of Co and Mn nitrate salts

The co-precipitation of the mixed metal nitrate solution (Co:Mn ratio of ~1:1) with ammonia had been shown to be optimum at a temperature of 70°C and pH = 8.3 ± 0.01 (62,85).

150 mℓ each of Co and Mn (1 M) nitrate solutions were mixed and preheated in a constant temperature water bath to 70°C. In addition 150 mℓ of the NH_3 precipitating solution (11 M) was also preheated to 70°C, in the same water bath. These preheated solutions were then introduced into the precipitation reactor by means of a peristaltic pump, at a combined pumping rate of ~8 mℓ min^{-1}. The pH of the reactor was monitored by a pH probe and meter, and was maintained at pH = 8.3, by further addition of an ammonia solution (concentrated) dropwise into the reactor. The precipitating solution was continuously stirred with the use of a magnetic stirrer. The duration of the co-precipitation was ca. one hour, during which time ~15 g of catalyst had precipitated out of ~500 mℓ of solution and recovered by filtration (using Whatman No. 31 wide mesh filter paper) and then washed with distilled water (~500 mℓ). The catalyst was then dried in vacuo (50 kPa) at 110°C for 16 hours. Atomic adsorption spectroscopy was used to determine the metal content of the catalyst according to the method given in Section 2.1.4.

A schematic representation of the co-precipitation apparatus is given in Figure 2.1
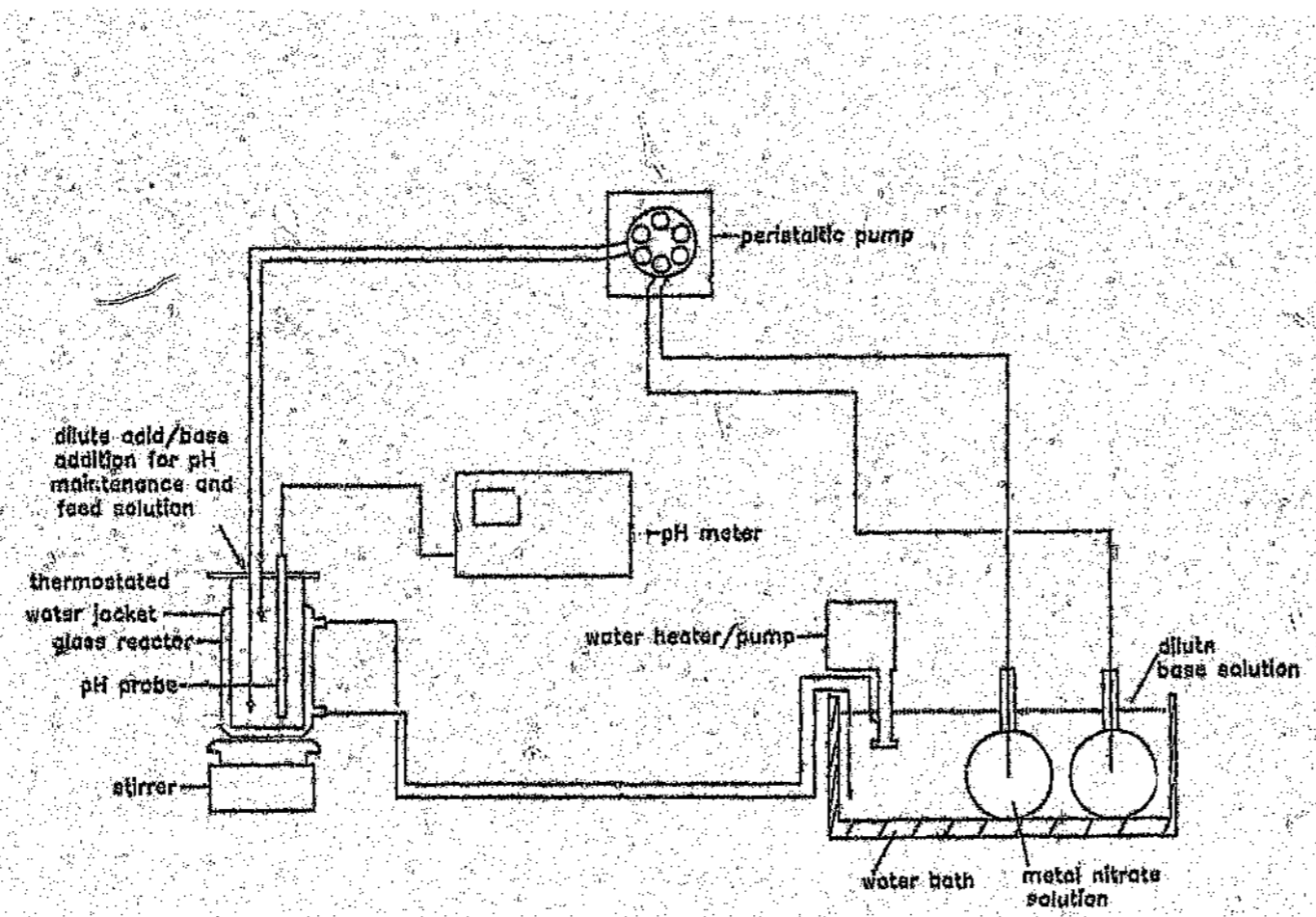
Figure 2.1: A schematic representation of the co-precipitation apparatus.

APPENDIX 2

Reactor housing, insert and dual seal assembly

The detailed design of the reactor, consisting of a reactor housing (with dual seal assembly) and insert, is depicted in Figure 2.4 and 2.5 respectively. The design was adapted from that of Korf and Espinoza (105a) and displayed behaviour characteristic of plug–flow reactors. The reactors were constructed from 316 stainless steel and showed that blank thermal reactions in the absence of catalysts were negligible at below 350°C. Leak free performances under relatively high temperatures (400°C) and pressures (1400 kPa) was accomplished by having an all welded and dual sealing system. Use was made firstly of a Helico flex seal which was compressed in the recess (see Figure 2.4), which allowed for the springloaded O–ring to develop sufficient torus for a good seal. Unlike most sealing systems that have an increasing leak rate with increasing pressure, this metal O–ring has a decreasing leak rate with increasing pressure, due to the gas pressure inside the seal (105b). In conjunction with this, a vacuum type seal employing a thin aluminum ring (1 mm thickness) and fine cutting edges on the top and bottom flanges (see Figure 2.4), with which the aluminum seal will ultimately be consolidated when the reactor housing is closed by tightening the 46 mm hexa nut.

The reactor insert (Figure 2.5) which is placed within the reactor housing has the following features which allow for ideal exploratory heterogeneous catalyst research (105b).

- easy charge of catalyst, which is quantitatively recoverable after reaction,
- no reactant by–pass of catalyst bed and a uniform gas distribution over the catalyst bed,

– diffusion and other transport limitations are minimized or non-existent,

– a preheater before the catalyst zone,

– an axial thermocouple well, running through the catalyst bed. This allows a thermocouple to travel through the bed, so that catalyst temperature is monitored during synthesis reactions.
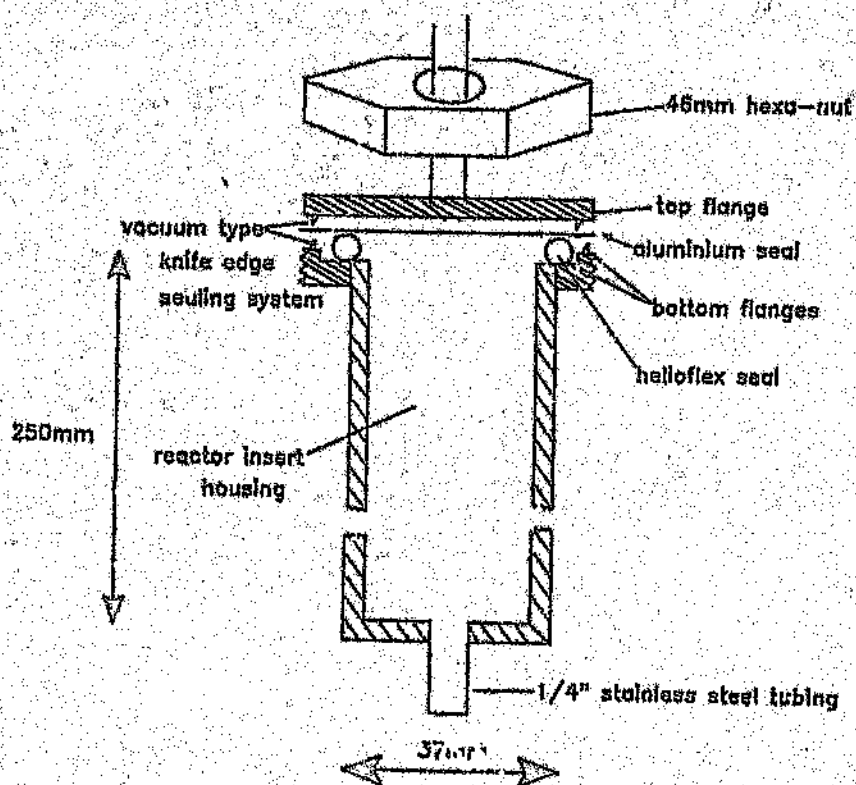
Figure 2.4:   Reactor housing showing the dual seal assembly.

APPENDIX 3

Liquid and solid knock-out systems

The trapping out of the various condensate fractions (i.e. light to medium wax fractions and aqueous layers containing dissolved oxygenates), was achieved using post–reactor condensors shown in Figures 2.2 and 2.3, and Figure 2.6(a) and (b). Initially use was made of only one condensor, kept at room temperature (Figure 2.6(a)) for studies performed on the K promoted Co/MnO catalysts – cf. Chapter 3. After a suitable mass balance period, the condensor was removed from the reactor system with the use of quick connect fittings, coupled with four–way valves between reactor and trap, enabling this removal with ⁀f the reaction pressure or flow rate. The condensate cₒₘₒₐ , ⁀ (wax) and aqueous layer was then removed from the ₒₒₗₐₐ 'ghtening the hexa nut, used in conjunction with a teflon bₐₐ. ·· ressure within the condensor. The organic and aqueous layers were then separated from each other, weighed and subsequently analysed using off–line capillary gas chromatography (as described in Section 2.3). This knock–out system was later modified for studies involving Cr promoted Co/MnO catalysts (cf. Chapter 4), for improved wax handling capabilities, as previously described in Section 2.2. Use was now made of a hot (120°C – see Figure 2.6(b)) and cold (room temperature) condensor combination. This knock–out combination could be isolated from the reactor system during condensate collection with the use of two three–way high temperature valves (again enabling condensate removal without interruption of reactor operating parameters), as shown in Figure 2.3. Firstly, hot melted wax was tapped from the hot condensor (which could also be pressurized from an independent N₂ source) through a one–way Nupro valve, after which the condensate material from the room temperature

APPENDIX 6

Publications arising from this thesis

1. Carbon monoxide hydrogenation using cobalt manganese oxide catalysts: Initial catalyst optimization studies.

   S.E. Colley, R.G. Copperthwaite, G.J. Hutchings adn M. van der Riet, *Ind. Eng. Chem. Res.* 1988, 77, 1339

2. Identification of body-centred cubic cobalt and its importance in CO hydrogenation.

   S.E. Colley, R.G. Copperthwaite, G.J. Hutchings, S.P. Terblanche and M.M. Thackeray, *Nature*, 1989, 339, 6220, 129

3. Unusual cobalt phases in CO-hydrogenation catalysts, studies by *in situ* X-ray diffraction.

   S.E. Colley, R.G. Copperthwaite and G.J. Hutchings, accepted for publication, *Catalysis Today*.

6. POSTER — Cobalt manganese CO hydrogenation catalysts: Solid state and surface characterization. Faraday Discussion — Catalyst Characterization, University of Liverpool, Liverpool, England, U.K., September 1979.

Inlet   outlet

—16mm hexa—nut

—top flange

—teflon seal

—bottom flange

150mm

34mm

44mm

a

Inlet

outlet

120mm

25mm

—one—way tap

hot wax

b
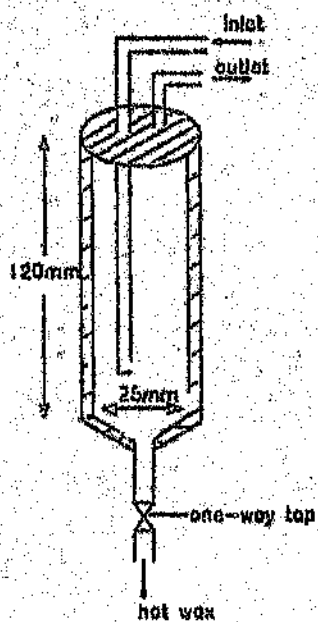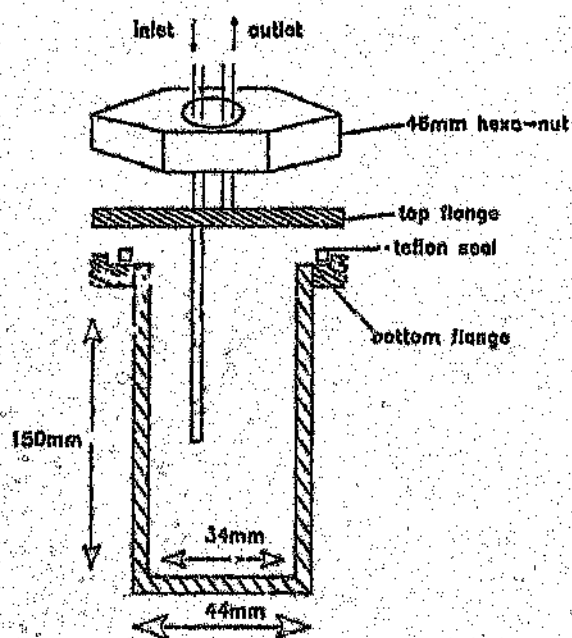
Figure 2.6(a) and (b):   Schematic representation of a, the cold (room temperature) condensor and b, hot (120°C) condensor.

condensor (i.e. oxygenated aqueous layer and in some cases also contained low boiling waxes that were subsequently manually separated), was removed as previously (using the quick connect fittings). The various fractions were then weighed and analysed as previously.

APPENDIX 4

Evaluation of data

In order to obtain quantitative data in the form of individual product selectivities from the integrated response of the respective gas chromatographs (over the total mass balance period), a procedure of data manipulation and evaluation was required. Initially, the varying response of the detector to each product component had to be corrected for, by multiplying each component's area count (integrated response) by a correction factor, outlined by Dietz (105c) and Purnell (105d). Since the selectivity of each component of the product yield (over a mass balance period) from a catalyst was quoted in percent by mass derived from equation (1).

$$\text{selectivity of component } i = \frac{\text{mass of } i}{\text{total mass of all components}} \times \frac{100}{1} \qquad (1)$$

a consolidation of the various product fractions i.e. gaseous, wax and oxygenated aqueous fractions, was required. In order to do this the conversion of the gaseous product's concentration from mass percent to grams per component was necessary. This calculation was performed by firstly converting the gaseous product's concentration from mass percent to a volume percent, using standard gas mixtures with known volume percent; with the method detailed by Mikes (105e) — see equation (2) and (3). The gaseous component's volume percent could then be converted to grams per component — see equation (4).

Factor for correcting % m/m to % v/v

$$\epsilon = (\% \text{ v/v} \times Mw)/\% \text{ m/m} \qquad (2)$$

where Mw = molecular weight of the component

Then by using a standard gas calibration for a 1% v/v for a given gas, ϵ may be calculated.

From equation (3), the volume percent of the gas components may then be calculated.

$$\% \text{ v/v} = (\% \text{ m/m} \times \epsilon)/Mw \qquad (3)$$

The grams of gaseous products per component was then calculated from the ideal gas law

$$n = PV/RT \qquad (4)$$

where n (the number of moles) is used to calculate the mass per component from the following equation

$$\text{mass of component } i = N_i \times Mw_i$$

and V = inlet flow rate (mℓ/hr) x mass balance period (hrs) x % v/v

After addition to the liquid and solid phase masses, (which had previously been weighed), the percentage of each component (in terms of mass) could then be calculated. This complete operation was performed by computer (IBM PC-XT) using the software derived by van der Riet (82).

APPENDIX 5

Indexing of the body centered cubic pattern by $\sin^2 \Theta$ ratios

The three observed diffraction lines at $2\Theta = 44.73°$, $65.13°$ and $82.54°$, were found not to fit any of the Co compounds listed in the JCPDS powder diffraction files, sets $1 - 37$. The fact that only three peaks were observed between $2\Theta = 10°$ and $90°$ suggested high symmetry, and indexing the pattern by the method of $\sin^2 \Theta$ ratios to a body-centered cubic lattice was used. The method of indexing by $\sin^2 \Theta$ ratios is derived from the following (174a):

According to the Bragg equation

$$n\lambda = 2d \sin \Theta \qquad\qquad 1.1$$

where   n = order of reflection

      d = interplanar spacing = a, for a cubic crystal

      λ = radiation wavelength (CuKα)

      Θ = diffraction angle

and the expression for an interplanar spacing of a cubic crystal,

$$a = \frac{\lambda}{2} \frac{\sqrt{h^2 + k^2 + \ell^2}}{\sin \Theta} \qquad\qquad 1.2$$

two reflections $(h_1 k_1 \ell_1)$ and $(h_2 k_2 \ell_2)$ satisfy the equations

$$\sin^2 \Theta_1 = \frac{\lambda^2}{4a^2} (h_1^2 + k_1^2 + \ell_1^2)$$

$$\qquad\qquad 1.3$$

$$\sin^2 \Theta_2 = \frac{\lambda^2}{4a^2} (h_2^2 + k_2^2 + \ell_2^2)$$

in which the order of reflection n, has been combined with the Miller indices. Division of the first equation by the second gives

$$\frac{\sin^2 \Theta_1}{\sin^2 \Theta_2} = \frac{n_1}{n_2} \qquad\qquad 1.4$$

where m_1 and m_2 are the integral sums of the squares of the respective indices. This indexing procedure consists essentially of determining the simplest integral relationship existing between the experimental $\sin^2 \Theta$ that does not yield forbidden integers (7,15,23,18 etc.), i.e. which is a number not expressible as the sum of three squares. It is necessary that all the data be referred to a common wavelength (a condition that was assumed in deriving equation 1.4 from equation 1.3). Thus, for some constant spacing d, a value of $\sin^2 \Theta$ for one wavelength is related to $\sin^2 \Theta$ for a second wavelength as follows:

$$\frac{\sin^2 \Theta_1}{\sin^2 \Theta_2} = \frac{\lambda_1^2}{\lambda_2^2} \qquad\qquad 1.5$$

This relationship follows directly from the square of the Bragg law written for two wavelengths.

Experimental data from the cobalt powder pattern are used in Table 5.5 to illustrate the indexing procedure.

TABLE 5.5: <u>Indexing of a Cobalt Powder Pattern obtained in this study by the Method of sin² Θ Ratios[a]</u>

line	2Θ	sin² Θ	Calculated ratios		d	intensity	hkℓ
			1	2			
1	44.73	0.1448	1	2	2.024	100	110
2	65.13	0.2897	2	4	1.431	20	200
3	82.54	0.4351	3	6	1.168	30	211

[a] wavelength employed: $CuK\alpha = 1.54056$ Å.

The simplest set of approximately integral ratios is given in column 1, and the set listed in column 2 are doubled values from 1. The Miller indices (hkℓ) are deduced directly from the true integers by inspection. From the occurrence of only even values of $h + k + \ell$, the lattice type is identified as body–centered.

APPENDIX 7

Conference proceedings arising from this thesis

1. PAPER – The effect of potassium promotion on activity and selectivity of Co/MnO catalysts for Fischer–Tropsch synthesis. R & D Colloquim: Catalysis and catalytic reactor technology in the RSA. Riviera International Hotel, Vereeniging, South Africa, August 1988.

2. PAPER – Chromium promoted cobalt catalysts for the production of medium wax fraction hydrocarbons from synthesis gas. Annual Meeting – Catalysis and Catalytic Processing, Safari Hotel, Rustenburg, South Africa, September 1989.

3. PAPER – Unusual cobalt phases in CO–hydrogenation catalysts, studies by *in situ* X–ray diffraction. SURCAT group of the Royal Society of Chemistry – *In situ* Methods in Catalysis, University of Reading, Reading, England, U.K., September 1990.

4. PAPER – An *in situ* high temperature X–ray diffraction investigation of Co/MnO catalysts for the hydrogenation of carbon monoxide. Annual meeting – Catalysis and Catalytic Processing, van Riebeeck Hotel, Gordon's Bay, South Africa, October 1990.

5. POSTER – The effect of operating conditions on alkene selectivity for Co/MnO Fischer–Tropsch catalysts. 30th Convension of the South African Chemical Institute – Chemistry for Southern Africa, Johannesburg Sun, Johannesburg, South Africa, January 1989.

LIST OF ABBREVIATIONS

AAS — Atomic Absorption Spectroscopy

AES — Auger Electron Spectroscopy

BET — Brunauer, Emmett, Teller (surface area)

DSC — Differential Scanning Calorimetry

EDAX — Energy Dispersive Analysis by X-ray

EXAFS — Extended X-ray Absorption Fine Structure

FID — Flame Ionization Detector

F-T — Fischer-Tropsch Synthesis

GHSV — Gas Hourly Space Velocity

IR — Infra-red Spectroscopy

MBE — Molecular Beam Epitaxy

SEM — Scanning Electron Microscopy

S-F — Schulz-Flory Distribution

SIMS — Secondary-Ion Mass Spectrometry

SMAD — Solvated Metal Atom Dispersed

SMSI — Strong Metal-Support Interaction

TCD — Thermal Conductivity Detector

TEM — Transmission Electron Microscopy

TGA — Thermal Gravimetric Analysis

TPO — Temperature Programmed Oxidation

TPR — Temperature Programmed Reduction

TPSR — Temperature Programmed Surface Reaction

UHV — Ultra High Vacuum

UPS — Ultraviolet Photoelectron Spectroscopy

XPS — X-ray Photoelectron Spectroscopy

XRD — X-ray Diffraction

REFERENCES

1. Hoffman E.J., in *"Synfuels — The problem and the promise"*, The Energon Company, Loramie, Wyoming, 1982.

2. McAuliffe, C.A., in *"Hydrogen and Energy — Energy Alternative Series"*, Macmillan Press, London, 1980.

3. Keim, W., *Am. Chem. Soc., Symp. Ser.*, 1987, 328 (*Ind. Chem C₁ Process*), chap. 1, 1.

4. Grosvenor, ...B. (ed.), *National Geographic*, Special Report on "Energy", February, 1981.

5. Derbyshire, F. and Gray. D.,(in "Coal Liquefaction"), *Ullmanns Encyclopaedia*, 5th revised edition. Vol. 7, VCH, Veinweinheim, 1986.

6. Anderson, R.B., in *"The Fischer–Tropsch Synthesis"*, Academic Press, Florida, 1984.

7. Probstein, R.F. and Hicks, R.E., in *"Synthetic Fuels"* McGraw–Hill, New York, 1982.

8. Haggin, J., *Chem. Eng. News.*, 1981, (Feb 23) 39.

9. Bell, A.T., *"Catalyst Design — Progress and Perspective"*, L.L. Hegedus et al. (eds.) John Wiley and Sons, New York, 1985, Chap. 4.

10. Dry, M.E., in *"Catalysis — Science and Technology — Vol. 1"*, J.R. Anderson and M. Boudardt (eds.), Springer Verlag, Berlin, 1981, Chap. 4, 159.

11. Henrici–Olivé, G. and Olivé, S, in *"The Chemistry of the Metal–Carbon Bond — Vol. 3"*, F.R. Hartley and S. Patai (eds.), John Wiley and Sons, New York, 1985, 391.

12. Taylor, P. and Wojciechowski, R.W., *Fuel Processing Technology*, 1984, 8, 135.

13. Storch, H.H.; Golumbic, N. and Anderson, R.B. in *"The Fischer–Tropsch and related synthesis"*, John Wiley and Sons, New York, 1951.

14. Anderson, R.B., in *"Catalysis — Vol. 4"*, P.H. Emmett (ed.), Von Nostrand–Reinhold, New Jersey, 1956.

15. Vannice, M.A., *Catal. Rev.–Sci. Eng.*, 1976, 14, 153.

16. Ponec, V., *Catal. Rev.–Sci. Eng.*, 1978, 18, 151.

17. Bell, A.T., *Catal. Rev–Sci. Eng.*, 1981, 23, 203.

18. Vannice, M.A., in *"Catalysis–Science and Technology — Vol. 3"*, J.R. Anderson and M. Boudart (eds.), Springer Verlag, Berlin, 1982, chap. 3.

19. Sabatier, P. and Senderens, J.B., *C.B. Hebd. Seonces Acad. Sci.*, 1902, 134, 514, 680.

20. BASF: *German Patent*, 1913, 293, 787.

21. Fischer, F. and Tropsch, H., *Brennst.–Chem.*, 1923, 4, 276.

22. Fischer, F. and Tropsch, H., *German Patent*, 1922, 411, 216.

23. Fischer, F. and Tropsch, H., *Brennst.–Chem.*, 1924, 5, 201, 217.

24. Pichler, H., *Brennst.–Chem.*, 1938, 19, 226.

25. Pichler, H. and Shulz, H., *Chem. Ing. Tech.*, 1970, 42, 1162.

26. Pichler, H., in *"Advances in Catalysis — Vol. 4"*, W.G. Frankenburg; V.I. Komarewsky and E.K. Rideal (eds.), Academic Press, New York, 1952.

27. Courty, P., and Chaumette, P., *Energy Progress*, 1987, 7, 1, 23.

28. Kofer–De Poorter, C.H., *Chem. Rev.*, 1981, 81, 447.

29. Vannice, M.A., *J. Catal.*, 1975, 37, 462.

30. Vannice, M.A., *J. Catal.*, 1976, 43, 129.

31. Vannice, M.A., *J. Catal.*, 1975, 37, 449.

32. Vannice, M.A., *J. Catal.*, 1979, 50, 278.

33. Colley, S.E.; Copperthwaith, R.G.; Hutchings, G.J. and van der Riet, M., *Ind. Eng. Chem. Res.*, 1988, 27, 1339.

34. Venter, J.; Kaminsky, M.; Geoffrey, G.L. and Vannice, M.A., *J. Catal.*, 1987, 103, 450.

35. Tronconi, E.; Cristiani, C.; Ferlazzo, N.; Forzatti, P.; Villa, P.L. and Pasquon I. *Appl. Catal.*, 1987, 32, 285.

36. Post, M.F.M., Shell Internationale Research, *European Patent*, 1985, EP 0, 174, 696

37. van Erp, W.A.; Nanne, J.M. and Post, M.F.M., Shell Internationale Research, *European Patent*, 1986, EP 0, 178, 008

38. Tauster, S.J.; Fung, S.C. and Garten, R.L., *J. Am. Chem. Soc.*, 1978, 100, 170.

39. Dry, M.E.; Schingles, T. and Botha, C.S., *J. Catal.*, 1970, 17, 341.

40. Dry, M.E.; du Plessis, J.A.K. and Leuterity, G.M., *J. Catal.*, 1966, 194, 6.

41. Tauster, S.J., *Am. Chem. Soc., Symp. Ser.*, 1986, 298 (Strong Met. – Support Interact.) 1, 1.

42. Hutchings, G.J., *S. Afr. J. Chem.*, 1976, 34, 65.

43. Kugler, E.L., *Prepr – Am. Chem. Soc., Div. Pet. Chem.*, 1980, 564.

44. King, D.L., *J. Catal.*, 1978, 51, 397.

45. Kellner, C.S. and Bell, A.T., *J. Catal.*, 1982, , 75, 251.

46. Dry, M.E. and Oosthuizen, G.J., *J. Catal.*, 1968, 11, 18.

47. Simon, M.; Mortreaux, A.; Petit, F.; Vanhove, D. and Blanchard, M., *J. Chem. Soc., Chem. Commun.*, 1985, 17, 1170.

48. Pierantozzi, R., *J. Catal.*, 1987, 106, 327.

49. Blanchard, M. and Bonnet, R., *Bull. Soc. Chim. Fr.*, 1977, (*1–2, Pt.*1), 7.

50. Blanchard, M.; Vanhove, D.; Petit, F. and Mortreux, A., *J. Chem. Soc., Chem. Commun.*, 1980, 19, 908.

51. Kani, H.; Tan, B.J. and Klabunde, K.J., *Langmuir*, 1986, 2(6), 760.

52. Klabunde, K.J.; David, S.C. and Hattori, H., *J. Catal.*, 1978, 54, 254.

53. Meier, P.F.; Pannella, F.; Klabunde, K.J. and Imiza, J., *J. Catal.*, 1986, 101(2), 545.

54. Dry, M.E., *Ind. Eng. Chem., Prod. Res. Dev.*, 1976, 15, 282

55. Henrici–Olivé, C. and Olivé, S., *Angew. Chem., Int. Ed. Engl.*, 1976, 15(3), 136.

56. Satterfield, C.N.; Huff, G.A.; Stenger, H.G.; J.L. and Madon, R.J., *Ind. Eng. Chem. Fundam.*, 1985, 24, 450.

57. Satterfield, C.N. and Huff, G.A., *J. Catal.*, 1982, 73, 187.

58. Donnelly, T.J.; Yates, I.C. and Satterfield, C.N., *Energy and Fuels*, 1988, 2, 6, 734.

59. Henrici–Olivé, G. and Olivé, S. in "*The chemistry of the hydrogenation of carbon monoxide*", Springer Verlag, Berlin, 1984.

60. Flory, P.J. in "*Principles of Polymer Chemistry*", Cornell University Press, Ithaca, New York, 1967.

61. King. D.L.; Cusumano, J.A. and Garten, R.L., *Catal. Rev. – Sci. Eng.*, 1981, 23, (1 and 2), 233.

62. van der Riet, M., *PhD Thesis*, University of the Witwatersrand, Johannesburg, South Africa, 1988.

63. Dry, M.E., *Catalysis Today*, G.J. Hutchings and M.S. Scurrell (eds.), January 1990, 183.

64. Dry, M.E., *J. Mol. Catal.*, 1982, 17, 133.

65. Dry, M.E., in "*Applied Industrial Catalysis — Vol. 2*", K.M. Samuel et al. (eds.), 1983, chap. 5, 167.

66. *ChemSA*, K.M. Samuel *et al.* (eds.) August 1989, p. 264 (Sasol Mirror).

67. *ChemSA*, K.M. Samuel *et al.* (eds.) p. 309 (Sasol Mirror).

68. Hurlich, A.H., *Met. Progr.*, 1977, 112(5), 67.

69. Hurlburt, C.S. (Jr.), in "*Dana's Manual of Mineralogy*" 17th edition, John Wiley and Sons, New York, 1966.

70. Morral, F.R., (in "Cobalt and Cobalt Alloys"), *Kirk-Othmer Encyclopaedia*, 3rd edition, Vol. 5, John Wiley and Sons, New York, 1979.

71. Cotton, F.A. and Wilkinson, G., in "*Advanced Inorganic Chemistry*", 4th edition, John Wiley and Sons, New York, 1980, p. 766.

72. Dent, A.L. and Lin, M., *Am. Chem. Soc., Adv. Chem. Series*, 178 (Hydrocarb. Synth. from CO and H₂), chap. 6, 1979, 47.

73. Borghard, W.G. and Bennett, C.D., *Ind. Eng. Chem. Prod. Res. Dev.*, 1979, 18, 18.

74. Vanhove, D.; Makambo, P. and Blanchard, M., *J. Chem. Soc., Chem. Commun.*, 1979, 605.

75. Vanhove, D.; Zhuyong, Z.; Makambo, L. and Blanchard, M., *Appl. Catal.*, 1984, 9, 327.

76. Zowtiak, J.M. and Bartholomew, C.H., *J. Catal.*, 1983, 83, 103.

77. Reuel, R.C. and Bartholomew, C.H., *J. Catal.*, 1984, 85, 63.

78. Reuel, R.G. and Bartholomew, C.H., *J. Catal.*, 1984, 85, 78.

79. Gopalakrishnan, R. and Viswanathan, B., *J. Chem. Soc., Faraday Trans. 1*, 1986, 82, 2635.

80. Gopalakrishnan R., and Viswanathan, B., *Surf. Tech.*, 1948, 23, 173.

81. Viswanathan, B. and Gopalakrishnan, R., *J. Catal.*, 1986, 99, 342.

82. Moon, S.H. and Yoon, K.E., *Appl. Catal.*, 1985, 16, 289.

83. Lee, H.W. and Bartholomew, C.H., *J. Catal.*, 1989, 120, 256.

84. van der Riet, M.; Hutchings, G.J. and Copperthwaite, R.G., *J. Chem. Soc., Chem. Commun.*, 1986, 788.

85. Copperthwaite, R.G.; Hutchings G.J.; van der Riet, M. and Woodhouse, J., *Ind. Eng. Chem. Res.*, 1987, 26, 869.

86. Varma, R.L.; Dan-Chu, L.; Mathews, J.F. and Bakhshi, N.W., *Can. J. Chem. Eng.*, 1985, 63, 72.

87. Derule, H.; Blanchard, M. and Canesson, P., *Appl. Catal.*, 1989, 50, L1–L4.

88. Meier, P.F.; Pannella, F.; Klabunde, K.J. and Imian, Y., *J. Catal.*, 1986, 101, 545.

89. Frankel, D. and Gates, B.C., *J. Am. Chem. Soc.*, 1980, 102, 7, 2478.

90. Ishihara, T.; Egachi, K. and Arai, H., *Appl. Catal.*, 1987, 30, 225.

91. Fornasari, G.; Gusi, S.; Tritiro, F. and Vaccari, A., *Ind. Eng. Chem. Res.*, 1987, 26, 1500.

92. Barrault, J. and Guilleminot, A., *Appl. Catal.*, 1986, 21, 307.

93. Pannell, R.B. and Kibby, C.L., *Proc. Int. Congr. Catal.*, 7th, 1980, T. Seigunn and K. Tanabe (eds.), Part A, p. 447, Elsevier, Amsterdam, 1981.

94. Yokota, K. and Fujimoto, K., *Feul*, 1989, 68, 225.

95. Withers, H.P. (Jr.); Eliezer, K.F. and Mitchell, J.W., *Ind. Eng. Chem. Res.*, 1990, 29, 1807.

96.   Haag, W.O.; Kuo, J.C. and Wender, I., *Energy*, 1987, 12, 689.

97.   Pan, W. X.; Cao, R. and Griffin, G.L., *J. Catal.*, 1988, 114, 447.

98.   Takeuchi, K.; Matsuzaki, T.; Arakawa, H.; Hanaoka, T. and Sugi, Y., *Appl. Catal.*, 1989, 48, 149.

99.   Swan, T.S., Shell International Research, *UK Patent*, 1985, UK 2, 158, 090.

100.   Kim, C.J., Exxon Research and Eng. Co., *European Patent*, 1990, EP 355218, A1.

101.   Kim, C.J., Exxon Research and Eng. Co., *European Patent*, 1989, EP 339923, A1.

102.   Iglesia, E.; Soled. S. and Fiato, R.A., Exxon Research and Eng. Co., *US Patent*, 1988, US 4, 794, 099.

103.   Acres, G.J.K.; Bird, A.J.; Jenkins, J.W. and King, F., in *"Catalysis — Specialist Periodical Reports — Vol. 4"*, The Royal Society of Chemistry, London, 1981, chap 1.

104.   Maiti, G.C.; Malessa, R. and Baerns, M., *Appl. Catal.*, 1983, 5, 151.

105.   Deckwer, W.D.; Serpemen, Y.; Ralek, M. and Schmidt, B., *Ind. Eng. Chem. Process Des. Dev.*, 1982, 21, 222.

105a. Korf, C.J. and Espinoza, R., *CSIR (CENG), Report*, 1986, 584 (Pretoria, South Africa).

105b. Snel, R., *Chemica Scripta*, 1982, 20, 99.

105c. Dietz, W.A., *J. of Gas. Chromatogr.*, 1967, 68.

105d. Purnell, H. in *"Gas Chromatography"*, John Wiley and Sons, New York, 1967.

105e. Mikeš, D., *"Laboratory handbook of chromatographic and allied methods"*, John Wiley and Sons, New York, 1979.

106. Richardson, J.T., in *"Principles of Catalyst Development"*, Fundamental and Applied Catalysis (series), M.V. Twigg and M.S. Spencer (eds.), Plenum, New York, 1989, chap. 6, p. 95.

107. Shah, Y.T. and Perrotta, A.J., *Ind. Eng. Chem. Prod. Res. Develop.*, 1976, 15, 123.

108. van der Lee, G.; Bastein, G.T.M.; van den Boogert, I.; Schuller, B.; Luo, H.Y. and Ponec, V., *J. Chem. Soc., Faraday Trans.*, 1987, 83, 2013.

109. Löchner, V.; Papp, H. and Bearns, M., *Appl. Catal.*, 1986, 23, 339.

110. Jaggi, N.K.; Schwartz, C.H.; Butt, J.B.; Papp, H. and Baerns, M., *Appl. Catal.*, 1985, 13, 347.

111. Bussemeier, B.; Frohning, C.D. and Cornils, B., *Hydrocarbon Processing*, 1976, 55, 105.

112. Kölbel, H. and Tillmetz, K.D., *US Patent*, 1977, US 4, 177, 203.

113. Kreitman, K.M.; Baerns, M. and Butt, J.B., *J. Catal.*, 1987, 105, 319.

114. Cornils, B.; Frohning, C.D. and Morow, K., *Proc. 8th Int. Congr. Catal. – Vol. 2*, Berlin, 1984.

115. Boeyens, J.C.A. and Hutchings, G.J., *J. Catal.*, 1986, 100, 537.

116. Copperthwaite, R.G.; Hack, H.; Hutchings, G.J. and Sellschop, J.P.F., *Surf. Sci.*, 1985, 164, L827.

117. Barrault, J., in *"Met. Supp – Met. Addt. Eff. Catal."*, C. Imelik *et al.* (eds.), 1982, 225.

118. van der Riet, M.; Copperthwaite, R.G. and Hutchings, G.J., *J. Chem. Soc., Farraday Trans.*, 1987, 1, 83, 2963.

119. Dry, M.E.; Shingles, T.; Boshoff, L.J. and Oosthuizen, G.J., *J. Catal.*, 1969, 15, 190.

119a. Bartholomew, C.H., *Catalysis Letters*, 1190, 7, 27

119b.   Rankin, J.L. and Bartholomew, C.H., *J. Catal.*, 1986, 100, 533

120.   Konig, L. and Gaube, J., *Chem. – Ing. – Tech.*, 1983, 55, 14.

121.   Bonzel, H.P., *J. Vac. Sci. Technol.*, 1984, 2(2), 866.

122.   Wesner, D.A.; Linden, G. and Bonzel, H.P., *Appl. Surf. Sci.*, 1986, 26, 335.

123.   Ertl, G.; Lee, S.B. and Weiss, M., *Surf. Sci.*, 1981, 111, L711.

124.   Miller, D.G. and Moskovits, M., *J. Phys. Chem.*, 1988, 92, 6081.

125.   Yang, G.H. and Oblad, A.G., *Am. Chem. Soc., Div. Pet. Chem., Prepr.*, 1978, 23(2), 513.

126.   Yeh, E.B.; Schwartz, L.H. and Butt, J.B., *J. Catal.*, 1985, 91, 241.

127.   Chen, A.A.; Kaminsky, M.; Geoffroy, G.C. and Vannice, M.A., *J. Phys. Chem.*, 1986, 90, 4810.

128.   Chuang, S.C.; Goodwin, J.G. (Jr.) and Wender, I., *J. Catal.*, 1985, 95, 435.

129.   Arakawa, H. and Bell, A.T., *Ind. Eng. Chem. Process Des. Dev.*, 1983, 22, 97.

130.   Campbell, C.T. and Goodman, D.W., *Surf. Sci.*, 1982, 123, 413.

131.   Koel, B.E.; Peebles, D.E. and White, J.M., *Surf. Sci.*, 1981, 107, 367.

132.   Betts, M.J., *Masters Dissertation*, University of the Witwatersrand, Johannesburg, South Africa, 1989.

133.   Lindner, U. and Papp, H., *Appl. Surf. Sci.*, 1988, 32, 75.

134.   Gonzalez, R.D. and Miura, H., *J. Catal.*, 1982, 77, 338.

135.   Bonzel, H.P. and Krebs, H.J., *Surf. Sci.* 1981, 109, L527.

136. Huff, G.A. (Jr.) and Satterfield, C.N., *J. Catal.*, 1984, 80, 370.

137. Schliebs, B. and Gaube, J., *Ber. Bunsenges. Phys. Chem.*, 1985, 89, 68.

138. Stenger, H.G. (Jr.), *J. Catal.*, 1985, 92, 46.

139. Schulz, H., *C₁ Mol. Chem.*, 1985, 1, 231.

140. Schulz, H. and Gokcebay, H., *Proc. Organic React. Conf.*, Charleston, S.C., April 1982.

141. Rao, V.V.S. and Gormley, R.J., *US Patent*, 1982, US 4, 340, 503.

142. Katzer, J.R.; Sleight, A.W.; Gajardo, P.; Michel, J.B.; Gleason, E.F. and McMillan, S., *Faraday Discuss.*, 1979, 72, 72.

143. Lang, N.D. and Williams, A.R., *Phys. Rev. Lett.*, 1976, 37, 212.

144. Garfunkel, E.L.; Crowell, J.E. and Somorjai, G.A., *J. Phys. Chem.*, 1982, 86, 310.

145. Crowell, J.E.; Garfunkel, E.L. and Somorjai, G.A., *Surf. Sci.*, 1982, 121, 303.

146. Broden, G.; Gafner, G. and Bonzel, H.P., *Surf. Sci.*, 1979, 84, 295.

147. Krebs, H.J.; Bonzel, H.P. and Gafner, G., *Surf. Sci.*, 1979, 88, 269.

148. Dwyer, D.J. and Hardenbergh, J.H., *Appl. Surf. Sci.*, 1984, 19, 14.

149. Luftman, H.S.; Sun, Y.M. and White, J.M. *Surf. Sci.*, 1984, 140, L259.

150. Dry, M.E. and Ferreira, L.C., *J. Catal.*, 1967, 7, 352.

151. Dry, M.E., in "*Chemicals from Coal New Processes*", John Wiley and Sons, New York, 1984, chap. 4.

152. Le Roux, J.H., in "*Fischer-Tropsch Waxes*", Sasol Report on Waxes, 1984, Sasolburg, South Africa.

153.   Dry, M.E. and Hoogendoorn, J.C., *Cat. Rev. – Sci. Eng.*, 1981, 23, 265.

154.   Bode, D., Shell Internationale Research, *European Patent*, 1986, EP 0, 188, 304.

155.   Everson, R.C.; Woodburn, E.T. and Kirk, A.R.M., *J. Catal.*, 1978, 53, 186.

156.   Vermaire, D., *Personal Communication*, 1987, Sastech (R and D), Sasolburg, South Africa.

157.   Groeneveld, G.; Wittgen, P.M.M.; van Kersbergen, A.M.; Mestrom, P.L.M.; Nuijten, C.E. and Schuit, G.C.A., *J. Catal.*, 1979, 59, 153.

158.   McDaniel, M.P. and Welch, M.B., *J. Catal.*, 1983, 82, 98.

159.   Welch, M.B. and McDaniel, M.P., *J. Catal.*, 1983, 82, 110.

160.   McDaniel, M.P.; Welch, M.B. and Dreiling, C.H., *J. Catal.*, 1983, 82, 118.

161.   Riva, A.; Trifiró, F. Vaccari, A.; Busca, G.; Mintchev, L.; Sanfilippo, D. and Manzatti, W., *J. Chem. Soc., Faraday Trans. 1*, 1987, 83, 2213.

162.   Szilagyi, T.; Praliaud, H.; Primet, M. and Martin, G.A., *Appl. Catal.*, 1984, 11, 235.

163.   Sheffer, G.R. and King, T.S., *Appl. Catal.*, 1988, 44, 153.

164.   Satterfield, C.N.; Huff, G.A. and Longwell, J.P., *Ind. Eng. Chem. Process Dev. Des.*, 1982, 21, 465.

165.   Satterfield, C.N. and Stenger, H.G., *Ind. Eng. Chem. Process Des. Dev.*, 1984, 23, 849.

166.   Caldwell, L., *CSIR (CENG)*, *Report*, 1980, 330 (Pretoria, South Africa).

167.   Bauer, H.H.; Christian, G.D. and O'Reilly, J.E., in *"Instrumental Analysis"*, Allyn and Bacon, Inc., Boston, 1978.

168.   King, D.L., *J. Catal.*, 1978, 51, 386.

169. McDaniel, M.P., *Adv. Catal.*, 1985, 33, 47.

170. Robenstorf, B., *J. Catal.*, 1989, 117, 71.

171. Loggenberg, P.M., *Personal Communication*, 1990, Sastech (R and D), Sasolburg, South Africa.

172. Leith, I., *CSIR (CENG), Report*, 1983, 457 (Pretoria, South Africa).

173. Sexton, B.A.; Hughes, A.E. and Turney, T.W., *J. Catal.*, 1986, 97, 390.

174. Idzerda, Y.U.; Elam, W.T., Jonker, B.T. and Prinz, G.A., *Phys. Rev. Lett.*, 1989, 62, 21, 2480.

174a. Klug, H.P. and Alexander, L.E., in *"X-ray Diffraction Procedures for Polycrystalline and Amorphous Materials"*, Wiley Interscience, New York, 1974.

175. Hamadek, I.H.; King, D. and Griffiths, P.R., *J. Catal.*, 1984, 88, 264.

176. Copperthwaite, R.G.; Loggenberg, P.M.; Derry, T.E. and Sellschop, J.P.F., *Vacuum*, 1988, 38, 413.

177. Kaminsky, M.P.; Winograd, N.; Geoffroy, G.L. and Vannice, M.A., *J. Am. Chem. Soc.*, 1986, 108, 1315.

178. Newman, R.A.; Blazy, J.A.; Fawcett, T.G.; Whiting, L.F. and Stowe, R.A., *Adv. X-ray Anal.*, 1987, 30, 493.

179. Walmsley, R.; Thompson, J.; Friedman, D.; White, D. and Geballe, T.H., *IEEE Trans. Magn.*, 1983. 19, 1992.

180. Gates, D.J.C. and Prestridge, E.B., *J. Catal.*, 1987, 106, 549.

181. Rayment, T.; Schlögl, R. and Thomas, J.M., *Nature*, 1985, 315, 311.

182. Johnston, C.; Jorgensen, N. and Rochester, C.H., *J. Chem. Soc., Faraday Trans. I*, 1988, 84(1), 309.

183. Nix, R.M.; Rayment, T.; Lambert, R.M.; Jennings, J.R. and Owen, G., *J. Catal.*, 1987, 106, 216.

184. Walker, A.P.; Rayment, T. and Lambert, R.M., *J. Catal.*, 1989, 117, 102.

185. Dhere, A.G. and De Angellis, R.J., *J. Catal.*, 185, 92, 145.

186. Colley, S.E.; Copperthwaite, R.G.; Hutchings, G.J.; Terblanche, S.P. and Thackeray, M.M., *Nature*, 1989, 339, 129.

187. Biloen, P. and Sachter, W.M.H., *Adv. Catal.*, 1981, 30, 65.

188. Fisher, V., Catalysis – Specialist Periodical Report, *Royal Soc. Chem.*, London, 1982, 5, 48, London.

189. Vannice, M.A., *J. Catal.*, 1982, 74, 199.

190. Barrault, J.; Forguy, C. and Pernchon, V., *Appl. Catal.*, 1983, 5, 119.

191. Costa, J.L.; Noels, A.F.; Demonceau, A. and Hubert, A.J., *J. Catal.* 1987, 105, 1.

192. Barrault, J., *Stud. Surf. Sci. Catal.*, 1982, 11, 225.

193. Palmer, R.L. and Vroom, D.A., *J. Catal.*, 1977, 50, 244.

194. Ignatrev, A. and Matsuyama, T., *J. Catal.*, 1979, 58, 328.

195. Barrault, J. and Renard, C., *Appl. Catal.*, 1985, 14, 133.

196. Grzybek, T.; Papp, H. and Baerns, M., *Appl. Catal.*, 1987, 29, 335.

197. Kuznetsova, L.I.; Suzdorf, A.R.; Vsmanova, I.V.; Moiseeva, G.A. and Chumakov, V.G., *Kinet-Katal.*, 1988, 29, 491.

198. Adams, D.M., in *"Inorganic Solids"*, John Wiley and Sons, New York, 1974.

199. Venter, J.; Vannice, M.A.; Kaminsky, M. and Geoffroy, G.L., *Am. Chem. Soc., Div. Petr. Chem.*, New York, 1986, 219.

200. Venter, J.; Kaminsky, M.; Geoffroy, G.L. and Vannice, M.A., *J. Catal.*, 1987, 105, 155.

201. Srinivasan, R.; De Angelis, R.J.; Rencroft, P.J.; Dhere, A.G. and Bently, J., *J. Catal.*, 1989, 116, 144.

202. Sato, K.; Inoue, Y.; Kojima, I.; Miyazaki, E. and Yajumori, I., *J. Chem. Soc., Faraday Trans. 1*, 1984, 80, 841.

203. Chin, R.L. and Hercules, D.M., *J. Phys. Chem.*, 1982, 86, 3079.

204. Chin, R.L. and Hercules, D.M., *J. Phys. Chem.*, 1982, 86, 360.

205. Declerck-Grimee, R.I.; Canesson, P.; Friedman, R.M. and Friplat, J.J., *J. Phys. Chem.*, 1978, 82, 885.

206. Nandi, R.K.; Pitchai, R.; Wong, S.S.; Cohen, J.B.; Burwell, R.L. and Butt, J.B., *J. Catal.*, 1981, 70, 298.

207. Riedi, P.C.; Dumelow, T.; Rubenstein, M.; Prinz, G.A. and Qadri, S.B., *Phys. Rev.*, 1987, B36, 4595.

208. Prinz, G.A., *Phys. Rev. Lett.*, 1985, 54, 1051.

209. Moruzzi, V.L.; Marcus, P.M.; Schwarz, K. and Mohn, P., *J. Magn. Magn. Mater.*, 1986, 955, 54.

210. Bagayoko, D.; Ziegler, A. and Callaway, J., *Phys. Rev. B.*, 1983, 27, 7046.

211. Min, B.I.; Oguchi, T. and Freeman, A.J., *Phys. Rev.* 1986, B33, 7852.

211a. Johnson, B.G., Bartholomew, C.H. and Goodman, D.W., *J. Catal.*, 1991, 128, 231.

212. Mellor, J.R., *Personal Communication*, 1990, Catalysis Research Programme, University of the Witwatersrand, Johannesburg, South Africa.

213. Lee Sheng, Y. and Aris, R., *Catal. Rev. - Sci. Eng.*, 1985, 27(2), 207.

214. Delmon, B.; Grange, P.; Jacobs, P.A. and Poncelet, G., *"Preparation of Catalysts - Vol. 4"*, Proc. 4th Int. Symp., Sep 1986, Elsevier, Amsterdam, 1987.

215.   Komiyama, M., *Catal. Rev. – Sci. Eng.*, 1985, 27(2), 341.

215a.   Chu, P.; Petersen, E.E. and Radke, C.J., *J. Catal.*, 1989, 117, 52.

215b.   Dougherty, R.C. and Verykios, X.E., *Catal. Rev. – Sci. Eng.*, 1987, 29(1), 101.

215c.   Shadman-Yazdi, F. and Petersen, E.E. *Chem. Eng. Sci.*, 1972, 27, 227.

215d.   Ernst, W.R. and Daugherty, D.J., *AIChEJ.*, 1978, 24, 935.

215e.   Juang, H.D. and Weng, H.S., *Ind. Eng. Chem. Fundam.*, 1983, 22, 224.

215f.   Johnson, D.L. and Verykios, X.E., *J. Catal.*, 1983, 79, 156.

215g   Cukierman, A.L.; Laborde, M.A. and Lemcoff, N.O., *Chem. Eng. Sci.*, 1983, 38, 1977.

215h.   Dadyburjor, D.B., *Ind. Eng. Chem. Fundam.*, 1985, 24, 16.

215i.   Vayenas, C.G. and Pavlou, S., *Chem. Eng. Sci.*, 1987, 42, 1655.

215j.   Vayenas, C.G. and Pavlou, S., *Chem. Eng. Sci.*, 1988, 43, 2729.

215k.   Vayenas, C.G.; Pavlou, S. and Pappas, A., *Chem. Eng. Sci.*, 1989, 44, 133.

216.   Hurst, N.W.; Gentry, S.J.; Jones, A. and McNicol, B.D., *Catal. Rev. – Sci. Eng.*, 1982, 24(2), 233.

217.   Tauster, S.J. and Fung, S.C., *J. Catal.*, 1978, 55, 29.

218.   Adesina, A.A., *J. Catal.*, 1990, 124, 297.

219.   Cagnoli, M.V.; Sergio, M.G.; Gallegos, N.G.; Alvarez, A.M.; Mercader, R.C. and Yeramian, A.A., *J. Catal.*, 1990, 123, 21.

220. Armstrong, R.S.; Bell, T.; Chaffee, A.L.; Chin, V.W.L.; Loeh, H.J.; Lucchere, A.B.J.; Masters, A.F. and Williams, M.A., *Appl. Catal.*, 1989, 47, 243.

221. Vermaire, D., *Sastech report No. 60*, October, 1985, Sasol 1, Sasolburg, South Africa.

222. Espinoza, R., *Personal Communication*, 1990, Sastech (R and D), Sasol 1, Sasolburg, South Africa.

223. Orchard, S.W., *ChemSA*, August, 1987, 222.

224. MacDonald I., *"Electroplating Engineering Handbook"*, 4th edition, L.J. Dasney (ed.), Van Rostrand, New York, 1984.

225. Pearlstein, F., *"Modern Electroplating"*, 3rd edition, F.A. Lowenheim (ed.), Wiley, New York, 1973, chap. 31.

226. Molenaar, A. in *"Proceedings of the Symposium on Electroless deposition of Metals and Alloys"*, Volume 88 – 12, M. Paunovic and I. Ohno (eds.), The Electrochemical Society, Inc., 1988, p. 77.

227. Wiese, H. and Weil, K.G., in *"Proceedings of the Symposium on Electroless deposition of Metals and Alloys"*, Volume 88 – 12, M. Paunovic and I. Ohno (eds.), The Electrochemical Society, Inc., 1988, p. 53.

228. Nakahara, S. and Okinaka, Y., in *"Proceedings of the Symposium on Electroless deposition of Metals and Alloys"*, Volume 88 – 12, M. Paunovic and I. Ohno (eds.), The Electrochemical Society, Inc., 1988, p. 157.

229. Stremsdoefer, G.; Perrot, H.; Martin, J.R. and Cléchet, P., in *"Proceedings of the Symposium on Electroless deposition of Metals and Alloys"*, Volume 88 – 12, M. Paunovic and I. Ohno (eds.), The Electrochemical Society, Inc., 1988, p. 61.

230. Miyabayashi, T.; Wakayama, H.; Miyatn M., Kobagashi, K.; Yasuda, M. and Hine, F., in *"Proceedings of the Symposium on Electroless deposition of Metals and Alloys"*, Volume 88 – 12, M. Paunovic and I. Ohno (eds.), The Electrochemical Society, Inc., 1988, p. 196.

231. Frieze, A.S.; Sard, R. and Weil, R., *J. Electrochem. Soc.*, 1968, 115, 6, 556.

232. Fisher, R.D. and Chilton, W.H., *J. Electrochem. Soc.*, 1962, 109, 6, 485.

233. Ting, C.H., in *"Proceedings of the Symposium on Electroless deposition of Metals and Alloys"*, Volume 88 – 12, M. Paunovic and I. Ohno (eds.), The Electrochemical Society, Inc., 1988, p. 223.

234. Holm, V.C.F. and Clark, A., *J. Catal.*, 1968, 11, 305.

235. Schlesinger, M.; Meng, X.; Evans, W.T.; Saunders, D.A. and Kampert, W.P., *J. Electrochem. Soc.*, 1990, 6, 137, 1706.

236. Haggin, J., *Chem. Eng. News*, July 23, 1990, p. 27.

Author: Colley Saul Eric.
Name of thesis: Hydrogenation Of Carbon Monoxide Over Modified Cobalt-based Catalysts.

PUBLISHER:
University of the Witwatersrand, Johannesburg
©2015

LEGALNOTICES: